

ULTRA RED GALAXIES IN THE DISTANT
UNIVERSE:
*The first quiescent galaxies and their hidden
progenitors*

DISSERTATION SUBMITTED FOR THE DEGREE OF
PHILOSOPHIÆ DOCTOR
TO THE PHD SCHOOL OF THE FACULTY OF SCIENCE,
KØBENHAVNS UNIVERSITET

Katriona Mai Landau Gould

Advised by:
Gabriel Brammer
& Francesco Valentino

Assessment Committee:
Prof. Paschal Oesch
Prof. Mariska Kriek
Prof. Ross McLure

APRIL 2024

© COPYRIGHT BY KATRIONA MAI LANDAU GOULD, 2024. ALL RIGHTS RESERVED.

ABSTRACT

Understanding the story of how galaxies formed and evolved over cosmic history is the shared quest of extra-galactic astronomers. If one were to look out into the universe around us, it would become evident that galaxies fall roughly into two groups: those that still actively form stars (blue galaxies), and those that have long since become quiescent (red galaxies). These populations arise as a natural consequence of the interplay between galaxies, the dark matter halos they live in, and the gas that surrounds these environments that is the key ingredient of star formation. But what cannot be explained, is how only 1-2 billion years after the Big Bang, quiescent galaxies began to appear, seemingly having assembled billions of solar masses in a few hundred million years, and quenched their star formation in equally rapid timescales. These are the first massive quiescent galaxies (MQGs). This issue has been the subject of much examination over the past few decades, increasingly so since these galaxies were spectroscopically confirmed only in the past decade. Despite these studies, several challenges remain, ranging from how best to select these galaxies in our data sets, to understanding their physical origins. This thesis presents the exploration of these first quiescent galaxies and their possible origins via the study of data taken with both ground and spaced based telescopes, including *JWST*, using two new codes presented in this work.

The first part of this thesis presents a novel selection method designed to find high redshift quiescent galaxies in photometric catalogs, specifically tailored to their unique colours. This method was designed to allow for a wide variety of colours, and therefore allows us to select more recently quenched galaxies, as they are bluer than the typical quiescent galaxy. First tuning the method using cosmological simulations, I found that my method outperforms a classical at colour selection at $z > 3$. I then applied the selection method to the widest and deepest optical/near-infrared photometric catalog of the COSMOS field, COSMOS₂₀₂₀. Therein I explored the number densities to understand the rarity of these galaxies, and compared to similar galaxies in simulations in order to understand their physical origins. I calculated the number density of MQGs from $z = 5$ to $z = 2$, confirming this is period of tremendous

growth in the early universe. I compared these number densities to those produced from cosmological simulations and found that no simulations can reproduce the number densities of MQGs found observationally at $z > 3$, implying that new recipes are needed.

In the second part of the thesis, I applied this method to eleven public imaging fields taken in the first three months of *JWST* observations, finding number densities for massive ($\log(M_*/M_\odot) > 10.6$) quiescent galaxies at $3 < z < 4$ on the order of 10^{-5} Mpc^{-1} , with field to field variations and cosmic variance playing a huge role in deriving these estimates, highlighting the importance of searching for these galaxies over multiple fields. Tuning the selection allowed for the discovery of lower mass quiescent galaxies, something which was expected, but highly difficult to study prior to the launch of *JWST*. Finally, a quiescent galaxy candidate at $z > 4$ selected by the method was later confirmed to be one of the most distant and old quiescent galaxies ever found to date, highlighting the method’s flexibility in finding all types of galaxies. I also used this colour selection to identify quiescent galaxy candidates at $z > 2$ in the CANUCS survey, and presented a preliminary sample of spectra of quiescent galaxies at $z \sim 2$ observed with *JWST*/NIRSpec, including two galaxies at $z > 3$. These galaxies exhibit a range of spectra of different apparent ages, further demonstrating the colour selection method as a way to explore galaxies in all stages of quenching.

Finally, in the third part of the thesis, I presented novel observations of an optically invisible, dusty star forming galaxy at $z = 3.65$ (dubbed “BB”) observed both with *JWST*/NIRCam and NIRSpec. I developed a new software specifically to fit the spectrum of this galaxy, and explored its stellar populations and inter-stellar medium (ISM) properties using a combination of photometry and spectroscopy. I found that BB is a massive, star forming, highly dust obscured galaxy, with a strongly ionized ISM. Line ratios based on standard diagnostics as well as significant residuals indicating a broadened HeI λ 10830 line imply the galaxy is either hosting an active black hole, is experiencing shocks, or has strong stellar winds from evolved stars. This galaxy is already as small as $z \sim 3$ quiescent galaxies, and combined with its stellar mass and fast gas depletion timescale, I hypothesised that BB will join the compact quiescent galaxy population by $z \sim 2$. Based on BB’s similarity to other optically dark main sequence galaxies at $z > 3$, it is possible this population could also be progenitors of the high redshift massive quiescent galaxy population.

ABSTRACT PÅ DANSK

Forståelsen af galaksernes dannelses- og udviklingshistorie gennem kosmisk tid, er den fælles søgen for ekstragalaktiske astronomer. Ser man ud i universet omkring os, bliver det tydeligt, at galakser groft kan inddeles i to grupper: Dem, der stadig aktivt danner stjerner (blå galakser), og dem, der for længst er døde, altså har stoppet stjernedannelse (røde galakser). Disse populationer opstår som en naturlig konsekvens af samspillet mellem galakser, haloerne af mørkt stof de befinder sig i, og nøgleingrediensen i stjernedannelse, gassen gassen omkring disse miljøer. Men det, der ikke kan forklares, er, hvordan kun 1-2 milliarder år efter Big Bang begyndte døde galakser at dukke op. Det er tilsyneladende sket efter at have samlet billioner af solmasser på få hundrede millioner år, og slukket deres stjernedannelse på samme tidsskala. Disse er de første massive døde galakser (MQG'er). Dette problem har været genstand for meget undersøgelse gennem de seneste årtier, og i stigende grad, siden disse galakser blev spektroskopisk bekræftet i løbet af det forrige årti. På trods af disse studier forbliver flere udfordringer, fra hvordan man bedst udvælger disse galakser i vores datasæt, til at forstå deres fysiske oprindelse. Denne afhandling præsenterer udforskningen af disse første døde galakser og deres mulige oprindelser gennem studiet af data taget med både jord- og rum-baserede teleskoper, inklusive *JWST*, ved brug af to nye koder præsenteret i dette arbejde.

Den første del af afhandlingen præsenterer en ny udvælgelsesmetode designet til at finde høj-rødforskydnings døde galakser i fotometriske kataloger, specifikt tilpasset deres unikke farver. Metoden blev designet til at tillade et bredt udvalg af farver og gør det derfor muligt for os at udvælge nyligt døde galakser, da de er blåere end den typiske døde galakse. Efter først at have justeret metoden ved hjælp af kosmologiske simuleringer, fandt jeg, at min metode overgår en klassisk farveudvælgelse ved $z > 3$. Derefter anvendte jeg udvælgelsesmetoden på det bredeste og dybeste optiske/nær-infrarøde fotometriske katalog af COSMOS-feltet, COSMOS₂₀₂₀. Her udforskede jeg antalstæthed for at forstå disse galakseres sjældenhed, og sammenlignede med lignende galakser i simuleringer for at forstå deres fysiske oprindelse. Jeg beregnede antalstætheden af MQG'er fra $z = 5$ til $z = 2$ og bekræftede, at dette er en peri-

ode med enorm vækst. Jeg sammenlignede disse antalstætheder med dem produceret fra kosmologiske simuleringer og fandt, at ingen simuleringer kan reproducere de observerede antalstætheder af MQG'er ved $z > 3$, hvilket tyder på, at nye simuleringsteknikker er nødvendige.

I afhandlingens anden del anvendte jeg denne metode på elleve offentlige billedfelter taget i de første tre måneder af *JWST*-observationerne og fandt antalstætheder for massive ($\log(M^*/M_\odot) > 10.6$) døde galakser ved $3 < z < 4$ på størrelsesordenen 10^{-5} Mpc^{-1} , med variationer fra felt til felt og kosmisk varians, som spiller en stor rolle i disse estimater, hvilket fremhæver vigtigheden af at undersøge disse galakser på tværs af flere felter. Justering af udvælgelsen gjorde det muligt at opdage døde galakser med lav masse, noget som var forventet, men meget vanskeligt at studere før *JWST*'s opsendelse. Endelig blev en kandidat til en død galakse ved $z > 4$ udvalgt af metoden, og senere bekræftet som en af de fjerneste og ældste døde galakser nogensinde fundet, hvilket fremhæver metodens fleksibilitet i at finde alle typer galakser. Jeg brugte også denne farveudvælgelse til at identificere kandidater til døde galakser ved $z > 2$ i CANUCS-programmet og præsenterede et foreløbigt udvalg af spektre af døde galakser ved $z \sim 2$ observeret med *JWST*/NIRSpec, inklusivt to galakser ved $z > 3$. Disse galakser udviser en række meget forskellige spektre, hvilket yderligere demonstrerer farveudvælgelsesmetoden som en måde at udforske galakser i alle stadier af afkøling.

Endelig i afhandlingens tredje del præsenterer jeg nyskabende observationer af en optisk usynlig, støvet stjerneformende galakse ved $z = 3.65$ (kaldet "BB") observeret både med *JWST*/NIRCam og NIRSpec. Jeg udviklede en ny software specifikt til at forstå spektret for denne galakse og udforskede dens stjernepopulationer og interstellart medium (ISM) ved hjælp af en kombination af fotometri og spektroskopi. Jeg fandt, at BB er en massiv, stjerneformende, stærkt støvskjult galakse, med et kraftigt ioniseret ISM. Linjeratioer baseret på standarddiagnostik samt betydelige rester, der indikerer en udvidet He I $\lambda 10830$ linje, tyder på, at galaksen enten huser et aktivt sort hul, oplever chokbølger, eller har kraftige stjernevinde fra udviklede stjerner. Denne galakse er allerede lige så lille som døde galakser ved $z \sim 3$, og kombineret med dens stjernemasse og hurtige gasudtømmingstid, hypotetiserede jeg, at BB vil tilslutte sig populationen af kompakte døde galakser ved $z \sim 2$. Baseret på BB's lighed med andre optisk mørke hovedsekvensgalakser ved $z > 3$, er det muligt, at populationen af høj-rødforskydnings massive døde galakser kan være efterkommere af galakser som BB.

THIS THESIS IS DEDICATED TO MY BIG SISTER JESS. BRAISED BEANS!

ACKNOWLEDGMENTS

This PhD could not have been completed without the help and support of what amounts roughly to a small village. I would like to profess my thanks to those people here. I would firstly like to thank the thesis committee Pascal Oesch, Mariska Kriek, and Ross McLure for taking the time to read this thesis and being my opponents. To my supervisor Gabe, thank you for being my teacher. We are both similar (you know what I mean!) but that similarity is the basis for our shared passion for rigorous science, technical details, and messing around in the weeds of the data. Thank you for nurturing my passion for distant red galaxies, helping me debug my code countless times, teaching me your tricks of the trade, and introducing me to your networks and collaborations. To my supervisor Francesco, thank you for being my mentor. Whenever I doubted my abilities or was stuck with where to go with my science, you were there to listen to me and guide me. You always checked in with me to make sure I was okay. Thank you for providing useful and fast feedback on every single talk abstract, poster, talk, paper draft, proposal and thesis chapter. Thank you for continuing supervision even after you had left DAWN. This field is incredibly lucky to have you. To both of you - I am so proud of our shared achievements, of our shared values of collaboration, careful science, kindness, and having fun. Thank you both for being my PhD Parents. Hail Elmo.

Thank you to Kate Whitaker and Claudia del P. Lagos for providing much needed expertise and mentorship with writing my first paper. I couldn't have done it without your immense support and collaboration. To everyone in CANUCS, thank you all for being so great. Being a part of the team has been wonderful, and I still can't believe I get to explore the universe through the eyes of JWST not only with you all, but thanks to the group's amazing efforts of reducing data, making catalogs, and being excellent science collaborators (and holiday buddies - JELLYFISH!!). Thank you Chris for trusting me with the task of NIRSpec candidate selection, and to represent CANUCS at multiple conferences. Kartheik, thank you for teaching me about SED fitting, sharing your enthusiasm for cool methods, and showing me all the best food and bubble tea spots in Toronto. Ghassan, I'm glad you're pretty much always awake when I am, for science chat and all things otherwise (including doggo pics). Jasleen and Victoria, thank you for being my astro big sisters and hiking buddies. I love you both, 10/10.

To all my collaborators and co authors, including those at DAWN - thank you for working

with me on this PhD. I have learned so much from all of you - special thanks to Francesca and Kasper for helping me with the papers. To all the folks at DAWN - wow, it has been truly amazing to be part of this center with you. Sune, thanks for always taking an interest in my work, and for convincing me to lead a JWST proposal five days before the deadline when I'd never written one before (and thanks to Marko for that too!). John, thanks for being my -almost daily - work buddy and mentor during my first year. First year pandemic PhD would have been a lot slower and boring without you. Vasily, thank you for the 120 comments, and I'm sorry I forgot about them. Thank you Natalie for being the bestest bud, and thank you Rasmus for translating my abstract. Shout out to the other DAWN PhD's who went through it with me: you are all now too many to list, but I appreciate all of you!! Huge thanks to Helena and Guarn for all the admin help and emotional support. Arianna, thanks for being an awesome collaborator and awesome friend, and being there for me when my life was a tyrannosaurus wreck. Kimi, thank you for being my ESA (and, have a nice day). Thank you Rashmi for staying with me until the (not so) bitter end.

To my friends, and my family: thank you for not only supporting me through multiple health issues that made this PhD more difficult than it needed to be, but also for never doubting my abilities despite my set-backs. Your unwavering support was crucial, and is deeply appreciated. Special thanks to all the incredible people who kept me going during the final month - keeping me company, working together, bringing me food, encouraging daily texts and calls. You know who you are. To Jacob and Claudia, thank you for picking me up and setting me straight when I fell apart. Nikolai, thanks for reminding me I can always quit. I didn't, but it was a good reminder. Helen, thank you for being my art buddy / brick buddy / you get the picture. Russ, thanks for the kick ass playlist. Thanks to my housemates for the support, in particular Adem. To my equally crazy St Andrews friends - Tom, Caitlin, Glen - who also decided to move countries, do a Physics PhD, and pursue the academic adventure - I'm glad we got to share it together. Alisa - I'm so glad I followed you to Copenhagen - thank you for being my sister no matter the time zone.

Jess and Mum, thank you for checking on me and calling me every day in the final few months. You are both my guardian angels and I love you both very much. I really could not have done it without your constant support. Thank you dad, for sharing my enthusiasm in Astrophysics and physics in general, for taking me to the monthly Lancaster astronomical society meetings, driving me up to Clougha fell to stargaze when you'd rather be in bed, and teaching me how to write technical documents. Thank you for telling me "Kerpluch!" Before every single exam. To both my parents: my training as a scientist began with you and made me the astrophysicist I am today.

If I forgot anyone - let it be known - I am most thankful to all of you, even if your name is not listed here.

CONTENTS

ABSTRACT	iii
ABSTRACT PÅ DANSK	iv
I INTRODUCTION	7
1.0.1 From frogs to superclusters	7
1.1 A brief history of distant red galaxies	12
1.1.1 It all began with Hubble	12
1.1.2 Seeing the universe in (fra) red with <i>Spitzer</i>	15
1.2 The first quiescent galaxies	16
1.2.1 The birth of the <i>UVJ</i> selection method	17
1.2.2 The medium band era	18
1.2.3 Everything we know (pre- <i>JWST</i>)	19
1.2.3.1 Number densities	21
1.2.3.2 Stellar populations	23
1.2.3.3 Chemical enrichment	25
1.2.3.4 Dust content	28
1.2.3.5 Star formation histories	28
1.2.3.6 Sizes and morphology	29
1.2.3.7 Environment	30
1.2.3.8 Gas fractions and AGN	31
1.3 The progenitors of the first quiescent galaxies	34
1.3.1 The cosmic star formation rate density	34
1.3.2 The possible progenitors explored thus far	36
1.4 The aims of this thesis	39
2 A NEW DEFINITION OF QUIESCENT	41
2.1 Introduction	42
2.2 Data	47
2.2.1 COSMOS ₂₀₂₀	47

2.2.2	3D-HST	48
2.2.3	Simulated data	49
2.3	SED fitting with eazy-py	50
2.3.1	Eazy-Py	50
2.3.1.1	Rest-frame flux densities	51
2.3.1.2	Stellar masses and Star formation rates	54
2.4	Selecting a robust sample of massive galaxies	55
2.4.1	Introducing the GMM	57
2.4.2	Defining the separator	58
2.4.2.1	The $p(q)$ threshold for quiescence	60
2.4.2.2	UVJ versus GMM in SHARK	62
2.5	Application to COSMOS2020	62
2.5.1	Comparing GMM/ $NUV - VJ$ to UVJ and $NUVrJ$ colour selections	63
2.5.2	Full spectral energy distribution	66
2.5.3	Spectroscopically confirmed QGs	69
2.6	Number densities	69
2.7	What fraction of QGs at $3 < z < 5$ are post-starburst?	72
2.8	Will we find old quiescent galaxies at $z > 4$ with $JWST$?	74
2.9	Summary and conclusions	75
A.1	Rest-frame flux densities	77
A.2	Star-galaxy separation	78
A.3	Robustness of rest-frame J band estimate	80
A.4	Performance of an extended UVJ color selection	81
3	THE QUIESCENT UNIVERSE AS SEEN BY $JWST$	83
3.1	Searching far and wide for quiescent galaxies with $JWST$	84
3.1.1	Quiescent galaxy selection using the GMM method	85
3.1.2	The big picture at $3 < z < 4$	86
3.1.3	Lower masses, higher redshifts	88
3.2	Searching deep for quiescent galaxies with $JWST/CANUCS$	91
3.2.1	CANUCS	91
3.2.2	Data reduction	92
3.2.3	Spectroscopy of quiescent galaxies	93
3.2.3.1	Selection of candidates	93
3.2.3.2	Spectroscopic reduction	95
3.2.3.3	A spectroscopic sample of quiescent galaxies at cosmic noon	96

4	A DISTANT RED GALAXY OBSERVED BY <i>JWST</i>	101
4.1	Introduction	102
4.2	Observations and Data Reduction	105
4.2.1	Photometry	105
4.2.2	Spectroscopy	107
4.3	Methods	108
4.3.1	Correcting for slit losses	109
4.3.2	Strong lensing correction	109
4.3.3	Photometric fitting	109
4.3.4	Spectroscopic fitting	110
4.3.4.1	Models	110
4.3.4.2	Priors	111
4.3.4.3	Sampling	111
4.3.4.4	Final fitting setup	112
4.3.5	Physical properties measured from line fluxes	112
4.3.6	Size	113
4.4	Results	113
4.4.1	Redshift and line widths	122
4.4.2	Dust and SFR	123
4.4.3	Stellar mass	124
4.4.4	BBand the star forming main sequence	125
4.4.5	Ionization conditions	127
4.4.6	Colours and morphology	131
4.4.6.1	Colour gradients	132
4.4.6.2	Morphology and size	132
4.5	Discussion	135
4.5.1	Optical vs FIR SFRs	135
4.5.2	Does BB host an AGN?	136
4.5.3	Placing BB in context	137
4.6	Conclusions	138
B.1	Testing the line ratio fitting	140
B.2	Redshift differences between spectra	140
5	CONCLUSIONS AND FUTURE PERSPECTIVES	143
5.1	Conclusions	143
5.2	Future perspectives	146
	REFERENCES	207

LISTING OF FIGURES

1.1	Galaxy evolution	9
1.2	The Hubble Deep Field	14
1.3	The UVJ colour diagram	17
1.4	SEDs of $z \sim 2 - 4$ quiescent galaxies from the ZFOURGE survey	20
1.5	Spectrum of a $z = 3.7$ massive quiescent galaxy	21
1.6	Number densities of massive quiescent galaxies	22
1.7	The key features of quiescent galaxy spectra	24
1.8	Age indices for massive quiescent galaxies	26
1.9	Formation and quenching times of massive quiescent galaxies at $2 < z < 5$	30
1.10	The interplay of gas and quenching in galaxies	32
1.1.1	Obscured vs unobscured contribution to cosmic star formation rate density since $z \sim 7$	35
1.1.2	Dusty star forming galaxies on the main sequence	38
2.1	Photometric vs spectroscopic redshifts of galaxies in COSMOS2020	52
2.2	Comparison of stellar masses and star formation rates between two codes	53
2.3	Side by side comparison of UVJ and $NUVUVJ$ colour diagrams	56
2.4	$NUVUVJ$ diagram coloured by probability of quiescence	58
2.5	Validating the GMM method against simulations	61
2.6	Comparing cross selection between UVJ and $NUVUVJ$ methods at $2 < z < 3$	64
2.7	Comparing cross selection between UVJ and $NUVUVJ$ methods at $3 < z < 5$	65
2.8	Multi-wavelength postage stamps and SEDs of example $NUVUVJ$ selected MQGs at $3 < z < 5$	67
2.9	Median rest frame SED of 259 $NUVUVJ$ selected MQGs at $3 < z < 5$	68
2.10	Number densities of MQGs at $2 < z < 6$ from observations and simulations	70
A.1	Star galaxy separation projected in gzK diagram	79
A.2	SNR versus redshift at $3 < z < 5$ in IRAC channels for massive galaxies at $3 < z < 5$ in COSMOS2020	82
3.1	$NUV - U, V - J$ colours of quiescent galaxies at $z > 3$ observed with $JWST$	85

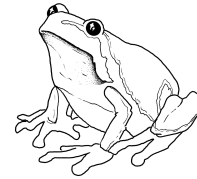
3.2	Mass probability distributions of quiescent galaxies at $3 < z < 5$	86
3.3	Compilation of number densities of massive quiescent galaxies at $3 < z < 4$	87
3.4	SEDs and RGB cutouts of quiescent galaxies at $z > 4$ observed with <i>JWST</i>	89
3.5	Spectrum of the highest redshift quiescent galaxy to date	90
3.6	Schematic of the CANUCS observing strategy	92
3.7	Colour selection of quiescent galaxies for spectroscopic follow-up	94
3.8	Spectroscopic vs photometric redshift for 14 quiescent galaxies observed with <i>JWST</i>	96
3.9	Rest frame 1D spectra of quiescent galaxies at cosmic noon	97
3.10	Rest frame 1D spectra of quiescent galaxies at cosmic noon (continued)	98
3.11	RGB cut-outs of spectroscopic galaxies at cosmic noon observed with <i>JWST</i>	100
4.1	RGB composite image of the MACS J0417.5 – 1154 observed with <i>JWST</i> / NIRCcam	107
4.2	Three observed frame NIRSpec/PRISM spectra of BB, an optically invisible galaxy observed with <i>JWST</i>	108
4.3	Multi-wavelength SED of BB ₁	114
4.4	Multi-wavelength SED of BB ₂	115
4.5	Multi-wavelength SED of BB ₃	116
4.6	Best fit spectral models for BB	120
4.7	Posterior distributions of best fit properties	121
4.8	Stellar mass distributions measured from photometry of BB	125
4.9	BB on the main sequence at $z = 4$	126
4.10	sSFR measured from EW(H α) for BB	128
4.11	Line ratio diagnostic diagrams showing the ionization conditions of BB	129
4.12	Measured colour gradients of BB	132
4.13	Model sizes of BB and 1D size profile	133
4.14	Size mass relation for quiescent galaxies and optically invisible galaxies at $1 < z < 5$	134
B.1	H α / [NII] $\lambda\lambda$ 6549, 6585 distributions measured from low and medium resolution NIRSpec spectra	141
B.2	Velocity offsets for the spectra of BB	142

INTRODUCTION

I

With magic, you can turn a frog into a prince. With science, you can turn a frog into a Ph.D and you still have the frog you started with.

Terry Pratchett
THE SCIENCE OF DISCWORLD



I.O.I FROM FROGS TO SUPERCLUSTERS

The universe is unfathomably large to humans. In our daily lives, the size scales we experience are much, much smaller, despite spanning up to seven orders of magnitude. On Earth, we experience these distance scales through a multitude of senses - from the things we touch, to the objects we see, to the sounds we hear. Astronomy is unique from the other physical sciences, because unlike a chemist mixing solutions or a biologist listening to frogs, we are limited to studying our subject almost exclusively via observation of the electromagnetic spectrum. The light from stars and galaxies we observe has traveled countless human lifetimes before it was even seen by us. Even before humans existed, light was emitted from the first stars as a byproduct of nuclear fusion between elements, primarily Hydrogen. When a star is born from a collapsing cloud of Hydrogen gas, the pressure at its center overcomes the electrostatic repulsion between negatively charged Hydrogen atoms, forcing them to fuse to create Helium, and energy packets called photons. This energy comes from a difference in the binding energy before and after the fusion, and was first postulated as the power source of stars by physicist Arthur Eddington in 1921 ([Eddington, 1926](#)). The extreme density of stellar interiors prevents a quick escape, but after a few thousand to a few million years, the photons from those stars reach the surface, and travel on through space and time, eventually ending up as seemingly stationary pinpricks on the indigo canvas of our night sky, or galaxies in our telescopes.

The galaxy we inhabit, which is fairly typical as galaxies go, is just one of hundreds of billions in the observable universe. The Milky Way (so called because of its dramatic white-ish

appearance in our night sky) is home to ~ 100 billion stars including our own. Despite the fact that we live inside it, astronomers have managed to discern the size, shape, and color of our home Galaxy, as well as the masses and compositions of its constituent ingredients. Furthermore, using careful analysis and smart statistical techniques, they have even managed to map its history and potential origins. Each and every galaxy in the universe has its own story, which can also be inferred indirectly from studying its light across the electromagnetic spectrum. It is through this study of millions of galaxies, both nearby and distant, that we are able to construct a story of how the present day populations came to be.

If the evolution of galaxies took place in a day, then there are three major epochs: cosmic dawn, the birth of galaxies, cosmic noon, the peak of cosmic star formation, and cosmic evening - the present day. At each of these snapshots, the properties of the galactic population as a whole, and of the average galaxy, is different. We make use of something called redshift to study this evolution. The fundamental speed limit of the universe is $299792458 \text{ ms}^{-1}$, which is the speed of light in a vacuum. Thus, light emitted from very distant objects takes some time to arrive, meaning that observing galaxies at greater and greater distances is equivalent to looking back in time. This neat property of space-time allows astronomers to study galaxies at different epochs of cosmological history. Due to the expansion of the universe, light from distant objects is stretched as it travels to us, a phenomenon known as cosmological redshift, which is defined as

$$z = \frac{\Delta\lambda}{\lambda_{\text{rest}}} = \frac{\lambda_{\text{obs}} - \lambda_{\text{rest}}}{\lambda_{\text{rest}}} \quad (\text{I.1})$$

Subsequently, light from distant galaxies is shifted further and further into the infra-red regime. Redshift is a convenient replacement when referring to distance, because of its logarithmic behaviour. Thus, we usually refer to distances or time epochs using redshift instead of distance units, whilst time is usually measured in millions or billions of years. To an astronomer, 100 million years is a short amount of time.

Figure 1.1 presents the evolution of galaxies as a function of time and redshift. Our current understanding is that cosmic dawn began roughly 300 million years after the Big Bang, at roughly $z \sim 14$ (Bromm and Yoshida, 2011) when the first galaxies formed from pristine hydrogen gas accumulating onto the most massive dark matter halos, creating clumpy,

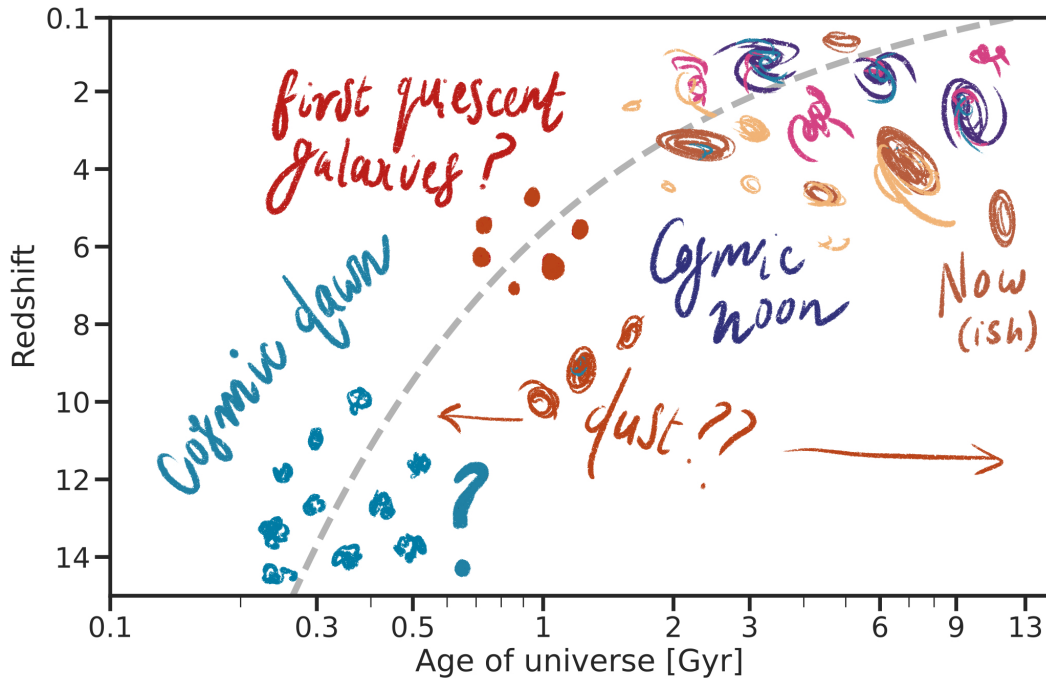


Figure 1.1: Representation of galaxy evolution; the x axis shows age of the universe in Gyr, whilst the y axis shows the corresponding redshift. These quantities are related by the grey dashed line, which assumes a flat Λ CDM cosmology. Various epochs and populations are shown: at the bottom left, cosmic dawn, where the first galaxies form, cosmic noon in the middle at the peak of star formation, and the present day at top right with the local galaxy zoo. At some point around $z \sim 4$, the first quiescent galaxies appear.

tiny, galaxies forming hundreds of stars per year. The first galaxies grew and evolved in a dynamic universe - new galaxies continued to appear until the cosmic star formation rate density peaked some 3 billion years later at $z \sim 2$ (cosmic noon) (Madau and Dickinson, 2014). Over the following 10 billion years, the birth of new galaxies slowed, and the existing populations matured and calmed their production of growth and new stars. By the time we arrive at the present day ($z \sim 0$), galaxies exist predominantly in two groups: those still actively forming stars, and those who are done and now passively exist, their stellar populations quietly maturing (Schawinski et al., 2014).

Connecting the dots between the first galaxies, the present day universe, and everything that happens in between, is the shared quest of extra-galactic astronomers. Over the last century, our understanding of the story of galaxy evolution has grown enormously thanks to technological innovation in both engineering and computing. In the 1970s, a typical astrophysics publication presented observations of a handful of nearby galaxies observed with a singular ground-based telescope, the analysis of which was likely carried out using foundational, but limited, languages such as FORTRAN, performed on a computer with at most several kilo-bytes of RAM.

In 2024, things are a bit different. There are now multiple ground-based and space-based observatories designed to observe wavelength regimes along the entire electromagnetic spectrum, from X-rays to optical to radio. Many of these are equipped with multiple instruments, making it possible to image at specific wavelengths, collect spectra of individual galaxies or en masse via multi object spectroscopy, and design synergistic programs to address global questions (community surveys) or specific questions (proposals). Astronomers have then pushed these instruments further, some discovering ingenious ways to hack the operations of some telescopes in order to push them to their limit.

Advances in computing and internet technologies have revolutionized astrophysics research: we now have searchable public data bases storing terabytes of data that are easy to query, communications platforms that facilitate collaborative research, and cloud based computing services that provide a wide variety of virtual computers and super-computers. Developments in programming have also contributed: the most popular language used by astrophysicists in 2023 is python, for which there are endless open source packages one can use to aid research. Some are generically useful - array manipulation, plotting, machine learning meth-

ods, sampling tools - and some are specifically designed to aid astrophysics research, either written for the community (for example, `astropy` (Astropy Collaboration et al., 2018)) or by the community itself.

It is through this technological and engineering revolution that our deep knowledge of distinct galaxy populations came to be, because it is only with advanced instrumentation and modeling that we are able to study such curious things. In the 1990's, astrophysicists began finding fuzzy red blobs in their images, which were given many nicknames*, such as "Extremely Red Objects" (EROs; McCarthy, 2004) and "Distant Red Galaxies" (DRGs; Franx et al., 2003). The nature of these galaxies was highly uncertain - calculating distances, stellar masses and star formation rates from only a few data points was not trivial. Over the following three decades, an enormous effort pushing near-infrared instrumentation to their limits (and even inventing new technologies) combined with multiple imaging and spectroscopic surveys revealed that those fuzzy red blobs actually contained an entire galaxy zoo, and now we have a lot more nicknames for these galaxies, some of which are still equally as vague. Confusingly, the existence of some populations were impossible to explain under the present cosmological framework. Whilst it was easy to ignore such things when these galaxies were unresolved blobs with very uncertain properties, the issue has to be faced when spectroscopy confirms they are actually real (Glazebrook et al., 2017).

As such, there is now undeniable evidence that unusually evolved galaxies characterised by extreme stellar masses and little to no active star formation suddenly appeared within the first 1-2 billion years after the Big Bang. These are the first massive quiescent galaxies (MQGs). How they accumulated such mass, and how they stopped forming stars, is still unknown. This is important, because we can understand galaxy evolution through the lens of studying the first quenched galaxies. They provide clues not only into the subsequent growth of the quiescent galaxy population, but crucially, studying their origins directly leads to understanding the initial conditions of the universe that seeded the first galaxies and ultimately led to the cosmos we see today.

This has been a topic of debate in the past months since the launch of *JWST*, with claims of galaxies "too massive" leading the community to question the cosmological foundation of Lambda-CDM upon which we base our entire theory of galaxy evolution (Labbé et al., 2023).

*My favourite is "Faint Red Outlier Galaxies", or FROGS (Moustakas et al., 1997).

Concurrently, many studies have pointed out that the analysis techniques and assumptions made in performing these calculations can lead to incorrect results (Giménez-Arteaga et al., 2024; Desprez et al., 2023), thereby leading the community to infer that impossible galaxies exist (such as “Schrodinger’s galaxy”; (Arrabal Haro et al., 2023; Donnan et al., 2023; Naidu et al., 2022)).

Prior to the launch of the James Webb Space Telescope (*JWST*), even obtaining robust measurements of the properties required to investigate the nature and origin of the first quiescent galaxies (and similarly distant red fuzzies) was inherently limited by the lack of instruments probing the near-infrared wavelength regime, the inability to resolve blended sources in large extra-galactic imaging surveys, and the expensive integration times required to even confirm the distant of such galaxies using ground-based spectroscopy, which suffers enormously from telluric interference in the NIR. Fortunately, we now have a shiny new space telescope, and *JWST*’s instrument suite has proven its ability to spectroscopically confirm hundreds of Myr years old MQG candidates in trivial exposure times, easily resolve quiescent and dust obscured galaxies in imaging, and resolve multi-component emission lines. These are exactly the data we require to press forward successfully in our exploration of this exciting cosmic epoch. This thesis presents my endeavors to understand the distant red universe through the development of two novel analysis techniques and their application to two fabulous data sets. We begin with this chapter, the introduction, which provides the necessary background needed to understand the thesis work in context of the literature.

I.1 A BRIEF HISTORY OF DISTANT RED GALAXIES

I.1.1 IT ALL BEGAN WITH HUBBLE

The launch of NASA’s Great Observatories was a pivotal moment for the study of galaxy evolution. Conceived in 1975, the concept was simple: to discover and explore areas of astrophysics that were currently out of reach, due to the difficulty of studying certain regions of the electromagnetic spectrum from the ground. Four observatories would see the universe in all colours from the infrared to the optical to the UV to X-rays and to gamma rays, shedding new light on fundamental questions that could only be answered with space telescopes. Amongst these were the key pillars of the field of extra-galactic astrophysics: when did the

universe begin? how do stars - and therefore also galaxies - form? what are the laws that guide the evolution of the cosmos and its matter? It was these observatories, combined with leading ground-based instruments, that saw through a new area in the study of galaxies and their evolution in the past three decades (Armus et al., 2021).

The Hubble Space Telescope (*HST*) (1990-present) was the first optical space observatory designed to study stars and galaxies. *HST* happened in great part thanks to the work of Lyman Spitzer, who spent years campaigning for an observatory in space, and supported efforts paramount to this goal such as the first space balloon and the first UV space telescope, Copernicus, launched in 1972. In 1965, Spitzer was appointed to lead a committee to design the objectives of a proposed large space telescope (Lyman Spitzer, 1990), but it wasn't until a decade later in 1975 that *HST* was realised. The launch followed in 1990, and after a few years and astronaut trips to fix its blurry vision, the telescope finally revealed a new view of the universe. Within its first few years after the primary mirror was corrected, observations already revealed a wealth of new findings (Ferguson et al., 2000; Williams et al., 1996).

The success of the first few GO and GTO programs in Cycles 1-5 encouraged Robert Williams, then Director of the Space Science Telescope Institute, to push the boat (or telescope) out, and use ten days of Director's Discretionary Time (DDT) to observe a blank patch of sky continuously for ten days (Williams et al., 1996). The result of this endeavour, the Hubble Deep Field (see Figure 1.2), is arguably the most transformative result to change the field of extra-galactic astronomy since its inception in the early twentieth century - particularly because it was not expected by all of the community. Predictions for what Hubble would find can be summed up by this quote from Bahcall et al. (1990): "*We do not expect HST to reveal a new population of galaxies ... the major contribution of HST for galaxy research will be in revealing the shapes, sizes and content of previously unresolved galaxies*". Instead, the Hubble Deep Field revealed thousands of galaxies out to unseen distances, in sizes, shapes and colours that were not only resolved, but also unexpected (e.g Fernández-Soto et al., 1999; Abraham et al., 1996).

It was then possible to investigate the existence and infer the evolution of quiescent galaxies at distances further than before (see Ferguson et al., 2000 for an excellent overview). At the time, it was well established that the $z \sim 0$ quiescent galaxy population must have manifested over a significant fraction of the universe's history in order to build up to present day

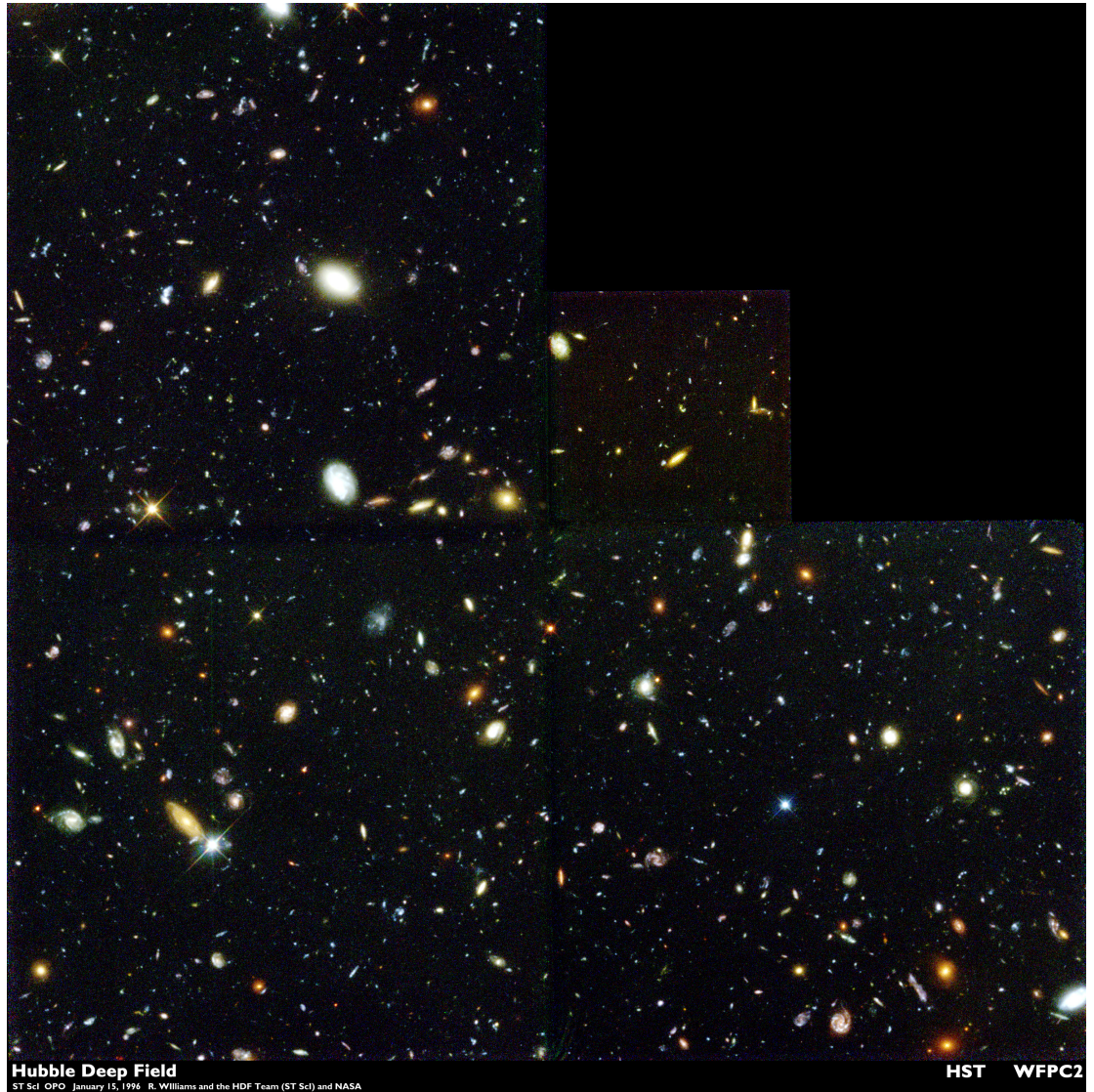


Figure 1.2: False colour image of the Hubble Deep Field, the result of pointing the Hubble Space Telescope (*HST*) at an area of sky less than 1% of the moon, for over 100 hours. The image contains over 3000 galaxies and was the first deep extra galactic field of many observed with *HST*. Credit: Williams et al. (1996) and the HDF team.

Milk-way stellar masses and solar or super-solar metallicities. The pertinent question was whether they formed from monolithic collapse in the early universe and passively evolved to $z \sim 0$ (Eggen et al., 1962), or rather grew their mass via mergers in a hierarchical scenario (van Dokkum et al., 1999; Kauffmann et al., 1993). Whilst the former would manifest as a constant number density of ellipticals as function of look-back time, the latter would see the elliptical luminosity function increase with time, for which the evidence was conflicting. Studies using different selection methods and analyses would find completely opposite results - evolution (Kauffmann et al., 1996) vs no evolution (Lilly et al., 1996; Totani and Yoshii, 1998). Ferguson et al. (2000) commented on this;

”This debate highlights the difficulties inherent to defining samples based on a color cut in the margins of a distribution, where small changes in the boundary, as well as systematic and even random photometric errors in the data, can have substantial consequences for the conclusions.” — Section 5.3, The Hubble Deep Fields (Ferguson et al., 2000)

And in fact, this is a problem that persisted for the next two decades. Despite this, multiple works presented massive quiescent galaxy candidates at $z \sim 1$ photometrically selected from *HST* imaging, indicating the local field elliptical population began its assembly at least as early as $z \sim 1 - 3$ in order to establish the population at $z \sim 1$. Thus, *it was HST that introduced a real possibility of higher redshift quiescent galaxies.*

1.1.2 SEEING THE UNIVERSE IN (FRA) RED WITH *SPITZER*

The *Spitzer Space Telescope* (AKA *Spitzer*), launched in 2003 (Werner et al., 2004), yet again revealed new galaxy populations, but this time, some of them were invisible even to Hubble. Franx et al. (2003) and Yan et al. (2004) found a sample of galaxies detected in *Spitzer*’s Infrared Array Camera (IRAC) instrument at $3.6 \mu\text{m}$ but undetected in *HST*, which were implied as galaxies with evolved stellar populations around cosmic noon. The powerful combination of ground-based instruments and space-based observatories also made it possible to conduct multi-wavelength studies of distant red galaxies, and therefore measure the stellar populations, dust obscuration and stellar assembly of these populations.

Papovich (2006) used both *HST*, ground-based and *Spitzer* observations to study massive ($\log(M_*/M_\odot) > 11.5$) distant red galaxies at $1.5 < z < 3$, finding a mix of galaxies including those with evolved stellar populations, dust obscured star formation, and 10% having evidence for suppressed star formation, as well as 25% of their sample having evidence for hosting an AGN. Reddy et al. (2005) studied the MIPS $24\mu\text{m}$ emission of red galaxies selected using the novel BzK colour selection method (Daddi et al., 2004b) as well as those with $\text{red}J - K_s > 2.3$ colours. They found both optically and NIR selected $z \sim 2$ galaxies to be massive, with some having bolometric luminosity's comparable to local Ultra Luminous IR Galaxies (ULIRGS) ($\langle LIR \rangle \sim 2 \times 10^{12} L_\odot$) - but again, finding a small number seemingly passive. Labbé et al. (2005) studied the $3.6 - 8\mu\text{m}$ emission of *HST* selected DRGs with IRAC, and demonstrated an observed colour selection ($I - K_s$ and $K_s - 4.5\mu\text{m}$) that could be to separate passive galaxy candidates from dusty star forming. From this, they calculated that 30% of their sample as passive galaxies at $z \sim 2.5$ with stellar masses of $\langle \log(M_*/M_\odot) \rangle = 10.5$. Notably, Labbé et al. (2005) commented that the existence of such systems would require extreme quenching scenarios such as AGN feedback or galactic outflows, in order to produce massive quiescent galaxies by $z = 2 - 3$ based on the inferred quenching epoch of $z = 5$ or earlier. In the years following, studies continued to present handfuls of photometrically selected massive quiescent galaxies at $z \sim 2 - 3$ (Brammer and van Dokkum, 2007; Toft et al., 2007) and even up to $z \sim 9$ (Rodighiero et al., 2007; Wiklind et al., 2007), as well as spectroscopic confirmation of $z \sim 2$ quiescent galaxies (Kriek et al., 2006, 2007). Besides a tenuous candidate $z \sim 6.5$ post-starburst galaxy (Mobasher et al., 2005), there was no strong evidence for a substantial population of massive quiescent galaxies at $z \geq 3$.

1.2 THE FIRST QUIESCENT GALAXIES

The search for the elusive quiescent galaxies held the promise of understanding the entire tale of early galaxy formation and evolution, but it was clearly hampered by something. The reason why it was so difficult to find high redshift quiescent galaxies at that time was because of technology - or rather, lack of it. Precisely, the poor efficiency and small field of view of contemporary NIR imaging detectors made conducting deep, wide area surveys very difficult (Williams et al., 2009). This all changed with a new generation of NIR instrumen-

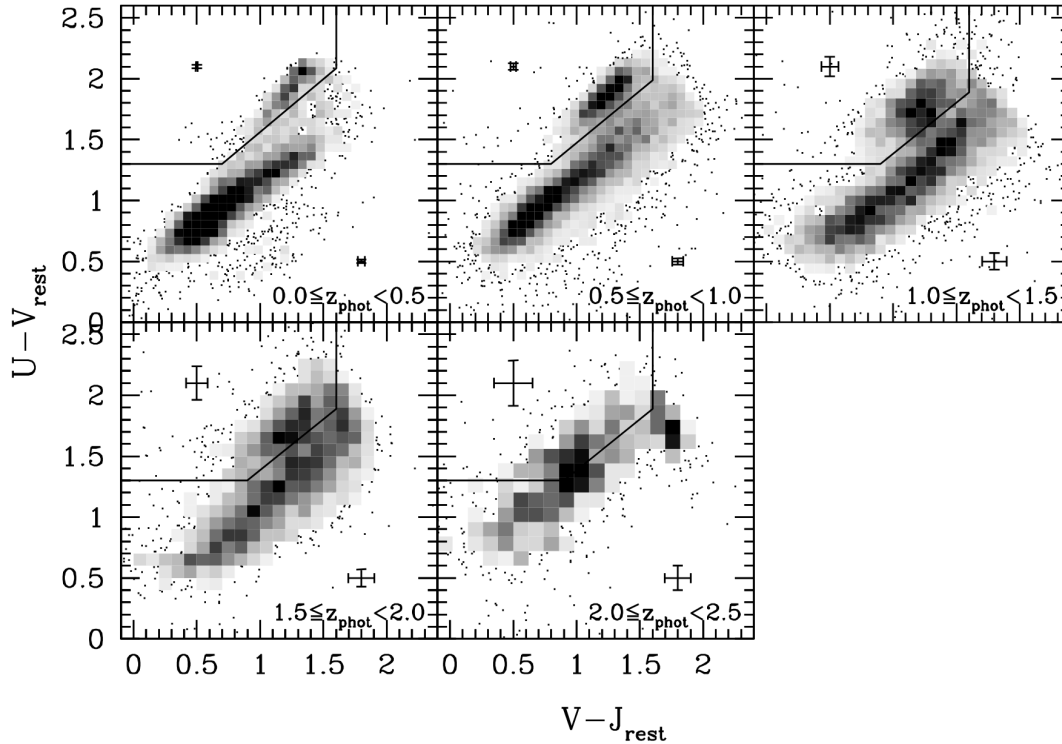


Figure 1.3: $U - V$ vs $V - J$ rest frame colours in bins of redshift from $z \sim 0$ to $z \sim 2.5$ of K selected galaxies from the UDS survey. Quiescent and star forming galaxies each occupy distinct loci, where each population can be separated by the colour criteria $U - V > 1.3$, $V - J < 1.6$ and $U - V > 0.88 \times (V - J) + (0.69, 0.59, 0.49)$ at $(0 < z < 0.5, 0.5 < z < 1.0, 1.0 < z < 2.0)$ (Williams et al., 2009).

tation, paving the way for large scale imaging surveys such as UKIDSS (Williams et al., 2009; Lawrence et al., 2007), WIRDS Bielby et al. (2012) and ULTRA-VISTA (McCracken et al., 2012; Dalton et al., 2006; Emerson et al., 2006), which published its fifth data release earlier this year, and was a foundational component in the Cosmic Evolution Survey catalogs (Weaver et al., 2021; Laigle et al., 2016; Muzzin et al., 2013; Ilbert et al., 2013).

1.2.1 THE BIRTH OF THE UVJ SELECTION METHOD

Data-sets and methods developed during this time were foundational for the next decade of high redshift red galaxy research. For example, instead of following the norm of selecting DRGs with observed colour cuts, Williams et al. (2009) binned galaxies by their photometric

redshift and subsequently allocated them as star forming or quiescent based on their UVJ rest frame colours. The choice of UVJ was motivated by their proximity to the observed filters J , K , and IRAC $4.5\ \mu\text{m}$ at $z \sim 2.5$, meaning it was possible to accurately measure the rest frame colours up to this redshift, and observe any trends. A clear trend appeared: in the UVJ colour diagram, quiescent galaxies occupied a locus separate to star forming galaxies, one which persisted out to at least $z \sim 2$, but migrating towards bluer colours, reflecting younger stellar populations (Figure 1.3). Their quiescent nature was confirmed through lack of emission in the MIPS $24\ \mu\text{m}$ filter, which at $z \sim 1 - 2.5$ would pick up emission from poly-aromatic hydrocarbons (PAHs), which would only be observable if heated by young stellar populations, indicating dust obscured star formation, or AGN.[†] This was corroborated by Brammer et al. (2011). Further exploration found UVJ colours not only correlated with dust, but also with morphology Papovich et al. (2012) and age (Belli et al., 2019; Whitaker et al., 2010).

The establishment of a fast, easy and reliable method to select high redshift quiescent galaxy populations from imaging then made it possible for the community to select and study these populations with relative ease. (Forrest et al., 2020b; Schreiber et al., 2018; Pacifici et al., 2016; Straatman et al., 2015; Ma et al., 2015; Tomczak et al., 2014; Straatman et al., 2014; Spitler et al., 2014; Fumagalli et al., 2014; Whitaker et al., 2014; Muzzin et al., 2013; Whitaker et al., 2012, 2011; Brammer et al., 2011; Whitaker et al., 2010). Although, it should be stated that UVJ was just a different implementation of the basic idea of a colour cut (Daddi et al., 2004b)

1.2.2 THE MEDIUM BAND ERA

At the same time, the use of NIR medium band filters was introduced to bridge the gap between spectroscopy of quiescent galaxy candidates, which was too expensive for large samples, and photometry carried out with broad-band filters, which resulted in large photometric redshift uncertainties for red galaxies, and lacked the depth required to detect the exact location of the Balmer break at $z \geq 1.5$. The NEWFIRM Medium Band Survey (NMBS; Whitaker et al. (2011); van Dokkum et al. (2009b)) introduced five medium band filters

[†]However, these omissions would also exclude galaxies with dust warmed by old stellar populations (e.g. Belli et al., 2021).

J_1, J_2, J_3, H_1, H_2 in place of J, H , resulting in a twofold photometric redshift accuracy and, for the first time, strong evidence for the quiescent galaxy population existing out to at least $z \sim 3$ [Whitaker et al. \(2011\)](#). NMBS was also used to measure the dust attenuation properties of galaxies at $0 < z < 2.5$: [Kriek and Conroy \(2013\)](#) found that different galaxy types prefer different dust attenuation curves, leading to the important conclusion that assuming a global dust law for all galaxies is probably not a good idea.

The FOURSTAR galaxy Evolution Survey (ZFOURGE; [Straatman et al. \(2016\)](#)) took this idea further (or rather, deeper), with a NIR medium band survey integrated to depths that were unattainable with ground-based spectroscopy ($AB \sim 25 - 26$, 25, 25 in J, H, K medium bands) (Figure 1.4). ZFOURGE demonstrated the awesome power of medium band observations for multiple science cases: the evolution of low mass star forming and quiescent galaxies since $z \sim 2$ [Tomczak et al. \(2014\)](#), tracing the history of Milky-Way like galaxies back to $z \sim 3$ [Papovich et al. \(2015\)](#), the possibility of dusty star forming galaxies with low specific star formation rates at $z \sim 3$ [Spitler et al. \(2014\)](#) and most surprisingly, the undeniable existence of quiescent galaxies at $z \sim 4$ [Straatman et al. \(2014\)](#).

1.2.3 EVERYTHING WE KNOW (PRE-*JWST*)

Finally, spectroscopic confirmation cast all doubt of quiescent galaxies at $z > 3$ aside, when [Glazebrook et al. \(2017\)](#) presented the spectrum of a massive ($\log(M_*/M_\odot) = 11.2$) galaxy at $z_{spec} = 3.717$ with no current star formation ($SFR < 0.2 M_\odot \text{yr}^{-1}$) (Figure 1.5). The presence of deep Balmer absorption lines were indicative of a predominantly A star type stellar population, something that had been observed in $z \sim 0$ post-starburst galaxies, a population that had negligible star formation but had signs of a recent vigorous star formation episode (e.g. [Wild et al. \(2009\)](#)). This is due to the relatively short lifetime of the A stars, at 20-1000 Myr. [Glazebrook et al. \(2017\)](#) found that the existence of such a massive, dormant system only 1.5 billion years after the Big Bang could only be explained by a rapid formation (< 250 Myr) and quenching (< 500 Myr), with a peak star formation rate of at least $> 350 M_\odot \text{yr}^{-1}$ (95% CI). Over the following years, more studies presented spectroscopic confirmation of quiescent galaxies at $3 < z < 4$ from optical/NIR spectra, albeit in small numbers. This was complimented by a plethora of statistical studies based on multi-wavelength imaging data

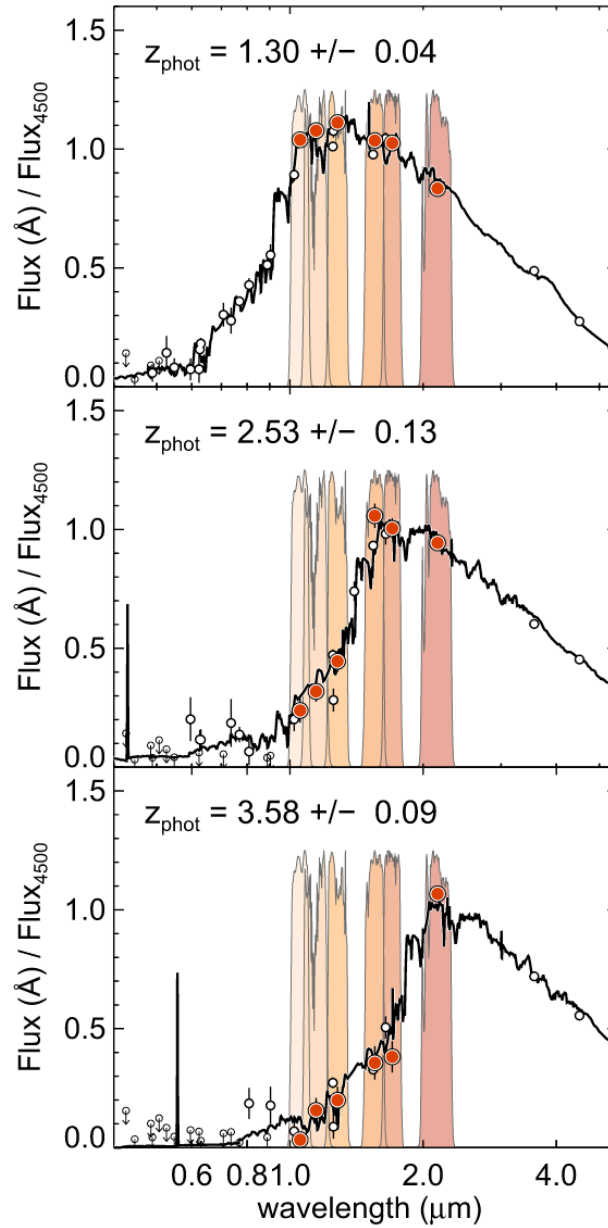


Figure 1.4: Demonstration of the utility of NIR medium bands from [Straatman et al. \(2016\)](#): each panel shows broadband photometry (white) and medium band photometry (red points) with best fit models (black) of quiescent galaxies at progressively higher redshifts from top to bottom. The medium band filter transmission curves are shown behind each SED, demonstrating the ability of the filter set to be used to probe quiescent galaxies out to $z \sim 4$ via measurement of the Balmer/4000 break.

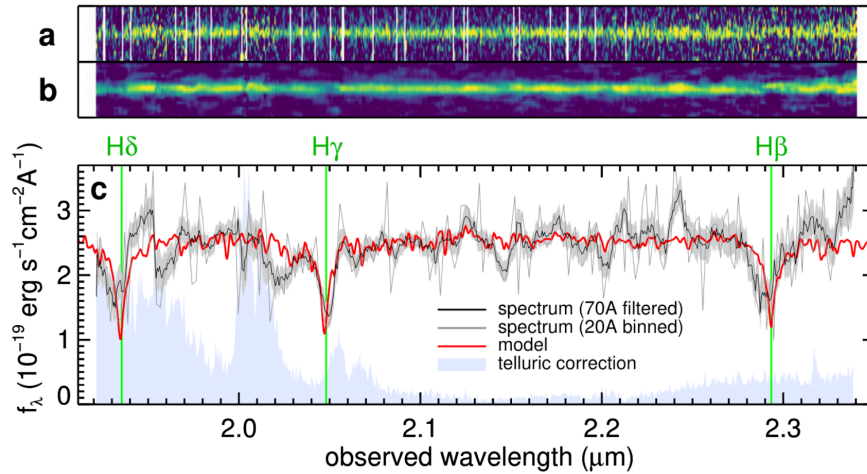


Figure 1.5: Top panel: original 2D MOSFIRE spectrum (a) with smoothing applied (b). Bottom panel: 1D spectrum (black) and best fit model (red) of a massive quiescent galaxy at $z_{spec} = 3.717$. The prominent Balmer absorption line features are marked in green ($H\delta, H\gamma, H\beta$). Figure taken from [Glazebrook et al. \(2017\)](#).

from the UV to the radio, as well as simulations. In this section, I will provide an overview of our knowledge of first quiescent galaxies (and how properties are measured) from studies in the literature conducted prior to this thesis.

1.2.3.1 NUMBER DENSITIES

Counting the number of galaxies as a function of cosmic time provides information on their evolution. This exercise has been carried out often over the past decades via the calculation of luminosity functions, mass functions and number densities, often splitting populations by their morphology, colour or star forming status (e.g [Muzzin et al., 2013](#)). This allows the charting of populations over cosmic time, in order to understand both individual populations, and also relationships between different types of galaxies. Furthermore, comparing the number densities of galaxies at fixed mass, or better, fixed velocity dispersion to avoid progenitor bias ([Stockmann et al., 2019](#)), can be used to infer the evolution from compact quiescent galaxies at $z \sim 2$ to the present day elliptical population. Comparing these numbers to simulations allows one to check whether the ingredients in simulations can reproduce galaxy populations observed with telescopes.

Below $z \sim 3$, the number densities of quiescent galaxies can generally be reproduced by

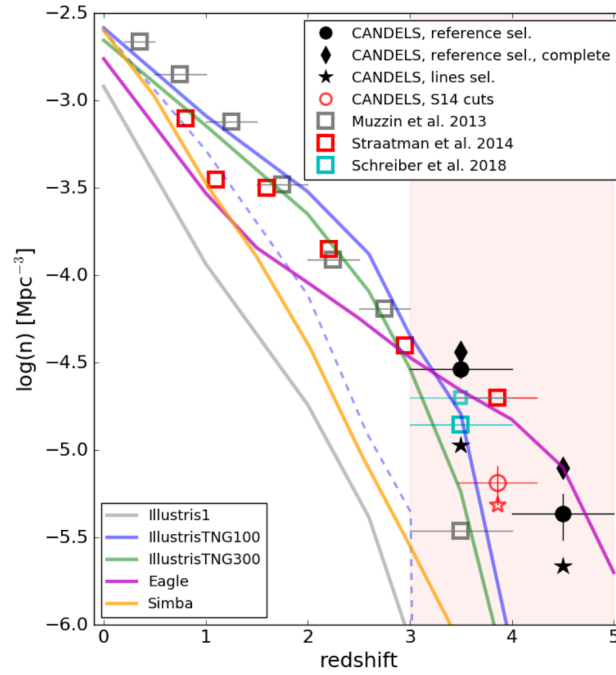


Figure 1.6: Number densities of massive quiescent galaxies in both observations and simulations from $z \sim 5$ to $z \sim 0$. Above $z > 3$, simulations struggle to reproduce the number densities of MQGs; only the EAGLE simulation manages this, but falls short at predicting numbers at $z < 3$. Figure taken from [Merlin et al. \(2019\)](#).

simulations. Above this redshift, multiple studies found an excess of these galaxies compared to simulations, implying that either the number densities of MQGs are overestimated, or that alternate quenching recipes are required in simulations to reproduce the observations (e.g. [Merlin et al., 2019](#); Figure 1.6). The combined results of many studies over the past decade found that between $z \sim 5$ and $z \sim 2$, the number density of these galaxies increases 100-fold, pointing towards a period of tremendous growth acceleration ([Ilbert et al., 2013](#); [Straatman et al., 2014](#); [Davidzon et al., 2017](#); [Schreiber et al., 2018](#); [Merlin et al., 2018, 2019](#); [Girelli et al., 2019](#); [Shahidi et al., 2020](#); [Carnall et al., 2020](#); [Santini et al., 2020](#); [Valentino et al., 2020](#)). This then raises questions - why this particular epoch? how are galaxies growing so fast, and why are these ones then ceasing their star formation so quickly? Having assessed the situation from a statistical perspective, we may now turn to studying their physical properties for clues.

1.2.3.2 STELLAR POPULATIONS

We turn first to the baryonic content of massive quiescent galaxies. Quiescent galaxies at all epochs can be characterised by a break in their spectral energy distribution at 4000 \AA . The break is a defining feature of quiescent galaxies at all cosmic epochs, and its strength is directly related to the age of the stellar populations. Like their low redshift counterparts (e.g. [Wild et al., 2009](#)), the $z > 3$ QG's exhibit Balmer / 4000 \AA breaks due to a combination of two main factors. Firstly, the stellar populations: a lack of radiation from young, hot stars of the O/B spectral class leads to a drop in the spectrum blue-wards of $\sim 4000 \text{ \AA}$, and the Balmer absorption line series caused by older, A type stars spans this wavelength regime. Secondly, the presence of elements heavier than Helium (referred to as metals) produces a cooling effect, as they absorb high energy photons, leading to a series of absorption lines at rest frame $\sim 3000 - 6000 \text{ \AA}$ (see top panel of Figure 1.7). The strength of the break is used as a direct measurement of the light-weighted age, and can be measured using the D_{4000} index, which is calculated by taking the ratio above and below the break ([Balogh et al., 1999](#); [Hamilton, 1985](#)) (see Equation 1.2). Emission above the break is predominantly from older,

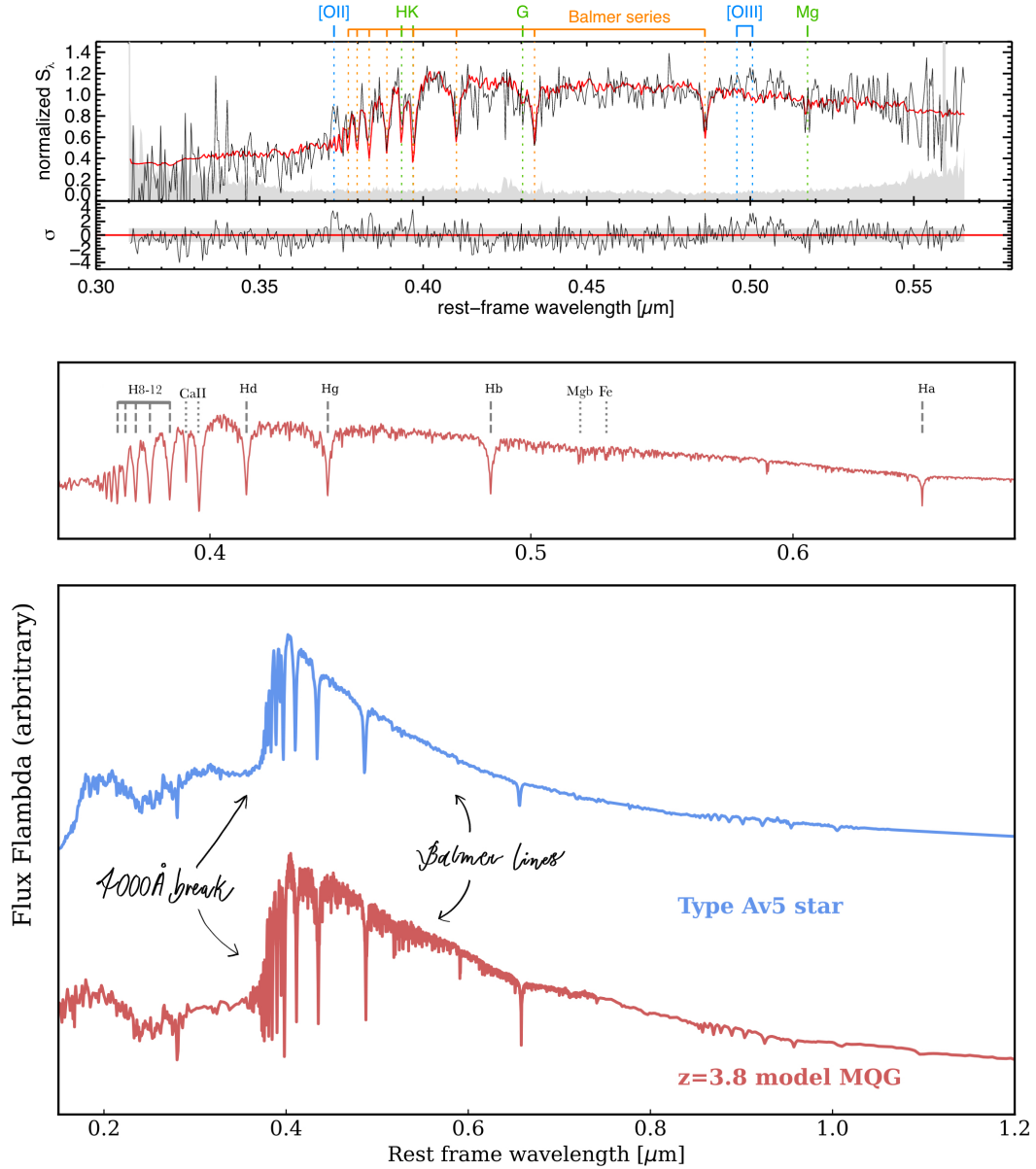


Figure 1.7: *Upper panel:* Rest frame optical stacked spectrum (black; residuals to best fit model (red) shown in sub panel below) of a sample of eight massive quiescent galaxies at $z > 3$ exhibiting the Balmer absorption line series (marked in orange) as well as metal absorption lines (green) and Oxygen emission lines (blue). (Schreiber et al., 2018).

Lower panel: A model spectrum of a type AV5 star, with main features of the Balmer break at 4000 and Hydrogen Balmer absorption line series μm (Pickles, 1998), and an example rest frame model spectrum of a $z \sim 3.8$ massive quiescent galaxy produced using eazy-py (Brammer, 2021; Brammer et al., 2008), which exhibits the same main features.

low mass stars which make up the bulk of the stellar population.

$$D4000 = \frac{\int_{4000}^{4100} f_{\lambda} d\lambda}{\int_{3850}^{3950} f_{\lambda} d\lambda} \quad (1.2)$$

Galaxies which have undergone recent quenching, either coeval or a recent burst, exhibit stronger Hydrogen Balmer absorption lines from as well as continuum emission blue-wards of the break. This is caused by A type stars of around $1 - 1.2M_{\odot}$ whose ages span a few hundred million years, indicating recent (< 800 Myr) star formation. Combined with a lack of ongoing star formation, this means the galaxy is classed as either post-star burst, or recently quenched (e.g French, 2021). This, as well as moderate Balmer breaks, is a defining feature of QGs at $z > 3$, which seem to exhibit these features both in spectroscopic data, as well as photometry, where best fit models are often those with spectra resembling an A star (see Figure 1.7). Forrest et al. (2022) measured the break strength of a sample of spectroscopically confirmed MQGs at $3 < z < 4$ and found them to have breaks much weaker than present day QGs (Figure 1.8). Furthermore, they found that these galaxies have much stronger H δ absorption lines, further cementing them as having undergone recent star formation, and therefore, recent quenching.

1.2.3.3 CHEMICAL ENRICHMENT

The chemical composition of galaxies is an important property because of its relationship to processes internal (star formation, metal production, gas recycling and feedback processes) and external (galaxy interactions and mergers, IGM, cluster physics). The metallicity of a galaxy is defined as the abundance of elements heavier than Helium, usually measured using indices calculated using certain emission or absorption lines. Commonly it is presented as an abundance ratio relative to solar, e.g. the logarithmic ratio of Iron to Hydrogen. This is easy for star forming galaxies at a range of redshifts due to their bright emission lines which are detectable in the UV/optical regime, but presents as a challenge for quiescent galaxies at intermediate redshifts ($z \sim 0.5 - 1$), due to their weak absorption lines, which are shifted into the near-infrared (Kriek et al., 2023). At $z > 2$, this becomes harder because the integration times required to measure required features amounts to many nights of telescope time for

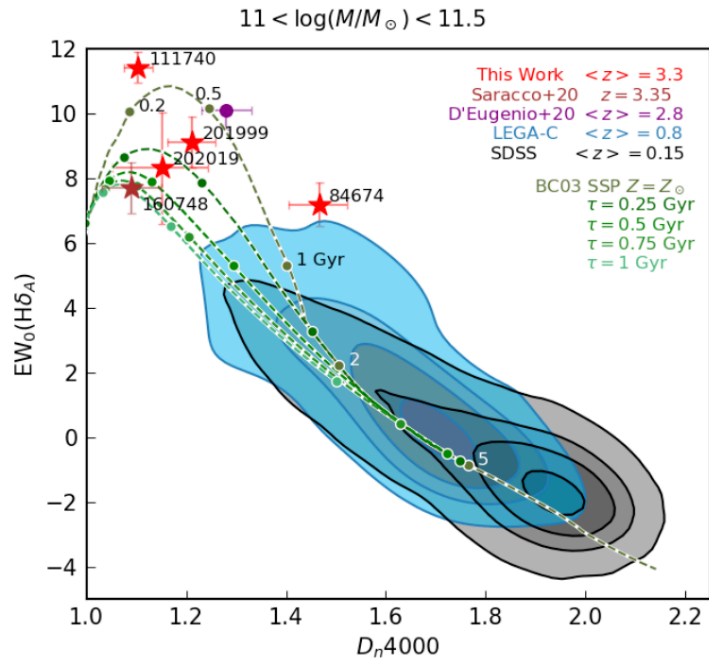


Figure 1.8: Equivalent width (EW) of the $H\delta$ absorption line vs D_n4000 , the strength of the 4000 \AA break for several samples of quiescent galaxies at $11 < \log(M_*/M_\odot) < 11.5$ (upper left) in context of the lower redshift galaxy population (blue and grey contours). The green tracks show the evolution expected for these galaxies as they age, in which they pass rapidly through the post-starburst phase with strong EW $H\delta$ and weaker breaks (i.e. lower D_n4000) before slowly evolving to the lower right over many billions of years, by which time the lower redshift MQG population exhibits weak or no EW $H\delta$ and strong ($D_n4000 \geq 2$) Balmer breaks (Forrest et al., 2022).

single galaxies (e.g. 29 hours for a quiescent galaxy spectrum at $z=2.186$ (Kriek et al., 2009; van Dokkum et al., 2009a)).

The state of the art in this area using pre-*JWST* instrumentation is the KECK Heavy Metals Survey, which aimed to chart the chemical properties of quiescent galaxies at $z \sim 1.4$ and $z \sim 2.1$, requiring 4-16 hours integration with KECK/MOSFIRE per band, for a total of 26 allocated nights of observing time for 21 galaxies (Kriek et al., 2023; Beverage et al., 2023). They found that quiescent galaxies at $1.4 < z < 2.1$ have sub-solar Fe abundances, whilst those at $z \sim 2.2$ have increased Mg abundances compared to those at $z \sim 1.4$. For the $z \sim 2.2$ population, the results imply rapid formation between $z \sim 2 - 8$. Overall, their results suggest that at progressively higher redshifts, massive quiescent galaxies are more metal poor than present day quiescent galaxies, form rapidly, and experience short star formation periods.

Given the instrumental challenges, it is not surprising that little is known about the chemical properties of massive quiescent galaxies at $z > 3$, and what is known is uncertain. Saracco et al., 2020 presented a 17 hour optical/NIR spectrum of a massive quiescent galaxy at $z = 3.352$ hosting an AGN, which was first shown in Marchesini et al., 2010 and was spectroscopically confirmed by Marsan et al., 2015. Although some weak metal absorption lines were present (MgB $\lambda 5175$, Fe $\lambda 5270$), investigations using models showed that features at shorter wavelengths such as the Balmer absorption lines, break strength and continuum shape were better indicators of metallicity for a young stellar population.

By comparing line indices to models at a range of metallicities and ages, they measured a super-solar light-weighted metallicity ($[Z/H] = 0.27_{-0.20}^{+0.03}$) and young light-weighted ($0.24_{-0.05}^{+0.11}$ Gyr), indicating rapid formation. This agreed with the mass-weighted and light-weighted values calculated using the full spectrum. This result was also supported by models with alpha enhancement, which results from alpha process that occurs in the final life stage of massive stars whereby a ladder of elements (C,O,Ne,Mg,Si,S and so on) are produced in successive Helium burning shells outward from the central Hydrogen to Helium burning shell. Holistically, the results suggest for at least this galaxy that it rapidly formed its stellar population from low metallicity pristine gas, the most massive of which then became core-collapse alpha process supernovae after living extremely short lives (10-50 Myr) (Nanayakkara et al., 2021; Kriek et al., 2016; Nomoto et al., 2006).

Looking forward, *JWST* will make it significantly easier to assess the chemical properties of the $z > 3$ MQG population. With high SNR (~ 100) medium resolution NIRSpec spectra, it will be possible to accurately measure ages, metallicities and alpha element abundances using a range of features such as the Balmer absorption lines, Fe and Mgb lines (Nanayakkara et al., 2021; see Figure 4 for details).

1.2.3.4 DUST CONTENT

Most QGs that have been studied at $z > 3$ exhibit little to no signs of dust (Straatman et al., 2014; Schreiber et al., 2018; Merlin et al., 2018, 2019; Girelli et al., 2019; Shahidi et al., 2020; Carnall et al., 2020; Santini et al., 2020; Valentino et al., 2020; Marsan et al., 2020; Forrest et al., 2020b). There are two explanations for this - first, that the dissipative processes that cause extreme compaction and quenching also lead to dust destruction, and hence the population is dust free (Akins et al., 2021). Or, that there exists a population of quenched galaxies with high dust obscuration that are not currently observable, and may be revealed with *JWST*. In fact, the few QGs in this epoch that have been studied spectroscopically are usually the brightest, and works such as (D'Eugenio et al., 2020b) suggest we may be biasing the conclusions of how the entire population is by studying these bright, dust-free post-starbursts.

1.2.3.5 STAR FORMATION HISTORIES

Both the sheer existence of MQGs at $z > 3$, and their tension with simulations, motivates the understanding of how they came to be. This can be explored by measuring their star formation histories (SFHs), which can be inferred from modelling spectra and their age sensitive features (the Balmer break and the Balmer absorption lines, for example). Attempts have also been made to infer ages, formation times and quenching times from photometric observations only. As a whole, the literature agrees that the $z > 3$ MQG population formed in rapid bursts and quenched equally as fast, with formation redshifts around $6 < z < 10$ and quenching redshifts around $3 < z < 6$ (Valentino et al., 2020; Forrest et al., 2020b; Schreiber et al., 2018; Merlin et al., 2019; Glazebrook et al., 2017). However, prior to *JWST*, the number of studies inferring SFHs from spectra are few, and results derived from photometry alone result in large uncertainties on formation times (~ 0.5 Gyr, Carnall et al. 2020).

Previous SFH studies at $z \sim 1$ have shown the importance of spectra for constraining SFH quantities such as burst mass and burst mass fraction; for just photometry, the prior is likely to be returned (Wild et al., 2020). Moreover, whilst it has been popular to assume parametric SFH shapes for quiescent galaxies (e.g. delayed tau models), the use of parametric SFHs has been shown to under-estimate early mass formation (Lower et al., 2020). The recent popularity of fully Bayesian non parametric star formation history fitting codes, such as Dense Basis (Iyer and Gawiser, 2017, Iyer et al., 2019) or Prospector (Leja et al., 2017), provides a viable solution to these problems: non parametric SFHs do not suffer from the same biases (Leja et al., 2019a) (alternatively, Alarcon et al., 2022 provide a more physically justified parametric star formation history fitting code). Furthermore, Suess et al. (2022b) show that SFHs of galaxies which have recently quenched their star formation cannot adequately be recovered by parametric methods, which can under-estimate post-starburst age by up to 200 Myr, but instead benefit from more flexible models. *JWST* will make it easier to study the assembly of MQGs at $z > 3$ with the possibility of probing the entire rest frame optical spectral range ($0.6 - 5.3\mu\text{m}$) with NIRSpec. Although, given the precision required to accurately measure ages even from spectra (Zibetti et al., 2024), it is likely that medium resolution spectra or higher, in tandem with non-parametric models, will be required to infer accurate star formation histories.

1.2.3.6 SIZES AND MORPHOLOGY

$z > 3$ QG's are highly compact, with rest frame optical sizes of $R_e \sim 0.5 - 1.5$ kpc (Forrest et al., 2020a; Esdaile et al., 2020; Saracco et al., 2020; Kubo et al., 2021). Straatman et al. (2015) found that the rest frame UV sizes of $z \sim 4$ QGs are $3\times$ smaller than similarly massive star forming galaxies at $z \sim 4$, and $6\times$ smaller than quiescent galaxies at $z \sim 0$. Similar conclusions were drawn from studying the rest frame optical sizes of 8 massive quiescent galaxies at $3 < z < 4$ (Forrest et al., 2020a) and 5 massive QGs at $z \sim 4$ (Kubo et al., 2021). This implies that the $z \sim 4$ massive QG population are the progenitors of present day elliptical galaxies, growing their size through dry minor mergers. Of course, this is not entirely certain, given that the population of quiescent galaxies in the universe has also grown (AKA “progenitor bias” (Stockmann et al., 2019; van Dokkum et al., 1999)).

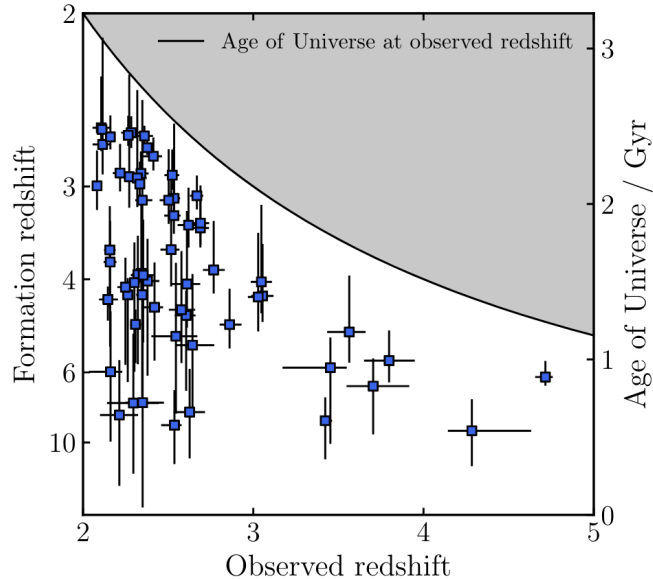


Figure 1.9: Formation and quenching times of massive quiescent galaxies at $2 < z < 5$, showing that quiescent galaxies in the early universe both formed and quenched rapidly. Figure taken from [Carnall et al. \(2020\)](#).

[Kubo et al. \(2021\)](#) commented that such high stellar masses and compact sizes implies a density comparable to MW Globular Clusters, which contain the galaxy’s oldest stars and are theorized to have formed quite early on from dense environments. It could then be postulated that dense pockets of gas could lead to the formation of $z \sim 4$ QGs. This would result in a top-heavy IMF whereby the first stellar populations are predominantly massive stars. [Esdaile et al. \(2020\)](#) attempted to test this using measurements of the dynamical mass, but found it was not possible to distinguish between different IMFs using kinematics measured from spectra taken using ground-based instruments (see also [Forrest et al. \(2022\)](#)).

1.2.3.7 ENVIRONMENT

The environment of quiescent galaxies at low redshift is important because interactions between galaxies in groups and clusters may contribute to the star formation rate. X-ray studies have charted a large number of massive lensing clusters ([Planck Collaboration et al., 2016](#)) where the brightest cluster galaxies are the most massive and also quiescent. Many studies both observational and simulations have shown gas can be removed via mergers (fast path),

or slower paths such as gas removal (see Section 1.2.3.8). Naturally, searches have extended to higher redshift, both statistically and of unique galaxies, in order to study the contribution of environment to the build up of quiescence. Searches have also been conducted for proto-clusters which contain only quiescent galaxies. If proto-clusters contain a statistically significant fraction of quiescent galaxies compared to the field, this indicates environmental quenching. Prior to *JWST*, these searches have been limited to searches for proto-clusters (the progenitors of modern day massive clusters) at or before cosmic noon, with a handful of studies pushing the frontier at $z = 2.5 \sim 3.5$. Such endeavours have been hampered by both the costliness of spectroscopic confirmation, as well as a dearth of well sampled photometry to statistically confirm quiescent status.

Despite this, investigations of the quiescent fraction in proto-clusters at $z \geq 3$ using photometry have found that there are significant densities of massive ($\log(M_*/M_\odot) \gtrsim 11$) quiescent galaxies in proto-clusters ($> 50\%$) compared to the field ($\sim 10 - 20\%$) (e.g. Shi et al., 2021; Ando et al., 2020; Kubo et al., 2013). Spectroscopy has also been used to confirm quiescent members in proto-clusters. Recently, McConachie et al. (2021) searched for over densities in photometric catalogs around spectroscopically confirmed massive galaxies at $z \sim 3.3$, finding two new proto-clusters with over 20 members each, both of which had quiescent members. They measured quiescent fractions of $\sim 70\%$ in these proto-clusters at $\log(M_*/M_\odot) > 10.85$ compared to $\sim 10 - 20\%$ in the field. Meanwhile, Kubo et al. (2021) confirmed the existence of a massive quiescent galaxy in the proto-cluster presented in their previous works with evidence for sudden recent quenching (~ 0.6 Gyr) and possible interaction with neighbours, indicating the quiescent galaxy underwent a merger. The combined imaging and spectroscopic capabilities of *JWST* will allow us to delve further into the environment of quiescent galaxies at $z \gtrsim 3$ and chart the contribution of environment to quenching.

1.2.3.8 GAS FRACTIONS AND AGN

Not only is a continual supply of gas required to fuel ongoing star formation, but also environmental conditions that promote accretion and cooling of gas so it can collapse to form stars. Following Figure 1.10 (adapted from Man and Belli (2018)), there are five situations

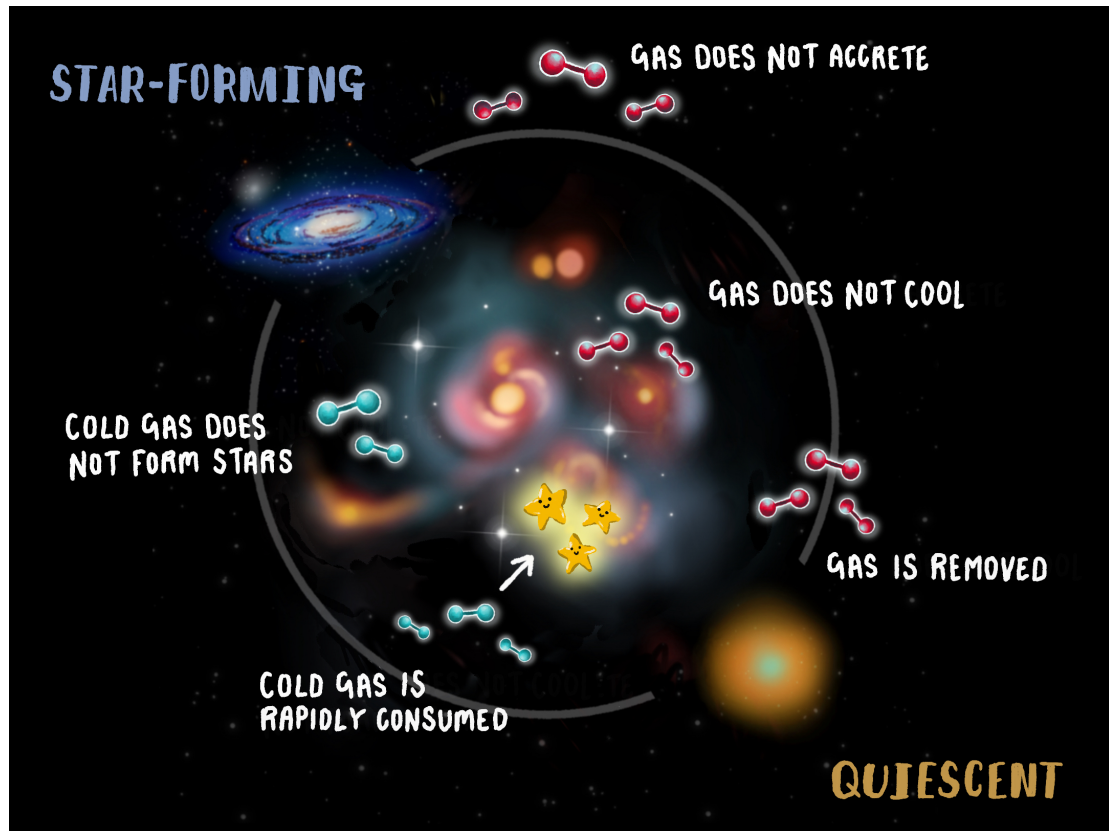


Figure 1.10: Infographic showing the five main reasons why a galaxy is not actively forming stars. From top middle, clockwise: Gas is present in the halo but does not accrete, gas is present in the galaxy but does not cool, gas is removed, gas has been consumed to form stars, or cold gas is present and cannot collapse to form stars. I created this infographic as an artistic adaptation of Figure 1 in (Man and Belli, 2018).

where gas may be present in, or nearby a galaxy, but only one of them leads to star formation. If the halo has a gas reservoir, the flow of gas into the galaxy can be reduced or stopped completely - so no supply of new fuel (Daddi et al., 2022; Feldmann et al., 2016). Perhaps the accretion of gas from the halo to the galaxy is successful, but the conditions prevent cooling, because the gas is supported thermally (AGN heating (e.g. Di Matteo et al., 2005)), or virial shock heating (Rees and Ostriker, 1977) or kinetically (stellar and AGN winds (Ostriker et al., 2010; Pellegrini and Renzini, 1991)). Even if the gas meets the requirements for collapse - i.e., meets the Jeans mass criterion and is sufficiently cold that collapse could occur, there may be some non thermal support preventing this collapse, such as support from magnetic fields, bars, or AGN (D'Eugenio et al., 2023; Khoperskov et al., 2018; Tabatabaei et al., 2018; Alatalo et al., 2014; Martig et al., 2009). Observations also show that gas can be removed from the galaxy through secular processes (AGN jets, winds, (e.g. Di Matteo et al., 2005)), as well as environmental processes (gas donation or sharing with group or cluster members; see Mao et al. 2022 for a recent overview). Even if gas is rapidly consumed to form stars, possibly triggered by mergers, disc instabilities or AGN (Zolotov et al., 2015; Ishibashi and Fabian, 2012; Mihos and Hernquist, 1996), there still needs to be some maintenance mode for quenching, such that the galaxy remains quiescent over time.

Two observables that can therefore be used to help understand quenching in high redshift galaxies are the gas fractions, and AGN prevalence. The molecular gas fraction ($f_{gas} = M_{gas}/(M_* + M_{gas})$) combined with the gas depletion timescale ($t_{dep} = M_{gas}/SFR$) are useful quantities to measure, because they can be used to infer cause of quenching (Suzuki et al., 2022). The gas mass can be measured directly via observations of molecular carbon via CO lines (e.g. Belli et al., 2021; Spilker et al., 2018), and then converting to molecular hydrogen, or indirectly via measuring the dust continuum emission and converting to a gas mass by assuming a dust to gas mass ratio (e.g. Whitaker et al., 2021; Magdis et al., 2021). Both of these methods have been used to investigate gas fractions at $z < 3$, but only a few studies have pushed to higher redshift. At $z < 3$, massive quiescent galaxies appear to have little cold gas ($f_{gas} < 0.1$), which depletes in less than a Gyr, implying strong feedback mechanisms, or rapid gas consumption (e.g. Whitaker et al., 2021).

There are only a few studies that have measured the gas fractions of $z > 3$ QGs. Suzuki et al. (2022) constrained upper limits on $f_{gas} = 10 - 20\%$ for a sample of four gravitation-

ally lensed galaxies using CI ($^3P_1-^3P_0$, $\nu_{\text{rest}} = 492.16$ GHz), supporting the scenario of gas expulsion or consumption rather than high star formation rate efficiency. Using the CII $158\mu\text{m}$ emission line, which for fixed integration time is able to go deeper than both CO and continuum dust emission, D'Eugenio et al. (2023) measured a range of gas fractions ($f_{\text{gas}} < 3.2\%$, $< 21\%$, $< 72\%$) for three $z > 3$ quiescent galaxies. The deep upper limit of $f_{\text{gas}} < 3.2\%$ for one galaxy, as well as suppressed star formation in its neighbour (Schreiber et al., 2020), implies the presence of an AGN to heat gas to such temperatures, possibly via kinetic feedback (e.g Ostriker et al., 2010) that the galaxy remains quenched despite inhabiting a massive dark matter halo (Shuntov et al., 2022) where cold gas accretion could occur (Daddi et al., 2022).

This therefore explains the interest in finding AGN in MQGs at $z > 3$, because AGN could be responsible for quenching, or maintenance of quiescence. Indeed, AGN have been noted in the $z > 3$ quiescent population, using both photometry and spectroscopy. Single galaxy studies have revealed post-starburst galaxies “caught in the act” of quenching, that also happen to harbour AGN (Schreiber et al., 2020; Saracco et al., 2020; Marsan et al., 2017, 2015), detected using the presence of emission line ratios indicating strong ionization (Díaz-Santos et al., 2017; Baldwin et al., 1981). Furthermore, stacking (as well as single galaxy) analyses have been used to study the prevalence of AGN in quiescent galaxies using X-ray and radio data (Ito et al., 2022; Marsan et al., 2020, 2017, 2015). However, studying AGN and its correlation with quenching in high redshift quiescent galaxies is limited by the availability and cost of obtaining rest-frame optical spectra. The rest-frame optical and NIR emission lines can be used to trace the ionization conditions in the galaxy (see Kewley et al. (2019) for a review), which prior to *JWST*, was only possible for the brightest galaxies. With the launch of *JWST*, it is finally possible to begin measuring quantities to deduce AGN presence in a systematic and statistical way, for larger samples of galaxies.

1.3 THE PROGENITORS OF THE FIRST QUIESCENT GALAXIES

1.3.1 THE COSMIC STAR FORMATION RATE DENSITY

Referring again to Figure 1.10, it is only in the rare case that the stars align and none of these impediments are present to gas collapse, that virial instability may lead to cloud collapse and

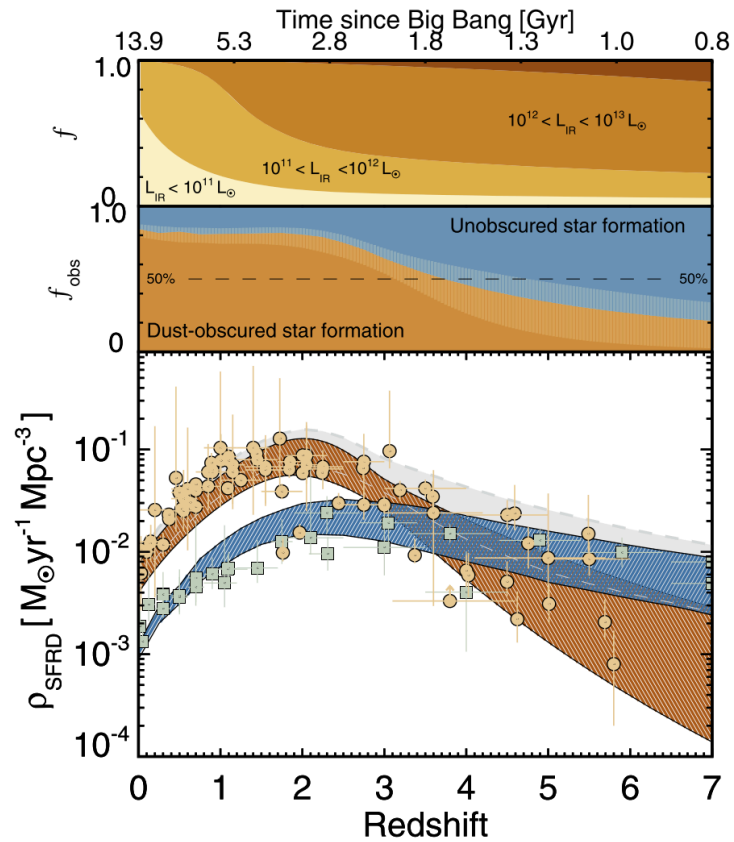


Figure 1.11: *Top panel:* Relative contribution of galaxies at different infrared luminosities to the total star formation rate density since $z \sim 7$. *Middle panel:* Fractional contribution to the cSFRD from obscured (ochre) vs unobscured (blue) star formation. *Lower panel:* Obscured vs unobscured contribution to cosmic star formation rate density since $z \sim 7$ from independent IR/sub-mm (orange points) and UV (blue points) surveys. Figure taken from [Zavala et al. \(2021\)](#).

star formation (Stahler and Palla, 2004). How rare, exactly, is a function of the availability of hydrogen gas, and the conditions of the galactic environment. Consequently, the cosmic star formation rate density (cSFRD) of the universe has evolved over time (Madau and Dickinson, 2014). Prior to the launch of *JWST*, measurements of the cSFRD show that star formation began some 600 million years after the Big Bang, accelerating until peaking at $z \sim 2$, which is nicknamed “cosmic noon”, for this reason. In the 11 billion years since, the star formation rate density has fallen, with the average SFR of Milky-Way mass galaxies at present day forming ~ 1 solar mass per year compared to galaxies at $z \sim 2$ with SFRs of $\sim 100 M_{\odot} \text{yr}^{-1}$. Somewhere along the way, the progenitors of the massive quiescent galaxy population were born, lived mysteriously fast and short lives, and became the quenched populations that first began to pop up around $z \sim 4$.

Whilst the contribution of unobscured star formation to this evolution has been probed well into to the first billion years with UV/optical telescopes, it has only been possible to study the contribution of obscured SF out to $z \sim 6$. As shown in Figure 1.11, Zavala et al. (2021) and Casey et al. (2021) showed that there is a significant contribution to the cosmic star formation rate density by highly dust obscured star forming galaxies, and confirmed earlier findings that 50% of all stellar light in the universe is obscured by dust (Driver et al., 2008). This is important because the progenitors of quiescent galaxies may well be dust obscured.

1.3.2 THE POSSIBLE PROGENITORS EXPLORED THUS FAR

It is still unknown what the mysterious progenitor population is, but studying different populations of galaxies at $z > 4$ holds the key to answering this question. In particular, there are several requirements that this population must meet: firstly, the number densities must be enough to sufficiently match the number densities of massive quiescent galaxies that begin to appear at $z \sim 4$, via either observed number densities, or by inferring them assuming a particular duty cycle (e.g Valentino et al., 2020). Secondly, they must have either already accumulated a sufficient body of stellar mass, or if not, they need to have high enough gas reservoirs and star formation rates such that they would become sufficiently massive in good time. Finally, they need to match their progenitors morphological properties, on average. The majority of quiescent galaxies at and beyond cosmic noon are compact (Kubo et al.,

2021; Marsan et al., 2020; Stockmann et al., 2019), and given that galaxies do not shrink in size, the progenitors must already be small (Williams et al., 2017). This may be due to compaction via gas funelling to the center, forming a massive core (Zolotov et al., 2015; Cimatti et al., 2008).

There is now mounting evidence that the progenitors of the $z \sim 3$ MQG population are dust obscured star forming galaxies at $z > 4$; I will briefly discuss the possible candidates here. Given the apparent burstiness of star formation histories of MQGs (e.g. Schreiber et al., 2018), it has been suggested that highly star forming galaxies known as starbursts, which shine at sub-mm and longer wavelengths (see Casey et al., 2014 for a review), could be possible progenitors (Spilker et al., 2018; Toft et al., 2014; Cimatti et al., 2008). These galaxies have extreme SFRs of up to thousands of solar masses per year required to match the star formation histories of some MQGs. However, sub-mm galaxies lack the number densities (Jin et al., 2018; Michałowski et al., 2017; Ivison et al., 2016) and gas reservoirs (Spilker et al., 2018; Aravena et al., 2016) to become the quiescent population by $z \sim 3$ (Williams et al., 2019). Furthermore, Valentino et al. (2020) selected both quiescent galaxies and sub-mm galaxies in a suite of simulations and found that whilst the majority of sub-mm galaxies at $z = 4 - 5$ that can be detected in shallow surveys quench by $z \sim 3$, not all $z \sim 3$ quiescent galaxies evolve from sub-mm galaxies. Furthermore, some of these quiescent galaxies instead originated from more normal star forming galaxies that emit sub-mm light only detectable by the deepest surveys at the time.

A promising new population of galaxies has emerged in the past few years. Bright in the near-infrared and beyond, but faint or invisible in the optical wavelengths, these galaxies have been dubbed “*HST*-dark” amongst other names, to signify their invisibility in the optical (Sun et al., 2021; Talia et al., 2021; Wang et al., 2019; Williams et al., 2019; Wang et al., 2016; Caputi et al., 2015). Evidence for the connection to $z > 3$ MQGs is already promising, given that the large scale clustering properties (in particular, the correlation function) of the sample presented in Wang et al. (2019) matches the quiescent sample presented in Schreiber et al. (2018) (see Fig. 4. in Wang et al. (2019)). Other attempts to connect the populations have been encouraging. Long et al. (2022) constructed a numerical model to calculate the number densities of dusty star forming galaxies out to $z \sim 5$, and forward modelled these galaxies to evolve into the quiescent population at $z \sim 3$. They successfully produced a

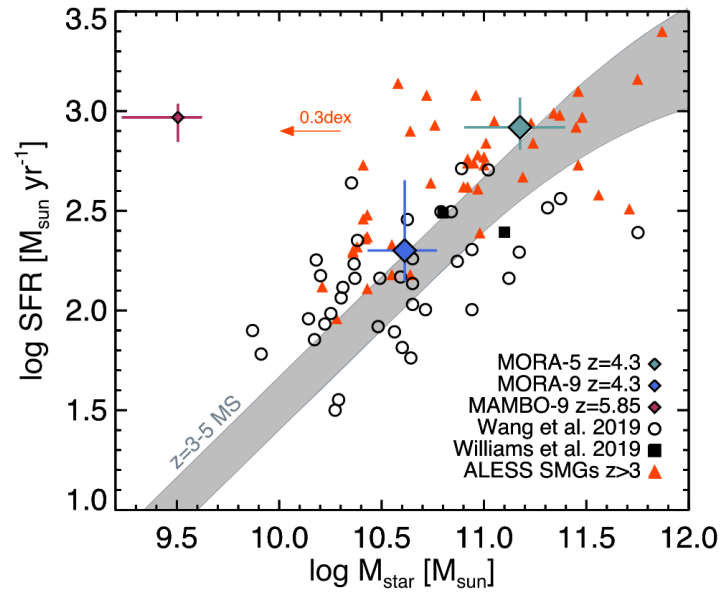


Figure 1.12: Dusty star forming galaxies on the [Schreiber et al. \(2015\)](#) star forming main sequence at $3 < z < 5$. Optically invisible galaxies from [Manning et al. \(2022\)](#) are shown as blue, teal and maroon points, $3MM-1$ from [Williams et al. \(2019\)](#) is shown as the black circle, the sample from [Wang et al. \(2019\)](#) is shown as open black circles. Figure taken from [Manning et al. \(2022\)](#).

model whereby high redshift DSFGs are the ancestors of the $z \sim 3$ population, some of which could be the mysterious optically invisible population. Single galaxy studies have also revealed encouraging links: Williams et al. (2019) reported the discovery of a massive dusty star forming galaxy at $z = 5.5$ that met the requirements to become quiescent by $z \sim 3$, including an inferred space density of these types of galaxies to reproduce the population as a whole. Manning et al. (2022) reported similar findings and conclusions for two galaxies at $z \sim 5$ (see Figure 1.12). Both of these studies relied on the detection of these galaxies at sub-mm wavelengths using ALMA, but lacked coverage in the rest-frame optical to confirm their stellar masses with precision (stellar mass estimates vary by 0.2-0.4 dex). In order to make a robust connection between these dusty main sequence galaxies at $z \sim 4 - 5$ and the MQG population at $z > 3$, observations using both *JWST*/NIRCam in conjunction with sub-mm facilities will be crucial.

1.4 THE AIMS OF THIS THESIS

The aforementioned studies expanded the knowledge of the $z > 3$ red galaxy population considerably, but also opened Pandora's box. The existence of multiple massive galaxy populations in the early universe provokes questions not only about their formation and evolution, but also about how we can best study these galaxies, starting with their selection. The discovery of quiescent galaxies with bluer colours motivates us to return to the drawing board about how we can best design a quiescent galaxy selection criterion. This is especially pertinent in the age of *JWST*, with an ever-growing body of space based imaging of unprecedented quality (Rigby et al., 2022) ready to be searched for rare massive galaxies. Another issue to address is our physical understanding of this galaxy population: advancements in simulations have been fast in the past few years, but do they now have the recipes and ingredients needed to reproduce the observed number densities of MQGs at $z > 3$? Finally, the existence of optically dark galaxies detected at NIR and longer wavelengths can finally be explored with *JWST*, allowing connections to be drawn between massive dusty galaxies and quiescent galaxies at $z > 3$. In particular, are these galaxies the possible progenitors of the high redshift MQG population?

Questions addressed in this thesis

1. Is there a better way to select massive quiescent galaxies at $z > 3$ from imaging than the current methods?
2. What are the number densities of massive quiescent galaxies at $z > 3$?
3. Can simulations reproduce the observed number densities of these galaxies?
4. Can we find old and low mass quiescent galaxies at $z > 3$ with *JWST*?
5. What are the properties of the “NIR-dark” population?
6. Could these optically invisible galaxies be the progenitors of $z > 3$ quiescent galaxies?

This thesis sets out to address these questions in the following way. In Chapter 2, I present a new colour selection method specifically tailored for finding quiescent and quenching galaxies at $z > 3$, tested on the latest COSMOS2020 catalog (Weaver et al., 2021), and compare number densities with those produced from contemporary simulations. In Chapter 3, I demonstrate the selection method in action on a compilation of *JWST* imaging from public fields taken in the first three months, highlighting the ability of the method not only to find $z > 4$ MQG candidates, but also low mass MQG candidates too. I further apply the selection method to the CANUCS *JWST* GTO survey (Willott et al., 2022), where I select MQG candidates for spectroscopic follow-up across five lensing clusters and present a preliminary sample of spectroscopy of MQGs at cosmic noon. Looking to the ancestors of $z > 3$ MQGs, I present the joint spectro-photometric analysis of an optically dark, compact main sequence star forming galaxy at $z = 3.65$ in Chapter 4, and discuss this galaxy’s future as a compact quiescent galaxy by $z > 2$. Finally, in Chapter 5 I conclude the work that this thesis has contributed to the (rapidly growing) body of literature, and briefly discuss some avenues for future work.

A NEW DEFINITION OF QUIESCENT

“When I use a word,’ Humpty Dumpty said, in rather a scornful tone, ‘it means just what I choose it to mean – neither more nor less.’

‘The question is,’ said Alice, ‘whether you can make words mean so many different things.’”

Lewis Carroll

ALICE THROUGH THE LOOKING
GLASS



This chapter contains the following article:

“COSMOS2020: Exploring the dawn of quenching for massive galaxies at $3 < z < 5$ with a new colour selection method”

Published in the Astronomical Journal (AJ): Volume 165, Number 6, Article 248, 18 pp. (June 2023)

Authors: Katriona M. L. Gould, Gabriel Brammer, Francesco Valentino, Katherine E. Whitaker, John. R. Weaver, Claudia del P. Lagos, Francesca Rizzo, Maximilien Franco, Bau-Ching Hsieh, Olivier Ilbert, Shuowen Jin, Georgios Magdis, Henry J. McCracken, Bahram Mobasher, Marko Shuntov, Charles L. Steinhardt, Victoria Strait, & Sune Toft.

ABSTRACT

We select and characterise a sample of massive ($\log(M_*/M_\odot) > 10.6$) quiescent galaxies (QGs) at $3 < z < 5$ in the latest COSMOS₂₀₂₀ catalogue. QGs are selected using a new rest-frame colour selection method, based on their probability of belonging to the quiescent group defined by a Gaussian Mixture Model (GMM) trained on rest-frame colours ($NUV - U, U - V, V - J$) of similarly massive galaxies at $2 < z < 3$. We calculate the quiescent probability threshold above which a galaxy is classified as quiescent using simulated galaxies from the SHARK semi-analytical model. We find that at $z \geq 3$ in SHARK, the GMM/ $NUVU - VJ$ method out-performs classical rest-frame UVJ selection and is a viable alternative. We select galaxies as quiescent based on their probability in COSMOS₂₀₂₀ at $3 < z < 5$, and compare the selected sample to both UVJ and $NUVrJ$ selected samples. We find that although the new selection matches UVJ and $NUVrJ$ in number, the overlap between colour selections is only $\sim 50 - 80\%$, implying that rest-frame colour commonly used at lower redshifts selections cannot be equivalently used at $z > 3$. We compute median rest-frame SEDs for our sample and find the median quiescent galaxy at $3 < z < 5$ has a strong Balmer/4000 Å break, and residual NUV flux indicating recent quenching. We find the number densities of the entire quiescent population (including post-starbursts) more than doubles from $3.5 \pm 2.2 \times 10^{-6} \text{ Mpc}^{-3}$ at $4 < z < 5$ to $1.4 \pm 0.4 \times 10^{-5} \text{ Mpc}^{-3}$ at $3 < z < 4$, confirming that the onset of massive galaxy quenching occurs as early as $3 < z < 5$.

2.1 INTRODUCTION

In the past few years it has become evident that there exists an extraordinary population of massive galaxies which have already ceased their star formation and become quiescent when the universe was just 2 billion years old ($z \geq 3$). The first hints of this population were candidates selected from optical/near-infrared (NIR) surveys such as in the GOODS-South field (Fontana et al., 2009), and later the Newfirm Medium-Band Survey (NMBS, Whitaker et al., 2011; Marchesini et al., 2010) and the FourStar Galaxy Evolution Survey (ZFOURGE, Straatman et al., 2014; Spitler et al., 2014). Targets were selected using various indicators, either on the basis of their specific star formation rate (sSFR) or rest-frame colours. Although

these candidates were tentative then, the recent influx of spectroscopically confirmed massive galaxies at $z > 3$ puts aside any doubt that these galaxies were already passive, and rapid evolution in the first few billion years caused the onset of the dawn of quenching. There are several examples of single galaxies (e.g., Marsan et al., 2015; Forrest et al., 2020a; Valentino et al., 2020; Saracco et al., 2020; Carnall et al., 2023), as well as full samples (Marsan et al., 2017; Schreiber et al., 2018; Forrest et al., 2020b; D’Eugenio et al., 2020a; McConachie et al., 2021; Nanayakkara et al., 2022), that have been spectroscopically confirmed as both massive (usually $\log(M_*/M_\odot) \gtrsim 10$) and quiescent ($\log(\text{sSFR}) \text{ yr}^{-1} \lesssim -9.5$), as well as a number of studies which selected and analysed massive quenched galaxies in large photometric data sets (Merlin et al., 2018; Girelli et al., 2019; Merlin et al., 2019; Guarnieri et al., 2019; Cecchi et al., 2019; Carnall et al., 2020; Shahidi et al., 2020; Santini et al., 2020; Stevans et al., 2021; Ito et al., 2022).

Thanks to the named studies, we now know about the properties of massive quiescent galaxies (QGs) at $z > 3$. These galaxies exhibit significant Balmer/4000 Å breaks indicative of ages between 100 Myr and ~ 1 Gyr, although the ages can be quite uncertain (e.g. Schreiber et al., 2018; Carnall et al., 2020; Forrest et al., 2020a; D’Eugenio et al., 2020a; Nanayakkara et al., 2022; Carnall et al., 2023). A few spectroscopically confirmed galaxies exhibit weak flux blue-wards of the break (a “blue bump”), indicating a stellar population comprising predominantly A-type stars, and therefore likely recent quenching (< 1 Gyr). This is distinct from the UV-upturn observed in local quenched galaxies, which seems to be due to emission from post main sequence stars such as Horizontal Branch (HB) or Asymptotic Giant Branch (ABG) stars (Greggio and Renzini, 1990; Yi et al., 1997; see Dantas et al., 2020 for a more recent overview). The age and mass of such early QGs implies a rapid formation period and recent quenching, much like post-starburst, or E/K+A galaxies observed at $z < 3$ (e.g. Dressler and Gunn, 1983; Goto, 2005; Wild et al., 2009; Ichikawa and Matsuoka, 2017; Wu et al., 2018; Chen et al., 2019; Wild et al., 2020; Wu et al., 2020; Wilkinson et al., 2021; see French, 2021 for a review of post-starburst galaxies). An onset of rapid quenching at $z \sim 4 - 6$ as suggested by the previous works would result in a fairly young massive quiescent population at $z \sim 3$ which had recently undergone an intense period of star formation.

Recently quenched QGs at $z > 3$ also seem to be fairly dust-free (Schreiber et al., 2018;

Kubo et al., 2021). This could be because dust is being destroyed in the post-starburst phase (e.g., Akins et al., 2021) and our selections for QGs at $z > 3$ are dominated by PSBs and relatively dust-free QGs, or because our selections and surveys are blind to dusty QGs at $z > 3$ (D'Eugenio et al., 2020a). The upcoming investigations into galaxies appearing in NIR observations with no optical flux (*HST*-dark galaxies) with the *James Webb Space Telescope* (*JWST*) will hopefully address this pertinent debate (Wang et al., 2019; Long et al., 2022; Barrufet et al., 2021, 2023).

Quiescent populations are commonly selected using rest-frame colour-colour diagrams, with an increasing number of studies further analyzing the correlations of physical properties relative to the sample location within these diagrams (e.g. Whitaker et al., 2012, Belli et al., 2019). The four most popular in use are the *UVJ* selection criteria (Wuyts et al., 2008, Williams et al., 2009), or variations thereof (e.g. Whitaker et al., 2012), *BzK* (Daddi et al., 2004a), and *NUVrK* or *NUVrJ* (Arnouts et al., 2013, Ilbert et al., 2013, Davidzon et al., 2017, Noirod et al., 2022). Rest-frame colour-colour diagrams have been favoured for their quick and easy use with large photometric data sets; galaxies tend to occupy distinct parameter spaces within these diagrams, making selection for quiescent populations moderately straightforward. Critically, the use of two colours allows for the separation of quiescent from star forming galaxies, with the $U - V$ or $NUV - r$ colour separating star forming galaxies from quiescent, and the $r - J$ or $V - J$ colour separating red dusty galaxies from those that are quiescent.

These selections were originally designed to separate galaxy populations at low redshift, but as newer data has emerged demonstrating that the bi-modality in populations clearly extends to higher redshift (e.g. Whitaker et al., 2011; Muzzin et al., 2013; Ilbert et al., 2013; Straatman et al., 2014), the selections and variations thereof are now often adopted at $z > 2$ (e.g., Whitaker et al., 2012; Straatman et al., 2014; Hwang et al., 2021; Suzuki et al., 2022; Ji and Giavalisco, 2022). In sum, rest-frame colour colour diagrams are ideal to select quiescent populations as they are computationally cheap, straight-forward. They can also be model dependent, but this depends on the way in which the rest-frame colours are calculated.

However, the application of rest-frame colour diagram selection boxes to higher redshift samples (in particular, $z > 3$) should be cautioned. Several studies (Belli et al., 2019;

D'Eugenio et al., 2020a) find that 10 – 30% of UVJ selected QGs at higher redshift are either low redshift interlopers or dusty star-forming galaxies. Lustig et al. (2022) show that this contamination occurs more frequently in the UVJ area populated by older QGs, at the top right corner of the quiescent selection box. Moreover, despite sSFR decreasing with redder $U - V$ and bluer $V - J$ colours, Leja et al. (2019c) demonstrate that a UVJ selection cannot differentiate between moderate and low specific star formation rates. Such a distinction in specific star formation rate is critical at high redshift where recently quenched galaxies, or those in the process of quenching, are more prevalent. Furthermore, Antwi-Danso et al., 2022 show that the extrapolation of rest frame J (which can be common at $z > 3$) leads to galaxies being wrongly classified.

Whilst rest-frame colour diagram selections remain useful, particularly for large ground based surveys, the current methods explored above are less reliable at $z > 3$ for several reasons. Firstly, many studies clearly show that $3 < z < 5$ is the epoch where QGs first appear (e.g. Marsan et al., 2020, Valentino et al., 2020), and so the galaxy population is *not yet bimodal*. Instead, as Marsan et al., 2020 find, massive galaxies in this epoch exhibit a wide spectrum of properties, with varying amounts of dust and star formation, as well as some harbouring an Active Galactic Nucleus (AGN) (see also Marsan et al., 2015, Marsan et al., 2017 and Ito et al., 2022). It therefore does not make sense anymore to apply a colour colour cut that was designed to separate galaxies in a bimodal universe when that bi-modality does not yet exist. Secondly, it takes on the order of \sim Gyrs for galaxies to evolve and become truly red (without dust), which implies that we would not expect to find the upper edge of the UVJ quiescent box highly populated at $z > 3$. Instead, it is more likely that galaxies found in this parameter space are instead dusty star forming galaxies that have scattered in over the $V - J < 1.5$ line. This is seen clearly in Lustig et al., 2022, who compare observations of QGs at $z \sim 3$ with several simulations. They find that the contamination of the UVJ quiescent box at $z \sim 2.7$ is most significant at reddest edge of the box, near the $V - J < 1.5$ line. To remedy this, they suggest changing the $V - J$ constraint from $V - J < 1.5$ to $V - J < 1$, which effectively cuts the selection area in half.

The third reason is that galaxies in the high redshift universe are faint, and thus even state-of-the-art ground-based surveys will have fairly large photometric errors for most galaxies

which propagate to uncertainties a factor of two larger in colours (see Appendix C in [Whitaker et al., 2010](#)). This is further antagonised by the fact that surveys such as *COSMOS* are limited to the resolution of the now decommissioned *Infra Red Array Camera (IRAC)* on the *Spitzer Space Telescope*, which, besides having a large point spread function (PSF), also barely probes the Balmer break at $z > 4$ for QGs. The use of rest-frame $V - J$ colour as a separator between dusty star forming galaxies and red QGs becomes highly uncertain at $z > 5$, where rest-frame J moves beyond $\sim 9\mu\text{m}$ (*IRAC/Channel 4*) and must therefore be extrapolated. For surveys limited to $\sim 5\mu\text{m}$ (*Channel 2*), this becomes $z > 3$. All of these reasons together imply that simply drawing a dividing line over a non bimodal, noisy population will result in both incomplete and quite significantly contaminated samples.

Given the arguments against them, one might reconsider the usefulness of rest-frame colour-colour selections when there are multiple options for spectral energy distribution (SED) fitting tools to calculate sSFRs which can be used to select for QGs. Whilst this alternative is often used (e.g. [Carnall et al., 2020](#); [Ito et al., 2022](#); [Carnall et al., 2022](#)), more complex methods may require careful tuning, time, and sometimes vast computing resources. Finally, this still does not solve the problem because these approaches require a sSFR cut or otherwise to select QGs in a population where the lines between star forming and quiescent are blurred. Whilst these methods offer opportunities to study the statistical properties and their stellar assembly, the selection of QGs should still be possible with simpler methods. It is therefore important that we take care in optimizing the rest-frame colour-colour selections as they are fast and can be easily applied to different surveys irrespective of the filters used, therefore serving as crucial tools for the selection of candidates for spectroscopic follow up with instruments such as *JWST*. This is something that the community has already begun to explore, e.g. [Leja et al., 2019c](#) (efficient selection of QGs at $z < 1$) and [Antwi-Danso et al., 2022](#) (efficient selection of QGs at $z > 3$ using synthetic *ugi* filters).

In this paper, we present a new rest-frame colour colour diagram and selection method specifically designed to find and select high confidence massive QGs at $z \sim 3$ and beyond. Using the latest *COSMOS* catalogue, *COSMOS₂₀₂₀*, we explore the utility of this new selection technique. In Sections 2.2 and 2.3, we describe the data and a modified *COSMOS₂₀₂₀* catalogue made specific to this study. In Section 2.4 we describe the selection of a robust sam-

ple of massive galaxies at $3 < z < 5$. In Section 2.4, we introduce the new colour selection method. In Section 4.4, we present this new selection applied to COSMOS2020 and the main results. Finally, we summarise our conclusions and outlook in Section 2.9. For all calculations we use the WMAP9 flat LambdaCDM cosmology (Hinshaw et al., 2013) with $H_0 = 69.3 \text{ km s}^{-1} \text{ Mpc}^{-1}$, $\Omega_m = 0.307$. All magnitudes are in the AB system defined by Oke and Gunn, 1983 as $m_{AB} = -2.5 \log_{10} \left(\frac{f_\nu}{3631 J} \right)$.

2.2 DATA

2.2.1 COSMOS2020

The Cosmological Evolution Survey (*COSMOS*) is currently the deepest NIR wide-field multi-wavelength survey that provides data over 2 square degrees of the sky (Scoville et al., 2007, Koekemoer et al., 2007). The latest version of the *COSMOS* photometric catalogue, *COSMOS2020* (Weaver et al., 2021), improves on previous version (Laigle et al., 2016) in many ways. Firstly, with the improved depth (~ 1 mag) and uniformity in the u-band data, taken from the CFHT Large Area U band Deep Survey2 (CLAUDS) (Sawicki et al., 2019); secondly, with the addition of ultra-deep optical data from *Hyper-Suprime Cam* (*HSC*; Miyazaki et al., 2018; Aihara et al., 2018); thirdly, the fourth data release of *Ultra-VISTA* (DR4) (McCracken et al., 2012; Moneti et al., 2019), effectively 1 mag deeper in K_s over the entire field; and finally, the inclusion of all *Spitzer/IRAC* data ever taken in the *COSMOS* field (Weaver et al., 2021; Moneti et al., 2022). *COSMOS2020* contains four catalogues, combining two source extraction methods and two photometric redshift codes. The Classic catalogue is produced using classical aperture based photometry method using *SOURCE EXTRACTOR* (Bertin and Arnouts, 1996), whilst *THE FARMER* catalogue is produced using a profile fitting photometry method (Weaver et al., 2023), which is a wrapper written for the source profile fitting code *THE TRACTOR* (Lang et al., 2016). *THE FARMER* has a distinct advantage over classical photometry methods due to its ability to correctly model and de-blend overlapping sources. This is particularly beneficial in deep fields where source crowding and overlapping is common. Both photometry catalogs are fit with two different photometric redshift codes (Le Phare, Arnouts and Ilbert 2011, and eazy-py (Brammer et al., 2008; Brammer, 2021). Weaver et al., 2021 show that *THE FARMER* performs equivalently to *SOURCE EXTRACTOR*

and excels at $i < 24$, independent of the redshift code used. For this analysis we use THE FARMER photometric catalogue combined with redshift and physical parameter estimation using `eazy-py`.

Although THE FARMER photometry and its associated uncertainties are suitable for general use SED fitting, [Weaver et al. \(2021\)](#) noted that it is likely the photometric uncertainties are underestimated. To test this, we ran the custom code `GOLFIR` ([Kokorev et al., 2022](#)) on a small subset of the COSMOS2020 *IRAC* images. `GOLFIR` uses a prior based on the highest available resolution imaging to model the flux in the *IRAC* photometry. Overall, the agreement of both photometric catalogs is high, however the *IRAC* errors derived with THE FARMER are smaller by a factor of ~ 5 . This is similar to the approach and conclusions in [Valentino et al. \(2022\)](#). At $z > 3$, the *IRAC* photometry plays a crucial role in the identification of massive galaxies. This is due to the fact that the light emitted from the bulk of the stellar mass is measured at observed frame $\lambda_{obs} > 2.5\mu\text{m}$, which is measured predominantly by the *IRAC* bands. Although the depths probed by the first two *IRAC* bands Channels 1 and 2 are comparable to those in *Ultra-VISTA* bands *JHK_s* (~ 25.5 mag, 3σ), *IRAC* channels 3 and 4 are shallower by ~ 3 mags. For massive QGs at $z > 3$, this may result in the *IRAC* bands approaching the detection limit of the survey. For this reason and the investigations explained above, for this work we conservatively boost the *IRAC* photometric errors by a factor of 5 and refit the COSMOS2020 FARMER photometry with `eazy-py` (see Section 2.3). As with [Weaver et al. \(2021\)](#), we do not include the *Subaru Suprime-Cam* broad band photometry or the *GALEX FUV* and *NUV* photometry, due to their shallow depth and broad PSF, respectively. In total, we use 27 photometric bands for SED fitting, probing observed frame $\sim 0.3 - 8\mu\text{m}$.

2.2.2 3D-HST

In Section 2.3, we will introduce the latest python implementation of `eazy`, `eazy-py` and its newer features. To demonstrate their validity, in particular the computation of physical properties such as stellar mass and star formation rate, we use an observational catalog with similar properties as COSMOS2020 to benchmark the performance. We consider the PROSPECTOR version of the 3D-HST catalog from ([Leja et al., 2019b](#)). The 3D-HST survey ([Skelton et al.,](#)

2014) is a 248-orbit Hubble Treasury program completed in 2015, providing *WFC3* and *ACS* spectroscopy for galaxies in 5 extra-galactic deep fields, including *COSMOS*, covering 900 square arc-minutes (199 square arc-minutes in *COSMOS*). The catalog includes photometry in up to 44 bands in *COSMOS* covering 0.3–8 μ m in the observed frame, with the inclusion of *Spitzer MIPS* 24 μ m photometry from Whitaker et al. (2014). The version that we considered contains a representative sub sample of 58,461 galaxies from the 3*D-HST* survey (roughly 33%) which span the observed star formation rate density and mass density at $0.5 < z < 2.5$. These galaxies are fit with the Bayesian SED fitting code PROSPECTOR (Leja et al., 2017; Johnson et al., 2020). PROSPECTOR uses galaxy models generated using PYTHON-FSPS (Conroy et al., 2009; Conroy and Gunn, 2010), non parametric star formation histories, variable stellar metallicities and a two-component dust attenuation model, under the assumption of energy balance. For this paper, we cross match our catalog and the 3*D-HST* PROSPECTOR catalog using a 0."6 matching radius, resulting in 8964 galaxies in common.

2.2.3 SIMULATED DATA

To test the robustness of our quiescent galaxy selection method, we use simulated galaxies from the SHARK semi-analytical model (SAM, Lagos et al., 2018). SHARK models the formation and evolution of galaxies following many physical processes, including star formation, chemical enrichment, gas cooling, feedback from stars and active galactic nuclei, among others. Critically for this work, SHARK includes a two-phase dust model for light attenuation that is based on radiative transfer results from hydrodynamical simulations (Trayford et al., 2020). This model was combined with the stellar population synthesis model of Bruzual and Charlot (2003), adopting a Chabrier (2003) initial mass function, and a model for re-emission in the IR in Lagos et al. (2019). SHARK does this using the generative SED mode of the PROSPECT SED code of Robotham et al. (2020). The predicted SED of each galaxy is then convolved with a series of filters to get their broad-band photometry. Lagos et al. (2019) showed that SHARK is very successful in reproducing the FUV-to-FIR emission of galaxies in observations at a wide redshift range, including luminosity functions, number counts and cosmic SED emission. Lagos et al. (2020) used this model to show that the con-

tamination fraction of dusty, star-forming galaxies (those with $870\ \mu\text{m}$ flux > 0.1 mJy) in the UVJ diagram increases with increasing redshift, reaching $\approx 47\%$ at $z = 3$, showing that the commonly adopted UVJ colour selection could be improved to reduce contamination. Here, we use a lightcone presented in [Lagos et al. \(2019\)](#) (see their Section 5) that has an area of $\approx 107\ \text{deg}^2$, and includes all galaxies in the redshift range $0 \leq z \leq 8$ that have a dummy magnitude, computed assuming a stellar mass-to-light ratio of $1, < 32$. The method used to construct lightcones is described in [Chauhan et al. \(2019\)](#).

2.3 SED FITTING WITH EAZY-PY

2.3.1 EAZY-PY

In this study, we use photometric redshifts, stellar masses, star formation rates and rest-frame colours derived with `eazy-py`* ([Brammer, 2021](#)). Here we detail this process, including an updated description and presentation of the `eazy-py` code. `eazy-py` is a pythonic photometric redshift code adapted from the original `eazy` code written in C+ ([Brammer et al., 2008](#)). `eazy-py` estimates redshifts by fitting non-negative linear combinations of galaxy templates to broad-band photometry to produce a best fit model. The flexibility of the code means that in theory, any kind of template can be used, e.g., quasar or AGN templates. The templates used in this paper are comprised of 13 stellar population synthesis templates from FSPS ([Conroy et al., 2009](#); [Conroy and Gunn, 2010](#)) spanning a wide range in age, dust attenuation and log-normal star formation histories. This template set is designed to encompass the expected distribution of galaxies in UVJ color space at $0 < z < 3$, and in theory beyond. We use a Chabrier IMF ([Chabrier, 2003](#)) and the [Kriek and Conroy, 2013](#) two component dust attenuation law, which allows for a variable UV slope (dust index $\delta = -0.1$, $RV = 4.05$).

The latest version of `eazy-py` (version 0.5.2) has been adapted to be a general use SED fitting code, providing estimates of physical parameters such as stellar mass, star formation rate, and dust attenuation. These physical properties are assigned to each template and “propagate through” the fitting process with the same non-negative linear combination coefficients that return the best-fit SED model. This results in star formation histories that are non-negative

*<https://github.com/gbrammer/eazy-py>

linear combinations of a number of basis star formation histories, and therefore the star formation history of a galaxy best-fit model will mimic non-parametric methods such as those used in [Pacifci et al., 2016](#); [Iyer et al., 2019](#); [Leja et al., 2019a](#) and other works. This means that `eazy-py` is more similar to codes that implement non-parametric star formation histories than it is to traditional SED fitting codes, and can account for the mass that is often missed as a result of using parametric star formation histories ([Lower et al., 2020](#)). We demonstrate this in Section 2.3.1.2. Errors on physical parameters are calculated by drawing 100 fits from the best fit template error function and using the 16th and 84th percentiles as the extremes of the 1σ errors. It should be noted that the physical parameter errors are not marginalised over the redshift error, therefore it is likely that the errors from `eazy-py` are underestimated. Figure 2.1 shows a comparison of photometric and spectroscopic redshifts for all galaxies at $0 < z < 6$ in our catalog. We find similar outlier fractions and bias for both star forming and QGs compared to the official COSMOS2020 release ([Weaver et al., 2021](#)).

2.3.1.1 REST-FRAME FLUX DENSITIES

The rest-frame fluxes are calculated based on the approach of [Brammer et al. \(2011\)](#), which uses the best fit model as a guide to interpolate between the observed photometry. This interpolation itself is weighted by the photometric errors, and therefore the rest-frame flux errors reflect those of the photometry. This means that the rest-frame fluxes are almost entirely derived from the photometry with only partial guidance from the best fit template. The results also account for the filter shapes and relative depths, which is advantageous particularly for multi-instrument photometric catalogs. This essentially ensures a “model-free” approach, which is crucial for our method, as rest frame colours are used in the selection process, and should ideally reflect the *observed* universe and not our models. For a full description of calculation of the rest-frame fluxes we refer the reader to Appendix A.1. The rest-frame filters used in this paper are the GALEX *NUV* band ($\lambda = 2800\text{\AA}$) ([Martin et al., 2005](#)), the re-calibrated *U* and *V* filters by [Maíz Apellániz \(2006\)](#), and 2MASS *J* band ([Skrutskie et al., 2006](#)).

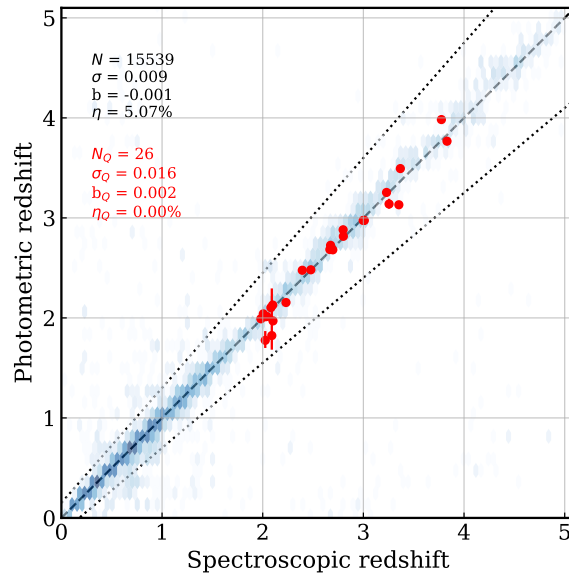


Figure 2.1: Photometric redshift vs spectroscopic redshift for all galaxies at $0 < z < 5$ in the combined UVISTA and HSC area with K_s SNR > 5 . Red points are spectroscopically confirmed QGs at $z > 2$ from Stockmann et al., 2019, D’Eugenio et al., 2020a, Schreiber et al., 2018, Forrest et al., 2020b, Valentino et al., 2020.

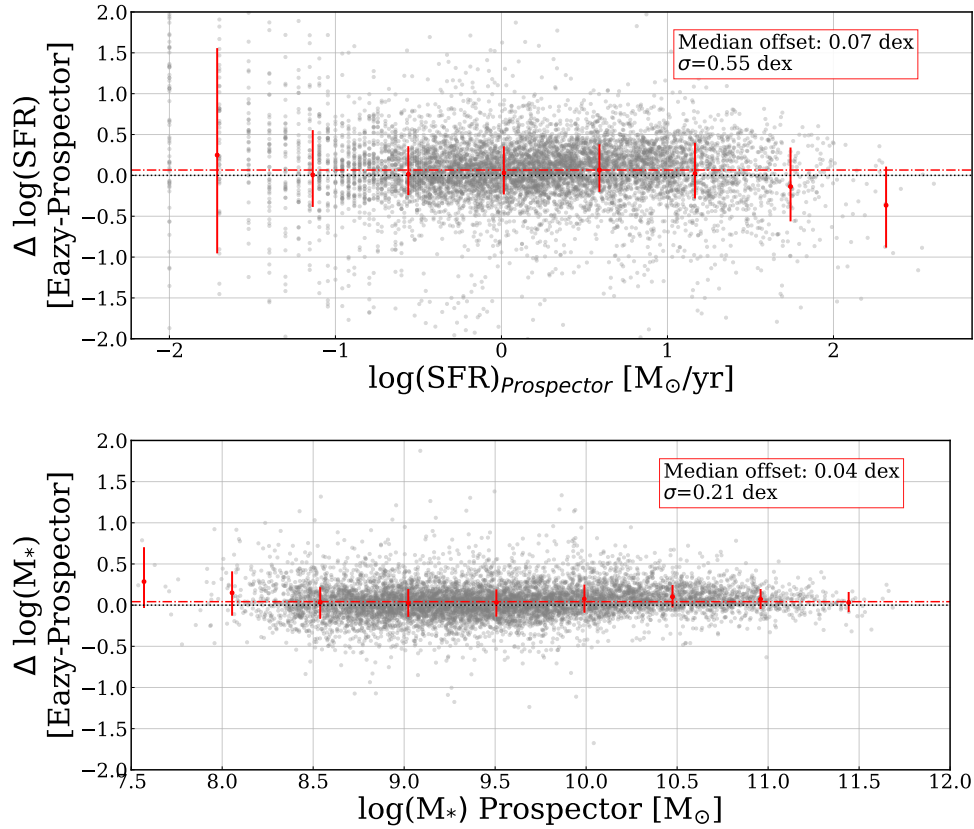


Figure 2.2: *Upper:* $\Delta \log(\text{SFR})$ (EAZY–PROSPECTOR) as a function of PROSPECTOR SFR for 8134 galaxies at $0.5 < z < 3.0$ matched to our catalogue with that of the 3D-HST survey in COSMOS. The median $\Delta \log(\text{SFR})$ is 0.07 dex (shown as red dashed line) and the scatter is 0.55 dex. The binned median offset and the associated 16th and 84th percentiles are shown as red points with error bars. *Lower:* $\Delta \log(\text{M}_{*})$ (EAZY–PROSPECTOR) as a function of PROSPECTOR stellar mass for the same sample. The median $\Delta \log(\text{M}_{*})$ is 0.04 dex and the scatter is 0.21 dex. The binned mean offset and the associated 16th and 84th percentiles are shown as red points with error bars.

2.3.1.2 STELLAR MASSES AND STAR FORMATION RATES

In this section we explore the stellar masses (M_*) and star formation rates (SFRs) derived with eazy-py. We note that it has been shown that star formation rates derived from broadband photometric SED fitting assuming parametric star formation histories can underestimate the SFR of a galaxy by several orders of magnitude (Lower et al., 2020). Sherman et al. (2020), who used eazy-py with default FSPS templates using a variety of realistic SFHs (rising, bursty), find that M_* are overestimated on average by 0.085 dex, and SFRs are underestimated on average by ~ 0.46 dex. As we fit with a different, newer set of templates using log-normal star formation histories, we cannot assume the derived masses and SFRs have from the same offsets.

To benchmark the eazy-py M_* and SFRs in this study, we use the 3D-HST catalog described in Section 2.2.2. From the PROSPECTOR 3D-HST catalog we use redshift (which are a compilation of spectroscopic redshifts, grism redshifts and redshifts derived using eazy), stellar masses and star formation rates, which are averaged over the past 100 million years. Here, we use the masses and star formation rates derived with Prospector as the “ground truth”. We select all galaxies with a photometric redshift agreeing within 15% of $\Delta z/(1+z)$ to the PROSPECTOR redshift, which results in 8134 galaxies spanning $0.5 < z < 3.0$. We then compute the difference (in dex) between our parameters (SFR, M_*) and the PROSPECTOR parameters. Due to differences in method, the K_s band magnitudes for COSMOS2020 are marginally brighter (~ 0.09 dex) than those in the Skelton et al., 2014 catalog that was used in Leja et al., 2019a. To facilitate a fairer comparison, we scale the Prospector masses and star formation rates accordingly. In practice, this results in a very small difference. We show both the SFR and mass comparisons in Figure 2.2 as a function of the estimates derived with PROSPECTOR. We calculate the median offset and scatter, and find that there is excellent agreement between the two catalogs, with only a minor overestimation of 0.04 dex for masses and 0.07 dex for SFRs by eazy-py with a scatter of 0.21 dex for mass and 0.55 dex for SFRs. The difference between the results of this investigation compared to Sherman et al., 2020 is notably that of the SFRs - whilst they find an underestimation of ~ 0.5 dex, we report a slight over-estimation. This is likely due to the different template sets used. In conclusion, given the agreement and no catastrophic bias in stellar masses or SFRs derived with eazy-py

we deem them acceptable for use.

2.4 SELECTING A ROBUST SAMPLE OF MASSIVE GALAXIES

We begin by selecting all objects within the area covered by both *HSC* and *Ultra-VISTA* (i.e., FLAG COMBINED = 0, area $\approx 1.27^{\circ 2}$), classified as galaxies according to the star galaxy separation criteria (see Appendix A.2), and with $K_s < 25.6$ mag, which is the 3σ limiting magnitude. From these, we select all galaxies with photometric redshifts $3.0 < z_{\text{phot}} < 5.0$, with a constraint that the lower 16% of the photometric redshift probability distribution, $p(z)$, should be contained above $z = 3$, and the upper 84% below $z = 5$. If a spectroscopic redshift is available in the catalogue we require $3 < z_{\text{spec}} < 5$. At $4.5 < z < 5$, the rest-frame *J* band is covered by IRAC channels 3 and 4, which means that it is still observationally constrained and not extrapolated (see Appendix A.3). This is vital to ensure the robustness of the sample (Antwi-Danso et al., 2022). For this reason, we do not extend beyond $z = 5.0$ in our sample selection. We next make a cut on stellar masses, $10.6 < \log(M_*/M_\odot) < 12$, which is the knee of the mass function at this redshift range and well above the stellar mass completeness (Weaver et al., 2021). However, it is important to note that at $4.5 < z < 5$, the Balmer/4000 break moves through the K_s band, which is the reddest band in the chi-mean *izYJHK*, detection image used in the photometric modelling. Therefore, our selection is likely not sensitive to older quiescent galaxies at this redshift range, if they exist. To our sample, we then add the following requirements to ensure the confidence in our massive galaxy sample is high. We choose to conservatively exclude anything with a reduced χ^2 equal to $\chi^2/(N_{\text{filt}})$ greater than 10. We also require K_s SNR > 5 . In summary, we require:

- Inside combined HSC/UVISTA area
- Classified as galaxy
- K_s MAG < 25.6
- $3.0 < z_{\text{phot}} < 5.0$ (or $3.0 < z_{\text{spec}} < 5.0$ if available)
- $z_{\text{phot},16\%} > 3.0$ and $z_{\text{phot},84\%} < 5.0$

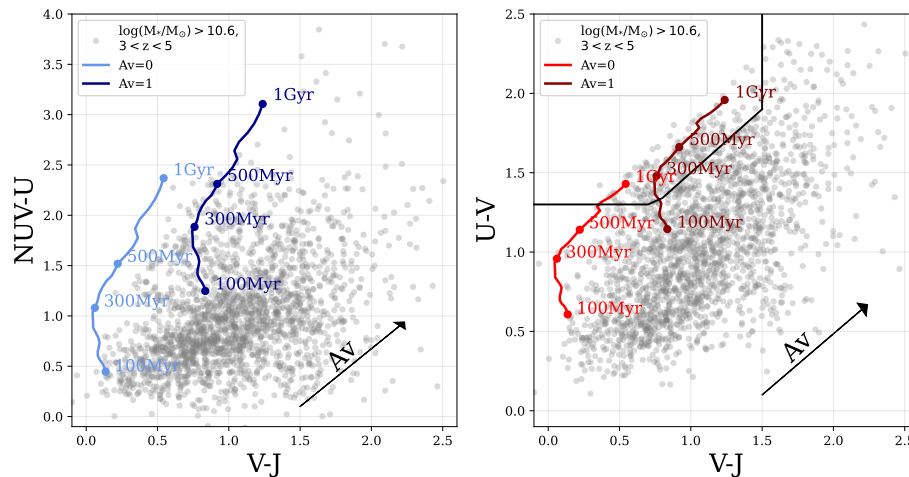


Figure 2.3: *Left:* $NUV - U$, $V - J$ colours of our massive ($10.6 < \log(M_*/M_\odot) < 12$) galaxy sample at $3 < z < 5$ (grey) and evolution tracks for an SSP with $A_V = 0$ (blue line on the left of the figure) and $A_V = 1$ (dark blue line) and Chabrier IMF aged to 1 Gyr. The dust vector representing the movement of a galaxy in this space by attenuation of $A_V = 1$ is shown by the arrow at the bottom right. *Right:* Same but for UVJ with the quiescent box defined by Whitaker et al. (2012) (defined as $U - V > 0.8 \times (V - J) + 0.7$, $U - V > 1.3$ and $V - J < 1.5$).

- $10.6 < \log(M_*/M_\odot) < 12$
- Reduced $\chi^2 < 10$
- $K_s \text{ SNR} > 5$

In total, this selection results in 1568 galaxies with a median redshift of $z_{phot} = 3.55$ and median stellar mass of $\log(M_*/M_\odot) = 10.94$. In addition to this, we select a sample at $2 < z < 3$ in a similar manner with a lower mass cut of $10 < \log(M_*/M_\odot) < 12$, in order to fit the Gaussian Mixture Model described in the following section. This gives a fitting sample of 12985 galaxies at $2 < z < 3$ with a median photometric redshift of $z_{phot} = 2.46$ and median stellar mass of $\log(M_*/M_\odot) = 10.52$.

2.4.1 INTRODUCING THE GMM

We present here a new colour selection designed to make finding QGs at $z > 3$ easier. Our new colour selection method combines the $NUV - U$, $U - V$ and $V - J$ colours, using the filters defined in Section 2.3.1.1. This colour selection method is *similar* to both UVJ and $NUVrJ$, with two major differences. The first is that four bands (three colours) are used instead of three, and the second is that the separation itself is not defined by a traditional “box” but rather using simple machine learning methods. Both are introduced to make the separation of QGs from (dusty) star forming more pronounced, and furthermore allow an easier separation between recently quenched and older QGs. The $U - V$ and $V - J$ colours are included to separate quiescent galaxies from star forming, as originally designed. The $NUV - U$ colour is added to measure the light emitted from recent star formation in the form of A-type stars and is similar to $NUV - r$, except that it probes a shorter baseline, specifically the flux directly blue-wards of the 4000 Å/Balmer break. Previous works have suggested $NUV - U$ is a viable indicator for time since quenching, for example [Schawinski et al. \(2014\)](#). Similarly, [Phillipps et al. \(2020\)](#) use $NUV - u$ as a means to remove passive galaxies with some residual star formation from a sample of truly passive galaxies. The reason for the use of four bands / three colours is twofold: firstly, the increase in dimensions allows us to extract more information whilst still only requiring 4 data points. Whilst this is similar to dimensionality reduction, it has the advantage of using information that is likely already available or easy to compute, and does not require imposing a high signal to noise cut to the data. Secondly, $NUV - U$ does not have a co-dependent variable with $V - J$, which allows for the spread of colours in $NUV - U/V - J$ to become more obvious, making it easier to both separate the quenched population from star forming, as well as explore the properties of galaxies within the quenched population with different amounts of recent star formation. This is particularly relevant at $z > 3$, where the fraction of PSB galaxies is high (e.g. [D’Eugenio et al., 2020b](#) and [Lustig et al., 2020](#) report a PSB fraction of 60-70% for photometrically selected QGs at $\log(M_*/M_\odot) > 11$). If we consider the 2D projection ($NUV - U, V - J$), it is clear that the star forming and quiescent populations separate more clearly due to the divergent alignment of the dust vector relative to the evolution tracks (see Figure 2.3). As an example, we plot the massive $3 < z < 5$ sample in this colour space with tracks showing the colour

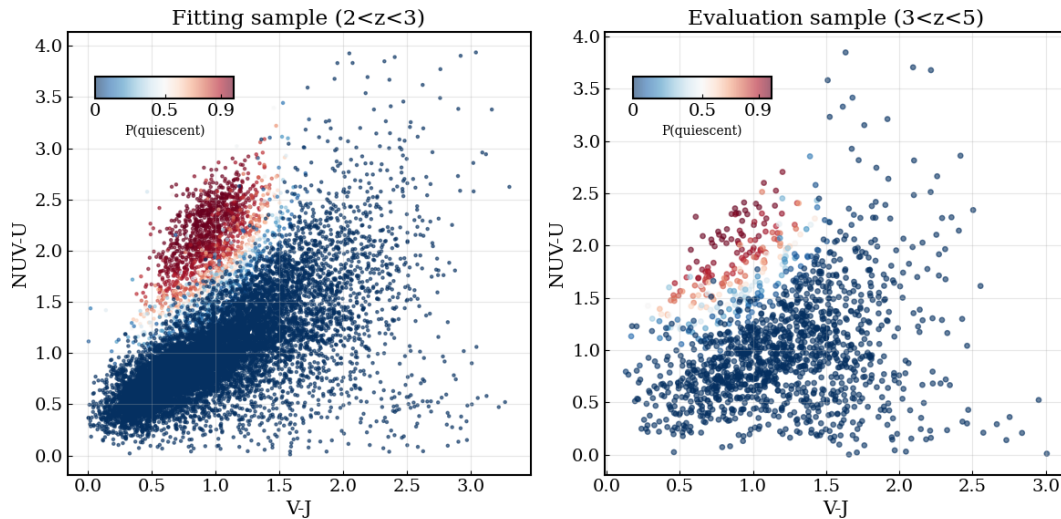


Figure 2.4: *Left:* $NUV - VJ$ diagram with the $2 < z < 3$ fitting sample coloured by $p(q)_{50\%}$, which is the median of the boot-strapped quiescent probability distribution based on the Gaussian Mixture Model. *Right:* Same but for the $3 < z < 5$ sample.

evolution of a single stellar population aged to 1 Gyr at both $A_V = 0$ and $A_V = 1$ generated using the Python-FSPS package. Both tracks move directly up through the quiescent area as they evolve over time. The lower portion of this area preferentially selects quenching or post-starburst galaxies, whilst the upper half encompasses older QGs. This age trend has been observed in the UVJ diagram (e.g. [Whitaker et al., 2012](#), [Whitaker et al., 2013](#), [Belli et al., 2019](#), [Carnall et al., 2019](#)), thus it is not entirely surprising that it appears in this colour diagram too – and in fact more pronounced due to the addition of the $NUV - U$ colour. We note that the direction of the age tracks diverge from the direction of the dust vector for $(NUV - U, V - J)$, resulting in red dusty star forming galaxies pushed downwards and to the left relative to old, red QGs, whereas for UVJ they follow the same direction, resulting in old, red QGs populating the same space as red dusty star forming galaxies.

2.4.2 DEFINING THE SEPARATOR

Most selections in rest-frame colour diagrams have been made by drawing a box empirically. We choose to separate QGs from star forming by using a Gaussian Mixture Model (GMM).

This is a probabilistic model that operates under the assumption that the data can be fit by a finite number of Gaussian curves, for which the parameters are not known. GMMs have already been employed successfully in multiple research areas in astrophysics, including to select and explore various galaxy populations such as quiescent and PSB galaxies (e.g. [Black and Evrard, 2022](#); [Ardila et al., 2018](#)). Probabilistic selection of QGs at $z > 3$ has also been carried out with great success by [Shahidi et al. \(2020\)](#) and [Santini et al. \(2020\)](#). We use the Gaussian Mixture Model package supplied by Scikit-learn ([Pedregosa et al., 2011](#)). Briefly, the GMM algorithm uses expectation-maximisation (EM), which is an iterative process used for classification when there are no “correct” labels (as is our case). EM works by choosing random components and iterating towards the best fit by computing the likelihood of each data point being drawn from the current model, and then adjusting the parameters to maximise that likelihood. In this approach, we choose to use all three colours: $NUV - U$, $U - V$ and $V - J$. We fit the model using the $2 < z < 3$ sample, which is first cleaned by requiring all colours have $0 < colour < 4$. To ascertain the optimal number of components, we fit multiple times using 1 – 10 Gaussian components and calculate the Bayesian Information Criterion (BIC) for each number of components, which is defined as

$$BIC = k \ln(n) - 2 \ln(L_{\max}) \quad (2.1)$$

where n is the number of model parameters, k is the number of data points fit and L_{\max} is the maximum likelihood of the fit. The BIC discriminates between models by penalising the number of parameters, which avoids over-fitting. We randomly select 60% of the sample, fit and compute the BIC for 1 – 10 components, and repeat 1000 times. We find that a 6–component model is best fit in $\sim 75\%$ of the repeated fits and adopt this as our baseline model. The GMM returns for each galaxy a likelihood of belonging to each group, which we convert to a probability. We could simply use this value to decide what to classify as quiescent, however, this does not account for the errors in a galaxy’s colours. To assign each galaxy a probability of belonging to the quiescent group, which is identified by eye as the component in the quiescent area of UVJ space, we instead take the following approach, inspired by [Hwang et al. \(2021\)](#). Each galaxy has rest frame fluxes in the NUV , U , V and J bands, and associated errors. Assuming these are Gaussian distributed, we boot-strap the fluxes 1000

times and compute the $NUV - U$, $V - J$ and $U - V$ colours for each set of rest frame fluxes. Each set of 1000 colours is then fit with the GMM and the percentiles (5, 16, 50, 84, 95) of the probabilities are calculated. This results in a quiescent probability distribution $p(Q)$ for each galaxy, which is marginalised over its rest frame flux errors. Therefore, the final distribution of $p(Q)$ for each galaxy accounts for flux errors. We refer mainly to $p(q)_{50}$ (abbrev. $p(q)$) throughout the text, which is the median quiescent probability calculated in this way. Here, we use the GMM purely as a tool to classify QGs and do not explore the other five groups defined by the model. In Figure 2.4 we show the $2 < z < 3$ fitting sample and the $3 < z < 5$ sample in the $NUVU - VJ$ plane, coloured by their quiescent probability $p(q)$. It is evident that the model correctly finds the boundary between quiescent and star forming, but a boundary that is a smooth gradient rather than a binary separation.

2.4.2.1 THE $p(q)$ THRESHOLD FOR QUIESCENCE

To calculate the $p(q)$ threshold above which a galaxy is classed as quiescent and assess the performance of the method, we use galaxies in the SHARK simulation (Section 2.2.3). At redshift snapshots of $z = 2$, $z = 3$, and $z = 4$ we select a massive galaxy sample ($\log(M_*/M_\odot) > 10$). We then define QGs in the sample as those with specific star formation rates $\log(\text{sSFR } t_H \text{yr}^{-1}) < 0.2$, where t_H is the age of the universe at that redshift snapshot and the sSFR is averaged over the last ~ 50 Myr. We fit the GMM to the $NUV - U$, $V - J$ and $U - V$ colours at each redshift snapshot. We then calculate the Receiver Operator Characteristic (ROC) curve, which is simply the False Positive Rate (FPR) as a function of True Positive Rate (TPR). The Area-Under-Curve (AUC) can be used as a measure of effectiveness of the classification method: an AUC very close to unity shows that the method correctly classifies objects with a high TPR and low FPR. We also compute the same numbers for the Whitaker et al., 2012 UVJ selection method (defined as $U - V > 0.8 \times (V - J) + 0.7$, $U - V > 1.3$ and $V - J < 1.5$). Figure 2.5 shows both the $NUVU - VJ$ and UVJ diagrams and the ROC curves for each redshift snapshot. The AUC increases from $z = 2$ to $z = 4$, meaning that the GMM has increasing chance of correctly identifying QGs (88%, 93% and 97% at $z = 2, 3, 4$ respectively). It is not possible to calculate the AUC for UVJ because there is only one selection “threshold”, which is whether or not a galaxy falls inside the UVJ quiescent area.

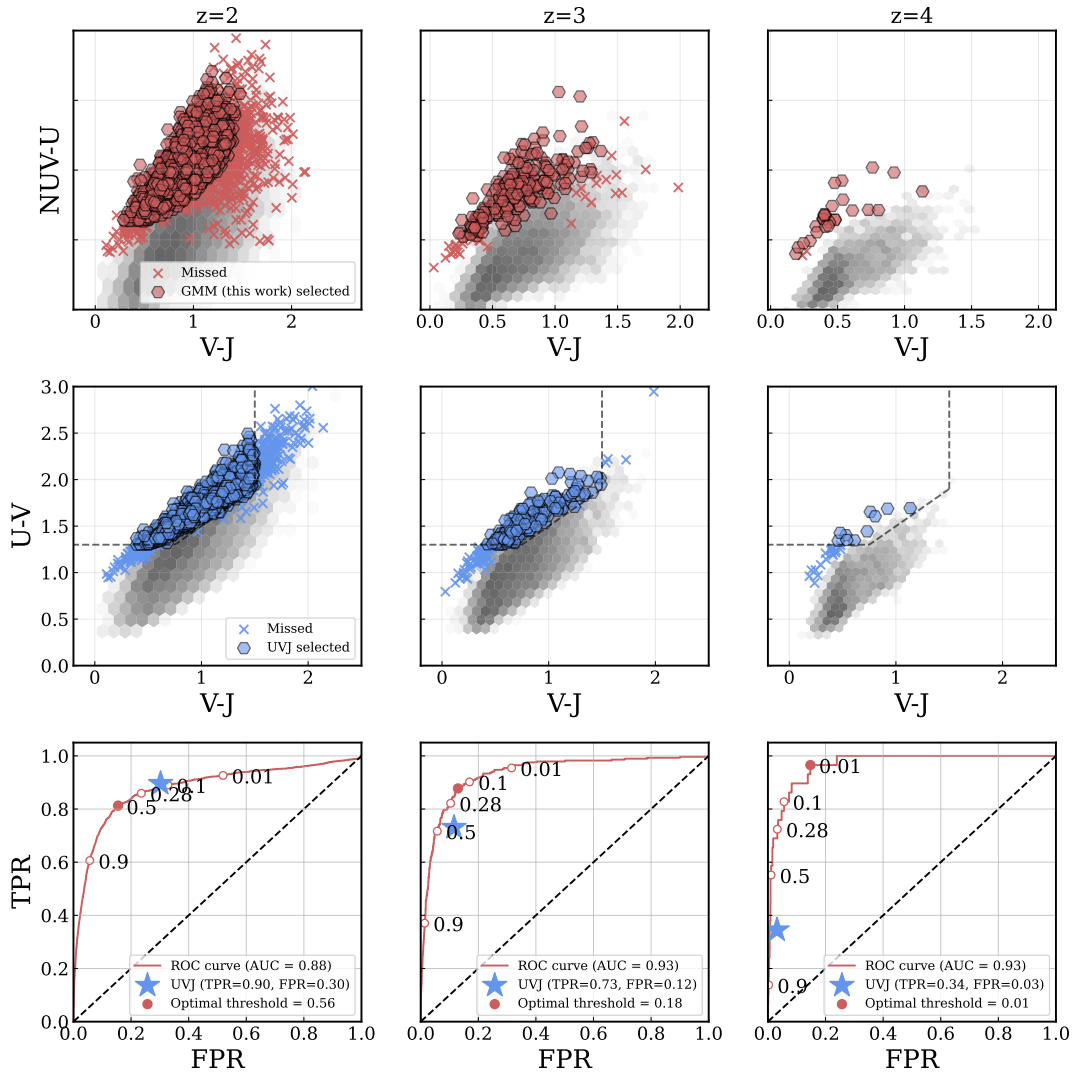


Figure 2.5: *Left column:* SHARK simulated galaxies in different colour planes. GMM/ $NUV - VJ$ (this work, top) and UVJ (middle) colour diagrams for massive ($\log(M_*/M_\odot > 10$) galaxies in the SHARK simulation (grey), with QGs found by each selection method as red (blue) hexagons and galaxies missed by both selection methods as red (blue) crosses. The bottom panel shows the Receiver Operator Characteristic (ROC) curve for the trained Gaussian Mixture Model as a function of quiescent probability ($p(Q)$) threshold. The Area Under the Curve (AUC), which represents the percentage probability of correctly classifying QGs, is reported, as well as the $p(Q)$ threshold, which is calculated as the geometric mean (shown on the figure as the coloured red circle on the red curve). The False Positive Rate and True Positive Rate is also presented for the [Whitaker et al., 2012](#) UVJ selection (blue star). *Middle column:* Same as left column but at $z = 3$. *Right column:* Same as left column but at $z = 4$.

Table 2.1: Quiescent probability ($p(q)_{50}$) thresholds for redshift ranges, defined by the maximum of the geometric mean of the ROC curve trained on SHARK simulated data.

Redshift	$p(q)_{50} >$
$2.0 < z < 3.0$	0.56
$3.0 < z < 4.0$	0.18
$4.0 < z < 5.0$	0.01

We can instead calculate the TPR and FPR for *UVJ*. The optimal $p(q)$ threshold is defined as the maximum of the geometric mean, which finds the threshold at which the TPR and FPR are perfectly balanced (or the top left most point on the ROC curve), and is defined as $\max(\sqrt{TPR * (1 - FPR)})$. The resulting $p(q)$ thresholds at $z = 2$, $z = 3$, and $z = 4$ are calculated using the geometric mean and are shown in Table 2.1.

2.4.2.2 UVJ VERSUS GMM IN SHARK

At $z = 2$, *UVJ* performs similarly to *NUV - VJ* at $p(q) \gtrsim 0.1$, with *UVJ* having FPR=30%, TPR=90% and *NUV - VJ* with FPR=33%, TPR=89%. However, the optimal threshold for *NUV - VJ* performs substantially better at this redshift, with a TPR only a few % lower (81%), whilst the FPR is more than halved, reducing from 33% to 15%. If we consider instead the contamination, which is defined as the number of galaxies defined as quiescent compared to the total number of *UVJ* quiescent galaxies, the conclusion changes. The contamination fraction of *UVJ* in SHARK at $z = 2, 3, 4$ is 80, 86, 91%, further highlighting the issues with *UVJ*. Looking to higher redshift, it is evident that *NUV - VJ*/ GMM classification not only out-performs *UVJ* classification, but also substantially increases in effectiveness with increasing redshift, highlighting the usefulness of the method especially at $z > 3$.

2.5 APPLICATION TO COSMOS₂₀₂₀

We apply the GMM to the massive galaxy sample in COSMOS₂₀₂₀ at $2 < z < 5$ selected in Section 2.4. Whilst SHARK produces galaxies at redshift snapshots of $z = 2, 3, 4$, observed galaxies are continuously distributed in redshift. We therefore choose not to assume that the $p(q)$ threshold is a step function, but rather a smoothly varying function of redshift. We

fit a second order polynomial to the three points $(z_{phot}, p(q)) = (2, 0.56; 3, 0.18; 4, 0.01)$ and use this function to determine if a galaxy is chosen as quiescent or not. This naturally incorporates the assumption that as we move to higher redshift, in order to be defined as quiescent, galaxies may look less like quiescent galaxies at $z = 2$, and more like post-starburst galaxies. We require that at $z = 2 - 4$, the median of the $p(q)$ distribution is above the threshold. At $z \geq 4$, we instead require that 95% of the $p(q)$ distribution is above $p(q) = 0.01$, in order to only select the highest confidence candidates. The application of redshift dependent $p(q)$ thresholds selects 1455 QGs at $2 < z < 3$ and 230 QGs at $3 < z < 5$. We visually inspect cut-outs of the $3 < z < 5$ sample in the optical and NIR bands, and remove nine QG candidates which are spurious, reducing the total $3 < z < 5$ sample to 221 in number. In the following sections, we present the properties of our sample of QGs, compare its statistics with those of galaxies selected using traditional colour diagrams, and discuss the differences between methods.

2.5.1 COMPARING GMM/ $NUV - VJ$ TO UVJ AND $NUVRJ$ COLOUR SELECTIONS

We apply both the [Whitaker et al. \(2012\)](#) UVJ selection as well as the [Ilbert et al. \(2013\)](#) $NUVRJ$ selection for quiescence to our massive galaxy samples at $2 < z < 3$ and $3 < z < 5$, and compare these traditional colour selections to the GMM colour selection method. For each panel of Figure 2.6, we calculate the overlap between selections, which is defined as the sample size divided by the sample size of the “main” selection for that row, which is highlighted by the coloured panel. At $2 < z < 3$, the overlap between all three selection methods is high: UVJ and $NUVRJ$ selections have an $\sim 85\%$ overlap, whilst the GMM selected sample also agrees well, sharing $\sim 80 - 90\%$ with UVJ and $NUVRJ$ selected QGs. This would be expected if the rest frame fluxes were measured directly from the template, but in this case they are weighted by the observed fluxes and so the conclusion is that the different selections are generally measuring the same *observed* SED shape. [Hwang et al. \(2021\)](#), who compared $NUVRJ$ and UVJ selected samples at $0 < z < 3$ in COSMOS2015, found a similar overlap ($\sim 85\%$). This suggests that the choice of rest-frame colour diagram selection at $z < 3$ is not crucial, although modifications to both UVJ and $NUVRJ$ colour selections may be in order.

At $3 < z < 5$ the agreement between colour selections is less clear: UVJ and $NUVRJ$ share

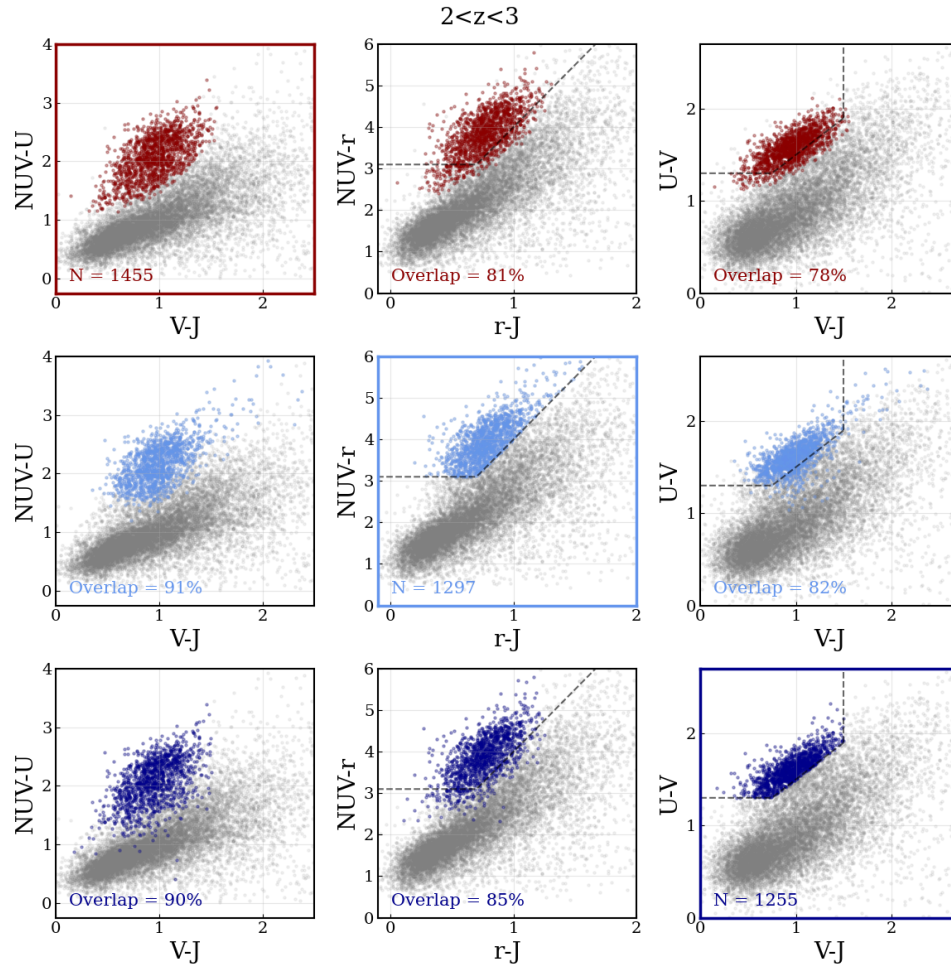


Figure 2.6: *Top row:* $NUV - VJ$ selected QGs at $2 < z < 3$ (dark red, left figure) shown in $NUV - VJ$ space, UVJ space and $NUVrJ$ space. *Middle row:* $NUVrJ$ selected QGs (middle figure, light blue) shown in $NUV - VJ$ and UVJ colour diagrams. *Bottom row:* UVJ selected QGs (right figure, dark blue) shown in $NUV - VJ$ and $NUVrJ$ colour diagrams. For each panel, the overlap is given, defined as the number of galaxies selected by that selection method divided by the number of galaxies selected by the main selection method for that row. In the first row we show the GMM selected sample at $2 < z < 3$ in the $NUV - VJ$ diagram, $NUVrJ$ diagram and UVJ diagram. The second row shows the $NUVrJ$ selected sample in $NUVrJ$ (light blue) as well as the other two colour colour diagrams and the third row shows the UVJ selected sample in UVJ as well as in the other two colour colour diagrams (dark blue).

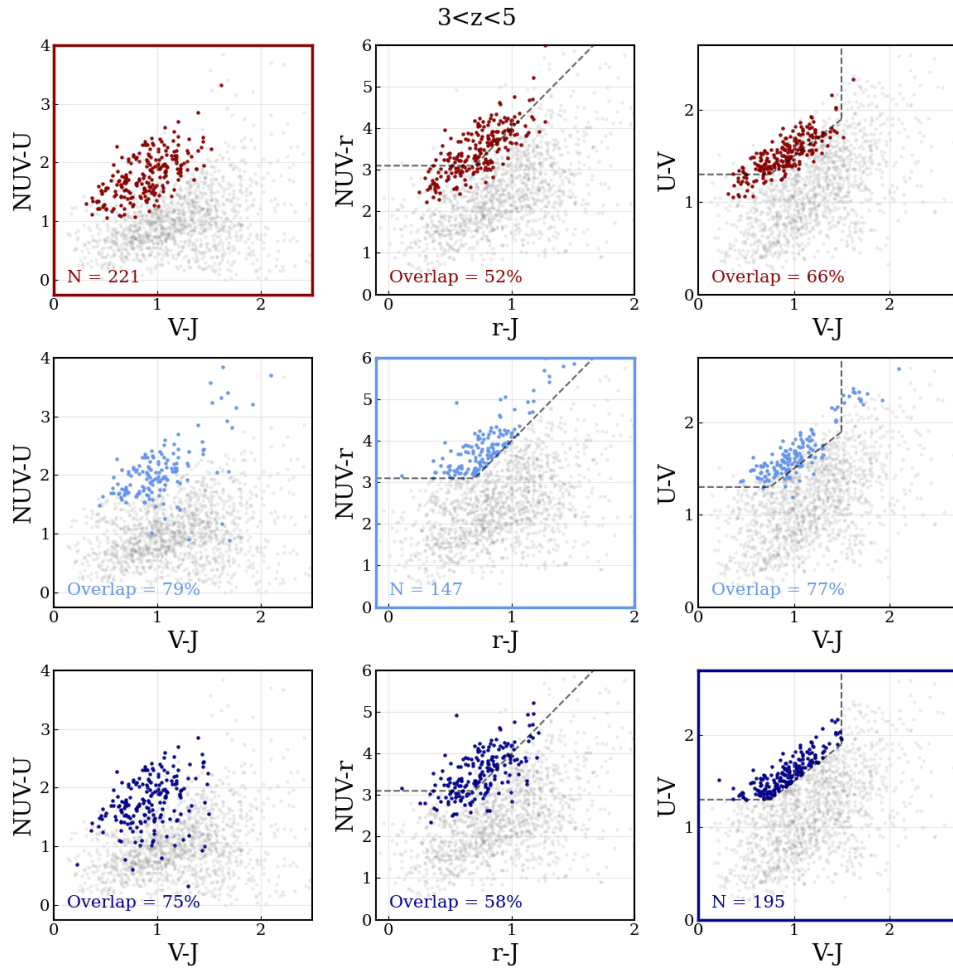


Figure 2.7: Same as figure 2.6 but for $3 < z < 5$.

58 – 77% of the same sample, whilst GMM shares 52 – 79% with $NUVrJ$ and 66 – 75% with UVJ . This difference is highlighted clearly in Figure 2.7. This is likely due to two reasons: firstly, that neither UVJ nor $NUVrJ$ selections include the region where post-starburst galaxies are most often found, which is at the lower edge beyond the $U - V < 1.3$ boundary. Secondly, the contamination fraction of UVJ and $NUVrJ$ is likely much higher than the GMM selection method. Whilst it is easy to remedy the first issue in both cases by simply lowering or removing the dividing line in $U - V/NUV - r$ as discussed above, this may also increase the contamination of the sample by introducing $U - V/NUV - r$ blue star forming galaxies. This is something that [Schreiber et al. \(2018\)](#) confirmed in their analysis. For completeness, we report the performance of an extended UVJ selection bench-marked against SHARK in Appendix A.4. The issue of contamination is more difficult to solve due to the nature of these colour selections, however our method aims to alleviate this problem by both the introduction of the third $NUV - U$ colour, and the option of choosing galaxies based on a probability distribution ideally makes it easier to sharpen the boundaries between different populations.

2.5.2 FULL SPECTRAL ENERGY DISTRIBUTION

To offer a more complete view of the full SEDs of our selected QGs, in Figure 2.8 we show both the cutouts from optical/NIR bands and best-fit SEDs for three candidates at $z_{phot} = 3.12, 3.92, \text{ and } 4.68$. We also compute the median rest-frame photometry and best-fit models for the whole GMM-selected sample normalized to $V = 1$ (Figure 2.9). The median values of K_s , observed magnitudes, M_* , SFRs, and sSFRs are also reported in the figure. The galaxies in our sample show a strong Balmer/4000 Å break indicating a dominant aged stellar population on average, as expected. However, they still have residual flux blue-ward of the break, indicative of a younger populations and recent quenching. The median mass ($\log(M_*/M_\odot) = 10.92$) of this sample is ~ 0.3 dex higher than the mass cut for the original sample selection, confirming that only the most massive galaxies have quenched their star formation at $z > 3$. The median $\log(\text{sSFR}/\text{yr}^{-1}) = -10.8$ indicates that these galaxies are best fit mainly by templates that include little or no ongoing star formation.

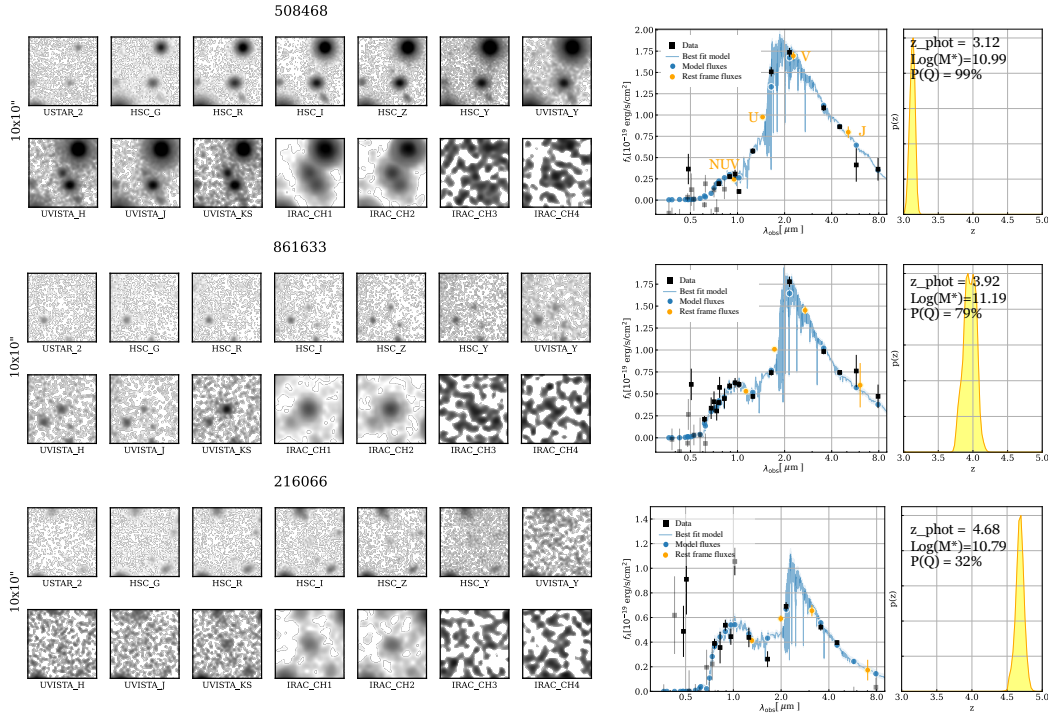


Figure 2.8: $10 \times 10''$ Postage stamp cutouts from selected bands in the optical to NIR scaled by $\pm 3\text{RMS}$ (left) and corresponding best fit SEDs (right) for three quiescent galaxy candidates selected using the $NUV - VJ$ method, taken from the main sample. The observed photometric points are shown as black circles (any with $\text{SNR} < 2$ in grey) and the best fit model is shown in blue. The rest frame NUV, U, V, J photometry is shown by the orange circles. The $p(z)$ is shown to the right of each SED in yellow, along with its best-fit photometric redshift, stellar mass, and quiescent probability median value ($P(q)_{50}$).

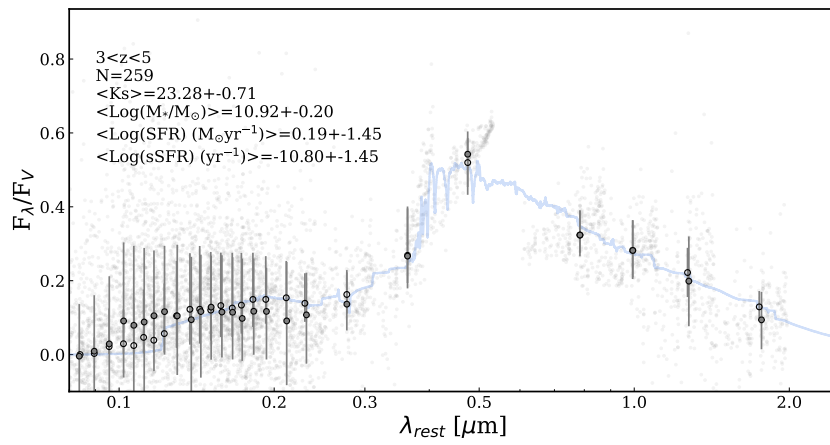


Figure 2.9: *Top:* Median smoothed rest frame SED for the GMM/*NUV* – *IJ* selected quiescent sample at $3 < z < 5$. Rest frame photometry for all galaxies is shown in grey, whilst the median per band and the associated 16th and 84th percentiles (error bars) are shown in dark grey. The median best fit (smoothed) model is shown in red. The median model photometry per band is shown by the open face circles. The location of the sample in *NUV* – *IJ* space is shown in the top right inset, whilst at the top left the sample median properties (number, median K_s band magnitude, median $\log(\text{stellar mass})$, median $\log(\text{SFR})$, median $\log(\text{sSFR})$) are shown, as well as the standard deviation.

Redshift	$N\text{Mpc}^{-3}$
$2.0 < z < 3.0$	$5.62 \pm 1.2 \times 10^{-5}$
$3.0 < z < 4.0$	$1.38 \pm 0.4 \times 10^{-5}$
$4.0 < z < 5.0$	$3.45 \pm 2.16 \times 10^{-6}$

Table 2.2: Number densities for galaxies in our sample at $2 < z < 3 \log(M_*/M_\odot) > 10$, $3 < z < 4 \log(M_*/M_\odot) > 10.6$ and $4 < z < 5 \log(M_*/M_\odot) > 10.6$. Errors are calculated by combining in quadrature the Poisson uncertainty and the fractional error due to cosmic variance.

2.5.3 SPECTROSCOPICALLY CONFIRMED QGS

As a confidence check, we cross-matched our sample of candidate QGs with a literature compilation of 7 spectroscopically confirmed $z \gtrsim 3$ QGs in COSMOS from [Forrest et al., 2020b](#) (4), [Forrest et al., 2020b/Marsan et al., 2015/Saracco et al., 2020](#) (1), [Valentino et al., 2020](#) (1) and [D’Eugenio et al., 2020a](#) (1). For 6/7 sources we retrieve $p(q) \gtrsim 10\%$, consistent with being QG according to our selection. To the remaining galaxy at $z_{\text{spec}} = 3.352$ ([Marsan et al., 2015; Forrest et al., 2020b; Saracco et al., 2020](#)), we assign $p(q) = 0.6\%$. This source would thus not be selected using our fiducial threshold at $3 < z < 4$. We note that this galaxy has experienced rapid quenching, possibly due to an AGN. The presence of the latter is inferred from the large [OIII]/H β emission line ratio, with the oxygen line possibly contaminating the K_s photometry (see the discussion in [Forrest et al. 2020a](#)).

2.6 NUMBER DENSITIES

The number densities of massive QGs at $z > 3$ is an important constraint on galaxy evolution and theory. The assembly of galaxies with such high stellar masses in an evolved state within only 1.5-2 billion years not only places important constraints on the formation of the first galaxies (e.g. [Steinhardt et al., 2016](#) and references within), but also on the cosmic star formation rate density (cSFRD) ([Merlin et al., 2019](#)). As such, the number density of these galaxies provides important context to early galaxy evolution. However, the number densities of massive QGs at $z > 3$ has been an intense topic of debate, due to both the disagreement between observations and theory, and between the observational studies themselves.

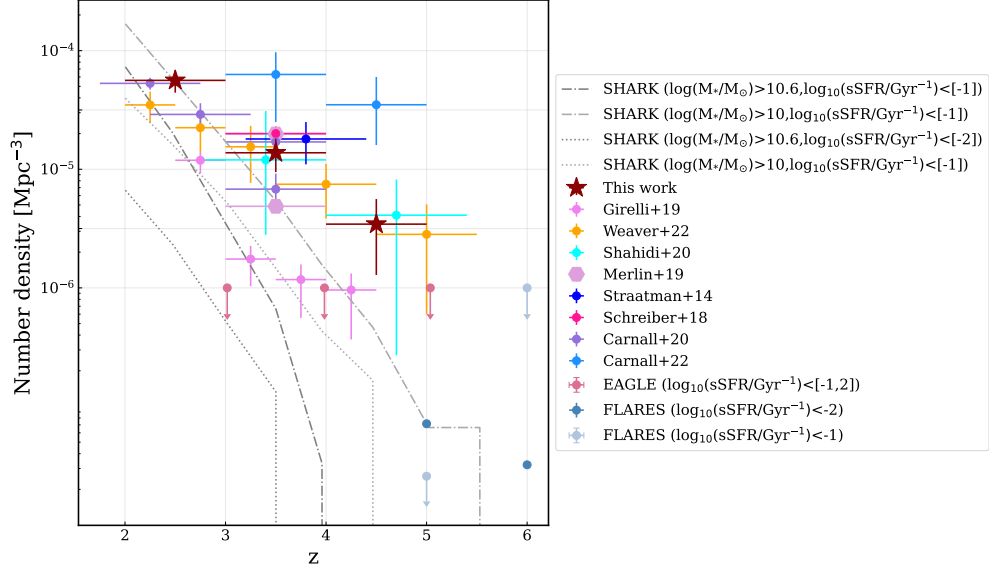


Figure 2.10: Number densities of massive QGs as a function of redshift at $2 < z < 5$. We report the number densities calculated for our sample (dark red stars) in redshifts bins of $2 < z < 3$ ($\log(M_*/M_\odot) > 10$), $3 < z < 4$ ($\log(M_*/M_\odot) > 10.6$) and $4 < z < 5$ ($\log(M_*/M_\odot) > 10.6$). The errors on the number densities include both Poisson noise and cosmic variance added in quadrature. We plot number densities from [Weaver et al., 2022](#), [Shahidi et al., 2020](#), [Straatman et al., 2014](#), [Schreiber et al., 2018](#), [Carnall et al., 2020](#), [Merlin et al., 2019](#), the extended sample from [Girelli et al., 2019](#) and [Carnall et al., 2022](#). Also shown are number densities for the FLARES and EAGLE simulations for massive galaxies ($\log(M_*/M_\odot) > 10.6$) at two quiescent selection thresholds ($\log_{10}(\text{sSFR}/\text{Gyr}^{-1}) < [-1, -2]$) ([Lovell et al., 2023](#)), as well as quiescent galaxies from the SHARK simulation at two mass ($\log(M_*/M_\odot) > [10., 10.6]$) and sSFR selection thresholds ($\log_{10}(\text{sSFR}/\text{Gyr}^{-1}) < [-1, -2]$)

Number densities derived from photometric and spectroscopic observations span ~ 2 dex, but they generally remain higher than those extracted from simulations (Ilbert et al., 2013; Straatman et al., 2014; Davidzon et al., 2017; Schreiber et al., 2018; Merlin et al., 2018, 2019; Girelli et al., 2019; Shahidi et al., 2020; Carnall et al., 2020; Santini et al., 2020; Valentino et al., 2020; Carnall et al., 2022; Valentino et al., 2023). The disagreement among observational works and with theoretical predictions is likely due to a mix of several factors, primarily different sample selections and quiescent criteria used together with analyses done using multiple diverse data sets. Of particular note is the size of such fields, as statistics can be affected by both the rarity of these galaxies and by cosmic variance. The latter is strongly mitigated by the large contiguous area of the COSMOS field. Here we compute and present the number densities for our sample of QGs in three bins at $2 < z < 3$, $3 < z < 4$ and $4 < z < 5$ (Table 2.2). Number densities are calculated using the survey area of the combined *HSC/UVISTA* coverage, which corresponds to 1.27 square degrees. We calculate the fractional error due to cosmic variance using the method of Steinhardt et al. (2021) who extend the method of Moster et al. (2011) for use in the early universe (for details, see Steinhardt et al., 2021 and Weaver et al., 2022). This is combined in quadrature with the Poisson error to get the total error budget.

In Figure 2.10, we show our number densities along with a compilation of number densities from other observational studies (e.g., Valentino et al. (2023) and references therein). Additionally, we show QG number densities from the SHARK simulation at two mass ($\log(M_*/M_\odot) > [10., 10.6]$) and sSFR selection thresholds ($\log_{10}(\text{sSFR}/\text{Gyr}^{-1}) < [-1, -2]$), as well as both the FLARES ($z \geq 5$) and EAGLE ($z \leq 5$) simulations for QGs at ($\log(M_*/M_\odot) > 10.6$) at two different selections ($\log_{10}(\text{sSFR}/\text{Gyr}^{-1}) < [-1, -2]$) (Lovell et al., 2022). It is important to note that the literature compilation of QGs at $z > 3$ comprise selections at different mass limits ranging from ($\log(M_*/M_\odot) > 10$, (Carnall et al., 2020) upwards, whilst our mass limit is much higher ($\log(M_*/M_\odot) > 10.6$). In general, our number densities at $3 < z < 4$ agree with the observational studies within 1σ errors. It is interesting to note that the number densities derived by Girelli et al. (2019) are much lower than those derived from COSMOS2020, which likely arises from the COSMOS2020 catalog including all UVISTA stripes, some of which have known over-densities (e.g. McConachie et al., 2021). Looking to higher redshift

2.7. WHAT FRACTION OF QGS AT $3 < z < 5$ ARE POST-STARBURST?

at $z > 4$, our estimates agree with those of [Weaver et al. \(2022\)](#) and [Shahidi et al. \(2020\)](#). Generally, it appears that number densities for massive QGs derived from a variety of different fields, selected with a variety of methods, are finally converging on agreement.

Previously, simulations were not able to reproduce the number densities of massive QGs at $z > 3$ observed in the real universe by a factor of 1-2 dex; this tension remains slightly with EA-GLE, which predicts only upper limits for QGs at $\log(M_*/M_\odot) > 10.6$ that are several times lower than most observations. At $z = 5$, the results from FLARES are $\sim 50\times$ smaller than our current limits at fixed M_* threshold, resulting in a direct tension. At $z > 5$, this simulation predicts similarly low number densities, but the lack of data from observations at $z \gtrsim 5$ means that for the first time at high redshift, simulations have QGs where observations have found none. SHARK performs the best at producing similar number densities of massive QGs to observations up to at least $z \sim 3$, but has a dearth of massive ($\log(M_*/M_\odot) > 10.6$) QGs at $z \gtrsim 4$. The only QGs at $z > 4$ in SHARK are ~ 4 times less massive than those in observations, and in fewer numbers too, implying that those galaxies which have been able to quench are still to accumulate mass. Finding QGs at $z \gtrsim 5$ will require both the combination of wide optical/NIR surveys to find such rare galaxies, and also deep NIR/MIR spectroscopy to confirm them.

2.7 WHAT FRACTION OF QGS AT $3 < z < 5$ ARE POST-STARBURST?

In the epoch of the universe where quenching begins, it may make more sense to instead differentiate between quenching, recently quenched, and older (or “true”) QGs. This issue confronts a more philosophical question in extra-galactic astrophysics: what is the definition of a quiescent galaxy? There appear to be two ways to deal with this population exhibiting a wide variety of quenching states: firstly, one can split the entire sample into young quiescent/PSB/recently quenched, and old quiescent (e.g. [Ichikawa and Matsuoka, 2017](#); [Schreiber et al., 2018](#); [Park et al., 2022](#)). Alternatively, the entire sample can be treated as homogeneous, which is what we have done with this analysis. The prevalence of QGs with recent star formation at $z > 3$ - the so-called PSB population - has been measured by a plethora of works, both from photometric and spectroscopic data. Whilst at low redshift,

the definitions of post-starburst, albeit broad, are based on measurements involving spectral indices or spectra-based PCA that encode information about strong Balmer absorption lines as well as weak or no emission lines (e.g. Wild et al., 2014, Chen et al., 2019, Wild et al., 2020, Wilkinson et al., 2021), this type of definition is not possible to apply to large photometrically selected samples. We instead consider how one might define a PSB galaxy in a sample of photometrically selected QGs based just on colours.

Marsan et al. (2020) proposed a definition of PSB based on a visual SED inspection and the presence of a UV peak brighter than the emission red-ward of the Balmer/4000Å break. This study estimates that PSB galaxies comprise 28% of the massive ($\log(M_*/M_\odot) > 11$) population at $3 < z < 4$ and 17% at $4 < z < 6$. Approximately twice higher fractions of PSB at $\log(M_*/M_\odot) > 11$ are reported by D’Eugenio et al. (2020a) based on their sample of spectroscopically confirmed objects at $z > 3$ with measured D_{n4000} , D_B and $H_{\delta A}$ indices. Thirty percent of the spectroscopic sample in Forrest et al. (2020b) ceased star formation less than 300 Myr prior the epoch of the observed redshift at $3 < z < 4$. At the same epoch, Schreiber et al. (2018) report that “young quiescent” galaxies, defined as UVJ -star forming galaxies with $V - J < 2.6$ but below some sSFR threshold, are just as numerous as classical QGs.

Here we base a definition of PSB on the strength of the “blue bump” in the SEDs traced by the $NUV - U$ colour. The distribution of $NUV - U$ colours for our QG sample of 221 galaxies peaks at $NUV - U = 1.75$. Only 28% of galaxies have $NUV - U > 2$ and only one galaxy has $NUV - U > 3$. Based on our single stellar population model from Section 2.4.1, a stellar population will not reach $NUV - U > 2$ until 0.5 – 1 Gyr has passed and $NUV - U > 3$ until well after 1 Gyr, assuming no dust attenuation. Based on this, we can define PSBs as those galaxies in our sample with $NUV - U < 2$, comprising 70% of QGs at $3 < z < 4$ and 87% at $4 < z < 5$. This is marginally higher than what previously reported (Schreiber et al., 2018). If we restrict our selection to only the most massive galaxies, i.e., those with $\log(M_*/M_\odot) > 11$, then these numbers change to 60% at $3 < z < 4$ and 86% at $4 < z < 5$. This agrees with the 60 – 70% value given by D’Eugenio et al. (2020a) for galaxies at $z \sim 3$. As a fraction of the entire ultra-massive galaxy population, PSBs only

comprise 7% at $3 < z < 4$, and 12% at $4 < z < 5$. Together with the results of the previous section, it is clear that $3 < z < 5$ is an active era in the history of the universe, one in which the transition to quiescence is fairly common.

2.8 WILL WE FIND OLD QUIESCENT GALAXIES AT $z > 4$ WITH *JWST*?

Qgs have already been spectroscopically confirmed with *JWST* (Nanayakkara et al., 2022; Carnall et al., 2023), however no old quiescent galaxies have been found at $z > 4$ yet. In general, the blue colours of our $3 < z < 5$ QG candidates indicates a lack of very red, evolved galaxies such as the one presented in Glazebrook et al., 2017. This could be because as an ensemble, the QG population at $z > 3$ has only recently quenched, and older QGs are much rarer. However, at $z > 4.5$, the reduced sensitivity to older/redder quiescent galaxies due to the lack of data directly covering the 4000 break could be biasing us to the bluest (and youngest) quiescent galaxies. Although this is easily side-stepped with *JWST*/*NIRSPEC*, it is difficult to solve even with *JWST* broad-band *NIRCAM* imaging; at $4.5 < z < 5$, the 4000 break falls at $2.2 - 2.4 \mu\text{m}$ and is straddled by *F200W* on the blue side and *F277W* (or redder bands such as *F350W*) on the red side (depending on the program), with no observations of quiescent galaxies at $z > 4.5$ currently spanning the midpoint or upper edge of the break (see e.g. Valentino et al. (2023) and Carnall et al. (2022)). This could easily be alleviated with the inclusion of *NIRCAM* narrow-bands covering $2.2-2.4 \mu\text{m}$, such as *F210M* or *F250M*. Currently, the only Cycle 1 program that has the combination of *F200W*, *F277W*/*F350W* and at least one medium band filter in between is the Canadian NIRISS Unbiased Cluster Survey (CANUCS; PI Willott (Willott et al., 2017)), which has both *F210M* and *F250M*. However, the combined area covered by these filters is ~ 50 arc-minutes squared, which would net less than one massive quiescent galaxy based on our number densities (see Section 2.6), assuming the same space distribution on the sky. In short, one would have to be incredibly lucky to find an evolved quiescent galaxy at $z > 4.5$ without both area and either spectroscopy or medium-band photometry.

2.9 SUMMARY AND CONCLUSIONS

In this work, we explore the massive quiescent galaxy population at $3 < z < 5$ in *COSMOS* using the latest photometric catalogue, *COSMOS2020*. We create a new catalogue using the *COSMOS2020* photometry, with *Spitzer/IRAC* errors boosted and derive redshifts and physical parameters with *eazy-py*. We motivate the need for a new rest-frame color diagram to select for QGs at $z > 3$ and present the Gaussian Mixture Model (GMM)/*NUVU - VJ* method as a viable alternative. We use a GMM to fit the *NUV - U*, *U - V*, *V - J* colours of massive galaxies at $2 < z < 3$ and galaxies are assigned a probability of being quiescent based on their bootstrapped rest frame colours. This GMM model is then applied to the colours of massive galaxies at $3 < z < 5$. Both the GMM model and code to calculate quiescent probabilities from rest frame flux densities are made available online[†]. Our key findings can be summarised below:

- We calculate the quiescent probability for simulated galaxies from the SHARK semi-analytical model at redshift snapshots of $z = 2, 3$, and 4 and find that GMM performs just as well as classical *UVJ* selection at $z = 2$, with both methods returning similar true positive and false positive rates (TPR $\sim 90\%$, FPR $\sim 30\%$). However, at $z > 3$, the GMM method outperforms classical *UVJ* selection and particularly excels at $z \geq 4$, where the TPR is almost 100% compared to *UVJ* that has less than 40% TPR. This highlights our proposed method as a viable alternative to traditional colour selection methods at $z > 3$.
- We compare our GMM-selected quiescent galaxies (QGs) in *COSMOS2020* to traditional rest-frame colour selected quiescent galaxies (*UVJ*, *NUVrJ*) and calculate the overlap between selection methods. We find that all three colour selections have high agreement at $2 < z < 3$, with methods selecting $\sim 85\%$ of the same galaxies, implying that the exact choice of rest-frame colour selection method at $2 < z < 3$ is not crucial. However, overlap between colour selections at $z > 3$ reduces to $\sim 65\%$, implying that one should be careful about using *UVJ* and *NUVrJ* colour selections interchangeably.

[†]<https://github.com/kmlgould/GMM-quiescent>

Generally, the bluer colours of GMM selected QGs at $3 < z < 5$ implies a dearth of any highly evolved QGs in this epoch.

- We compute the number densities of QGs at $2 < z < 5$ and confirm the overall abundance of QGs presented in many different works, which our values agree with within the uncertainties. Given the conservative nature of this work (the boosting of *IRAC* errors, the high mass limit and the probabilistic approach), we interpret the number densities as a lower limit.

The next few years will undoubtedly see our knowledge of QGs at $z > 3$ grow vastly with the recent launch and successful commissioning of *JWST* (Rigby et al., 2022), for which QGs at $z > 3$ have already been reported (Carnall et al., 2022; Pérez-González et al., 2022; Cheng et al., 2022; Rodighiero et al., 2023; Valentino et al., 2023) and even confirmed (Nanayakkara et al., 2022; Carnall et al., 2023), as well as ongoing large ground-based surveys such as the Cosmic Dawn Survey (Moneti et al., 2022, McPartland et al., 2023, in prep). Spectroscopic confirmation of multiple QG candidates with, e.g., *NIRSPEC* can be done in a matter of minutes (Glazebrook et al., 2021; Nanayakkara et al., 2022), and whilst ~ 8 hours with *VLT/X-shooter* or *Keck/MOSFIRE* are only sufficient to obtain a redshift and stellar populations, the same time (or less) with *JWST* could provide the required S/N to study detailed physics such as velocity dispersions and metallicities (Nanayakkara et al., 2021; Carnall et al., 2023). Whilst *JWST* will be crucial for confirming quiescent galaxy candidates and studying their physical properties in detail, wide area photometric surveys still have an important role to play, both for the selection of, and statistical study of these galaxies.

Acknowledgements

The Cosmic Dawn Center (DAWN) is funded by the Danish National Research Foundation under grant No. 140. S.J. acknowledges the financial support from the European Union’s Horizon research and innovation program under the Marie Skłodowska-Curie grant agreement No. 101060888.

The following software were used in this work:

Eazy-py (Brammer, 2021), scipy (Virtanen et al., 2020), numpy (Harris et al., 2020), matplotlib (Hunter, 2007), sci-kit learn (Pedregosa et al., 2011), astropy (Collaboration et al., 2013; Astropy Collaboration et al., 2018), python-fsps (Conroy and Gunn, 2010; Conroy et al., 2009).

A.1 REST-FRAME FLUX DENSITIES

Consider two methods for inferring the flux density of a given galaxy at redshift, z , in a rest-frame bandpass, e.g., the V (visual) band in the Johnson filter system (Johnson, 1955; Bessell, 1990), with a central wavelength* $\lambda_c \sim 5500 \text{ \AA}$. In the first method we identify two observed bandpasses with central wavelengths that bracket the redshifted rest-frame bandpass $\lambda_{c,A} < \lambda_c(1+z) < \lambda_{c,B}$ and perform a linear interpolation between the flux densities in the observed bandpasses A and B . In a second method we simply adopt the V band flux density of the best-fit model template that was used to estimate the photometric redshift of the galaxy. The first method has the benefit of being purely empirical, though it will be limited by noise in the two photometric measurements used for the interpolation. The second method incorporates constraints from all available measurements, but it will be more sensitive to systematic biases induced by the adopted model template library.

Here we adopt a methodology that is a hybrid between these two extremes that first makes better use of multiple observational constraints and second somewhat relaxes the dependence on the template library. Specifically, for a galaxy at redshift, z , and a given rest-frame bandpass with rest-frame central wavelength, λ_r , we compute a weight, w_i , for each observed bandpass with observed-frame central wavelength $\lambda_{o,i}$

$$\gamma_i = \exp(x_i^2/2/\log(1+\Delta)^2) \quad (\text{A.1})$$

$$w_i = W \cdot \left(\frac{2}{1 + \gamma_i/\text{Max}(\gamma_i)} - 1 \right), \quad (\text{A.2})$$

*The pivot wavelength is a convenient source-independent definition of the central wavelength of a bandpass (Tokunaga and Vacca, 2005)

where $x_i = \log(\lambda_r) - \log(\lambda_{o,i}/(1+z))$, and Δ and W are each parameters with a default value of 0.5. That is, the weights prioritize (i.e., are smallest for) observed bandpasses that are closest to the redshifted rest-frame bandpass. The templates are then refit to the observed photometry with least squares weights $\varepsilon_i^2 = \sigma_i^2 + (w_i \cdot F_i)^2$, where F_i and σ_i are the original photometric measurements and their uncertainties, respectively. The adopted rest-frame flux density is that of the template in this reweighted fit integrated through the target bandpass. In short, this approach uses the templates as a guide for a weighted interpolation of observations that best constrain a targeted rest-frame bandpass that fully accounts for all bandpass shapes and relative depths of a multi-band photometric catalog. Because the weights are localized for each target rest-frame bandpass, there is no implicit requirement that, e.g., the inferred rest-frame $V - J$ color is within the range spanned by the templates themselves. Finally, we note that this is essentially the same methodology as that in version 1.0 of the original eazy code[†] and now implemented in eazy-py

A.2 STAR-GALAXY SEPARATION

We use the same method for star-galaxy separation that is described in [Weaver et al. \(2021\)](#). Briefly, the catalogue is matched to the Hubble ACS morphology catalogue ([Leauthaud et al., 2007](#)) to isolate galaxies in the half-light radii versus magnitude plane. We fit each object with stellar templates from the PEGASUS library and compute the χ_{star}^2 . We calculate the reduced chi-squared χ_r^2 , where ($\chi_r^2 = \chi^2 / N_{filt} - 1$), of both the galaxy best fit template and star best template where N_{filt} is the number of filters used. Objects with HSC i -band magnitude < 21.5 or $HST/ACS\ F814W$ magnitude < 23 with $K_s\ SNR > 3$ or IRAC Channel 1 $SNR > 3$ are classified as stars if they lie on the point like sequence in the half-light radii versus magnitude plane or if they are fit better with a stellar template than a galaxy template (i.e, $\chi_{star}^2 < \chi_{galaxy}^2$). Additionally, objects that do not satisfy these criteria can be classified as a star if $\chi_{star}^2 + 1 < \chi_{galaxy}^2$. We find a similar fraction of stars to the number reported in the official COSMOS2020 catalogue and find a similar distribution in the gzK colour colour diagram (see Figure A.1).

[†]<https://github.com/gbrammer/eazy-photoz/tree/8be1c9>

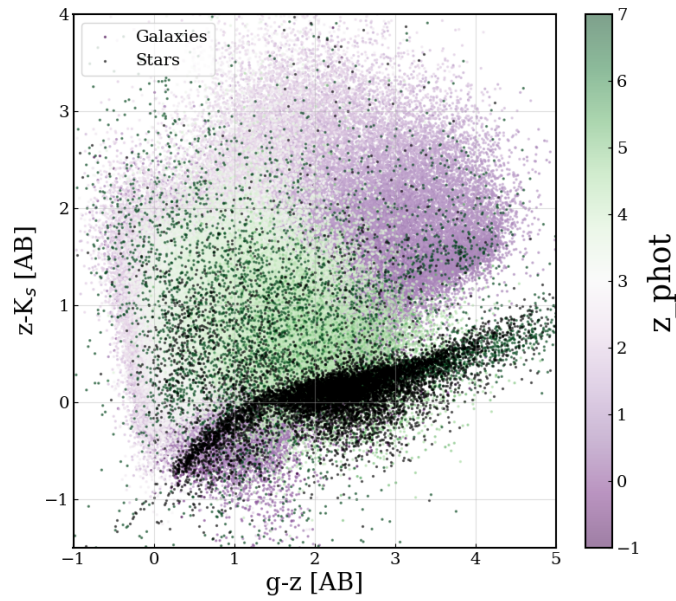


Figure A.1: gzK diagram for all galaxies in the combined UVISTA and HSC area with g , z and K SNR > 3 . Stars (black dots) occupy a locus across the lower part of the diagram, whereas galaxies (shown in green and purple dots) tend to occupy a wider spread of colours.

A.3 ROBUSTNESS OF REST-FRAME J BAND ESTIMATE

Although searches for massive QGs at $z > 3$ in the coming era will likely begin with rest-frame colour selections, we should be critical about which rest-frame colours should be used. The choice of rest-frame colours should depend on both the desired redshift range probed, and the ability of models to adequately measure rest-frame flux densities from the data. In particular, the colour used to discriminate between red dusty star forming galaxies and red QGs should be carefully chosen. [Antwi-Danso et al. \(2022\)](#) explored the effects of rest-frame J extrapolation for a flux limited sample of galaxies at $0.5 < z < 6$ and find that the flux is affected significantly at $z > 2$ when extrapolation occurs. This can result in the removal of QGs in standard selections and high contamination rates.

At $z > 3$, current ground-based surveys such as *COSMOS* rely on data from *Spitzer/IRAC* Channels 3 and 4. By $z \sim 5$, the rest-frame J -band is constrained entirely by Channel 4, which has a moderately shallow limiting 3σ depth of 23.1 mag in *COSMOS2020*. By comparison, *Spitzer/IRAC* Channels 1 and 2 are much deeper limited to 26.4 and 26.3 mags 3σ , respectively. However, the fraction of galaxies in *COSMOS2020* with $SNR \gtrsim 3$ in either Channel 3 or 4 at $3 < z < 5$ is only $\sim 5\%$. Making progress towards understanding the physical properties of the first quenched galaxies therefore mandates deeper data in the NIR, else inventive new methods, such as the use of a synthetic rest-frame i_s instead of J ([Antwi-Danso et al., 2022](#)). To ensure that rest-frame J is constrained for our sample, we limited the redshift upper bound at $z < 5$. Here, we compute the average SNR in bins of redshift for both Channels 3 and 4 for the entire massive sample and the quiescent sample (see Figure A.2). At $3 < z < 3.5$ and for both bands, the mean SNR for QGs is $\gtrsim 3$. At $3.5 < z < 4.0$, the mean SNR in Channels 3 and 4 is $2 - 3$, so rest-frame J is still constrained by reasonable photometry. At $z > 4$ however, both Channels have mean SNR between $1 - 2$, even after the $5\times$ boosting. This highlights the need for deeper observations in the NIR at $> 5 \mu\text{m}$. For part of the *COSMOS* field, this can be achieved with *JWST/MIRI* within the *COSMOS – Web* (PI: C. Casey, [Casey et al., 2022](#)) and *PRIMER* (PI: J. Dunlop) programs.

The issue of galaxies being classified incorrectly due to their rest-frame colours can partly be alleviated by our method of assigning a probability of quiescence to each galaxy, instead of a binary separator, which relies on the relative scatter within each population to be low –

evidently not the case at $z > 3$.

A.4 PERFORMANCE OF AN EXTENDED UVJ COLOR SELECTION

At high redshift ($z \geq 2$), it may make sense to lower, or remove, the $U - V > 1.3$ boundary, allowing for the selection of “recently quenched” or post-starburst galaxies. This has been suggested and implemented by multiple works. For example, [Schreiber et al. \(2018\)](#) suggested combining the lowering of the boundary with the use of a band measuring the contribution from more recent star formation, whilst [Marsan et al. \(2020\)](#), who studied ultra-massive galaxies in the COSMOS-Ultra-VISTA field, remove the line altogether. [Belli et al., 2019](#), [Forrest et al., 2020b](#), [Carnall et al., 2020](#) and [Park et al., 2022](#) also advocated for either removing or lowering the boundary. If the $U - V > 1.3$ constraint is entirely removed, the picture changes for UVJ . At $z = 2$ the results remain roughly the same: the TPR and FPR both increase by 4%. At $z > 3$, the improvement is marked: the TPR increases by 25% to 98%, whilst the FPR only increases by 3% by 15%. $z = 4$ sees the most improvement, with the TPR increasing from 34% to 97% whilst the FPR still remains low at 6%. Considering instead the contamination, which is defined as the number of galaxies defined as quiescent compared to the total number of UVJ quiescent galaxies, the conclusion changes. The contamination fraction of UVJ in SHARK at $z = 2, 3, 4$ is 81, 86, 87%, which is similar to the contamination including the border (80, 86, 91%). Therefore, although the TPR and FPR imply the extended UVJ selection is suitable for use, the contamination fraction suggests otherwise, which is the same conclusion as for the classical UVJ selection.

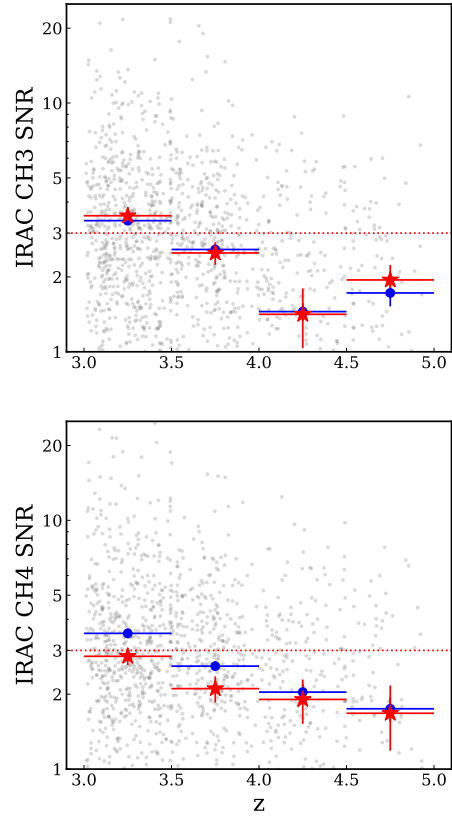
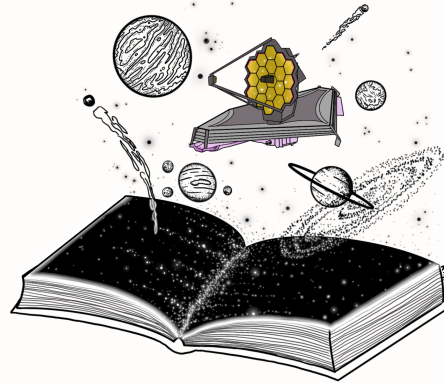


Figure A.2: Signal to Noise ratio (SNR) as a function of redshift at $3.0 < z < 5.0$ for IRAC Channel 3 (top) and IRAC Channel 4 (bottom) for the whole massive sample (gray). The average SNR for each channel is shown binned in redshift for the entire massive sample (blue dots) and the extended quiescent sample (red stars). The worst performance is at $4.5 < z < 5.0$ for both channels.

It should be emphasized, however, that the chief contribution of such a radically new and more powerful instrument would be, not to supplement our present ideas of the universe we live in, but rather to uncover new phenomena not yet imagined, and perhaps to modify profoundly our basic concepts of space and time.

Lyman Spitzer, Jr.

ASTRONOMICAL ADVANTAGES OF AN
EXTRA-TERRESTRIAL OBSERVATORY



This chapter contains materials reproduced from, and based on the following article:

“An Atlas of Color-selected Quiescent Galaxies at $z > 3$ in Public JWST Fields”

Published in the Astrophysical Journal (AJ): Volume 947, Number 1, 20 pp. (April 2023)

Authors: Francesco Valentino, Gabriel Brammer, Katriona M. L. Gould, Vasily Kokorev, Seiji Fujimoto, Christian Kragh Jespersen, Aswin P. Vijayan, John R. Weaver, Kei Ito, Masayuki Tanaka, Olivier Ilbert, Georgios E. Magdis, Katherine E. Whitaker, Andreas L. Faisst, Anna Gallazzi, Steven Gillman, Clara Giménez-Arteaga, Carlos Gómez-Guijarro, Mariko Kubo, Kasper E. Heintz, Michaela Hirschmann, Pascal Oesch, Masato Onodera, Francesca Rizzo, Minju Lee, Victoria Strait, and Sune Toft

The first cycle of observations with *JWST* resulted in not only new scientific results, but the publication of images from multiple different surveys which has the required area, depth, and filter coverage to execute a meaningful search for $z > 3$ quiescent galaxies. The advantage of searching multiple fields provides is that rarer galaxies, such as the most massive, are more likely to be found. Furthermore, the unprecedented depths make it possible to construct meaningful searches for a potential low mass quiescent galaxy population at $z > 2$, which would naturally be fainter given their low masses. This prospect was promising given that mere days after the first images were released, low mass quiescent galaxies at $z > 2$ were confirmed with *JWST* (Marchesini et al., 2023). In Chapter 2 I presented a new method that can be used to identify galaxies in various stages of quenching at high redshift. In this chapter, I present work I have done which is based on the application of this tool to various data-sets taken with *JWST*.

3.1 SEARCHING FAR AND WIDE FOR QUIESCENT GALAXIES WITH *JWST*

In Valentino et al., 2023, we presented the results of a search for quiescent galaxies at $z > 3$ in 11 public *JWST* fields observed in the first three months, based on the homogeneous reduction of the images to fully available catalogs. This was the inception of the DAWN *JWST* Imaging Archive (DJA), an effort to homogeneously reduce all public *JWST* data and create science ready data products. This first work of the DJA was intended to showcase what is possible with the power of *JWST*, and the DJA now contains an ever expanding compilation of public imaging and spectroscopy (Heintz et al., 2024).

For this work, the final reduction of the initial 3 months of imaging resulted in a total area of 145 arc-minutes squared with an average 5σ (0.5" aperture) *F200W* depth of 28.0 mag, over $100\times$ deeper than the 3σ (2" aperture) *K_s* ($\sim 2.1\mu m$) depth of the COSMOS2020 catalog used in chapter 2 (Weaver et al., 2021). Using both the traditional *UVJ* colour selection and the novel GMM selection method presented in Chapter 2, we produced a robust sample of 80 quiescent galaxy candidates at $3 < z < 5$. In this Section, I will describe the main results of the work, in particular focusing on the contribution of the novel colour selection method I designed.

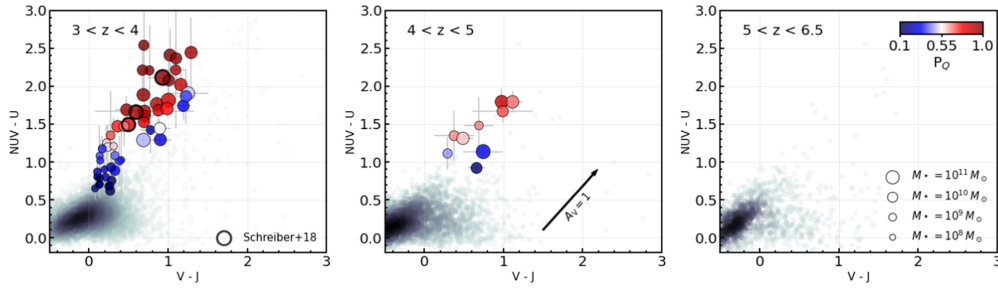


Figure 3.1: Rest frame $NUV - U$, $V - J$ colours of quiescent galaxies at $3 < z < 4$, $4 < z < 5$ and $5 < z < 6.5$ in eleven public *JWST* fields selected using the Gaussian Mixture Model method presented in Chapter 2. Galaxies are coloured by their quiescent probability $P_{Q,50\%}$ and sized according to their stellar mass. Those with a spectroscopic redshift from Schreiber et al., 2018 are circled in black. The background sample in grey shows the parent sample at those redshifts. Figure taken from Valentino et al., 2023 with permission (Figure 2. in the published article).

3.1.1 QUIESCENT GALAXY SELECTION USING THE GMM METHOD

Galaxies were selected on the basis of their rest frame $NUV - U$, $U - V$, $V - J$ colours if they had more than 50% chance ($P_{Q,50\%}$) of falling in the quiescent area of the GMM, and those with more than 70% probability ($P_{Q,70\%}$) were deemed passive, compared to the $P_{Q,50\%}$ sample deemed as recently quenched or quenching. This selection was performed via boot-strapping of the rest frame fluxes, assuming the errors are Gaussian distributed. Visual inspection of the cutouts and SEDS resulted in 50/71 (70%) and 18/20 (90%) of the $P_{Q,50\%}$ and $P_{Q,70\%}$ samples remaining (see Figure 3.1 for a projection of their colours in the $NUV - U$, $V - J$ plane).

Simultaneously, 251 galaxies were selected on the basis of their rest frame UVJ colours (allowing for their 1σ errors), but only 109/251 remained after visual inspection. The visual inspections were particularly unyielding for the candidates at $z > 5$, of which only 3/56 were kept - most were discarded due to the low quality of the SEDs. This is particularly interesting given that prior to the quiescent candidate selection, a number of selections were made on the catalogs to ensure candidates were chosen from a catalog with reliable photometry. This again highlights the advantage of using a method that a) uses more information and b) allows for a sliding scale of how candidates are selected; the resulting candidate pools in this case were of higher quality, and included much less junk to sort through post selection.

Similarly to Chapter 2, both methods select a large overlap of the same galaxies: 75% of

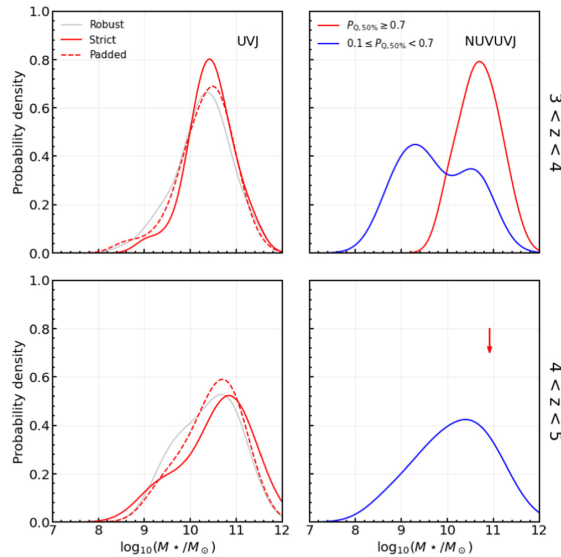


Figure 3.2: Mass probability density distributions for quiescent galaxies at $3 < z < 4$ (upper panels) and $4 < z < 5$ (lower panels) selected using both the traditional *UVJ* method (Williams et al., 2009) and the new Gaussian Mixture Model (*NUVUVJ*) method presented in Chapter 2. Interestingly, at $3 < z < 4$, the GMM method picks out lower mass quiescent galaxies when using a lower quiescent probability threshold (upper right panel, blue line). This figure is Figure C2 in the appendix of Valentino et al., 2023.

GMM selected and 50% of *UVJ* selected galaxies are within the shared sample. As expected, galaxies assigned a lower probability of quiescence were not selected by the *UVJ* method due to their bluer colours, highlighting the advantage of the GMM method for finding more recently quenched galaxies. Interestingly, these bluer galaxies which are not picked up by the *UVJ* selection were also on the lower end of the mass distribution (Figure 3.2), implying that GMM selection is more sensitive to lower mass quiescent galaxies.

3.1.2 THE BIG PICTURE AT $3 < z < 4$

In Valentino et al., 2023 we compute number densities for all galaxies in bins of redshift and mass for all fields. I focus here on the comparison to samples in the literature at fixed mass cut ($\log(M_*/M_\odot) > 10.6$), IMF and redshift range. Figure 3.3 shows the co-moving number densities of massive quiescent galaxies at $3 < z < 4$ computed by a number of works (including those computed in Chapter 2) based on both observations and simulations. Prior to 2022, it seemed that observations were not only at tension with simulations, but also themselves, with

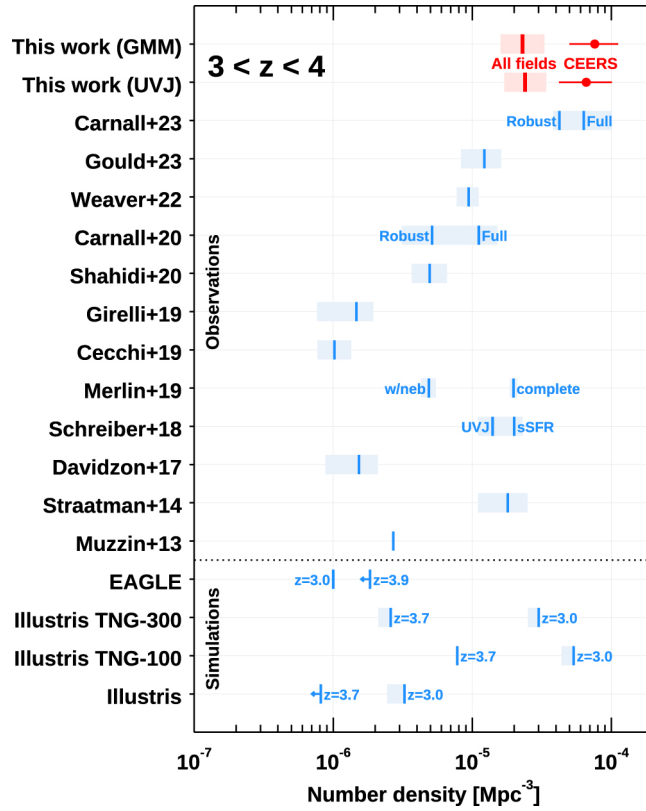


Figure 3.3: Number densities of massive ($\log(M_{*}/M_{\odot}) > 10.6$; corrected to [Chabrier, 2003](#) IMF) quiescent galaxies at $3 < z < 4$ from statistical studies over the past decade. The studies are separated into those using simulations (below dotted line) and observations (above dotted line). The number densities from 2022 converge towards an agreement towards higher number densities of order of 10^{-5} . The number densities computed from the work in Chapter 2 are shown ([Gould et al., 2023](#)) as well as the numbers discussed in this chapter (in red) ([Valentino et al., 2023](#)). This figure is Figure 5 in [Valentino et al., 2023](#).

number densities spanning an order of 2 dex. Since then, it seems that an agreement is being converged upon, at number densities on the order of 10^{-5}Mpc^{-1} , although it is interesting that in [Valentino et al., 2023](#) we find number densities twice as large as those measured using ground-based data sets, using similar selection methods ([Gould et al., 2023](#); [Weaver et al., 2022](#)). Moreover, field variation and cosmic variance play an important role, as some fields (in particular CEERS, see also [Carnall et al., 2022](#)) have even larger number densities of quiescent galaxies, and generally there are variations on the order of $2 - 3\times$ between fields. By searching across multiple fields, this study highlights the importance of conducting searches for quiescent galaxies across all possible fields and data-sets, in order to build a holistic picture of the quiescent galaxy population at $z > 3$. I will expand further on this topic in Section 3.2, where I present a search for quiescent galaxies at $z > 1$ across 5 deep lensing fields and their parallels, also observed with *JWST*.

3.1.3 LOWER MASSES, HIGHER REDSHIFTS

Prior to *JWST*, many studies selecting quiescent galaxies in photometric data imposed a stellar mass cut based on the completeness for massive galaxies, usually at $\log(M_*/M_\odot) > 10.6$. In this work, the selected quiescent galaxy samples span a wider mass range down to $9.5 < \log(M_*/M_\odot)$, with number densities consistent with those expected based on previous work ([Weaver et al., 2022](#); [Santini et al., 2022b](#)). This suggests a low mass quiescent galaxy population already assembled by $z \sim 3$, which seems to be the more the picture based on recent analyses using both ultra-deep data (size-mass relation of quiescent galaxies at $1 < z < 3$ in the UNCOVER and PRIMER fields; [Cutler et al., 2023](#)) as well as mid-infrared data from *JWST*'s MIRI instrument (identification of quiescent galaxies at $z > 3$ and $8.5 < \log(M_*/M_\odot)$ in JADES; [Alberts et al., 2023](#)).

Looking to high redshift, there are a handful of candidates at $z > 4.5$, almost all of which appear to be recently quenched based on their quiescent probability and bluer SEDs (see Figure 3.4), and one of which has a photometric redshift $z_{phot} = 5.18$, indicating the earliest epoch at which quiescent galaxies began to appear. In [Valentino et al., 2023](#), it was stated that spectroscopic observations were required to push beyond the $z > 4$ frontier and understand the beginnings of the epoch of galaxy quenching, by firstly confirming their redshifts.

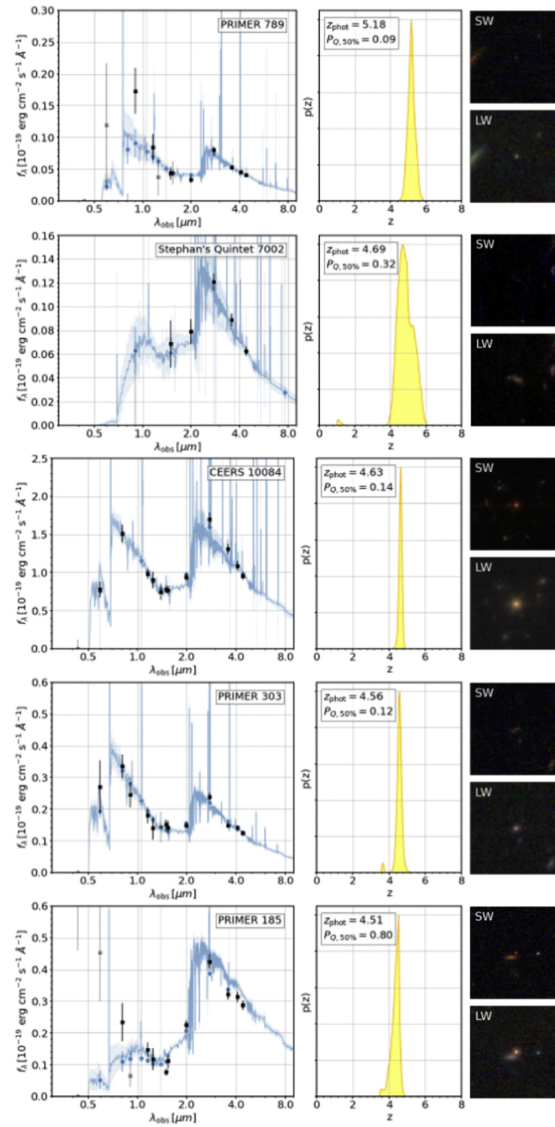


Figure 3.4: SEDs (photometry in black, best fit model in blue) of $z > 4$ quiescent galaxies selected in public *JWST* fields (this chapter; Valentino et al., 2023) using the Gaussian Mixture Model method presented in Chapter 2. To the right of each SED is the redshift probability distribution shown in yellow as well as short and long wavelength RGB image stamps. These galaxies show a wide diversity of quiescent probabilities (denoted in each panel as $P_{Q,50\%}$, and also shown by their SED shapes), suggesting a range of different evolutionary epochs. This figure is Figure 6 in Valentino et al., 2023.

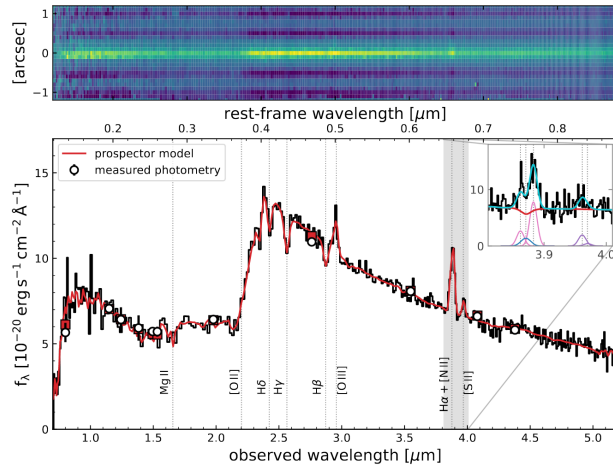


Figure 3.5: NIRSpec/PRISM spectrum (2D in upper panel, 1D in lower panel) of a quiescent galaxy at $z_{\text{spec}} = 4.896$ observed as part of the RUBIES *JWST* program (PI de Graaff; de Graaff et al., 2024 Figure 1). The spectrum has a strong Balmer break at 4000 as well multiple strong Balmer absorption lines, indicating recent star formation. Spectro-photometric modelling of the galaxy (shown in red) found it to be both massive ($\log(M_*/M_\odot)=10.9$), forming little to no stars over the past 100Myr ($\text{SFR}_{100} = 1.3M_\odot\text{yr}^{-1}$), and old ($t_{50} = 550\text{Myr}$). The inset shows the H α and [NII] $\lambda\lambda 6549, 6585$ lines, which are resolved in the G395M observations, allowing tight constraints on the low star formation rate.

Recently, CEERS-10084 (third panel in Figure 3.4) was observed as part of the RUBIES spectroscopic program (*JWST*-GO-4233^{*}; PI de Graaff) with both *JWST*PRISM and medium resolution grating G395M, confirming it as the highest redshift quiescent galaxy thus far at $z_{\text{spec}} = 4.896$ de Graaff et al., 2024 (Figure 3.5). The spectrum has a lack of strong emission lines that can be directly associated with SFR / HII regions ($\text{SFR}_{100} = 1.3M_\odot\text{yr}^{-1}$) and a clear Balmer break in the prism, confirming its quiescence. This galaxy is incredibly rare due its efficient formation, having formed half of its mass in just over half a billion years ($t_{50} = 550\text{Myr}$) and large stellar mass ($\log(M_*/M_\odot)=10.9$), highlighting the need for new recipes in simulations, which cannot produce such a galaxy at $z \sim 5$. Referring back to the question posed in Section 2.8 of Chapter 2: “Will we find old quiescent galaxies at $z > 4$ with *JWST*?” The answer is *yes!*

^{*}<https://www.stsci.edu/jwst/science-execution/program-information?id=4233>

3.2 SEARCHING DEEP FOR QUIESCENT GALAXIES WITH *JWST*/CANUCS

The second application of the GMM method to *JWST* data comes via the search for quiescent galaxies at and beyond cosmic noon in a set of five strong lensing clusters and their parallels. In this section I will introduce the CANUCS survey (the CANadian NIRISS Unbiased Cluster Survey; *JWST*-GTO-1208, PI Willott), and describe how I have used the method to select galaxies for spectroscopic follow-up with *JWST*/NIRSpec. In the previous section, I discussed the application of the selection method to a relatively wide area. The entire CANUCS area covered by NIRCам is approximately ~ 50 arc-minutes squared, almost three times smaller than the area searched in the previous section. Although the area covered is smaller, deep integration over a small area could make it possible to push the mass regime lower and search for low mass quiescent galaxies.

3.2.1 CANUCS

The CANadian NIRISS Unbiased Cluster Survey (**CANUCS**) is a Cycle 1 Guaranteed Time Observations (GTO) program (GTO-1208) led by members of the NIRISS GTO team, with the main aim of studying the properties and evolution of low mass galaxies across cosmic history via deep observations of five gravitational lensing clusters at $z \sim 0.5$ with three of the four *JWST* instruments (NIRCам, NIRISS and NIRSpec) (Willott et al., 2022, 2017). Among its chief science goals, many of which are already being realised, are to investigate extreme emission line galaxies, (Sarrouh et al., 2024; Withers et al., 2023) galaxies in the epoch of reionization (Bradač et al., 2024; Willott et al., 2023; Desprez et al., 2023; Asada et al., 2024), and complete high resolution studies (Matharu et al., 2023; Mowla et al., 2022).

Spread over a total of 200 hours of integration time, each cluster center is observed over two pointings with 7 NIRCам broad-bands and 1 medium band spanning $\sim 0.9 - 4$ microns, with the main pointing also covered with NIRISS 2 grism/3 filter combination. CANUCS makes efficient use of parallel observing to achieve this, resulting in two flanking fields for each cluster, each with a rich data set. To the north west of each cluster is the grism flanking field, named “NSF”, and to the south west are two NIRCам pointings each with the rich combination of 5 broad-bands and 9 medium bands (“NCF”). Figure 3.6 shows an example schematic of the observational configuration. All five fields benefit from some combi-

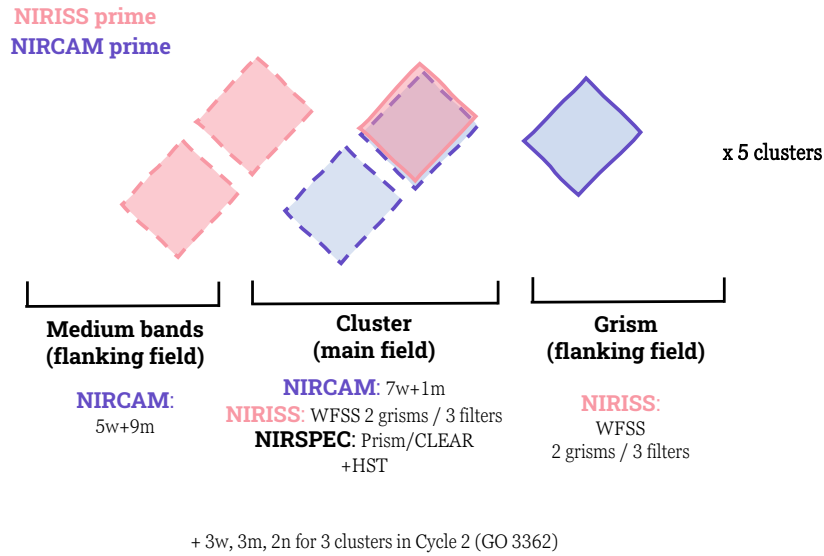


Figure 3.6: Schematic of the CANUCS observing strategy for each of the five deep lensing fields observed. The two pointings are shown in pink (NIRISS prime on the main field, NIRCAM on the flanking field) and purple (NIRCAM prime on the main field, NIRISS on the flanking field).

nation of optical and NIR data from HST observations, as well as FIR/sub-mm for MACS J0417.5–1154 from previous Herschel and ALMA programs (Fujimoto et al., 2023; Sun et al., 2022). Following the primary NIRCAM/NIRISS observations, each field is observed with low resolution NIRSpec/PRISM for approximately 3000s, limited to two pointings per field. This allows for further detailed studies of interesting candidates that arise in the first set of observations. The spectroscopy has already led to some exciting studies, including a low mass merger at $z = 5$ (Asada et al., 2023), a low mass post-starburst galaxy at the same epoch (Strait et al., 2023), and a previously optically invisible dusty star forming galaxy at $z = 3.65$, which will be discussed in Chapter 4.

3.2.2 DATA REDUCTION

The imaging reduction procedure is similar to Noirot et al., 2022 and is described in detail in Desprez et al., 2023 and Asada et al., 2024. A full description of the imaging and reduc-

tion is forth-coming (Sarrrouh&Asasa et al., in prep). I describe the image reduction briefly here. The images were first processed using the standard Space Telescope Science Institute (STScI) pipeline and the grism redshift and line analysis software (`grizli`; Brammer, 2023). The images for each cluster (which includes HST for some of them) were then drizzled onto a common pixel scale of 40 milli-arc-seconds per pixel using the Gaia DR₃ astrometry (Gaia Collaboration et al., 2023; Lindegren et al., 2021). The Brightest Cluster Galaxies and intra-cluster light (ICL) was modelled and removed for each cluster (see Martis et al., 2024) and then the images were convolved to the *F444W* Point Spread Function (PSF). Photometry was performed using a hot and cold detection mode in order to model the complexities of sources in the lensing fields. This works by detecting bright and extended sources in the “hot” mode without de-blending too much, and then going in with “cold” mode to find small and fainter sources (Galametz et al., 2013). The photometry is done with the `photutils` package (Bradley et al., 2024) via matched Kron (Kron, 1980) and circular apertures in a range of sizes for each filter image. The photometry were then corrected for galactic extinction and uncertainties were estimated by placing empty apertures and repeating the photometry procedure. For this work, I use the 0.7 arc-second aperture photometry catalog. Redshifts and rest frame *NUV*, *U*, *V*, *J* fluxes were measured using `eazy-py` (Brammer, 2021; Brammer et al., 2008), in particular the `tweak_fspqsf_12_v3` templates were used. An updated description of `eazy-py` can be found in Section 2.3 of Chapter 2.

3.2.3 SPECTROSCOPY OF QUIESCENT GALAXIES

3.2.3.1 SELECTION OF CANDIDATES

I used the GMM method to select quiescent galaxies for spectroscopic follow-up for each of the five lensing fields. For MACS 0417, both the main CLU field and NCF flanking field were observed with NIRSpec, but for all other fields only the central cluster was observed, and so NCF selections were made only for MACS 0417. The procedure was broadly the same for each cluster. I ran the GMM code using the rest frame *NUV*, *U*, *V*, *J* rest frame fluxes and their errors for each catalog in order to calculate the quiescent probability distributions and percentiles for all sources. Before selecting quiescent galaxies, I required a goodness of fit using the number of filters and χ^2 (typically reduced $\chi^2 < 5$), as well as requiring a minimum

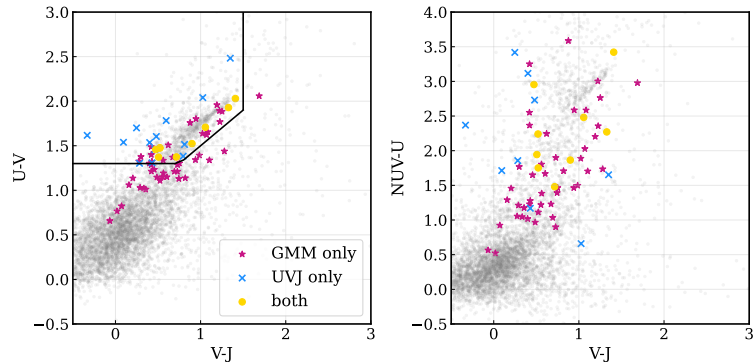


Figure 3.7: *Left:* rest frame UVJ colour diagram for MACS 0416 showing quiescent galaxy candidates selected by the GMM method only (pink stars), classical UVJ box selection (blue crosses) (Williams et al., 2009), and the intersection of both (yellow circles). The GMM selected quiescent galaxies extend both to the left of the traditional UVJ selection box (black lines) and also below it, where recently quenched galaxies are expected to be found. In the background in grey are galaxies in the same cluster brighter than $F200W$ SNR > 3. *Right:* $NUV - U$, $V - J$ projection of the same sample of galaxies.

$F200W$ SNR > 3 for the cluster fields, or $F210M$ SNR > 3 for the flanking fields. The quiescent probability criteria were loosened compared to previous works due to the nature of the selection; lowering the thresholds would prevent possibly rare and interesting transitioning galaxies from being left out of the selection. For galaxies between $1 < z < 4$, I required $P_{Q,50\%} > 0.001$, and for galaxies at $4 < z < 5$, this was loosened to $P_{Q,50\%} > 0.00001$. This decision was made after the first set of spectroscopy was done, in order to select for very recently quenched, low mass bluer galaxies like those presented in Strait et al. (2023) (from MACS0417) and Looser et al. (2023). I also applied the classical Williams et al. (2009) UVJ colour selection to explore the performance on these data. Figure 3.7 shows as an example both the UVJ and $NUVUVJ$ color diagrams with galaxies selected with each method and the intersection for the MACSJ0416.1–2403 cluster. As expected, the GMM method picks out bluer galaxies than extend below the edge of the quiescent selection area, as well as those on the border. Visual inspection of the galaxies selected by the UVJ (Williams et al., 2009) criteria but not by GMM showed that these sources had low quality SEDs or were junk, thus boosting confidence once again in the GMM method.

I then inspected the SEDs and multi-wavelength cutouts of the GMM selected galaxies for each cluster and ranked them based on the following criteria, where 1 is the highest priority:

1 - highly magnified/very bright or break/emission lines that are not observable in grism, or $z > 3$; 2 - bright or high redshift and prism observations would return a useful spectrum but the spectral coverage would not be ideal e.g. $1 < z < 2$; 3 - interesting high redshift candidate but unlikely to see much in 2.9ks of integration with the PRISM mode. It should be noted that these catalogs were used along with catalogs made by other members of the team to create the final masks, which was done by CANUCS PI C. Willott, so ranking something highly in my catalog would improve the chances of a galaxy falling in the final mask, but not guarantee its placement. Interestingly, there were a handful of quiescent galaxy candidates at $z > 3$ that did end up in the final spectroscopic follow-up catalogs, but no robust candidates at $z > 4$.

3.2.3.2 SPECTROSCOPIC REDUCTION

Spectroscopy was taken with the Multi-Object Spectroscopy (MOS) mode using the Micro-Shutter Assembly with the PRISM/CLEAR filter/grating combination, which provides low resolution coverage ($R \sim 100$) over $0.6 - 5.3\mu\text{m}$ with variable resolution, such that the blue end has an average resolution of $R \sim 60$ and the red end $R \sim 600$. Hence, the Balmer absorption lines will be observed at higher resolution for higher redshift galaxies. Each cluster was observed for three MOS configurations each 2.9ks integration time. The reduction is similar to the reduction describe in [Desprez et al. \(2023\)](#) and [Withers et al. \(2023\)](#). The level 1 data products were obtained using the STScI pipeline where the rate files were obtained from the raw data. The jump step option `expand_large_events` to remove residuals from snowballs, and a custom persistence mask was used to mask pixels that saturated after more than 1200s. `msaexp` ([Brammer, 2022](#)) was then used to do the level 2 processing including wavelength calibration, flat fielding, path-loss correction, slit-loss correction and finally create the 2D spectra. The 1D spectra were then obtained using an inverse variance weighted kernel ([Horne, 1986](#)). Finally, redshifts were fit using a basic fitting procedure in `msaexp` whereby the continuum is modelled as a series of splines and the emission and absorption lines are modelled as Gaussian curves with a fixed velocity width. For the presentation of these data we use these redshifts, but future work will involve more sophisticated fitting with the custom line fitting software presented in Chapter 4. The final catalog of spectra were visually inspected and given grades based on their redshift. The final spectra catalog was cross-checked

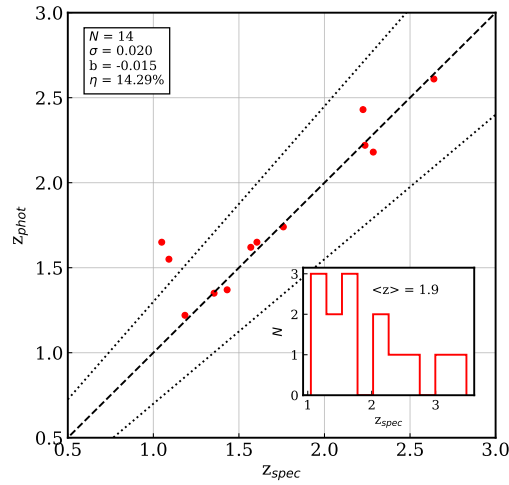


Figure 3.8: Spectroscopic vs photometric redshift for the preliminary spectroscopic sample of 14 quiescent galaxies observed with *JWST*/NIRSpec as part of the CANUCS spectroscopic follow-up over 5 lensing cluster fields. The average redshift is around cosmic noon, which is shown by the inset histogram ($\langle z_{\text{spec}} \rangle = 1.9$).

using co-ordinate matching with the quiescent galaxy candidate lists I compiled to determine matches, and then filtered by the inspection grade to include only those with robust redshifts.

3.2.3.3 A SPECTROSCOPIC SAMPLE OF QUIESCENT GALAXIES AT COSMIC NOON

Figure 3.8 shows the photometric vs spectroscopic redshifts of the preliminary sample selected with the GMM method (note that this is not the final sample as the work is still ongoing) of 14 galaxies observed across a range of redshifts from $1 < z < 4$, with a mean spectroscopic redshift of $\langle z_{\text{spec}} \rangle = 1.9$, and a highest spectroscopic redshift of $z_{\text{spec}} = 3.489$. Generally there is excellent agreement between photometric and spectroscopic redshifts, with $\sigma_{\text{NMAD}} = 0.02$.

Figures 3.9 and 3.10 show the rest frame spectra each normalised to their maximum flux and offset by an arbitrary amount on the y axis, sorted by descending redshift. These spectra exhibit Balmer breaks at a range of strengths, reflecting the flexibility of the GMM method in selecting for galaxies at a range of evolutionary stages. Both of the galaxies at $z > 3$ show prominent Balmer absorption lines as well as [OIII] $\lambda\lambda 4959, 5007$ and [NII] $\lambda\lambda 6549, 6585$

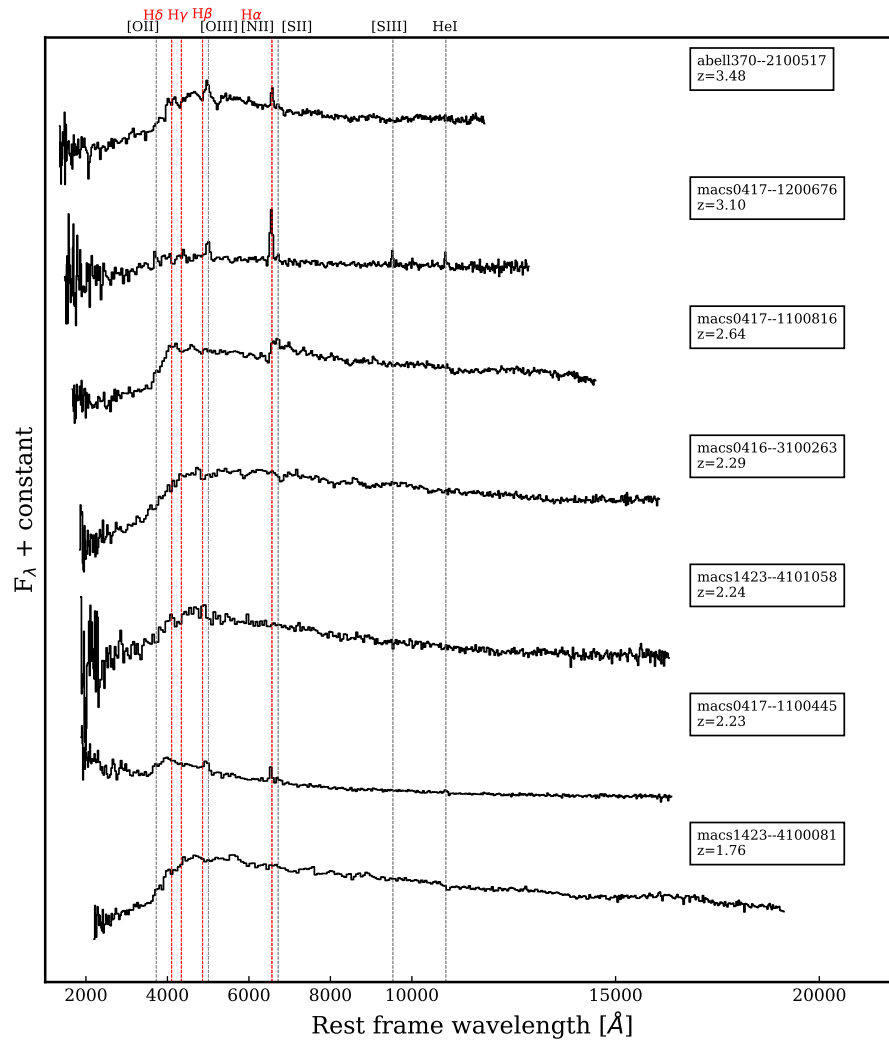


Figure 3.9: Rest frame 1D spectra of quiescent galaxies each normalised to their maximum and offset by an arbitrary amount on the y axis in order to show all of the spectra. The expected location of the Balmer line absorption series is shown by red lines, as well as other notable emission lines in black. At $z > 2$, there is a remarkable diversity in the spectral features of these galaxies, whereas at $z < 2$ (see the next figure), galaxies are more homogenous in their features.

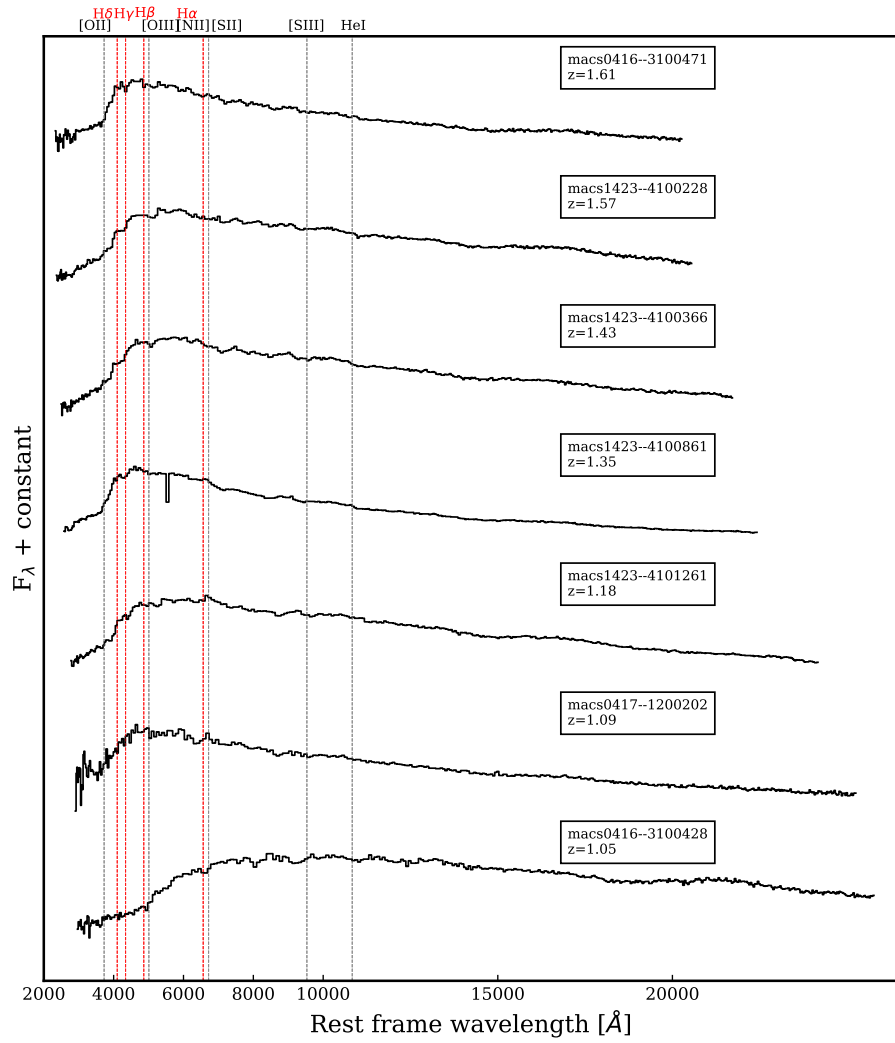


Figure 3.10: (continued)

+ H α emission, with macso417-1200676 also showing ionised sulfur [SIII] $\lambda\lambda$ 9069, 9531 and Helium HeI λ 10830 . Spectroscopic studies of MQGs at $z > 3$ have found emission lines and ratios indicating the presence of AGN (e.g. de Graaff et al., 2024; Setton et al., 2024; Carnall et al., 2023; Antwi-Danso et al., 2023; Saracco et al., 2020; Marsan et al., 2017, 2015), so it is not surprising to find such indications in our $z > 3$ spectra. All of the galaxies at $z > 2$ show a diversity in their spectral shapes, break strengths and line features compared to those at $z < 2$, which are more homogeneous and lack features besides the Balmer break. Some of these lower redshift galaxies, such as macso416-3100471 display absorption lines in H β and H δ but the low resolution will make accurately determining the H δ Lick index difficult, given it is defined at higher resolution (Balogh et al., 1999).

This sample provides many avenues for future work. Full spectro-photometric SED fitting of this sample will be done to determine the masses, assess their quiescence via H α emission, and constrain ages via SFH analysis, if possible. Furthermore, analysis of the line ratios can be done for the two highest redshift galaxies to assess AGN presence, and the presence of the sulfur lines can be used to determine the ionisation parameter using $S_{32} \equiv [\text{SIII}]\lambda\lambda 9069, 9531 / [\text{SII}]\lambda\lambda 6716, 6731$ (Kewley and Dopita, 2002). Given that the majority of the sample is resolved, this opens the door not only to measuring the sizes of these galaxies, but also their morphologies, which appear to be diverse. The cutouts in Figure 3.11 show not only compact galaxies as expected, but also disturbed morphologies. Finally, resolved photometric SED modelling could be advantageous to explore the dust and stellar populations of this sample (see e.g. Setton et al., 2024).

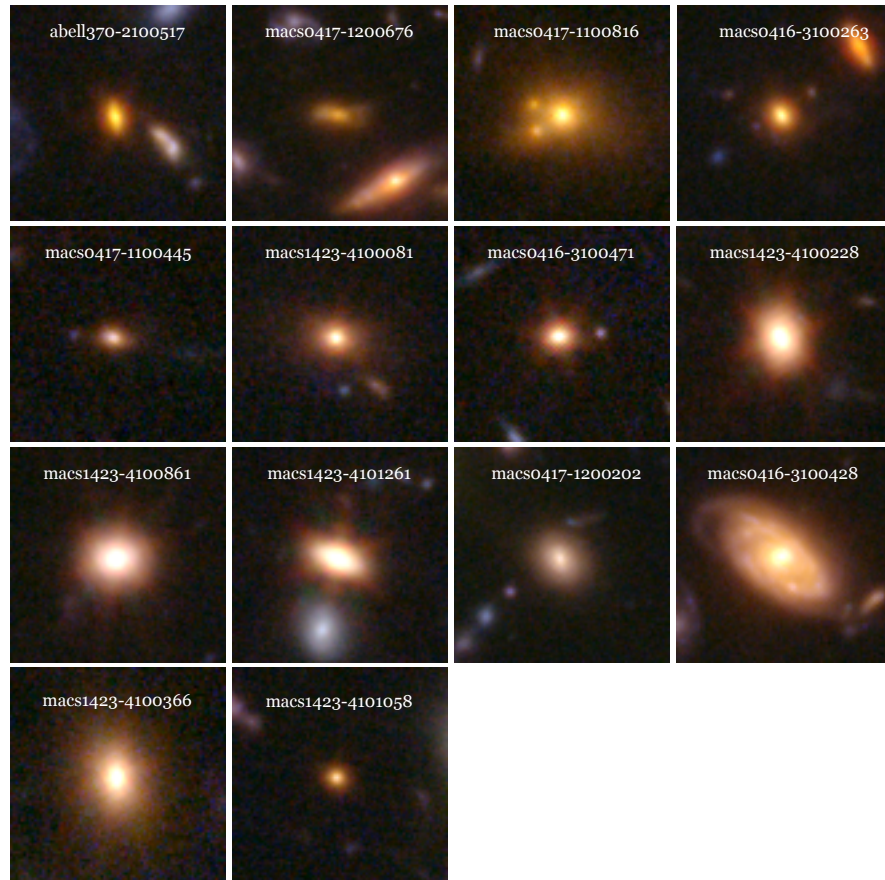


Figure 3.11: *F115W/F277W/F444W* RGB 4×4 arc-second cutouts of the quiescent galaxies shown in the previous three figures. There are a diverse range of morphologies, with some galaxies compact, some with apparent neighbours, and even a disc with clear spiral arm features.

A DISTANT RED GALAXY OBSERVED BY JWST

4

"If I take one more step, I'll be the
farthest away from home I've ever been."

Samwise Gamgee

THE FELLOWSHIP OF THE RING



This chapter contains the following article in preparation for submission to the Astrophysical Journal:

"JWST reveals the nature of an optically dark, multiply imaged, dusty star forming galaxy at $z = 3.65$ "

Authors: Katriona M. L. Gould, Gabriel Brammer, Francesco Valentino, Jasleen Matharu, Guillaume Desprez, Ghassan T. E. Sarroub, Lamiya Mowla, Victoria Strait, Chris Willott, Nicholas Martis, Roberto Abraham, Yoshi Asada, Marusa Bradac, Gaël Noirot, Kartheik Iyer, Adam Muzzin, Marcin Sawicki, Johannes Zabl, Vince Estrada-Carpenter, Kasper E Heintz

ABSTRACT

We present a spectro-photometric study of an optically invisible dusty star forming galaxy at $z_{\text{spec}} = 3.65$. The galaxy, nick-named BB, is lensed into three images by the MACSJ0417.5 – 1154 galaxy cluster with an average magnification factor of $\mu = 4.6 \pm 0.7$. This galaxy was observed as part of part of the CANadian NIRISS Unbiased Cluster Survey (CANUCS), and was previously un-detected in HST optical imaging whilst detected in FIR and sub-mm photometry as part of ALMA Lensing Cluster Survey, with a CO (4-3) spectroscopic redshift of $z_{\text{CO}} = 3.652$. We use optical to far-infrared photometry and low-resolution *JWST*/NIRSpec spectra of all three images of BB to investigate its stellar population, rest-frame optical size, and rest-frame optical interstellar medium emission. We measure blended $\text{H}\alpha + [\text{NII}]\lambda\lambda 6549, 6585$ emission lines, put an upper limit on the $\text{H}\beta$ flux, and use these lines to estimate a dust attenuation of $A_{\text{H}\alpha} > 4$, unambiguously confirming that this galaxy is extremely dusty. Standard diagnostic diagrams of additional detected emission lines, such as $[\text{OIII}]\lambda\lambda 4959, 5007$, $[\text{SII}]\lambda\lambda 6716, 6731$, $[\text{SIII}]\lambda\lambda 9069, 9531$, and $\text{HeI}\lambda 10830$, suggest a strong ionization source likely powered by an active galactic nucleus. This is also corroborated by the significant detection of the broadened He-I line. We derive an average magnification corrected stellar mass of $\log(M_*/M_\odot) = 10.3 \pm 0.2$, which combined with the SFR place this galaxy on the main sequence at $z \sim 4$. We measure a source plane half-light radius of $0.51 \pm 0.05 \mu^{-1} \text{kpc}$, finding that BB is already as compact as massive quiescent galaxies at the same epoch. This study suggests that galaxies like BB—heavily dust-obscured and forming stars at a rate consistent with the main sequence—could be common progenitors of the high-redshift MQG population.

4.1 INTRODUCTION

In the past decades, the combined power of optical and far-infrared/sub-mm telescopes has revealed a population of extremely red galaxies which are invisible or extremely faint in the optical, but bright at longer wavelengths. The first discoveries of predominantly red galaxies dates back to the early 2000's, when they were selected using new ground-based near-infrared capabilities (Franx et al., 2003). At that time, the available data lead to two main

possible conclusions: that these galaxies were high redshift $z > 3$, which was supported by the 1990's movement in Λ -CDM that extremely early galaxies must exist (e.g. [Kauffmann et al., 1993](#)), or that they were lower redshift, and either dusty or quiescent. Work over the following decades led to the discovery of a statistically significant population of galaxies at and beyond cosmic noon ($z \sim 2$) that had already accumulated significant stellar mass and had quenched their star formation ([Valentino et al., 2020](#); [Schreiber et al., 2018](#); [Straatman et al., 2014](#); [Kriek et al., 2016, 2006](#))

Concurrently, observations in the sub-mm/radio regime revealed galaxies with bright sub-mm emission but no detectable optical counter-parts, which led to the conclusion that a population of extremely dust-obscured, highly star forming galaxies (AKA dusty star forming galaxies; DSFGs) existed at $3 < z < 8$ ([Casey et al., 2021, 2014](#); [Chapman et al., 2005](#); [Smail et al., 1997](#)). Simulations struggled to both reproduce and explain these two populations both because of the difficulty in producing them at all, let alone with the observed abundance, as well as placing them in the greater context of how galaxy evolution proceeded in the first few billion years. Attempts to connect the two populations, with the sub-mm galaxies being ancestors of the massive quiescent galaxies, fell short—there are simply not enough sub-mm galaxies to explain the number of MQGs at $3 < z < 4$. Perhaps, instead, the progenitors of the first dormant galaxies could be more “normal” star-forming galaxies ([Valentino et al., 2020](#); [Wang et al., 2019](#); [Williams et al., 2019](#)). Indeed, this connection has already been made for quiescent galaxies at cosmic noon ([Toft et al., 2014](#)).

Recently, joint optical/NIR observations in deep extra-galactic fields revealed a “new” population of red galaxies, except this time, extremely faint, or invisible in the optical data, only appearing at wavelengths longer than $1\text{--}2 \mu\text{m}$. This population has been given many nicknames: “HST-dark” for those that are seen at longer wavelengths but undetected in available HST data; “HEIROS”/“NIR-galaxies”, named so because they are selected for using NIR colour information ([Sun et al., 2021](#); [Wang et al., 2019, 2016](#); [Caputi et al., 2015](#)). Thorough study of these galaxies has been limited due to several reasons. Firstly, their extremely red colours means they can only be detected using telescopes such as *Herschel* or *Spitzer*, and these data are usually too shallow, spatially unresolved, or both ([Kokorev et al., 2022](#)). Secondly, whilst dust continuum detections are cheap (minutes of integration for the brightest prototypical systems), and typically sufficient to confirm the star forming nature

of these galaxies, spectroscopic redshift confirmation with powerful interferometers, such as ALMA, is expensive due to the sensitivity and wavelength coverage required. Furthermore, FIR continuum observations provide information only about the dust content of these systems, and therefore obscured star formation and cold gas, but nothing about the stellar populations. Thus far, detailed studies have only been managed for relatively small samples of galaxies (Xiao et al., 2023b; Manning et al., 2022; Sun et al., 2021; Williams et al., 2019; Gómez-Guijarro et al., 2018; Franco et al., 2018), and statistical studies have relied on using gravitational lensing (Sun et al., 2021).

With the advent of *JWST*, the door is finally open to study the rest-frame optical properties of red galaxies in the early universe in high resolution. *JWST*'s wavelength coverage of $0.6\text{--}28\mu\text{m}$ with both imaging and spectroscopy allows us to delve into the varied populations of red galaxies that were previously difficult to study, and finally begin to forge evolutionary connections between them. Many studies have already embarked on new explorations of red galaxies, with a growing consensus that this population of red galaxies spans a diverse range of properties from extreme line emitters at $z > 6$, to dust-obscured main sequence galaxies at $z \sim 2 - 6$, to compact quiescent galaxies at $z > 3$ (Wang et al., 2024b; Kokorev et al., 2023; Williams et al., 2023; Pérez-González et al., 2022; Nelson et al., 2022). Thus far, spectroscopic studies have been few, but results thus far indicate that previously optically invisible galaxies indeed comprise a massive, main-sequence population that contributes significantly to the cosmic star formation rate density (cSFD) (Barrufet et al., 2024; Xiao et al., 2023a; Gottumukkala et al., 2023; Barrufet et al., 2023). Furthermore, observations of dust obscured galaxies at $z \sim 5 - 9$ revealed such massive galaxies that could bridge the gap between starburst galaxies and typical star forming galaxies at high redshift (Sun et al., 2024; Akins et al., 2023; McKinney et al., 2023; Williams et al., 2023), as well as a handful that are so massive that they challenge formation theories (Xiao et al., 2023a). Given the ongoing spectroscopic confirmations of similarly massive quiescent galaxies at progressively later epochs with *JWST* (Stawinski et al., 2024; de Graaff et al., 2024; Glazebrook et al., 2024; Setton et al., 2024; Carnall et al., 2023; Nanayakkara et al., 2022), and the lack of known progenitors, now it is possible to observationally explore whether more normal dust obscured galaxies at $z > 3$ may be the elusive progenitors of the massive quiescent galaxy population at $z > 3$.

In this work, we present new *JWST*/NIRCam and NIRSpec observations of a known “HST-faint” galaxy, taken as part of as part of the CANadian NIRISS Unbiased Cluster Survey (CANUCS GTO-1208; PI: Willott; Willott et al., 2022, 2017). This galaxy was first observed in the MACS J0417.5 – 1154 ($z_{\text{cluster}} = 0.443$, hereon referred to as MACS0417) as part of the ALMA Lensing Cluster Survey (Fujimoto et al., 2023; Sun et al., 2022). It is a triply-lensed source with a spectroscopic redshift of $z_{\text{spec}} = 3.652$ from the CO (4-3) emission line (Kohno et al. 2023; referred to as MACS0417 – 46/58/121 therein and also in Sun et al., 2022). Prior to *JWST* observations, this galaxy was only detected with $> 3\sigma$ significance in the FIR in both *Herschel*/SPIRE at $250\mu\text{m}$, $350\mu\text{m}$, $500\mu\text{m}$ (Sun et al., 2022), and ALMA band 6 ($\lambda = 1.15\text{mm}$). In October 2022, the galaxy was clearly detected at $> 1.5\mu\text{m}$ in CANUCS NIRCam imaging of MACS0417 and was later observed with NIRSpec’s low resolution filter/grating ($0.6 - 5.3\mu\text{m}$ PRISM/CLEAR) as part of the CANUCS spectroscopic follow-up observations in January 2023. Throughout the paper, we refer to this galaxy as the Baked Bean galaxy (BB for short), due to its visual resemblance to a baked bean. In Section 4.2, we discuss the the data and data reduction. We explain the spectrophotometric fitting and morphology measurement in Section 4.3.4. Finally, in Section 4.4, we present the results of the spectro-photometric analysis, and discuss BB in context in Section 4.5. In this analysis we use the WMAP9 flat Λ -CDM cosmology (Hinshaw et al., 2013) with $H_0 = 69.3 \text{ km s}^{-1} \text{ Mpc}^{-1}$, $\Omega_m = 0.307$ and Chabrier, 2003 IMF. All magnitudes are AB Oke and Gunn, 1983 as $m_{AB} = -2.5 \log_{10} \left(\frac{f_\nu}{3631 Jy} \right)$.

4.2 OBSERVATIONS AND DATA REDUCTION

4.2.1 PHOTOMETRY

BB was first observed in the MACS 0417 cluster ($z_{\text{cluster}} = 0.443$) as part of the ALMA Lensing Cluster Survey (ALCS: program #2018.1.00035.L, PI: K. Kohno), which observed 33 strong lensing galaxy clusters in band 6 at 1.2 mm using a two spectral scan setup spanning 15 GHz (Fujimoto et al., 2023). The galaxy (MACS0417 – 46/58/121) has a spectroscopic redshift of $z_{\text{spec}} = 3.652$ from CO (4-3) line (Sun et al., 2022; Kohno et al., 2023). It is gravitationally lensed by the cluster and appears in three places, with magnification factors

of $\sim 3 - 5$. It was also detected in Herschel SPIRE at $250\mu\text{m}$, $350\mu\text{m}$, and $500\mu\text{m}$ with high SNR of $\sim 30 - 50$ as reported by Sun et al. (2022), who presented it as an H-band dropout. It was not detected in the *HST*-selected catalog from Kokorev et al. (2022). We use the *Herschel*/SPIRE photometry from Sun et al. (2022) and ALMA photometry from Fujimoto et al. (2023), which reports a 1σ sensitivity of $84 \mu\text{Jy}/\text{beam}$ (rms) integrated over the full spectral windows. We confirm via coordinate cross-check that near-infrared emission for all sources is exactly aligned with the emission from the ALMA 1.2mm dust continuum emission.

We use NIRC*am* observations in eight filters ranging between 0.9 and $4.4 \mu\text{m}$ (F090W, F115W, F150W, F200W, F277W, F356W, F410M, and F444W), which were taken in October 2022 as part of the Canadian NIRISS Unbiased Cluster Survey (CANUCS GTO-1208; PI: Willott; Willott et al., 2022, 2017). Additionally, we use the F435W, F606W, and F814W images from *HST*/ACS observations of MACS0417 taken as part of the Reionization Lensing Cluster Survey (RELICS; HST-GO-14096, PI Coe; Coe et al. 2019). The imaging reduction procedure is similar to than performed by Noirot et al., 2022, and it is described in detail in Desprez et al., 2023 and Asada et al., 2024.

Briefly, the images were first processed using the standard Space Telescope Science Institute (STScI) pipeline and the grism redshift and line analysis software (*grizli*; Brammer, 2023). The images were then drizzled onto a common pixel scale of 40 milli-arc-seconds per pixel using the Gaia DR3 astrometry (Gaia Collaboration et al., 2023; Lindegren et al., 2021). The Brightest Cluster Galaxies (BCGs) and intra-cluster light (ICL) were modelled and removed for each target of the CANUCS survey (see Martis et al., 2024). The images were convolved to match the *F444W* Point Spread Function (PSF). The photometry was extracted with the *photutils* package (Bradley et al., 2024) via matched Kron (Kron, 1980) and circular apertures in a range of sizes for each filter image. The photometry was then corrected for galactic extinction (Schlafly and Finkbeiner, 2011) and uncertainties were estimated by placing apertures in empty regions of the sky and by repeating the photometry extraction. For this work, we use the photometry measured in $0.7''$ apertures scaled to total values within the Kron radius. These observations reach 3σ depths of F115W ~ 29.4 , F150W ~ 29.4 , F444W ~ 29.6 in $0.3''$ circular apertures; for a full table of depths we refer to Table A2 of Desprez et al., 2023. Figure 4.1 shows the F277W/F356W/F444W NIRC*am* RGB image of MACS0417

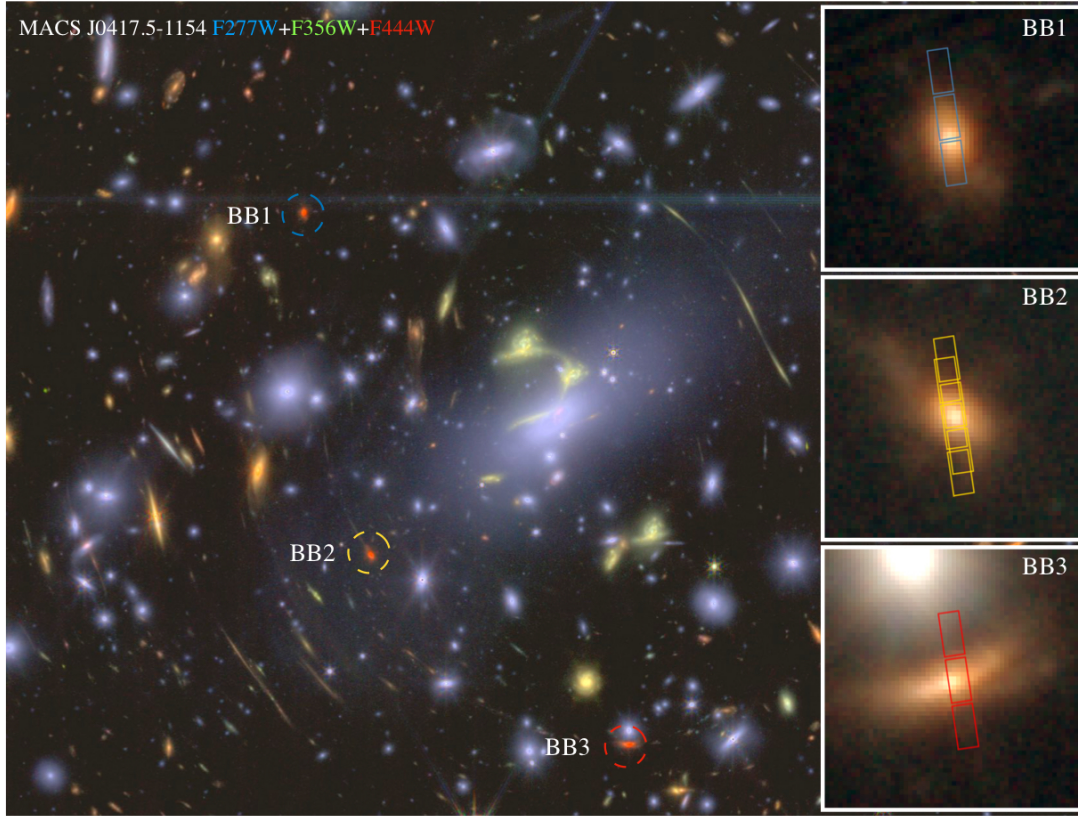


Figure 4.1: *Main panel:* F277W/F356W/F444W RGB composite image of MACS0417; each of the three lensed images of MACS0417-BB are denoted by coloured circle: BB-1 in blue, BB-2 in gold, and BB-3 in red. *Right panels:* 4×4 arc-second cutouts with the NIRSpec MSA slitlets shown.

and the locations of BB-1 (top-left), BB-2 (middle), and BB-3 (lower right). Insets showing $4 \times 4''$ cutouts show the alignment of the NIRSpec MSA slitlets.

4.2.2 SPECTROSCOPY

Low resolution ($R \sim 100$ over $0.6 - 5.3\mu\text{m}$ with variable resolution) spectra of BB-1, BB-2, and BB-3 were obtained as part of CANUCS GTO spectroscopic follow-up of MACS0417 with *JWST*/NIRSpec in January 2023 (Figure 4.2). All three images were observed using the Micro-Shutter Array (MSA) with the PRISM/CLEAR grating/filter combination for 2900 s using a three-slit nodding configuration. Level 1 data products were reduced using

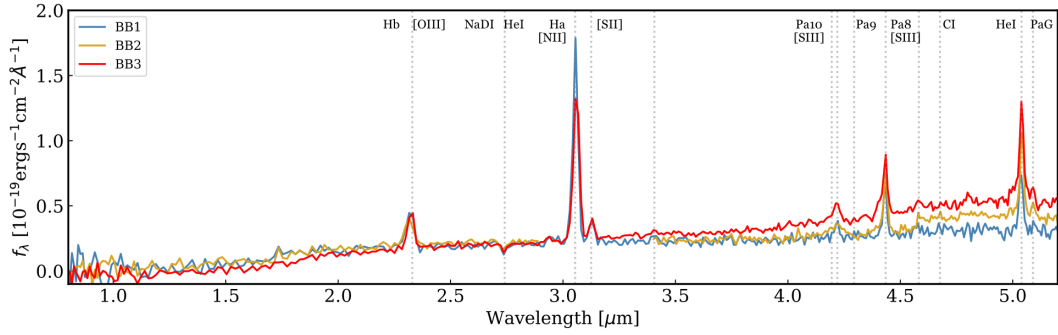


Figure 4.2: Observed frame NIRSpec/PRISM spectra of BB with prominent rest-frame optical and NIR emission / absorption lines shown. Note that the spectra of the separate lensed images show differences in their continuum shape and emission line strengths. These might arise from a combination of systematic extraction uncertainties and, potentially, from spectrally distinct sub regions of the resolved lensed images probed by the small NIRSpec MSA shutters (Fig. 4.1).

the *JWST* Pipeline, whilst Level 2 and 3 products were reduced using MSAEXP (Brammer, 2022). MSAEXP removes the background by taking differences of the nodded exposures and extracts an optimally-weighted 1D spectrum (Horne, 1986). Scaling of the spectra to the NIRCам photometry to account for losses from the small MSA shutters is performed as part of the fitting analysis described in Section 4.3.4. Additionally NIRISS slitless spectra were obtained in the F115W, F150W, and F200W bands, though unfortunately these do not sample any of the strong optical emission lines at the redshift of BB.

4.3 METHODS

In this section, we present the methods of the spectro-photometric fitting and size measurement. We conduct our multi-wavelength photometric analysis on all three images independently in the image plane (i.e., the observed data of the images magnified and distorted by gravitational lensing by the foreground cluster), and the majority of the spectro-photometric analysis on BB-1 and BB-3, as the spectrum of BB-2 has a significant detector gap between 3 – 4.5 μm where the key $H\alpha$ line falls.

4.3.1 CORRECTING FOR SLIT LOSSES

We scale the spectra to match the photometry in 8 NIRCcam bands by integrating the spectra through the filter bandpasses, and then fitting a second degree polynomial to the ratio of the observed to the synthetic photometry. This results in a correction factor of $1 - 3\times$. Substantial slit losses are to be expected considering the extension of the source outside the slit (Fig. 4.12). We anticipate little bias due to colour gradients or clumpiness, given the galaxy appearance in the NIRCcam images, and only very minor colour gradients measured (see Section 4.4.6.1). We proceed all spectral fitting with these slit-loss corrected spectra.

4.3.2 STRONG LENSING CORRECTION

We use the latest MACS0417 lens model generated by the CANUCS team (Desprez et al. in prep), which includes constraints from newly-discovered multiply imaged galaxies (see also Desprez et al., 2023; Strait et al., 2023; Asada et al., 2023). Because the general model is not optimised for our specific target, we reconfigure the model and run a custom analysis. We estimate the best fit magnification factor μ and its 1σ errors from the 16th and 84th percentiles of the posterior distribution from the optimisation. We find magnification factors consistent with those reported in Sun et al. (2022) for all three images (see Table 4.2). Whilst BB-1 is not severely distorted by lensing, both BB-2 and BB-3 show significant shear, and BB-3 appears to be doubly lensed by both the cluster and one of the brightest cluster galaxies. The light from the nearby cluster galaxy likely does not affect the modelling due to the removal of the BCG model prior to photometry, and the background subtraction that is applied when reducing the 2D spectra.

4.3.3 PHOTOMETRIC FITTING

We perform photometric SED fitting of each lensed image of the galaxy using two independent spectral energy distribution fitting codes: eazy-py (Gould et al., 2023; Brammer, 2021; Brammer et al., 2008) and STARDUST (Kokorev et al., 2021) in order to place constraints on the stellar populations using multiple methods. Photometric redshifts, stellar masses, star formation rates, V band dust attenuation (A_V), and $U - V$, $V - J$ rest-frame colours were

inferred with eazy-py* (Brammer, 2021) using all available *HST* and NIRC*am* photometry and adopting the latest tweak_fsp_s_QSF_12_v3 templates set. We derive alternative estimates of these quantities, as well as additional properties (L_{IR}), dust properties (A_V , dust mass M_{dust} , total SFR, IR AGN luminosity L_{AGN}), using the panchromatic SED fitting code STARDUST (Kokorev et al., 2021), which models the multi-wavelength emission from stars (Brammer et al., 2008), dust (Draine and Li, 2007; Draine et al., 2014) and AGN (Mullaney et al., 2011) without assuming the principle of energy balance. We fit all available photometry from *HST*, *JWST*, *Herschel*, and ALMA. For each fitting run, we fix the redshift to the estimate from the CO line detection $z_{\text{CO}(4-3)} = 3.652$, leaving all other parameters free.

4.3.4 SPECTROSCOPIC FITTING

To determine the redshift, line fluxes, velocity widths and equivalent widths from the rest-frame optical spectra, we use the novel Bayesian fitting software Spectrum Analysis Kit (speakeazy). speakeazy is specifically tailored for spectra taken using instruments with low resolution and/or variable resolution, such as *JWST*/NIRSpec’s PRISM/CLEAR configuration. Because the code is designed as a line fitting machine, minimal assumptions are used during fitting.

4.3.4.1 MODELS

The model consists of a stellar continuum component modelled using a fixed number of spline functions, as well as a library of emission and/or absorption lines, which are automatically chosen based on the redshift and instrument grating. All lines are modelled using 1D Gaussian curves. For a given line, the model is defined as a single Gaussian L_i with width σ_i , which depends on both an intrinsic velocity width v [km s^{-1}] as well as the wavelength dependent resolution curve, defined as $R = \frac{\Delta\lambda}{\lambda}$ at wavelength λ , where $\Delta\lambda$ is measured as a FWHM. We modify this using a rational scaling factor s_R to account for deviations from the instrument resolution curve (see de Graaff et al., 2023), which is multiplied by $2\ln(2)$ to

*<https://github.com/gbrammer/eazy-py>

convert it to a FWHM.

$$L_i = \frac{1}{\sqrt{2\pi\sigma_i^2}} \exp\left(-\frac{(\lambda - \lambda_i)^2}{2\sigma_i^2}\right) \quad (4.1)$$

$$\sigma_i^2 = \left[\left(\frac{v}{c}\right)^2 + \left(\frac{1}{2\sqrt{2\ln(2)}s_R R(\lambda_i)}\right)^2 \right] \lambda_i^2, \quad (4.2)$$

where $\lambda_i = \lambda_{\text{rest},i} \cdot (1+z)$ is the observed-frame wavelength of the line. Models are generated on the fly and the errors are estimated by sampling the full posterior space which is shaped by a minimal set of priors.

4.3.4.2 PRIORS

There is a number of options available for setting priors as either Gaussian or uniform. As a default, the redshift is set as a Gaussian prior around the best-fit redshift derived during the initial fit (or a given redshift by the user). s_R and velocity width v [km s^{-1}] are by default set to flat priors, but a future version of the code will include a joint prior which is currently in development. Additionally, we include a 2nd order polynomial to scale the spectral errors to account for unknown systematics during reduction from 2D to 1D spectra. Finally, the user has an option to allow for an extra set of broad line components in addition to narrow components for specified lines.

4.3.4.3 SAMPLING

An initial fit is found using a bounded least squares method. This initial solution is then used as a starting point for sampling using *EMCEE* (Foreman-Mackey et al., 2013), where the “walkers” are initialised from the prior distributions for z , v , s_R , and the error scaling coefficients, and from the covariance matrix of the line fluxes. Users have the option to run sampling either serial or using multiprocessing with a chosen number of cores, and can also choose the number of walkers per parameter, which we nominally set to 3 as recommended by Foreman-Mackey et al. (2013).

Defining a convergence criterion in a parameter space with high dimensions (often 20–100 depending on the priors) motivated the choice of a custom criterion instead of using the recommended method of using the auto-correlation time. We define that convergence is achieved when the relative change of the standard distribution for all walkers and all parameters is less than 10% for at least 1000 steps, and is checked every 500 steps. Once convergence is achieved, we discard the first 10,000 steps as burn-in and thin the chain with a thinning factor of 10. Derived quantities are taken as the median of the posterior distribution, with 1σ errors measured using the 16th and 84th percentiles of the flat samples.

4.3.4.4 FINAL FITTING SETUP

We fit the slit loss corrected spectra of BB-1 and BB-3 with the following setup. We model the continuum using a fixed number of splines ($n_{\text{spline}} = 21$). We set a loose Gaussian prior on the redshift ($z = 3.65 \pm 0.001$), flat prior on the line velocity ($1 < v < 1000 \text{ km s}^{-1}$), flat prior on the dispersion curve scaling ($1 < s_R < 2$), and we allow for a second degree polynomial error scaling, where we set a flat prior on the average error scaling ($1 < s_e < 3$). Initially, the code optimises for the best-fit redshift and line fluxes at fixed v , s_R , which are set to the median of the prior distribution. For the initial fit, we set a bound of > 2 on the $[\text{NII}]\lambda\lambda 6549, 6585 / \text{H}\alpha$ ratio, motivated by ratios of similarly red galaxies observed with *JWST* (de Graaff et al., in prep) and during sampling we set a lognormal prior on this ratio with shape parameter $s=1.3$, $\text{mean}=0.5$, and $\text{sigma}=3$.

4.3.5 PHYSICAL PROPERTIES MEASURED FROM LINE FLUXES

Following the method outlined in Domínguez et al. (2013) (see also Matharu et al. 2023), we use the Balmer decrement $\text{H}\alpha/\text{H}\beta$ to calculate the colour excess $E(\text{B-V})$ using the Calzetti et al. (2000) extinction curve and assuming case B recombination, for which the intrinsic $\text{H}\alpha/\text{H}\beta$ ratio is 2.79 (Reddy et al., 2023b). We then use this to infer the attenuation for $\text{H}\alpha$ ($A_{\text{H}\alpha}$). We measure the SFR from the dust corrected, magnification corrected $\text{H}\alpha$ flux following the prescription from Kennicutt (1998), using the correction from Muzzin et al. (2009) to convert from Salpeter Salpeter (1955) to Chabrier (2003) IMF.

	$BB - 1$	$BB - 3$	$BB - 2$
R.A. [deg]	64.404262	64.398569	64.388845
Decl. [deg]	-11.905519	-11.914794	-11.917598
F444W [mag]	22.70 $^{+0.00}_{-0.00}$	22.14 $^{+0.00}_{-0.00}$	22.45 $^{+0.00}_{-0.00}$
F150W [mag]	25.93 $^{+0.11}_{-0.10}$	27.75 $^{+0.87}_{-0.48}$	25.90 $^{+0.15}_{-0.13}$
F115W [mag]	29.44 $^{+1.24}_{-1.38}$	25.89 $^{+0.14}_{-0.12}$	28.08 $^{+0.32}_{-0.78}$
μ	4.3 $^{0.35}_{0.98}$	6.1 $^{0.51}_{-0.73}$	3.4 $^{0.14}_{0.11}$

Table 4.1: Summary of the basic observational quantities for each of the images of BB. From top to bottom: Right Ascension (degrees), Declination (degrees), observed F444W, F150W, and F115W magnitudes measured from 0.7 arc-second apertures, scalar lensing correction factor μ measured from the updated lensing model for MACS0417 (Desprez et al., in prep).

4.3.6 SIZE

We measure the size of BB-1 in the image plane for this work, while we defer a full morphological analysis of all lensed images to future work. At $z = 3.65$, rest-frame V is approximately covered by the F277W filter, which was thus used to model the stellar emission of our target. We measure the radius containing 50% of the galaxy’s light (r_{50}) using *imcascade*[†] (Miller and van Dokkum, 2021), which adopts a Multi-Gaussian Expansion approach to decompose PSFs and to model galaxies with a “cascade” of Gaussian curves.

4.4 RESULTS

Figures 4.3, 4.4 and 4.5 show all available data for BB-1 BB-2 and BB-3. The photometry from $\sim 0.4 \mu\text{m} - 1.15 \text{ mm}$ is shown along with the *JWST*/NIRSpec PRISM spectra. All data are shown on top of the best-fit STARDUST model fixed at $z_{\text{spec}} = 3.652$, which is fit only to the photometry. In Table 4.2 we present all derived quantities. If relevant, quantities are explicitly presented corrected for the indicated scalar magnification factor, μ .

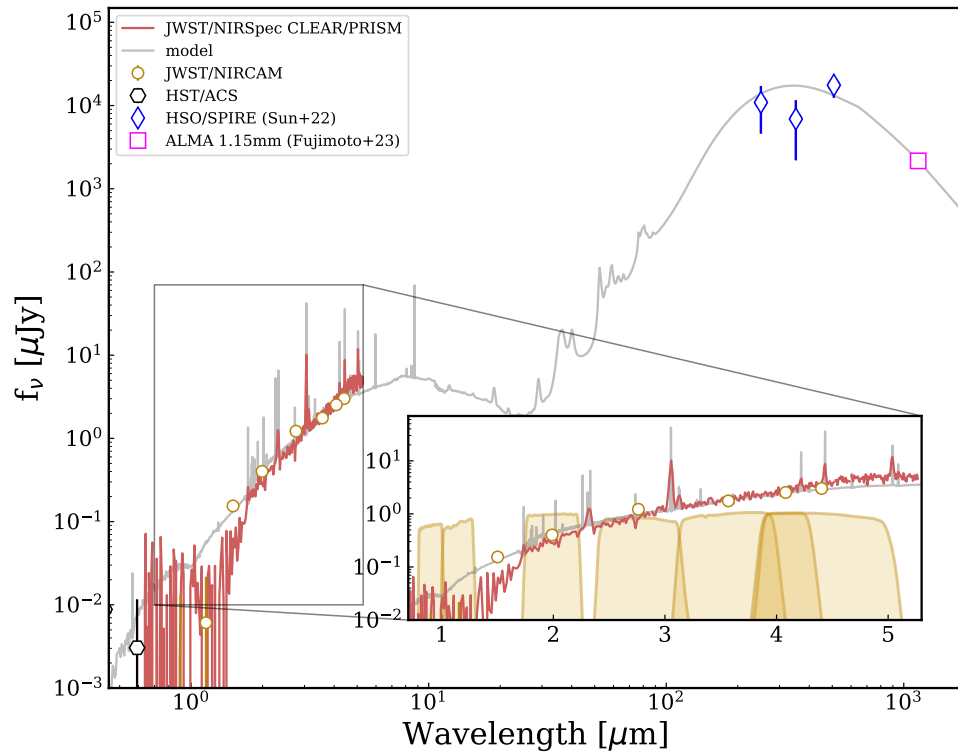


Figure 4.3: SED schematic of BB1, where data are shown on the best fit STARDUST model (grey), which is fit to multi-wavelength photometry (*HST* in black, NIRC*am* in gold, *Herschel* in blue (Sun et al., 2022), ALMA 1.15mm in pink (Fujimoto et al., 2023). The inset shows the PRISM spectrum (red) scaled to the NIRC*am* photometry (gold). The NIRC*am* bandpasses are shown in gold in the inset.

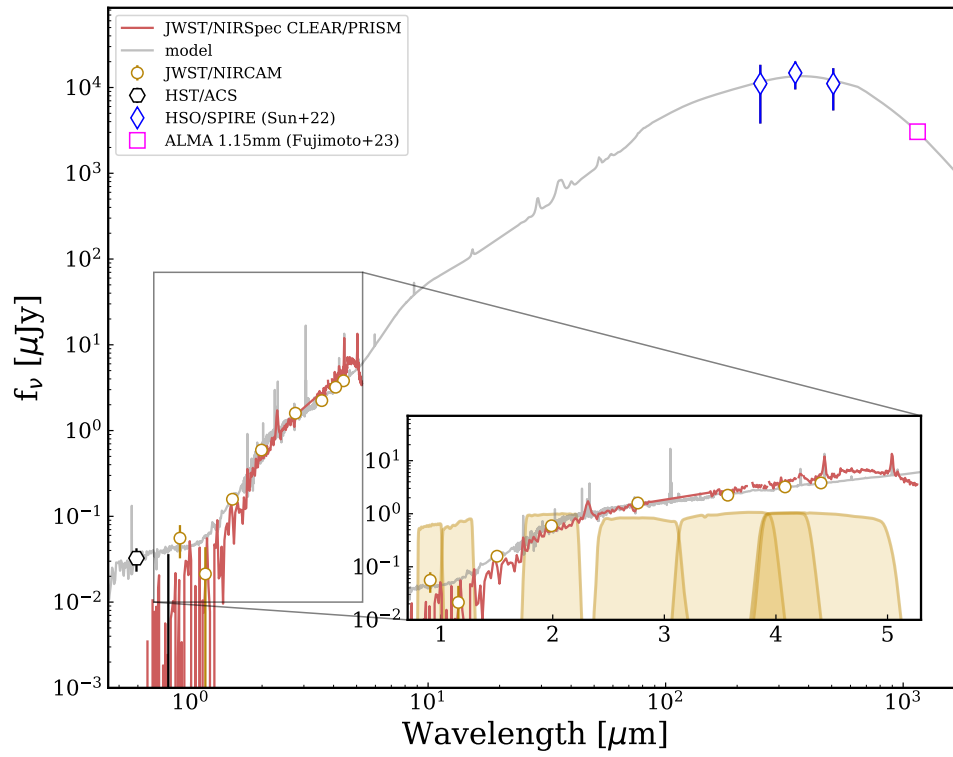


Figure 4.4: Same as Figure 4.3 but for BB2.

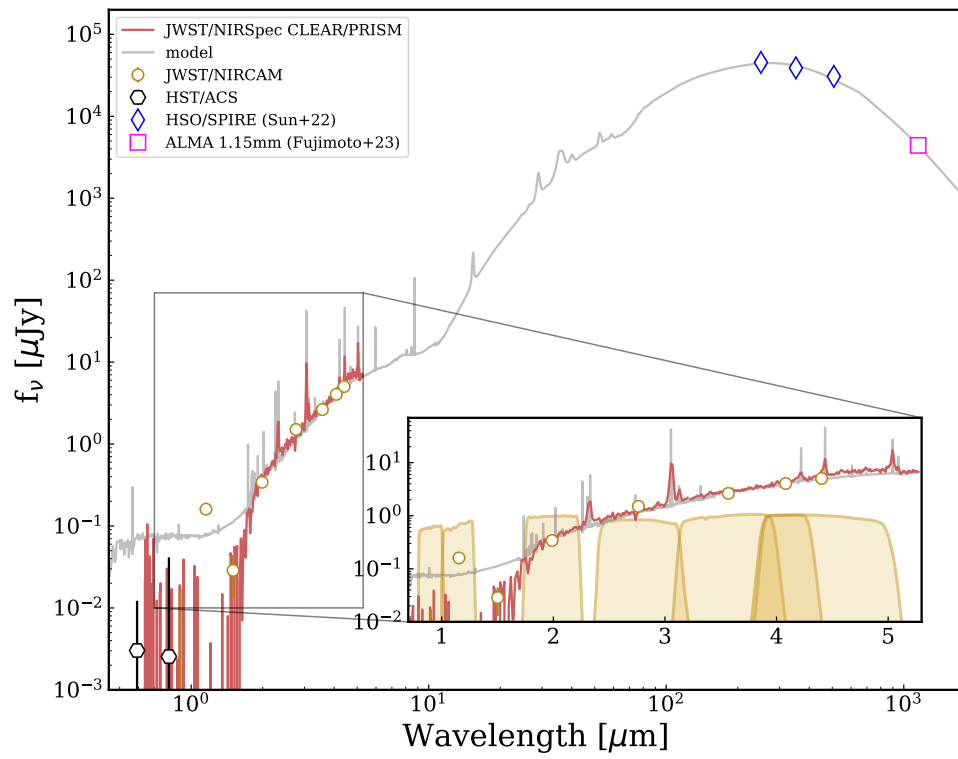


Figure 4.5: Same as Figure 4.3 but for BB₃.

	<i>BB</i> - 1	<i>BB</i> - 3	<i>BB</i> - 2
eazy-py			
z_{phot}	$3.54^{+0.07}_{-0.29}$	$3.50^{+0.05}_{-0.04}$	$3.53^{+0.10}_{-0.03}$
$\log(\mu^{-1}M_*/M_\odot)$	$10.02^{+0.56}_{-0.38}$	$10.57^{+0.64}_{-0.21}$	$10.21^{+0.57}_{-0.36}$
A_V (mag)	$3.65^{+0.04}_{-0.14}$	$3.49^{+0.12}_{-0.11}$	$3.58^{+0.10}_{-0.17}$
$\text{SFR} \log(\mu^{-1}M_\odot/\text{yr}^{-1})$	$1.95^{+0.50}_{-0.38}$	$1.94^{+0.62}_{-0.27}$	$2.07^{+0.52}_{-0.39}$
STARDUST			
$\log(\mu^{-1}M_*/M_\odot)$	10.15 ± 0.04	10.56 ± 0.02	10.64 ± 0.06
$\log(\mu^{-1}M_{dust}/M_\odot)$	8.31 ± 7.24	8.48 ± 0.28	8.82 ± 2.99
$\text{SFR}_{optical} \log(\mu^{-1}M_\odot/\text{yr}^{-1})$	1.33 ± 0.01	1.37 ± 0.07	0.75 ± 0.29
$\text{SFR}_{total} \log(\mu^{-1}M_\odot/\text{yr}^{-1})$	2.18 ± 0.14	2.81 ± 0.02	2.38 ± 0.12
A_V (mag)	2.46 ± 0.00	2.88 ± 0.00	0.53 ± 0.00
$L_{IR} \log(\mu^{-1}L_\odot)$	12.18 ± 0.14	12.81 ± 0.02	12.50 ± 0.21
$L_{AGN} \log(\mu^{-1}L_\odot)$	$< 10.47(1\sigma)$	$< 11.66(1\sigma)$	11.88 ± 0.72
f_{AGN}	0 ± 0.04	0 ± 0.33	0.25 ± 0.45

Table 4.2: Inferred galaxy properties from SED fitting. Using eazy-py to fit the 0.4 – 4.4 μm photometry from both *HST*/ACS and *JWST*/NIRCam we infer the magnification corrected stellar mass $\log(\mu^{-1}M_*/M_\odot)$, *V* band dust attenuation A_V , and magnification and dust corrected optical star formation rate $\text{SFR} \log(M_\odot/\mu\text{yr}^{-1})$. Using STARDUST to fit the 0.4 – 1150 μm photometry from *HST*/ACS, *JWST*/NIRCam, *Herschel*/SPIRE and ALMA, we infer the following global properties: magnification corrected stellar mass $\log(M_*/\mu M_\odot)$, magnification corrected dust mass $\log(M_{dust}/\mu M_\odot)$, optical SFR $\text{SFR}_{optical} \log(M_\odot/\mu\text{yr}^{-1})$, total SFR $\text{SFR}_{total} \log(M_\odot/\mu\text{yr}^{-1})$, *V* band dust attenuation A_V , magnification corrected IR luminosity $L_{IR} \log(L_\odot/\mu)$, magnification corrected AGN luminosity $L_{AGN} \log(L_\odot/\mu)$, and AGN fraction f_{AGN} , which is the fractional contribution of the AGN luminosity to the total infrared luminosity.

	<i>BB</i> - 1	<i>BB</i> - 3
z_{spec}	3.6500 ± 0.0007	3.6535 ± 0.0004
$A_{H\alpha} (H\alpha/H\beta)$ [mag]	$4.39^{+1.94}_{-1.16}$	$4.50^{+2.19}_{-1.31}$
$SFR_{H\alpha, dust\ corrected} \log(M_{\odot}/\mu yr^{-1})$	$1.43^{+2.23}_{-0.29}$	$1.19^{+2.83}_{-0.31}$
$\log(sSFR\ yr^{-1})(EW(H\alpha))$	$-8.47^{+0.10}_{-0.09}$	$-8.70^{+0.06}_{-0.06}$
$\log(U)$	$-2.47^{+0.10}_{-0.10}$	$-2.34^{+0.08}_{-0.08}$
FWHM [km s ⁻¹]	962^{+156}_{-164}	1372^{+179}_{-172}
$\log([NII]\lambda\lambda 6549, 6585 / H\alpha)$	$-0.04^{+0.14}_{-0.17}$	$0.25^{+0.02}_{-0.03}$
$\log([SII]\lambda\lambda 6716, 6731 / H\alpha)$	$-0.71^{+0.08}_{-0.09}$	$-0.50^{+0.05}_{-0.05}$
$\log([OIII]\lambda\lambda 4959, 5007 / H\beta)$	$1.04^{+0.41}_{-0.24}$	$1.33^{+0.47}_{-0.28}$
$\log(S_3)$	$0.47^{+0.10}_{-0.09}$	$0.59^{+0.09}_{-0.09}$
$\log(S_{32})$	$0.12^{+0.08}_{-0.08}$	$0.23^{+0.07}_{-0.06}$
$H\alpha / H\beta$	$21.05^{+34.88}_{-12.20}$	$17.73^{+37.76}_{-58.00}$

Table 4.3: Inferred galaxy properties from spectroscopic fitting for *BB*-1 and *BB*-3 - spectroscopic redshift z_{spec} , Attenuation to $H\alpha$ $A_{H\alpha} (H\alpha/H\beta)$ [mag], dust and magnification corrected SFR measured from the $H\alpha$ flux $SFR_{H\alpha, dust\ corrected} \log(M_{\odot}/\mu yr^{-1})$, specific star formation rate inferred from the rest-frame equivalent width of $H\alpha$ $\log(sSFR\ yr^{-1})(EW(H\alpha))$ (Mármol-Queraltó et al., 2016), ionization parameter $\log(U)$ inferred from S_{32} , (Kewley and Dopita, 2002), standard ionization diagnostic line ratios $\log([NII]\lambda\lambda 6549, 6585 / H\alpha)$, $\log([SII]\lambda\lambda 6716, 6731 / H\alpha)$, $\log([OIII]\lambda\lambda 4959, 5007 / H\beta)$ (Baldwin et al., 1981), and sulfur line ratios $S_3 \equiv [SII]\lambda 9531 / [SIII]\lambda 9069$ and $S_{32} \equiv [SIII]\lambda\lambda 9069, 9531 / [SII]\lambda\lambda 6716, 6731$ and the Balmer decrement $H\alpha / H\beta$.

Table 4.4: Magnification corrected line fluxes of BB-1 and BB-3 measured from 0.6 – 5.3 μ m low resolution NIRSpec PRISM/CLEAR spectra. Note that the fluxes in this table are not dust corrected.

Line	<i>BB</i> – 1		<i>BB</i> – 3	
	Flux (10^{-19} erg s $^{-1}$ cm $^{-2}$ μ^{-1})	SNR	Flux (10^{-19} erg s $^{-1}$ cm $^{-2}$ μ^{-1})	SNR
H β	15^{+14}_{-14}	<3	8^{+13}_{-13}	<3
H γ	-17^{+15}_{-15}	<3	-17^{+15}_{-15}	<3
H δ	10^{+18}_{-19}	<3	-15^{+18}_{-18}	<3
H α	432^{+78}_{-66}	6	314^{+17}_{-13}	22
[NII] $\lambda\lambda$ 6549, 6585	392^{+69}_{-79}	5	559^{+17}_{-19}	31
[OIII] $\lambda\lambda$ 4959, 5007	194^{+20}_{-19}	10	262^{+18}_{-18}	15
[SII] $\lambda\lambda$ 6716, 6731	87^{+13}_{-12}	7	103^{+11}_{-11}	9
[SIII] λ 9069	55^{+10}_{-10}	6	67^{+11}_{-11}	6
[SIII] λ 9531	184^{+29}_{-27}	6	294^{+37}_{-33}	8
OI λ 6302	23^{+16}_{-16}	<3	38^{+14}_{-14}	3
PaD	15^{+12}_{-12}	<3	3^{+12}_{-12}	<3
PaG	21^{+15}_{-15}	<3	25^{+12}_{-13}	<3
HeI λ 10830	186^{+18}_{-17}	11	266^{+19}_{-18}	15
Pa8	-30^{+28}_{-29}	<3	-118^{+31}_{-32}	4
Pa9	3^{+11}_{-11}	<3	-13^{+10}_{-11}	<3
Pa10	-2^{+10}_{-10}	<3	26^{+11}_{-11}	<3
HeI λ 5877	-15^{+25}_{-25}	<3	-24^{+22}_{-22}	<3
Cl λ 9580	24^{+12}_{-12}	<3	28^{+12}_{-12}	<3
NaDI	-26^{+26}_{-26}	<3	-19^{+22}_{-22}	<3

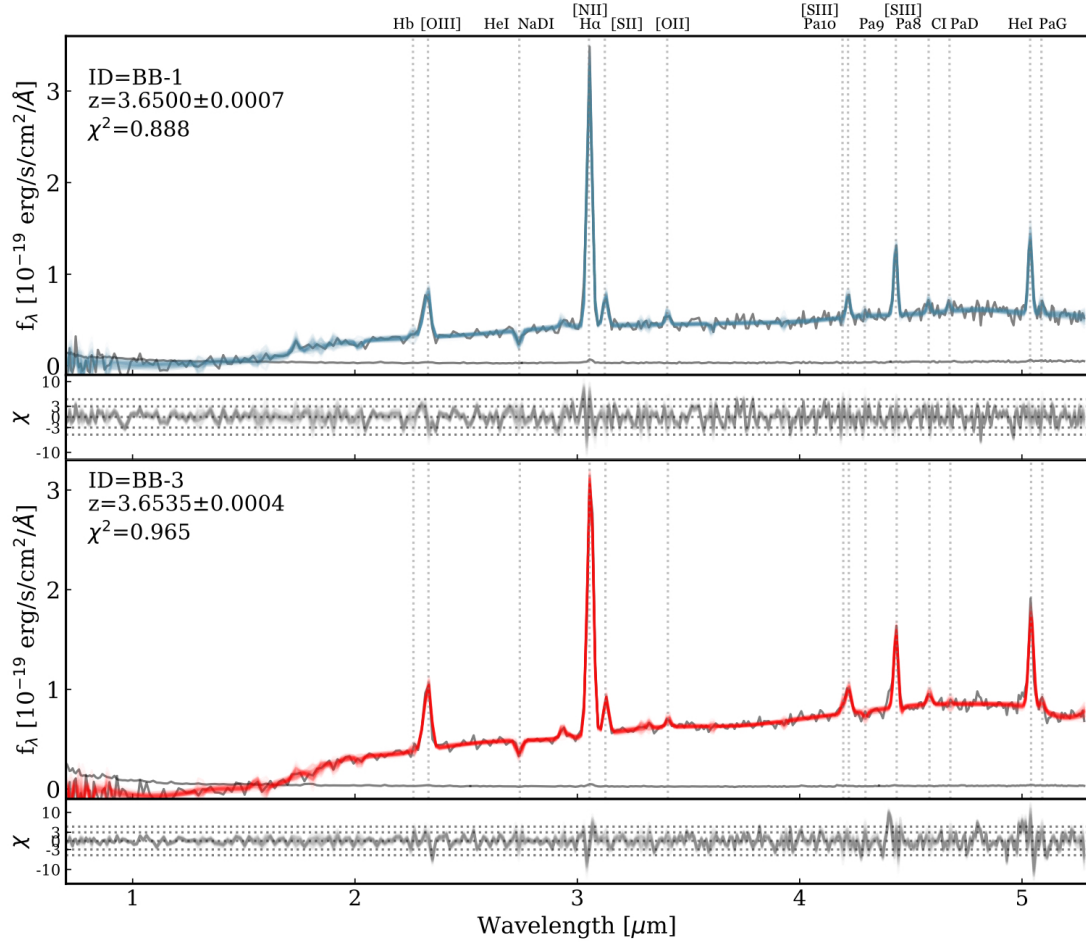


Figure 4.6: NIRSPEC/PRISM photometry scaled spectra of BB-1 (upper panel) and BB-3 (lower panel) and 1σ uncertainties (grey line) with 100 models randomly drawn from the posterior in blue/red. The residuals (χ) in units of σ are shown in a panel below each spectra, and for BB-3 there are significant ($\sim 10\sigma$) residuals around the [SIII] $\lambda\lambda$ 9069, 9531 and HeI λ 10830 lines, indicating possible broad line components.

Table 4.5: Rest-frame line equivalent widths for the set of well-detected lines measured from $0.6 - 5.3\mu\text{m}$ low resolution NIRSpec PRISM/CLEAR spectra of BB-1 and BB-3 (measured in the image plane, i.e. not corrected for magnification).

Line	<i>BB</i> - 1		<i>BB</i> - 3	
	rest-frame EW (\AA)	SNR	rest-frame EW (\AA)	SNR
H α	126_{-6}^{+8}	19	215_{-32}^{+37}	6
[NII] $\lambda\lambda 6549, 6585$	223_{-9}^{+12}	21	194_{-38}^{+38}	5
[OIII] $\lambda\lambda 4959, 5007$	142_{-10}^{+13}	13	136_{-14}^{+13}	10
[SII] $\lambda\lambda 6716, 6731$	40_{-5}^{+6}	8	43_{-6}^{+6}	7
[SIII] $\lambda 9069$	19_{-4}^{+3}	5	22_{-4}^{+4}	6
[SIII] $\lambda 9531$	77_{-9}^{+10}	8	72_{-11}^{+11}	7
HeI $\lambda 10830$	70_{-5}^{+7}	12	69_{-7}^{+8}	9

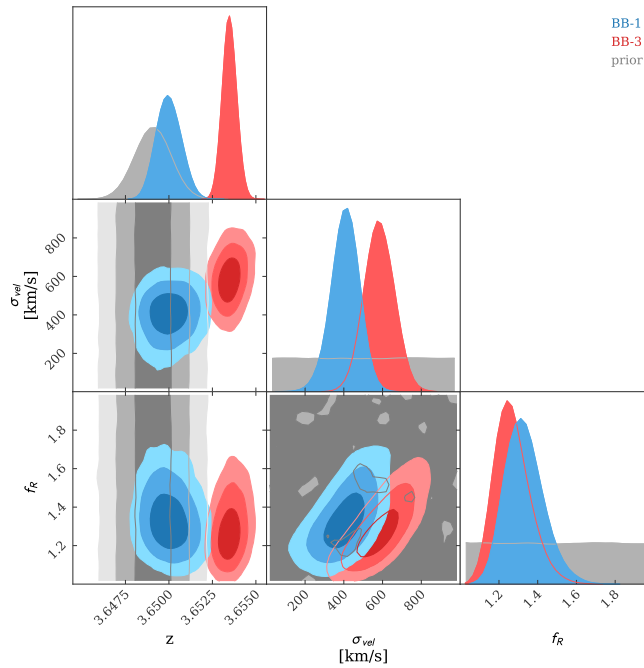


Figure 4.7: Posterior distributions of redshift, velocity dispersion and resolution curve scaling factor for BB1 (blue) BB3 (red) and the priors (grey).

4.4.1 REDSHIFT AND LINE WIDTHS

Figure 4.6 show the slit-loss corrected PRISM spectra and 100 random models drawn from the posterior parameters (blue for BB-1, red for BB-3). We find reduced $\chi^2 \sim 1$ with only minor error scaling required (errors are boosted by an average of $\sim \times 1.5$ for both spectra during the fitting procedure). The spectra have redshift solutions that lie directly either side of the CO (4-3) redshift $z_{CO} = 3.652$ from Kohno et al. (2023), with BB-1 at $z_{spec} = 3.6500 \pm 0.0007$ and BB-3 at 3.6535 ± 0.0004 . We find that this is due to an intrinsic offset between the spectra (see Appendix B.2), but whether this is due to a systematic in the reduction process, or as a result of the spectra possibly probing spectrally distinct sub regions of the galaxy, remains to be seen.

Both spectra of BB show a common set of prominent emission lines: H α (which is blended with the [NII] $\lambda\lambda 6549, 6585$ doublet), ionised sulfur [SII] $\lambda\lambda 6716, 6731$ and [SIII] $\lambda\lambda 9069, 9531$, ionised oxygen [OIII] $\lambda\lambda 4959, 5007$, and Helium HeI $\lambda 10830$. We also marginally detect a number of weaker lines in both spectra ($\sim 2\sigma$ or weaker), which we list in Table 4.4 for completeness. Figure 4.7 shows the posterior distributions for redshift (z), intrinsic velocity dispersion v [km s^{-1}] (note that this is not the FWHM), and the dispersion curve scaling factor (s_R). As expected, v and s_R are covariant, meaning that it is not possible to measure line widths precisely (i.e, with a small uncertainty). The fits seem to favour a dispersion curve slightly higher resolution than the one provided by the JDox ($\sigma_R \sim 1.3$), which was also found by (de Graaff et al., 2023). We find similar line widths for both spectra, with $\text{FWHM} = 962_{-164}^{+156} \text{ km s}^{-1}$ and $1372_{-172}^{+179} \text{ km s}^{-1}$ for BB-1 and BB-3, respectively. The posterior velocity dispersions of $400 - 600 \text{ km s}^{-1}$ are significantly higher than the velocity dispersions measured for star forming galaxies at this redshift (Price et al., 2020), and are similar to those measured for ultra-massive quiescent galaxies ($\sim 400 \text{ km s}^{-1}$; Forrest et al., 2022). However, systematics may contribute significantly to this measurement. We explore this in detail in Appendix B.1, where we employ an identical fitting set-up on an extremely similar galaxy at $z = 3.65$ that has both NIRSpec medium (G395M/F290LP) and low (PRISM/CLEAR) resolution spectra. We anticipate here that the intrinsic velocity width inferred from the PRISM spectrum is up to $\sim 3\times$ greater than that inferred from the medium resolution spectrum, indicating

[†]<https://github.com/tbmiller-astro/imcascade>

that our velocity width measurements for BB are also likely overestimated.

Bearing this caveat in mind, there is further evidence for broad lines in BB-3, which is fit with a higher velocity dispersion than BB-1. This seems to be driven by the HeI λ 10830 line, which is marginally resolved and for which a single velocity component fit returns significant residuals ($> 10\sigma$). This would indicate some internal process contributing to line broadening such as an AGN (see [Padovani et al., 2017](#)). Some studies have found broad HeI λ 10830 absorption in galaxies hosting active black holes ([Leighly et al., 2011](#)), including a recent observation of a compact AGN with *JWST*/NIRSpec by [Wang et al. \(2024a\)](#). As noted in this paper, the HeI λ 10830 can be a meta-stable transition state (2^3S , 19.7eV above ground state), populated by recombination from the HeII state, possibly indicating AGN activity. Alternatively, the HeI λ 10830 line can also be produced by strong winds from Wolf-Rayet stars, which are the final stable phase of massive star evolution ([Howarth and Schmutz, 1992](#)), and have terminal velocities of $\sim 1000 - 3000\text{kms}^{-1}$. Evidence of the presence of Wolf-Rayet stars has been found in the spectra of the progenitors of compact quiescent galaxies at $z \sim 2$ ([Williams et al., 2015](#)). In either case, higher resolution spectra are required to understand both the origin of the HeI λ 10830 line, and the reason for its apparent broadening.

4.4.2 DUST AND SFR

The spectra of BB exhibit strong H α emission, making it finally possible to measure a H α SFR for a galaxy of this type. Furthermore, we can put an upper limit on the dust attenuation by measuring the Balmer decrement. However, estimating the dust attenuation from the H α and H β line fluxes is not trivial, not only because the H α and [NII] $\lambda\lambda$ 6549, 6585 fluxes are strongly covariant, but also the ratios derived from each spectrum converge to different H α / [NII] $\lambda\lambda$ 6549, 6585 ratios (see Section 4.4.5). Furthermore, for both BB-1 and BB-3, H β is not detected even at the 1σ level. With these limitations in mind, we estimate very large decrements of H α / H β < 20 (1σ upper limit) for both images. It is possible that by not accounting for stellar H β and H α absorption, the H β and H α fluxes could be underestimated, but it is likely this would not make a difference given the variable and low resolution of the spectrum.

Assuming a [Calzetti et al. \(2000\)](#) dust law, we compute $A_{H\alpha}$ of $4.39_{-1.16}^{+1.94}$ for BB-1 and

$4.50_{-1.31}^{+2.19}$ for BB-3 . Even considering the lower bounds, both spectra imply $A_{H\alpha} \gtrsim 3.2$. This agrees with the stellar continuum attenuation of A_V of ~ 3.65 from fitting eazy-py to *HST*/ACS and *JWST*/NIRCam photometry, whilst fitting all available photometry from $\sim 0.4 - 1150\mu\text{m}$ with STARDUST gives A_V of ~ 2.7 for BB-1 and BB-3. Generally these results infer strong dust attenuation, which is further supported by the dust masses we fit with STARDUST (see Table 4.2), which are on the order of 1% of the stellar mass. This is also expected given the compact size of BB, which agrees with previous work that found H-faint compact galaxies with high dust obscuration were also compact (Sun et al., 2021). It may be noted the $H\alpha$ attenuation is ~ 1 magnitude greater than that inferred from the photometric SED fitting. We do not include a specific extra attenuation factor for nebular lines compared with stars (e.g. Kashino et al., 2013; Calzetti et al., 2000), but this would go in the direction of further increasing the dust correction derived from the Balmer decrement.

Finally, we estimate the intrinsic SFR on short timescales ($\sim 10\text{Myr}$) from the extinction corrected $H\alpha$ flux, returning $\log(\text{M}_\odot/\mu\text{yr}^{-1}) = 1.43_{-0.29}^{+2.23}$ for BB-1 and $\log(\text{M}_\odot/\mu\text{yr}^{-1}) = 1.19_{-0.31}^{+2.83}$ for BB-3. We measure similar optical SFRs from multi-wavelength SED fitting, whilst total SFRs based on L_{IR} are ~ 1 dex higher, and closer to the SFRs presented in Sun et al., 2022; we discuss this in Section 4.5.1.

4.4.3 STELLAR MASS

We estimate the stellar mass of all three images in both the optical/NIR with eazy-py and across the full wavelength range with STARDUST . After correcting for magnification, there is a ~ 0.6 dex spread in stellar mass across these measurements of all three images for masses derived with two different codes. Combining these measurements using an inverse weighted average gives $\langle \log(\text{M}_*/\mu\text{M}_\odot) \rangle = 10.29 \pm 0.24$, where the error is the standard deviation (see Figure 4.8). The stellar mass is below the characteristic stellar mass for pre-*JWST* mass functions at $z \sim 3.5$ (e.g. at $3.5 < z < 4.5$ the characteristic stellar mass is $\log(\text{M}_*/\text{M}_\odot) = 10.65 \pm 0.06$, Weaver et al., 2022; see also Long et al., 2022). However, BB is similarly massive to *HST*-dark selected galaxies at $z \sim 3.5$ presented in a number of works based on the Early Release Science (ERS) survey CEERS (Finkelstein et al., 2023). Similarly, Barrufet et al. (2023) presented a sample of dusty galaxies at $3 < z < 5$ selected using NIRCam colour

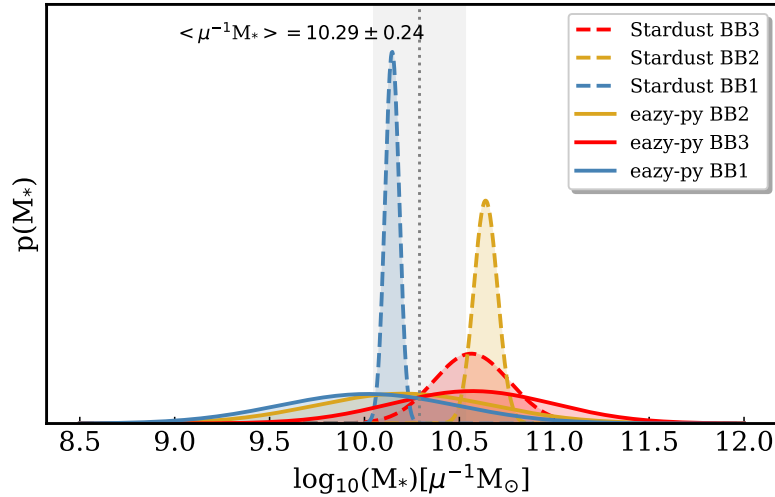


Figure 4.8: Stellar mass probability distributions for BB-1 (blue), BB-2 (gold) and BB-3 (red) measured with both eazy-py (solid lines) and STARDUST (dashed lines). The average stellar mass and standard deviation is denoted by the grey dotted line and area around it. All measurements are corrected for lensing.

selection, with an average stellar mass of $\log(M_*/M_\odot) \sim 9.5 - 10$. [Gottumukkala et al. \(2023\)](#) applied a similar colour selection and found dust obscured galaxies at $z \sim 3.5$ with average stellar masses of $\log(M_*/M_\odot) = 10.15^{+0.43}_{-0.50}$, and also compared their sample to the one selected by [Pérez-González et al. \(2022\)](#), who found dust obscured galaxies in a similar redshift and stellar mass ranges ($z \sim 3.7$, $\log(M_*/M_\odot) = 10.20^{+0.46}_{-0.73}$). All things considered, BB appears to be broadly similar to galaxies with similar observed colours (see Section 4.4.6) at the same redshift, indicating it could be a poster child for the population.

4.4.4 BBAND THE STAR FORMING MAIN SEQUENCE

Figure 4.9 shows the location of all three lensed images of BB in the Mstar-SFR plane. We show also the $z = 4$ main sequence computed by [Speagle et al. \(2014\)](#), along with HST-dark galaxies at $3 < z < 5$ from both [Barrufet et al. \(2023\)](#) and [Gottumukkala et al. \(2023\)](#). Results from fitting photometry (upper panel) generally suggest that that BB lies on the main sequence. All results based on eazy-py fall directly within the scatter of the empirical relation, whilst the total (i.e., based on the infrared luminosity) and optical SFR from STARDUST fall

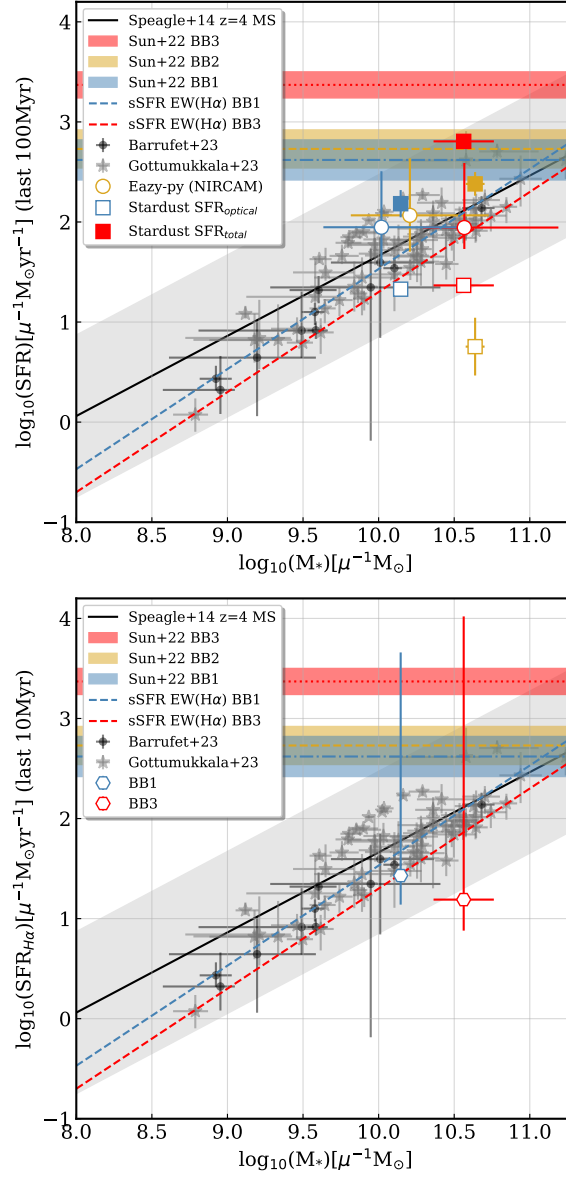


Figure 4.9: *Upper panel:* Star forming main sequence with results from photometric SED fitting for all three images shown as circles (eazy-py) and open (filled) squares points (STARDUST optical (total) SFR). The FIR derived SFR and 1σ errors from (Sun et al., 2022) are shown as dotted / dashed lines. The main sequence at $z = 4$ from Speagle et al., 2014 is shown as well as HST-dark galaxies at $3 < z < 4$ from Barrufet et al., 2023 and Gottumukkala et al., 2023. *Lower panel:* Same but showing the optical SFR's and 1σ errors derived from the $H\alpha$ line fluxes, with the mass plotted from photometric SED fitting with STARDUST. In both panels, we show the ssFR measured from $EW(H\alpha)$ as dashed lines, which also fall on the main sequence.

marginally both above and below the *eazy-py* points. In the lower panel of Figure 4.9, we also show the dust- and magnification-corrected SFRs as measured from the spectra, and assuming the stellar masses from *STARDUST* as a reference. These results are also consistent with the main sequence including the 1σ lower limit, which, together with the stellar mass measurements, confidently places BB *at least* on the main sequence. The 1σ upper limit would place BB in the same parameter space as highly star-forming sub-mm galaxies (Cunha et al., 2015; see also Figure 6 of Barrufet et al., 2023). This 1σ upper limit also overlaps with the FIR derived SFRs from Sun et al. (2022). The equivalent width (EW) of $H\alpha$ can be used to estimate the specific star formation rate (sSFR) independently of the measurements from photometry, and also a useful measure of sSFR that is invariant with age, nebular emission, and dust extinction (Mármol-Queraltó et al., 2016). We use the relation measured at $1 < z < 5$ measured by Mármol-Queraltó et al. (2016), $EW(H\alpha) = 63 \pm 7 \cdot \text{sSFR}$. In Figure 4.10, we show the sSFR distributions for BB-1 and BB-3 using the measured $H\alpha$ EWs (upper panel), as well as the sSFR as a function of $H\alpha / H\alpha + [\text{NII}]\lambda\lambda 6549, 6585$ (lower panel). From these measurements, we can ascertain that the $\log_{10}(\text{sSFR}/\text{yr}^{-1}) \sim -8.5$, which places BB exactly on the main sequence at $z \sim 4$, in agreement with the conclusions drawn from the photometric SED fitting.

4.4.5 IONIZATION CONDITIONS

The set of rest-frame optical emission lines detected in the spectra of this galaxy provide an opportunity to study not only the star formation activity and dust attenuation, but also the Interstellar Medium (ISM) conditions. Typically, line ratios calculated from combinations of the Balmer recombination lines ($H\alpha$, $H\beta$, etc) and collisionally excited metal lines (e.g. $[\text{OIII}]\lambda\lambda 4959, 5007$, $[\text{NII}]\lambda\lambda 6549, 6585$, $[\text{SIII}]\lambda\lambda 9069, 9531$, $[\text{SII}]\lambda\lambda 6716, 6731$) can be used to investigate properties such as gas-phase elemental abundances (i.e. metallicity), gas temperature and pressure, electron temperature, and the ionization conditions of the gas (Kewley et al., 2013). Ionization from star formation can be probed on recent (< 10 Myr) timescales, making it possible to infer whether an ionization potential is dominated by e.g. starburst activity or AGN activity (Kaasinen et al., 2018).

The foundational line ratio diagnostic is the BPT diagram ($[\text{NII}]\lambda\lambda 6549, 6585/H\alpha$ vs

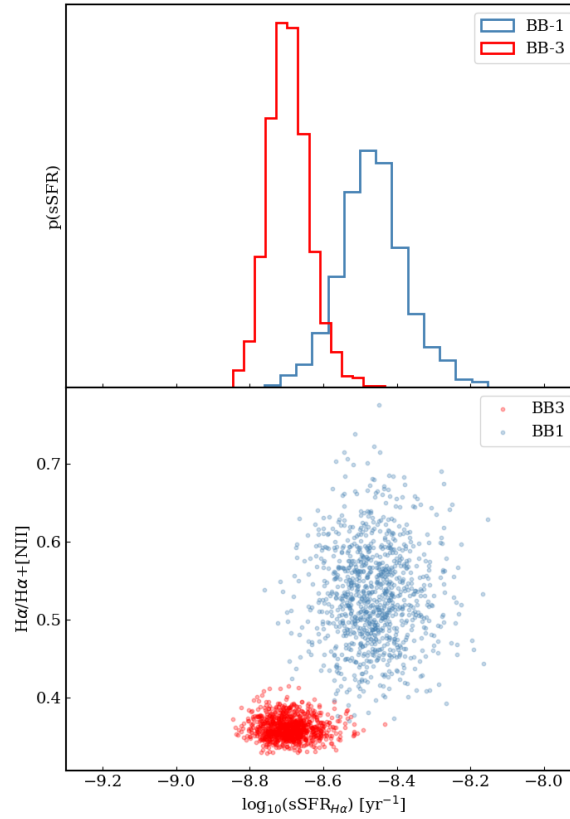


Figure 4.10: *Upper panel:* Distributions of $\log_{10}(\text{sSFR})$ [yr^{-1}] measured from EW($H\alpha$) distributions of BB-1 (blue) and BB-3 (red) using the relation from [Mármol-Queraltó et al. \(2016\)](#). *Lower panel:* $\log_{10}(\text{sSFR})$ [yr^{-1}] as a function of $H\alpha / H\alpha + [\text{NII}]$ (blue and red points for BB-1 and BB-3) posterior distributions.

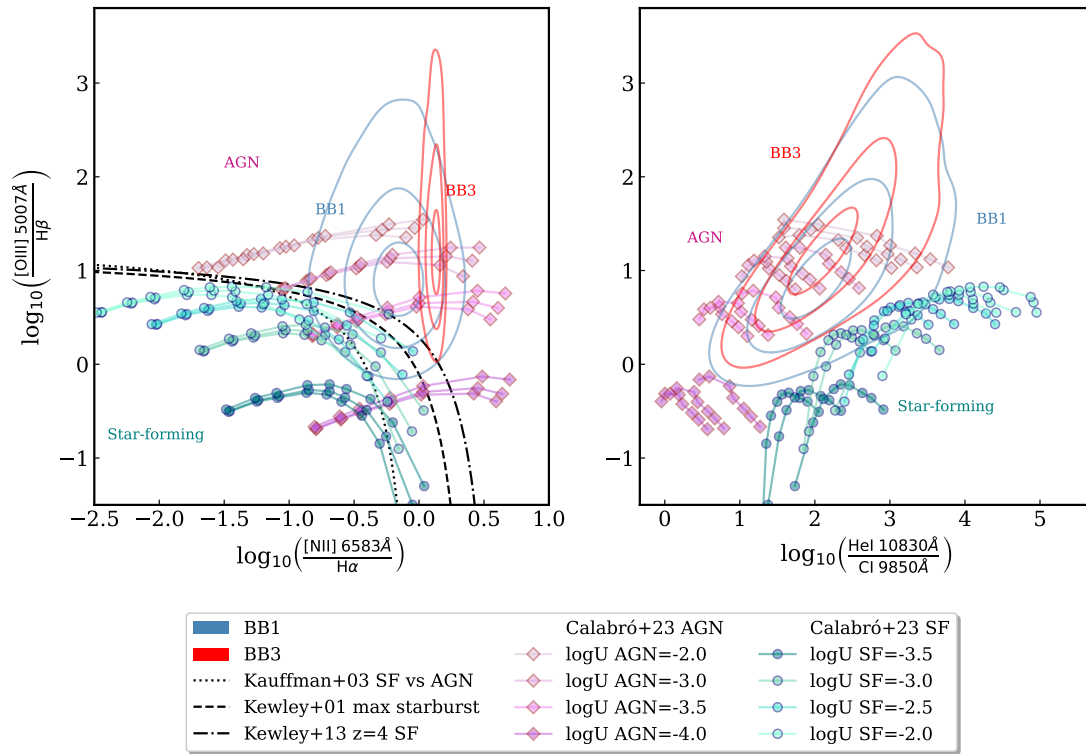


Figure 4.11: Location of posterior emission line ratios ($\text{NII}/\text{H}\alpha$ vs $\text{OIII}/\text{H}\beta$ a.k.a. BPT on the left, $\text{HeI}_{10830}/\text{Cl}_{9850}$ vs $\text{OIII}/\text{H}\beta$ on the right) for BB1 (blue contours) and BB3 (red contours) with star forming and AGN models for different ionization parameters generated from CLOUDY (Calabrò et al., 2023). In both diagrams, both BB1 and BB3 reside in the area populated by AGN models with $\log U \gtrsim -3$, indicating the possible presence of an AGN in the galaxy.

[OIII] $\lambda\lambda$ 4959, 5007/H β , Baldwin et al. 1981), in which galaxies fall into different areas depending on their primary ionization strength and source (e.g., star formation, shocks, AGN). In particular, it can be used to differentiate galaxies hosting an AGN from those without. This arises due to the extreme UV ionization from the AGN accretion disc contributing to enhanced levels of [OIII] $\lambda\lambda$ 4959, 5007 and [NII] $\lambda\lambda$ 6549, 6585 compared to ionization from star formation. Over the past decades, this has evolved to a set of line ratio diagnostic diagrams, and, in the age of *JWST*, entirely new diagnostics thanks to the new accessibility of lines previously unobserved due to redshift (e.g. Calabrò et al., 2023). Studies using photoionization models have further gleaned light on how different properties such as electron density and metallicity distribute on these diagrams, making it possible for observers to understand the conditions of the ISM simply from several sets of line ratios (Kewley et al., 2019).

For this particular galaxy, there are several strongly detected lines available in the rest-frame optical/NIR for exploring using these diagnostics, which is something entirely novel for this kind of galaxy at this redshift. We therefore make use of every available diagnostic in order to build a complete picture of the ISM. We calculate all line ratios from the posterior line flux distributions and correct resolution-separated line (i.e., lines that are not blended) for extinction as described in Section 4.4.2. We convert the total [NII] $\lambda\lambda$ 6549, 6585 and [OIII] $\lambda\lambda$ 4959, 5007 line fluxes to just the flux of the lines used in the diagnostic (i.e. the brightest) using the intrinsic line ratios.

Firstly, we calculate the positions of BB-1 and BB-2 in the original BPT diagram (Figure 4.11, left panel). Both spectra have high [OIII] $\lambda\lambda$ 4959, 5007/H β and [NII] $\lambda\lambda$ 6549, 6585/H α line ratios consistent with ionization from an AGN or shocks (see Figure 11a of Kewley et al., 2019). Curiously, despite setting a prior of ~ 0.5 on the [NII] $\lambda\lambda$ 6549, 6585/H α ratio, BB₃ is better fit with a higher [NII] $\lambda\lambda$ 6549, 6585/H α ratio (note that the tightness of this ratio is not necessarily due to precision, but rather that it hits the edge of the prior). BB₁ has a distribution that falls closer to both the $z = 4$ dividing line calculated from Equation 5 in Kewley et al. (2013) as well as the maximum starburst line from Kauffmann et al. (2003). We explore the accuracy of our code at estimating the correct [NII] $\lambda\lambda$ 6549, 6585/H α ratio in Appendix B.1 and find that our code can successfully distinguish the correct line flux contributions to the blended lines. Given the possibility of the shutters probing spectrally distinct

sub regions of the galaxy (see Figure 4.6), the difference in ratios could arise from the spectra probing different regions of the ISM with different gas properties.

We also plot photoionization models from Calabrò et al. (2023) at a range of ionization parameters and densities tailored for $z = 3$ galaxies. We explored different diagnostics using their models with the available lines from our spectra. We found that the most discriminating diagram making use of lines in the rest-frame NIR is $\text{HeI}\lambda 10830 / [\text{ClI}]\lambda 9850$ vs $[\text{OIII}]\lambda\lambda 4959, 5007 / \text{H}\beta$, which we show in the right panel of Figure 4.11. This shows both spectra clearly lining up with the photoionization models consistent with AGN or shocks.

In both panels, both spectra have line ratios consistent with models from Calabrò et al. (2023) at $-3.5 < \log(U) < -2.0$. We investigate this further by calculating the sulfur line ratio $S_{32} \equiv [\text{SIII}]\lambda\lambda 9069, 9531 / [\text{SII}]\lambda\lambda 6716, 6731$ which can be used to infer the ionization parameter (Sanders et al., 2019; Kewley and Dopita, 2002), and is invariant with metallicity. We use the calibrations from Morisset et al. (2016) to calculate $\log(U) = -2.47_{-0.10}^{+0.10}$ for BB-1 and $= -2.34_{-0.08}^{+0.08}$ for BB-3, results which are consistent with those inferred from Calabrò et al. (2023) models. Holistically, the line ratios paint a picture of an ISM that is strongly ionized by AGN or shocks.

4.4.6 COLOURS AND MORPHOLOGY

All three images of BB are detected at $\text{SNR} > 10$ in all bands rewards of F200W, whilst BB-1 and BB-2 are also detected at $\text{SNR} > 5$ in F150W. Accounting for the magnification factor, BB would qualify as “HST-dark” using the colour selection defined by Nelson et al. (2023) ($F_{444\text{W}} < 24.5$ mag; $F_{150\text{W}} > 25.5$ mag; $F_{115\text{W}} > 27$ mag), which they note is comparable to the selection employed by Barrufet et al. (2023) and also to foundational colour selections (Wang et al., 2016; Caputi et al., 2012). Therefore by the new *JWST* standards, BB keeps its original classification of “HST faint” first presented in Sun et al. (2022). However, BB is the only galaxy within the MACS0417 lensing cluster field that would qualify as such. The rest-frame *UVJ* colours (Whitaker et al., 2012; Williams et al., 2009) of BB are also very red ($U - V \sim 2.3$ and $V - J \sim 2.1$), as expected, placing the galaxy in the top right quadrant where dusty star forming galaxies are found.

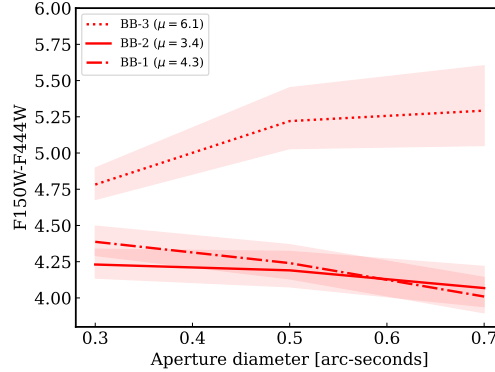


Figure 4.12: $F_{150W}-F_{444W}$ colour as a function of radial distance from the source center for all images.

4.4.6.1 COLOUR GRADIENTS

The composite images show a slight colour gradient, with the center of each image redder than the outskirts. To investigate this, we calculate the $F_{150W}-F_{444W}$ colour from the 0.3, 0.5, 0.7 arc-second apertures and bootstrap the flux errors to calculate the 1σ colour uncertainties (see Figure 4.1). Although we find that all sources have no significant colour gradients at the 1σ level, we do find that they are consistently red throughout, which is something that [Nelson et al. \(2023\)](#) also found for similarly red, massive field galaxies at $2 < z < 6$.

4.4.6.2 MORPHOLOGY AND SIZE

We show in Figure 4.13 our model fits to BB-1 in the F_{277W} band. The residuals imply some extended feature that is not accounted for (possibly tidal tails or companions), as well as a central spiral feature, which is likely an artefact due to the PSF. Both BB-2 and BB-3 also display the same features, and the RGB images (see Figure 4.1) show what could be a dust lane. We measure the image plane size of BB-1 as $R_{50\%,\text{image}} = 2.25 \pm 0.04\text{kpc}$, which we convert to a source plane size by dividing by the lensing magnification $\mu = 4.3$, giving $R_{50\%,\text{source}} = 0.52 \pm 0.05\text{kpc}$. Preliminary analysis conducted in the source plane confirms this size estimate; a full analysis in the source plane is left for future work.

To compare the size in context, we show in Figure 4.14 the position of BB-1 relative to the redshift size relations for galaxies at a range of stellar masses from both [Wel et al. \(2014\)](#) and

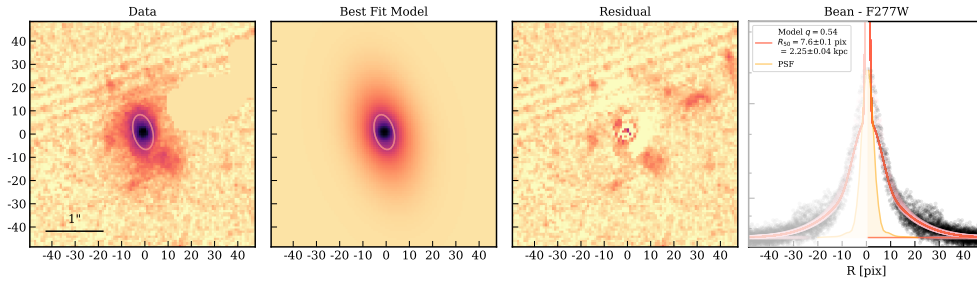


Figure 4.13: From left to right: F277W data, model, residuals and 1D size profile from fitting BB-1 with *imcascade* in the image plane. The X-Y units are in pixels. In the rightmost panel, the intrinsic profile is shown by the red line, the PSF is shown by the yellow area. BB-1 has a compact half-light radius of $R_{50\%,\text{source}} = 0.52 \pm 0.05\text{kpc}$, shown by the pink circle in the cutouts. BB-1 could easily be covered by the *JWST* NIRSpec Integral Field Unit (IFU) field of view (FOV), which is $3 \times 3''$.

Mowla et al. (2019), as well as quiescent galaxies at $1 < z < 3$ (Suess et al., 2022a) and at $3 < z < 5$ (Ito et al., 2024). We also show the sample of optically dark massive galaxies at $2 < z < 6$ presented in Nelson et al. (2022), which is the most similar measurement comparison that we can make. BB-1 has a remarkably compact size: it is much smaller than other optically faint/dark galaxies at the same epoch and it is as small as some quiescent galaxies in the same epoch. Pérez-González et al. (2022) measured the light-weighted and mass-weighted sizes of a sample of optically faint/dark galaxies with *JWST* and found that the majority of them lie on the Wel et al. (2014) size-mass relation for star forming galaxies. They also measured some remarkably compact galaxies, which were denoted as either quiescent or $z > 6 - 7$ extreme emission line galaxies. BB already has the structural parameters seen in the high-redshift quiescent galaxy population at $z \sim 2$, and is sufficiently compact to be a quiescent galaxy at its observed redshift. Assuming no more gas replenishment, and a gas depletion timescale of $t_{\text{d}} = 190_{-95}^{+266}\text{Myr}$ from Sun et al. (2022), at its current SFR BB-1 would at most triple its stellar mass to $\log(M_*/M_{\odot}) \sim 10.6$ by $z \sim 2.4$. Therefore, it is conceivable that based on these results, BB is set to become a compact quiescent galaxy by $z \sim 2.4$.

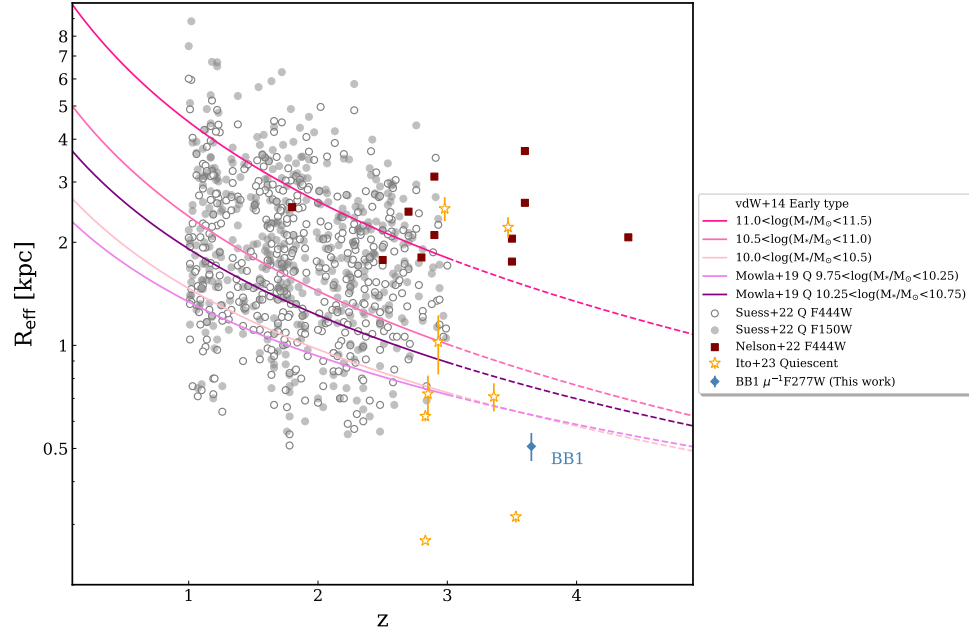


Figure 4.14: The position of BB-1 on the size relation relation using the half light radius measured from the F277W image (approximately rest-frame V band) using imcascade (Miller and van Dokkum, 2021). Relative to other dust obscured galaxies at $2 < z < 6$ (Nelson et al., 2022) BB-1 is much more compact, and is similarly compact to massive quiescent galaxies at $3 < z < 4$ (Ito et al., 2024). BB-1 is in the appropriate place relative to both the size-redshift relation (Mowla et al., 2019; Wel et al., 2014) and observations of quiescent galaxies at $2 < z < 3$ (Suess et al., 2022a) in order to be a progenitor of the massive quiescent galaxy population at or before cosmic noon.

4.5 DISCUSSION

4.5.1 OPTICAL VS FIR SFRs

Our SFRs agree within 1σ of the FIR derived values of $\log(\mu^{-1}M_{\odot}/\mu\text{yr}^{-1})= 2.62^{+0.2}_{-0.2}$ and $\log(\mu^{-1}M_{\odot}/\mu\text{yr}^{-1})= 3.37^{+0.13}_{-0.13}$ from Sun et al. (2022). However, the optical SFRs of BB-1 and BB-3 seem to be systematically lower than the FIR SFRs. There are three possible explanations for this: *a*) both are correct *b*) the optical SFR is underestimated due to underestimating the $H\alpha$ flux because of [NII] $\lambda\lambda 6549, 6585$ blending; and *c*) the FIR SFR is overestimated due to a luminosity source which is not accounted for. We explore all three scenarios here.

In the scenario *a*, we assume that the optical SFRs being lower than the FIR SFRs reflects a physical truth. This is possible because $H\alpha$ SFRs probe shorter timescales compared to FIR SFRs (~ 10 Myr compared to ~ 100 Myr) and therefore $H\alpha$ SFRs measure more recent star formation. This suggests a decrease in star formation activity in the last ~ 100 Myr, which could either be a natural lull in the global star formation history, the result of a burst in star formation, or the beginnings of a quenching epoch. This makes sense given the fast gas depletion timescale for the total sample presented in Sun et al. (2022) ($t_{\text{d}} = 190^{+266}_{-95}$ Myr).

In scenario *b*, the SFRs derived from the spectrum are underestimated due to two factors, which are related: firstly, the contribution of flux [NII] to the blended $H\alpha$ + [NII] line complex is overestimated, leading to an underestimated $H\alpha$ + flux. This directly leads to a lower SFR. Considering the effect this has on the derived attenuation, underestimating the $H\alpha$ flux leads to a smaller $H\alpha/H\beta$ ratio and therefore nebular line attenuation is underestimated, therefore skewing to lower dust extinction. Correcting the already underestimated $H\alpha$ flux with an underestimated attenuation then leads to a final SFR which falls significantly short. There is evidence for this in the highly skewed values of attenuation and SFR we derive from the spectrum. With the current data, it is not possible to derive a more precise SFR.

In scenario *c*, the FIR derived SFRs are overestimated, because the FIR luminosity is boosted by heating by an AGN, or older stellar populations. Although Sun et al. (2022) include AGN models in their SED fits, the model is only constrained by 4 photometry points in the FIR, whereas the region needed to constrain the AGN contribution is the mid infrared. This would be possible to test if it were possible to obtain mid-IR spectroscopy, which at

this redshift would detect polycyclic aromatic hydrocarbons (PAHs) from star formation and continuum emission from dust grains heated by the AGN torus. The mid-IR AGN strength can be related to the FIR AGN strength if the torus is particularly bright compared to the dust in the ISM in the mid-IR (Kirkpatrick et al., 2015). Unfortunately, the required rest-frame baseline of $6 - 13 \mu\text{m}$ is just beyond *JWST*/MIRI wavelength coverage. As a result, constructing a holistic understanding of the star formation and AGN activity of this galaxy must be done through disjointed study of the rest-frame optical/NIR and FIR. One potential avenue is exploring the rest-frame near-infrared. *JWST* would cover rest-frame $\sim 1 - 6 \mu\text{m}$ where emission from the stellar CO absorption line at rest-frame $2.29 \mu\text{m}$ can be used to infer the luminosity of the hot dust and therefore measure the AGN strength (Burtscher et al., 2015).

4.5.2 DOES BB HOST AN AGN?

Prior to *JWST*, the study of active super massive black holes (SMBH) was dominated by galaxies hosting bright quasars, because the identification of AGN in galaxies at $z > 3$ was prohibited by the lack of access to rest-frame UV/optical emission lines. We now have the opportunity to explore the AGN population at higher redshifts and investigate the AGN presence in different galaxy populations such as dSFGs and QGs, and their importance in physical processes such as dust production, dust destruction and quenching at $z > 3$.

For this galaxy, we have attempted to constrain the presence of an AGN using both multi-wavelength SED fitting as well as exploring the ionization diagnostics using rest-frame optical emission lines. Another possible avenue for testing for an AGN is by measuring the velocity dispersion of the emission lines. We fit a fixed velocity width for all lines and calculated FWHM line widths of $\sim 1000 \text{ km s}^{-1}$ for both spectra, which are much larger than the expected FWHM of a few hundred km s^{-1} for star forming galaxies at cosmic noon (Wisnioski et al., 2015). Testing the code on data with both prism and medium grating spectra showed that the velocity widths can be at least $3\times$ larger measured with the prism, so it is highly likely that our measurements for BB are over-estimated relative to the truth. There is, however, one piece of evidence to suggest line broadening. In the spectrum of BB-3, there are significant $> 10\sigma$ residuals around the [SIII] $\lambda\lambda 9069, 9531$ and HeI $\lambda 10830$ lines, sug-

gesting that the velocity width fit to all other lines cannot successfully fit these lines, therefore implying a broad component. In conclusion, there are several pieces of evidence that suggest BB is hosting an AGN. Higher resolution spectra and spatially resolved observations in the rest-frame optical and near infra-red regimes will give conclusive answers.

4.5.3 PLACING BB IN CONTEXT

Throughout this work we have studied the detailed physics of an optically invisible dusty, star forming galaxy at $z \sim 4$. However, is BB typical, or unique compared to the rest of the population? Comparing BB with other dusty star forming galaxies at $z \sim 4$ from [Barrufet et al. \(2023\)](#) and [Gottumukkala et al. \(2023\)](#), we found that BB lies on the star forming main sequence and is similarly massive to other optically invisible $z \sim 4$ galaxies observed with *JWST*. BB is typically smaller than similarly dusty, star forming galaxies at this epoch ([Barrufet et al., 2024](#); [Pérez-González et al., 2022](#)). So although BB is actually quite similar in its mass, star formation rate and dust obscuration to similar galaxies at this epoch, its size sets it apart.

Looking to the ISM conditions, BB has an ionization parameter that is directly in the center of the distribution for star forming galaxies at $z = 3-6$ with much lower dust obscuration ($-3.3 \leq \log(U) \leq -1.6$, [Reddy et al. 2023a](#); [Shapley et al. 2023](#)). Whilst dust can soften the hardness of the ionising radiation field ([Reddy et al., 2023a](#)), the ionization parameter suggests an ionising source which is strong enough to counter-act this effect. Interestingly, [Reddy et al. \(2023a\)](#) showed that $\log(U)$ is tightly correlated with star formation rate surface density, and this relationship is redshift invariant at least to $z \sim 6.3$. This could arise due to gas density directly elevating U via changes in electron density n_e , amongst other things. Although the lack of resolution with prism makes a measurement of n_e for these data unfeasible, higher resolution observations could provide a deeper look into the ISM and the role of dust via the resolved emission lines. In order to build a coherent picture of the interplay between gas and dust in the ISM of BB, higher resolution spectroscopic measurements are required, and IFU observations would be key for unravelling the mystery of whether the high line ratios are driven by AGN or shocks.

Finally, the holistic evidence for BB soon becoming quiescent is strong: BB already has

assembled the stellar mass, yet is sufficiently compact, to join the quiescent galaxy population at $z \sim 2$ (Stockmann et al., 2019). It has multiple signs of hosting an obscured AGN, from the line ratios, line widths, and the Helium emission line. Although it is still unknown how massive quiescent galaxies quench, multiple studies have found evidence for AGN in MQGs (e.g. Saracco et al., 2020), which seem to be the only way to quench star formation in high redshift galaxies in simulations (e.g. Xie et al., 2024). We do not yet know if there is any causation here, but the correlation exists, and through more observations we can begin to eliminate causal pathways. Finally, although we do not have a gas mass measurement, given the star formation rate and a maximal dust to gas mass ratio, BB will use up all of its fuel in at most 1 Gyr, assuming no more gas inflow.

4.6 CONCLUSIONS

In this work we have presented the photometric and spectroscopic analysis of a triply imaged, previously optically invisible, dusty star forming galaxy at $z \sim 4$, observed with *JWST*/NIRSpec. BB presents the unique opportunity to understand the ISM of a dusty star forming galaxy via access to rest-frame optical emission lines, opening the door to understanding the interplay of dust and gas in dusty star forming galaxies at high redshift. Furthermore, the unique perspective of having three images and spectra has made it possible to explore these avenues via different orientations of the galaxy. We have found that BB is similar to other optically invisible dusty star forming galaxies during this epoch in its colours, colour gradients, and stellar populations. BB lies not only on the star forming main sequence, confirmed by multiple measurements made from both multi-wavelength photometry as well as from the spectra. By exploring a rich set of rest-frame optical emission lines, we have determined that the ISM of BB is strongly ionized by either AGN or shocks. Further evidence for an AGN arises from the shape of the multi-wavelength SED as well as significant residuals in the emission line fits of BB-3 indicating the presence of broad line components in the HeI λ 10830 and [SIII] λ λ 9069, 9531 lines. Whilst much has been explored, many questions still remain, including the source of the ionization. Evidence of morphological disturbance in the form of tidal features hints that BB may have undergone a recent merger event; this could be tested by measuring the kinematics, as well as studying the star formation history and comparing

to simulations. We find that BB is significantly compact, and is a similar size to massive quiescent galaxies at $z \sim 3 - 4$. Together with the gas depletion timescale measured using the FIR data, this suggests BB is well on its way to quiescence by $z \sim 2$, and therefore is likely a progenitor of the $z > 2$ MQG population. Finally, this study highlights the importance of not only having multi-wavelength photometric observations, but also the possibilities of the science that can be done with NIRSpec/PRISM. Future observations of this galaxy will help to shed more light not only on the understanding of highly dust obscured main sequence galaxies at $z > 3$, but also on the connection to high redshift massive quiescent galaxies and their ancestors.

Acknowledgements

KG would like to thank Kimi Kardoso Kreilgaard and Jacob Osman for helpful discussions regarding sampling. The Cosmic Dawn Center (DAWN) is funded by the Danish National Research Foundation under grant No. 140. This work is based in part on observations made with the NASA/ESA/CSA James Webb Space Telescope. The data were obtained from the Mikulski Archive for Space Telescopes (MAST) at the Space Telescope Science Institute, which is operated by the Association of Universities for Research in Astronomy, Inc., under NASA contract NAS 5-03127 for JWST.

The following software were used in this work:

Eazy-py (Brammer, 2021), scipy (Virtanen et al., 2020), numpy (Harris et al., 2020), matplotlib (Hunter, 2007), sci-kit learn (Pedregosa et al., 2011), astropy (Collaboration et al., 2013; Astropy Collaboration et al., 2018), python-fsps (Conroy and Gunn, 2010; Conroy et al., 2009), emcee (Foreman-Mackey et al., 2013), msaexp (Brammer, 2022), grizli (Brammer, 2023).

B.1 TESTING THE LINE RATIO FITTING

In order to test whether it is possible to recover an accurate $H\alpha/[NII]$ ratio from fitting the PRISM spectra with our code, and to roughly assess the accuracy of the intrinsic line widths, we perform the following test. We select a galaxy at $z_{\text{spec}} = 3.65$ that has a similar PRISM spectrum to BB, which also has observations in the G395M/FL290P filter/grating combination. This galaxy was selected from the RUBIES spectroscopic survey (*JWST*-GO-4233; PI de Graaff), targeting ~ 5000 red sources with both low and medium filters across both the UDS and EGS fields with NIRSpec/MSA (see de Graaff et al., 2024 and Wang et al., 2024c for details; a full description of the RUBIES survey is forthcoming (A. de Graaff et al., in prep)). The 1D PRISM and medium resolution spectra are reduced similarly to the process described in Section 4.2.2. We then fit the PRISM spectrum with an identical setup to how the spectra of BB were fit, including imposing a prior on the $H\alpha/[NII]$ ratio. The medium resolution spectrum was fit using a bounded least squares method with a fixed intrinsic velocity width of 250 km s^{-1} , achieving a reduced $\chi^2 = 2.3$. We employ full sampling of the PRISM spectrum and after convergence the final best fit model has $\chi^2 = 1.2$. We then calculate the fully sampled $H\alpha/[NII]$ ratio and compare this to the “truth” ratio we calculate from the medium spectrum, where the errors on the medium spectrum derived ratio are calculated using the covariance matrix of the fit. Figure B.1 shows the posterior $H\alpha/[NII]$ ratio from fitting the PRISM spectrum and the medium resolution spectrum. We find that the results from the PRISM agree with the ratio from the medium resolution spectrum within 1σ errors, and are therefore confident that the measurement of the ratio from the PRISM for BB is also accurate.

B.2 REDSHIFT DIFFERENCES BETWEEN SPECTRA

The redshift solutions preferred by each spectrum are significantly different. In order to test whether the different $H\alpha/[NII]$ ratios preferred by each spectra are the cause of this, we calculate the velocity offset relative to $z = 3.652$ for each spectra to check if there are measurable offsets. We find that there is an apparent velocity offset of $\sim 225 \text{ km s}^{-1}$ between the spectra, which then leads to a redshift difference (see Figure B.2). It is unclear if this is

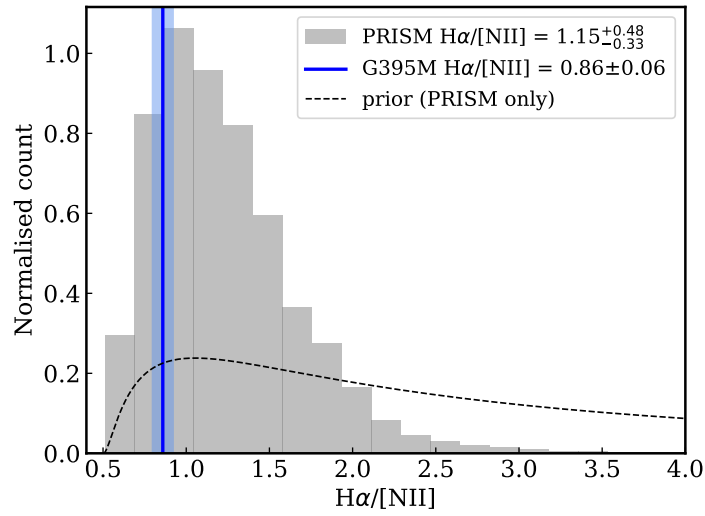


Figure B.1: The resulting $H\alpha / [NII]$ distributions from fitting a dusty $z=3.65$ galaxy that has been observed with both low (PRISM/CLEAR) and medium (G395M/FL290P) resolution *JWST*/NIRSpec spectra. Although the ratio fit from the low resolution spectra has a large dispersion, it correctly recovers the “truth” measured from the medium resolution spectrum.

a systematic error that arises due to the reduction pipeline, but we can rule out the blended $H\alpha / [NII]$ being the cause of this.

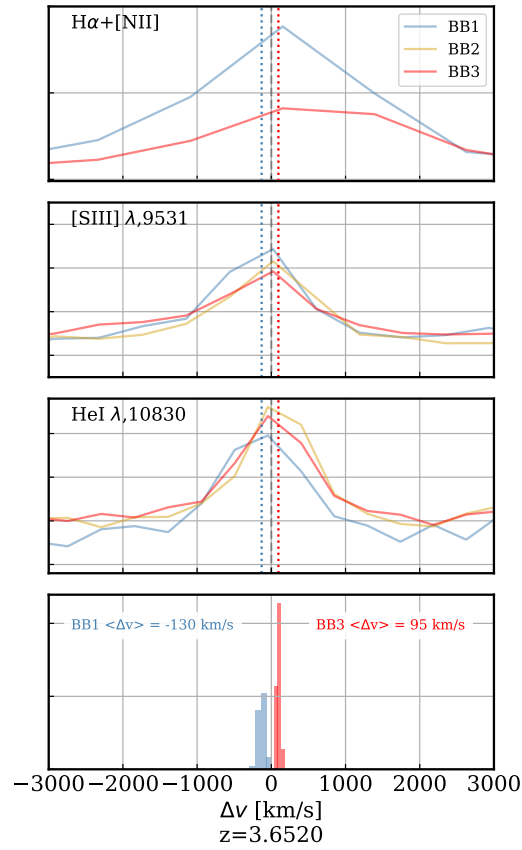


Figure B.2: Upper three panels: Velocity offsets relative to a common $z = 3.652$ for prominent emission lines for all three spectra. *Lower panel:* Velocity offset distributions measured from the redshift posteriors for BB-1 (blue) and BB-3 (red). demonstrating the distinct redshift difference between the two spectra arises due to a systematic offset in the data themselves.

"Next stop – Science!"

Mr. Ray
FINDING NEMO



5.1 CONCLUSIONS

This thesis has presented an in depth look into distant red galaxies via exploration of two sub-populations: high redshift $z > 3$ massive quiescent galaxies (MQGs), and optically dark, main sequence star forming galaxies that existed during the same epoch. I began by reviewing the pre-*JWST* literature in Chapter 1, where I set the scene on how we first came to understand the distant red galaxy populations from first explorations in the 1990s and 2000s with *HST* and *Spitzer*, and how our understanding evolved over the following decades thanks to numerous surveys and telescopes. At the end of this literature review, it was established that massive quiescent galaxies exist at $z > 3$, but their properties were poorly understood. At this time, statistical analyses could not agree on their number densities, likely due to differing selection techniques, and it was not possible to explain their physical origins in a multitude of simulations. Furthermore, questions arose as to where they came from: what is the galaxy population that directly precedes the first quiescent population? I then set out to tackle six questions related to these topics, which I will now address in turn, and summarise how each Chapter contributed to answering them.

Is there a better way to select massive quiescent galaxies at $z > 3$ from imaging than the current methods?

Prior to actually studying MQGs, it is crucial to know how to identify them. MQGs samples have been selected in large photometric catalogues using colour selections calibrated on the low redshift quiescent galaxy population (Schreiber et al., 2018; Straatman et al., 2014). At $z \sim 3$, these selection methods do not perform adequately due to differences in the fundamental properties between the high and low redshift quiescent galaxy populations, as well as the data quality (Lustig et al., 2022). In Chapter 2 I presented a novel colour selection for identifying massive quiescent galaxies $z > 3$ in photometric catalogs of imaging surveys

(Gould et al., 2023). Instead of using a binary divider in colour space to quantify quiescence, I invented a method to select MQGs based on the probability that they lie in a certain region of colour space. I tested this method using simulated MQGs at $z=2,3,4,5$ from the SHARK simulation (Lagos et al., 2018), and found that my method outperforms a classical UVJ colour selection at $z > 3$. In Chapter 3, I used this colour selection to identify quiescent galaxy candidates at $z > 2$ in the CANUCS survey (Willott et al., 2022), and presented a preliminary sample of spectra of quiescent galaxies at $z \sim 2$ observed with *JWST*/NIRSpec, including two galaxies at $z > 3$. These galaxies exhibit a range of spectra, highlighting the colour selection method as a way to explore galaxies in all stages of quenching.

What are the number densities of massive quiescent galaxies at $z > 3$, and can simulations reproduce the observed number densities of these galaxies?

In Chapter 2 I applied the selection method to the most recent catalog of the COSMOS field (Weaver et al., 2021). I calculated the number density of MQGs from $z = 5$ to $z = 2$, confirming this is period of tremendous growth in the early universe, and finding number densities similar to those calculated from previous studies (e.g. Schreiber et al., 2018). I compared these number densities to those produced from cosmological simulations and found that no simulations can reproduce the number densities of MQGs found observationally at $z > 3$, implying that new recipes are needed, or existing ones need to be altered. In Chapter 3, I presented work done in collaboration with others (Valentino et al., 2023) to apply my novel colour selection method to 11 homogeneously reduced public imaging fields in the first three months of *JWST*. We found number densities for massive ($\log(M_*/M_\odot) > 10.6$) quiescent galaxies at $3 < z < 4$ on the order of 10^{-5} Mpc^{-1} , with field to field variations and cosmic variance playing a huge role in deriving these estimates. Moreover, number densities from this study were $2\times$ greater than those measured recently using mainly ground-based data (Gould et al., 2023; Weaver et al., 2022), highlighting the importance of high spatial resolution NIR observations to identify and de-blend sources, and derive robust redshifts and stellar masses. Finally, we found that there is some convergence on the number densities of MQGs at $z > 3$ in the past few years, highlighting the power of *JWST* to confidently explore these galaxies.

*Can we find old and low mass quiescent galaxies at $z > 3$ with *JWST*?*

In Chapter 3, I presented the detection of low mass ($\log(M_*/M_\odot) < 9.5$) quiescent galaxies by tuning the parameters of my selection method. These galaxies were expected based on previous stellar mass functions (Weaver et al., 2022; Santini et al., 2022a). Looking to higher mass, older galaxies, we presented a candidate massive quiescent galaxy at $z_{phot} = 4.63$ se-

lected using a lower quiescence threshold (i.e., it wouldn't be selected by stricter traditional methods). This galaxy was later observed as part of the RUBIES *JWST* GO program (*JWST*-GO-4233; PI de Graaff) with both NIRSpec medium resolution and low resolution modes, and was confirmed to be high redshift ($z_{\text{spec}} = 4.896$), massive ($\log(M_*/M_\odot) = 10.9$), quiescent ($\text{SFR}_{100} = 1.3 M_\odot \text{yr}^{-1}$) and old ($t_{50} = 550 \text{Myr}$) (de Graaff et al., 2024). This particular galaxy challenges simulations once again, as it requires extremely formation to be so old and massive only 1.2 billion years after the Big Bang. This finding also confirms the power and the flexibility of my selection method to find old quiescent galaxies as well as young ones.

What are the properties of the “NIR-dark” population?

Prior to *JWST*, little was known about the elusive population of galaxies that were optically invisible, but brighter at longer wavelengths (“NIR-dark”), and spectroscopy in the rest-frame optical was not possible, making it difficult to accurately infer their stellar masses and study the ISM. In Chapter 4, I presented the spectro-photometric analysis of a previously known optically dark, dusty main sequence galaxy at $z_{\text{spec}} = 3.65$. This galaxy was a previously presented in Kohno et al. (2023) and Sun et al. (2022) as the brightest ALMA source in the lensing cluster MACS J0417.5 – 1154 and is lensed into three images. This galaxy (dubbed “BB”) was observed with both NIRCam and NIRSpec as part of CANUCS. I developed a new software specifically designed to measure the redshifts, line fluxes, and line widths of galaxies such as this one, which I then used to explore its properties. I found that BB is a massive $\log(M_*/M_\odot) = 10.3 \pm 0.2$, star forming $\log(M_\odot/\mu\text{yr}^{-1}) = 1.43_{-0.29}^{+2.23}$, highly dust obscured galaxy ($A_{\text{H}\alpha} > 4$), with a strongly ionized ISM. Line ratios based on standard diagnostics as well as significant residuals indicating a broadened He I $\lambda 10830$ line imply the galaxy is either hosting an AGN, is experiencing shocks, or has strong stellar winds, possibly from Wolf-Rayet stars.

Could these optically invisible galaxies be the progenitors of $z > 3$ quiescent galaxies?

In Chapter 4, we estimated the F277W size of the least distorted image, probing roughly rest frame optical V band, and converted to an intrinsic size of $0.51 \pm 0.05 \text{kpc}$. This makes BB already as small as quiescent galaxies at $z > 3$ (Ito et al., 2024). Combined with a short depletion timescale ($t_\dagger = 190_{-95}^{+266} \text{Myr}$) (Sun et al., 2022) and already large stellar mass ($\log(M_*/M_\odot) = 10.3 \pm 0.2$), this could mean that BB will join the compact quiescent galaxy population at $z \sim 2$. Although BB is only one galaxy, it has similar colours, stellar mass and sfr to other optically dark galaxies observed recently with *JWST* (e.g Barrufet et al., 2024; Gottumukkala et al., 2023; Barrufet et al., 2023; Pérez-González et al., 2022; Nelson et al., 2022), and could therefore be seen as a “poster child” for the population. Therefore, it is

possible that other optically dark galaxies with similar properties to BB could also be MQG progenitors.

5.2 FUTURE PERSPECTIVES

Already in the first 21 months of *JWST* observations, a deluge of data has been taken, reduced, and studied. In the era of the Great Observatories, detailed imaging and spectroscopy of high redshift dusty and quiescent galaxies was highly difficult, or impossible, due to prohibitively expensive exposure times, lack of wavelength coverage, or inadequate resolving power. This is now possible with *JWST*'s wavelength coverage and resolving power, which has revealed stunning imaging and spectra of red galaxy populations.

Spectroscopy with *JWST* is the most exciting avenue for the study of high redshift quenching. This is not only reflected in the number of studies since the launch (de Graaff et al., 2024; Setton et al., 2024; Glazebrook et al., 2024; Ito et al., 2024; Carnall et al., 2023; Sandles et al., 2023) but also in the generous share of proposals accepted in Cycle 2 using spectroscopy to study high redshift quenching*, which accounted for $\sim 10\%$ of the total allocated prime observing time for General Observer (Go) programs in the category of “Galaxies”. This likely resulted from the success of Cycle 1 in proving *JWST*'s capabilities - the first Cycle of observations proved that *JWST* could not only spectroscopically confirm quiescent galaxies in a fraction of the time required from the ground (e.g. Nanayakkara et al., 2024), but could also provide the resolution required to probe the physics of quenching (de Graaff et al., 2024; Slob et al., 2024; Davies et al., 2024; Carnall et al., 2023). Whilst this was already known theoretically (Nanayakkara et al., 2021), it has been notoriously difficult to convince TAC's to allocate time for spectroscopy of quiescent galaxies, as they require a significant amount of integration just to confirm redshifts. With *JWST*, this is in the past now.

When writing about the possibilities of a space-based telescope, Lyman Spitzer Jr. wrote “...that the chief contribution of such a radically new and more powerful instrument would be, not to supplement our present ideas of the universe we live in, but rather to uncover new phenomena not yet imagined” (Lyman Spitzer, 1990). Indeed, this has happened with *JWST*, although Spitzer was in fact referring to *HST*. The detection of low mass quiescent galaxies has been a new hot topic in the *JWST* era, with more “typical” low mass quiescent galaxies being presented (e.g. Cutler et al., 2023; Alberts et al., 2023; Marchesini et al., 2023) as well as so called “mini-quenched galaxies”. These galaxies are low mass galaxies with no measurable instantaneous star formation that could either represent a transitional phase from star-forming to quiescent, or a temporary lull in period of bursty star formation. Observations of these galaxies at $3 < z < 7$ (e.g. Looser et al., 2023; Strait et al., 2023) provoked a flurry of works

*<https://www.stsci.edu/jwst/science-execution/approved-programs/general-observers/cycle-2-go>

exploring the possibility of such galaxies in simulations (Gelli et al., 2024; Faisst and Morishita, 2024; Dome et al., 2024; Gelli et al., 2023), although previous work has shown that bursty star formation can occur at high redshift (Anglés-Alcázar et al., 2017). This has raised questions such as the definition of quiescent, which is exactly why having a sliding scale definition such as the one I designed can be very useful - a quiescent galaxy is defined by your selection criteria.

At the start of thesis, in 2020, the landscape for studying distant red galaxies was vastly different to today. *JWST* has opened the doors of discovery to study quiescent and dusty galaxies in glorious, gory detail, and it is the goriness of science that motivated the creation of the two new methods presented in this thesis. This thesis has contributed to our scientific understanding of the $z > 3$ universe: charting the properties and number densities of quiescent galaxies, assessing the status of simulations, and exploring the properties of “NIR-dark” galaxies and their possible status as quiescent galaxy progenitors. But, I have also specifically created tools to make not only my study of these galaxies easier, but also to make the job easier for the community. Both codes are publically available on github, and can be used both to select and explore quiescent galaxies in all imaging data, as well as study the spectra of galaxies observed with *JWST*/NIRSpec. The future work made possible by this thesis extends also to analysing the sample of quiescent galaxies at cosmic noon that I selected with the novel selection method. Other avenues include harnessing the power of the medium band data in CANUCS, which was explored in great detail during this PhD but sadly did not make it into the thesis. The foundational work based on medium bands in the 2010s (Straatman et al., 2014; Kriek and Conroy, 2013; Whitaker et al., 2011) has shown the power of medium bands for accurately constraining not only the redshifts, but stellar populations and ages of quiescent galaxies. Looking forward, there is much science to do. The next few years will undoubtedly reveal even more exciting galaxies, and with the power of computational methods and a vast data base of public *JWST* data, we have all the tools we need to understand when, and how, the first quiescent galaxies came to be.

REFERENCES

Abraham, R. G., Tanvir, N. R., Santiago, B. X., Ellis, R. S., Glazebrook, K., and Bergh, S. v. d. (1996). Galaxy morphology to $I=25$ mag in the Hubble Deep Field. *Monthly Notices of the Royal Astronomical Society*, 279(3):L47–L52.

Aihara, H., Arimoto, N., Armstrong, R., Arnouts, S., Bahcall, N. A., Bickerton, S., Bosch, J., Bundy, K., Capak, P. L., Chan, J. H. H., Chiba, M., Coupon, J., Egami, E., Enoki, M., Finet, F., Fujimori, H., Fujimoto, S., Furusawa, H., Furusawa, J., Goto, T., Goulding, A., Greco, J. P., Greene, J. E., Gunn, J. E., Hamana, T., Harikane, Y., Hashimoto, Y., Hattori, T., Hayashi, M., Hayashi, Y., Helminiak, K. G., Higuchi, R., Hikage, C., Ho, P. T. P., Hsieh, B.-C., Huang, K., Huang, S., Ikeda, H., Imanishi, M., Inoue, A. K., Iwasawa, K., Iwata, I., Jaelani, A. T., Jian, H.-Y., Kamata, Y., Karoji, H., Kashikawa, N., Katayama, N., Kawanomoto, S., Kayo, I., Koda, J., Koike, M., Kojima, T., Komiyama, Y., Konno, A., Koshida, S., Koyama, Y., Kusakabe, H., Leauthaud, A., Lee, C.-H., Lin, L., Lin, Y.-T., Lupton, R. H., Mandelbaum, R., Matsuoka, Y., Medezinski, E., Mineo, S., Miyama, S., Miyatake, H., Miyazaki, S., Momose, R., More, A., More, S., Moritani, Y., Moriya, T. J., Morokuma, T., Mukae, S., Murata, R., Murayama, H., Nagao, T., Nakata, F., Niida, M., Niikura, H., Nishizawa, A. J., Obuchi, Y., Oguri, M., Oishi, Y., Okabe, N., Okamoto, S., Okura, Y., Ono, Y., Onodera, M., Onoue, M., Osato, K., Ouchi, M., Price, P. A., Pyo, T.-S., Sako, M., Sawicki, M., Shibuya, T., Shimasaku, K., Shimono, A., Shirasaki, M., Silverman, J. D., Simet, M., Speagle, J., Spergel, D. N., Strauss, M. A., Sugahara, Y., Sugiyama, N., Suto, Y., Suyu, S. H., Suzuki, N., Tait, P. J., Takada, M., Takata, T., Tamura, N., Tanaka, M. M., Tanaka, M., Tanaka, M., Tanaka, Y., Terai, T., Terashima, Y., Toba, Y., Tominaga, N., Toshikawa, J., Turner, E. L., Uchida, T., Uchiyama, H., Umetsu, K., Uruguchi, F., Urata, Y., Usuda, T., Utsumi, Y., Wang, S.-Y., Wang, W.-H., Wong, K. C., Yabe, K., Yamada, Y., Yamanoi, H., Yasuda, N., Yeh, S., Yonehara, A., and Yuma, S. (2018). The Hyper Suprime-Cam SSP Survey: Overview and survey design. *Publications of the Astronomical Society of Japan*, 70:S4. ADS Bibcode: 2018PASJ...70S...4A.

Akins, H. B., Casey, C. M., Allen, N., Bagley, M. B., Dickinson, M., Finkelstein, S. L., Franco, M., Harish, S., Arrabal Haro, P., Ilbert, O., Kartaltepe, J. S., Koekemoer, A. M., Liu, D., Long, A. S., McCracken, H. J., Paquereau, L., Papovich, C., Pirzkal, N., Rhodes, J., Robertson, B. E., Shuntov, M., Toft, S., Yang, G., Barro, G., Bisigello, L., Buat, V., Champagne, J. B., Cooper, O., Costantin, L., de La Vega, A., Drakos, N. E., Faisst, A., Fontana, A., Fujimoto, S., Gillman, S., Gómez-Guijarro, C., Gozaliasl, G., Hathi, N. P., Hayward, C. C., Hirschmann, M., Holwerda, B. W., Jin, S., Kocevski, D. D., Kokorev, V., Lambrides, E., Lucas, R. A., Magdis, G. E., Magnelli, B., McKinney, J., Mobasher, B., Pérez-González, P. G., Rich, R. M., Seillé, L.-M., Talia, M., Urry, C. M., Valentino, F., Whitaker, K. E., Yung, L. Y. A., Zavala, J., Cosmos-Web Team, and Ceers Team (2023). Two Massive, Compact, and Dust-obscured Candidate $z \approx 8$ Galaxies Discovered by JWST. *The Astrophysical Journal*, 956:61. Publisher: IOP ADS Bibcode: 2023ApJ...956...61A.

- Akins, H. B., Narayanan, D., Whitaker, K. E., Davé, R., Lower, S., Bezanson, R., Feldmann, R., and Kriek, M. (2021). Quenching and the UVJ diagram in the SIMBA cosmological simulation. *arXiv:2105.12748 [astro-ph]*. arXiv: 2105.12748.
- Alarcon, A., Hearin, A. P., Becker, M. R., and Chaves-Montero, J. (2022). Diffstar: A Fully Parametric Physical Model for Galaxy Assembly History. *arXiv:2205.04273 [astro-ph]*.
- Alatalo, K., Lacy, M., Lanz, L., Bitsakis, T., Appleton, P. N., Nyland, K., Cales, S. L., Chang, P., Davis, T. A., Zeeuw, P. T. d., Lonsdale, C. J., Martín, S., Meier, D. S., and Ogle, P. M. (2014). SUPPRESSION OF STAR FORMATION IN NGC 1266. *The Astrophysical Journal*, 798(1):31. Publisher: The American Astronomical Society.
- Alberts, S., Williams, C. C., Helton, J. M., Suess, K. A., Ji, Z., Shivaei, I., Lyu, J., Rieke, G., Baker, W. M., Bonaventura, N., Bunker, A. J., Carniani, S., Charlot, S., Curtis-Lake, E., D'Eugenio, F., Eisenstein, D. J., de Graaff, A., Hainline, K. N., Hausen, R., Johnson, B. D., Maiolino, R., Parlanti, E., Rieke, M. J., Robertson, B. E., Sun, Y., Tacchella, S., Willmer, C. N. A., and Willott, C. J. (2023). To high redshift and low mass: exploring the emergence of quenched galaxies and their environments at $z \sim 3$. Publication Title: arXiv e-prints ADS Bibcode: 2023arXiv231212207A.
- Ando, M., Shimasaku, K., and Momose, R. (2020). A systematic search for galaxy proto-cluster cores at $z \sim 2$. *Monthly Notices of the Royal Astronomical Society*, 496(3):3169–3181.
- Anglés-Alcázar, D., Faucher-Giguère, C.-A., Kereš, D., Hopkins, P. F., Quataert, E., and Murray, N. (2017). The cosmic baryon cycle and galaxy mass assembly in the FIRE simulations. *Monthly Notices of the Royal Astronomical Society*, 470:4698–4719. Publisher: OUP ADS Bibcode: 2017MNRAS.470.4698A.
- Antwi-Danso, J., Papovich, C., Esdaile, J., Nanayakkara, T., Glazebrook, K., Hutchison, T. A., Whitaker, K. E., Marsan, Z. C., Diaz, R. J., Marchesini, D., Muzzin, A., Tran, K.-V. H., Setton, D. J., Kaushal, Y., Speagle, J. S., and Cole, J. (2023). The FENIKS Survey: Spectroscopic Confirmation of Massive Quiescent Galaxies at $z \sim 3$ -5. *arXiv:2307.09590 [astro-ph]*.
- Antwi-Danso, J., Papovich, C., Leja, J., Marchesini, D., Marsan, Z. C., Martis, N. S., Labbé, I., Muzzin, A., Glazebrook, K., Straatman, C. M. S., and Tran, K.-V. H. (2022). Beyond UVJ: Color Selection of Galaxies in the JWST Era. *arXiv:2207.07170 [astro-ph]*.
- Aravena, M., Decarli, R., Walter, F., Cunha, E. D., Bauer, F. E., Carilli, C. L., Daddi, E., Elbaz, D., Ivison, R. J., Riechers, D. A., Smail, I., Swinbank, A. M., Weiss, A., Anguita, T., Assef, R. J., Bell, E., Bertoldi, F., Bacon, R., Bouwens, R., Cortes, P., Cox, P., González-López,

- J., Hodge, J., Ibar, E., Inami, H., Infante, L., Karim, A., Fèvre, O. L. L., Magnelli, B., Ota, K., Popping, G., Sheth, K., Werf, P. v. d., and Wagg, J. (2016). THE ALMA SPECTROSCOPIC SURVEY IN THE HUBBLE ULTRA DEEP FIELD: CONTINUUM NUMBER COUNTS, RESOLVED 1.2 mm EXTRAGALACTIC BACKGROUND, AND PROPERTIES OF THE FAINTEST DUSTY STAR-FORMING GALAXIES. *The Astrophysical Journal*, 833(1):68. Publisher: The American Astronomical Society.
- Ardila, F., Alatalo, K., Lanz, L., Appleton, P. N., Beaton, R. L., Bitsakis, T., Cales, S. L., Falcón-Barroso, J., Kewley, L. J., Medling, A. M., Mulchaey, J. S., Nyland, K., Rich, J. A., and Urry, C. M. (2018). Shocked POststarburst Galaxy Survey. III. The Ultraviolet Properties of SPOGs. *The Astrophysical Journal*, 863(1):28.
- Armus, L., Megeath, S. T., Corrales, L., Marengo, M., Kirkpatrick, A., Smith, J. D., Meyer, M., Gezari, S., Kraft, R. P., McCandliss, S., Tuttle, S., Elvis, M., Bentz, M., Binder, B., Civano, F., Dragomir, D., Espaillat, C., Finkelstein, S., Fox, D. B., Greenhouse, M., Hamden, E., Kauffmann, J., Khullar, G., Lazio, J., Lee, J., Lillie, C., Lightsey, P., Mushotzky, R., Scarlata, C., Scowen, P., Tremblay, G. R., Wang, Q. D., and Wolk, S. (2021). Great Observatories: The Past and Future of Panchromatic Astrophysics. *arXiv:2104.00023 [astro-ph]*. arXiv: 2104.00023.
- Arnouts, S., Floc'h, E. L., Chevallard, J., Johnson, B. D., Ilbert, O., Treyer, M., Aussel, H., Capak, P., Sanders, D. B., Scoville, N., McCracken, H. J., Milliard, B., Pozzetti, L., and Salvato, M. (2013). Encoding of the infrared excess in the NUVrK color diagram for star-forming galaxies. *Astronomy & Astrophysics*, 558:A67. Publisher: EDP Sciences.
- Arnouts, S. and Ilbert, O. (2011). LePHARE: Photometric Analysis for Redshift Estimate. *Astrophysics Source Code Library*, page ascl:1108.009. ADS Bibcode: 2011ascl.soft08009A.
- Arrabal Haro, P., Dickinson, M., Finkelstein, S. L., Kartaltepe, J. S., Donnan, C. T., Burgarella, D., Carnall, A. C., Cullen, F., Dunlop, J. S., Fernández, V., Fujimoto, S., Jung, I., Krips, M., Larson, R. L., Papovich, C., Pérez-González, P. G., Amorín, R. O., Bagley, M. B., Buat, V., Casey, C. M., Chworowsky, K., Cohen, S. H., Ferguson, H. C., Giavalisco, M., Huertas-Company, M., Hutchison, T. A., Kocevski, D. D., Koekemoer, A. M., Lucas, R. A., McLeod, D. J., McLure, R. J., Pirzkal, N., Seillé, L.-M., Trump, J. R., Weiner, B. J., Wilkins, S. M., and Zavala, J. A. (2023). Confirmation and refutation of very luminous galaxies in the early Universe. *Nature*, 622:707–711. ADS Bibcode: 2023Natur.622..707A.
- Asada, Y., Sawicki, M., Abraham, R., Bradač, M., Brammer, G., Desprez, G., Estrada-Carpenter, V., Iyer, K., Martis, N., Matharu, J., Mowla, L., Muzzin, A., Noirot, G., Sarrouh, G. T. E., Strait, V., Willott, C. J., and Harshan, A. (2024). Bursty star formation

and galaxy-galaxy interactions in low-mass galaxies 1 Gyr after the Big Bang. *Monthly Notices of the Royal Astronomical Society*, 527:11372–11392. Publisher: OUP ADS Bibcode: 2024MNRAS.52711372A.

Asada, Y., Sawicki, M., Desprez, G., Abraham, R., Bradač, M., Brammer, G., Harshan, A., Iyer, K., Martis, N. S., Mowla, L., Muzzin, A., Noirot, G., Ravindranath, S., Sarrouh, G. T. E., Strait, V., Willott, C. J., and Zabl, J. (2023). JWST catches the assembly of a $z \approx 5$ ultra-low-mass galaxy. *Monthly Notices of the Royal Astronomical Society*, 523:L40–L45. ADS Bibcode: 2023MNRAS.523L..40A.

Astropy Collaboration, Price-Whelan, A. M., Sipőcz, B. M., Günther, H. M., Lim, P. L., Crawford, S. M., Conseil, S., Shupe, D. L., Craig, M. W., Dencheva, N., Ginsburg, A., VanderPlas, J. T., Bradley, L. D., Pérez-Suárez, D., de Val-Borro, M., Aldcroft, T. L., Cruz, K. L., Robitaille, T. P., Tollerud, E. J., Ardelean, C., Babej, T., Bach, Y. P., Bachetti, M., Bakanov, A. V., Bamford, S. P., Barentsen, G., Barmby, P., Baumbach, A., Berry, K. L., Biscani, F., Boquien, M., Bostroem, K. A., Bouma, L. G., Brammer, G. B., Bray, E. M., Breytenbach, H., Buddelmeijer, H., Burke, D. J., Calderone, G., Cano Rodríguez, J. L., Cara, M., Cardoso, J. V. M., Cheedella, S., Copin, Y., Corrales, L., Crichton, D., D’Avella, D., Deil, C., Depagne, ♦, Dietrich, J. P., Donath, A., Droettboom, M., Earl, N., Erben, T., Fabbro, S., Ferreira, L. A., Finethy, T., Fox, R. T., Garrison, L. H., Gibbons, S. L. J., Goldstein, D. A., Gommers, R., Greco, J. P., Greenfield, P., Groener, A. M., Grollier, F., Hagen, A., Hirst, P., Homeier, D., Horton, A. J., Hosseinzadeh, G., Hu, L., Hunkeler, J. S., Ivezić, ♦, Jain, A., Jenness, T., Kanarek, G., Kendrew, S., Kern, N. S., Kerzendorf, W. E., Khvalko, A., King, J., Kirkby, D., Kulkarni, A. M., Kumar, A., Lee, A., Lenz, D., Littlefair, S. P., Ma, Z., Macleod, D. M., Mastropietro, M., McCully, C., Montagnac, S., Morris, B. M., Mueller, M., Mumford, S. J., Muna, D., Murphy, N. A., Nelson, S., Nguyen, G. H., Ninan, J. P., Nöthe, M., Ogaz, S., Oh, S., Parejko, J. K., Parley, N., Pascual, S., Patil, R., Patil, A. A., Plunkett, A. L., Prochaska, J. X., Rastogi, T., Reddy Janga, V., Sabater, J., Sakurikar, P., Seifert, M., Sherbert, L. E., Sherwood-Taylor, H., Shih, A. Y., Sick, J., Silbiger, M. T., Singanamalla, S., Singer, L. P., Sladen, P. H., Sooley, K. A., Sornarajah, S., Streicher, O., Teuben, P., Thomas, S. W., Tremblay, G. R., Turner, J. E. H., Terrón, V., van Kerkwijk, M. H., de la Vega, A., Watkins, L. L., Weaver, B. A., Whitmore, J. B., Woillez, J., Zabalza, V., and Astropy Contributors (2018). The Astropy Project: Building an Open-science Project and Status of the v2.0 Core Package. *The Astronomical Journal*, 156:123. ADS Bibcode: 2018AJ....156..123A.

Bahcall, J. N., Guhathakurta, P., and Schneider, D. P. (1990). What the Longest Exposures from the Hubble Space Telescope Will Reveal. *Science*, 248(4952):178–183. Publisher: American Association for the Advancement of Science.

- Baldwin, J. A., Phillips, M. M., and Terlevich, R. (1981). Classification parameters for the emission-line spectra of extragalactic objects. *Publications of the Astronomical Society of the Pacific*, 93:5–19. ADS Bibcode: 1981PASP...93....5B.
- Balogh, M. L., Morris, S. L., Yee, H. K. C., Carlberg, R. G., and Ellingson, E. (1999). Differential Galaxy Evolution in Cluster and Field Galaxies at $z \approx 0.3$. *The Astrophysical Journal*, 527(1):54. Publisher: IOP Publishing.
- Barrufet, L., Oesch, P., Fudamoto, Y., Illingworth, G. D., Labbe, I., Magee, D. K., Stefanon, M., and van Dokkum, P. (2021). Quiescent or dusty? Unveiling the nature of extremely red galaxies at $z > 3$. *JWST Proposal. Cycle 1*, page 2198. ADS Bibcode: 2021jwst.prop.2198B.
- Barrufet, L., Oesch, P., Marques-Chaves, R., Arellano-Cordova, K., Baggen, J. F. W., Carnall, A. C., Cullen, F., Dunlop, J. S., Gottumukkala, R., Fudamoto, Y., Illingworth, G. D., Magee, D., McLure, R. J., Leod, D. J., Michałowski, M. J., Stefanon, M., van Dokkum, P. G., and Weibel, A. (2024). Quiescent or dusty? Unveiling the nature of extremely red galaxies at $z > 3$. arXiv:2404.08052 [astro-ph].
- Barrufet, L., Oesch, P. A., Weibel, A., Brammer, G., Bezanson, R., Bouwens, R., Fudamoto, Y., Gonzalez, V., Gottumukkala, R., Illingworth, G., Heintz, K. E., Holden, B., Labbe, I., Magee, D., Naidu, R. P., Nelson, E., Stefanon, M., Smit, R., van Dokkum, P., Weaver, J. R., and Williams, C. C. (2023). Unveiling the nature of infrared bright, optically dark galaxies with early JWST data. *Monthly Notices of the Royal Astronomical Society*, 522(1):449–456.
- Belli, S., Contursi, A., Genzel, R., Tacconi, L. J., Förster-Schreiber, N. M., Lutz, D., Combes, F., Neri, R., García-Burillo, S., Schuster, K. F., Herrera-Camus, R., Tadaki, K.-i., Davies, R. L., Davies, R. I., Johnson, B. D., Lee, M. M., Leja, J., Nelson, E. J., Price, S. H., Shangquan, J., Shimizu, T. T., Tacchella, S., and Übler, H. (2021). The Diverse Molecular Gas Content of Massive Galaxies Undergoing Quenching at $z \sim 1$. arXiv:2102.07881 [astro-ph]. arXiv: 2102.07881.
- Belli, S., Newman, A. B., and Ellis, R. S. (2019). MOSFIRE Spectroscopy of Quiescent Galaxies at $1.5 < z < 2.5$. II - Star Formation Histories and Galaxy Quenching. *The Astrophysical Journal*, 874(1):17. arXiv: 1810.00008.
- Bertin, E. and Arnouts, S. (1996). SExtractor: Software for source extraction. *Astronomy and Astrophysics Supplement Series*, 117:393–404.
- Bessell, M. S. (1990). UBVRI passbands. *Publications of the Astronomical Society of the Pacific*, 102:1181–1199. ADS Bibcode: 1990PASP..102.1181B.

- Beverage, A. G., Kriek, M., Suess, K. A., Conroy, C., Price, S. H., Barro, G., Bezanson, R., Franx, M., Lorenz, B., Ma, Y., Mowla, L., Pasha, I., van Dokkum, P., and Weisz, D. (2023). The Heavy Metal Survey: The Evolution of Stellar Metallicities, Abundance Ratios, and Ages of Massive Quiescent Galaxies Since $z \sim 2$. Publication Title: arXiv e-prints ADS Bibcode: 2023arXiv231205307B.
- Bielby, R., Hudelot, P., McCracken, H. J., Ilbert, O., Daddi, E., Le Fèvre, O., Gonzalez-Perez, V., Kneib, J. P., Marmo, C., Mellier, Y., Salvato, M., Sanders, D. B., and Willott, C. J. (2012). The WIRCam Deep Survey. I. Counts, colours, and mass-functions derived from near-infrared imaging in the CFHTLS deep fields. *Astronomy and Astrophysics*, 545:A23. ADS Bibcode: 2012A&A...545A..23B.
- Black, W. K. and Evrard, A. (2022). Red Dragon: A Redshift-Evolving Gaussian Mixture Model for Galaxies. arXiv:2204.10141 [astro-ph].
- Bradač, M., Strait, V., Mowla, L., Iyer, K. G., Noirot, G., Willott, C., Brammer, G., Abraham, R., Asada, Y., Desprez, G., Estrada-Carpenter, V., Harshan, A., Martis, N. S., Matharu, J., Muzzin, A., Rihtaršič, G., Sarrouh, G. T. E., and Sawicki, M. (2024). Star Formation at the Epoch of Reionization with CANUCS: The Ages of Stellar Populations in MACS1149-JD1. *The Astrophysical Journal*, 961:L21. Publisher: IOP ADS Bibcode: 2024ApJ...961L..21B.
- Bradley, L., Sipőcz, B., Robitaille, T., Tollerud, E., Vinícius, Z., Deil, C., Barbary, K., Wilson, T. J., Busko, I., Donath, A., Günther, H. M., Cara, M., Lim, P. L., Meßlinger, S., Burnett, Z., Conseil, S., Droettboom, M., Bostroem, A., Bray, E. M., Bratholm, L. A., Jamieson, W., Ginsburg, A., Barentsen, G., Craig, M., Pascual, S., Rathi, S., Perrin, M., Morris, B. M., and Perren, G. (2024). astropy/photutils: 1.12.0.
- Brammer, G. (2021). eazy-py.
- Brammer, G. (2022). msaexp: NIRSpec analysis tools.
- Brammer, G. (2023). grizli.
- Brammer, G. B. and van Dokkum, P. G. (2007). The Density and Spectral Energy Distributions of Red Galaxies at $z \sim 3.7$. *The Astrophysical Journal*, 654:L107–L110. ADS Bibcode: 2007ApJ...654L.107B.
- Brammer, G. B., van Dokkum, P. G., and Coppi, P. (2008). EAZY: A Fast, Public Photometric Redshift Code. *The Astrophysical Journal*, 686(2):1503–1513.

- Brammer, G. B., Whitaker, K. E., van Dokkum, P. G., Marchesini, D., Franx, M., Kriek, M., Labbé, I., Lee, K. S., Muzzin, A., Quadri, R. F., Rudnick, G., and Williams, R. (2011). The Number Density and Mass Density of Star-forming and Quiescent Galaxies at $0.4 < z <= 2.2$. *The Astrophysical Journal*, 739:24. ADS Bibcode: 2011ApJ...739...24B.
- Bromm, V. and Yoshida, N. (2011). The First Galaxies. *Annual Review of Astronomy and Astrophysics*, 49(1):373–407. _eprint: <https://doi.org/10.1146/annurev-astro-081710-102608>.
- Bruzual, G. and Charlot, S. (2003). Stellar population synthesis at the resolution of 2003. *Monthly Notices of the Royal Astronomical Society*, 344:1000–1028. ADS Bibcode: 2003MNRAS.344.1000B.
- Burtscher, L., Xivry, G. O. d., Davies, R. I., Janssen, A., Lutz, D., Rosario, D., Contursi, A., Genzel, R., Graciá-Carpio, J., Lin, M.-Y., Schnorr-Müller, A., Sternberg, A., Sturm, E., and Tacconi, L. (2015). Obscuration in active galactic nuclei: near-infrared luminosity relations and dust colors. *Astronomy & Astrophysics*, 578:A47. Publisher: EDP Sciences.
- Calabrò, A., Pentericci, L., Feltre, A., Arrabal Haro, P., Radovich, M., Seillé, L.-M., Oliva, E., Daddi, E., Amorín, R., Bagley, M. B., Bisigello, L., Buat, V., Castellano, M., Cleri, N. J., Dickinson, M., Fernández, V., Finkelstein, S. L., Giavalisco, M., Grazian, A., Hathi, N. P., Hirschmann, M., Juneau, S., Kartaltepe, J. S., Koekemoer, A. M., Lucas, R. A., Papovich, C., Pérez-González, P. G., Pirzkal, N., Santini, P., Trump, J., de la Vega, A., Wilkins, S. M., Yung, L. Y. A., Cassata, P., Gobat, R. A. S., Mascia, S., Napolitano, L., and Vulcani, B. (2023). Near-infrared emission line diagnostics for AGN from the local Universe to $z \sim 3$. *Astronomy and Astrophysics*, 679:A80. ADS Bibcode: 2023A&A...679A..80C.
- Calzetti, D., Armus, L., Bohlin, R. C., Kinney, A. L., Koornneef, J., and Storchi-Bergmann, T. (2000). The Dust Content and Opacity of Actively Star-forming Galaxies. *The Astrophysical Journal*, 533:682–695. ADS Bibcode: 2000ApJ...533..682C.
- Caputi, K. I., Dunlop, J. S., McLure, R. J., Huang, J.-S., Fazio, G. G., Ashby, M. L. N., Castellano, M., Fontana, A., Cirasuolo, M., Almaini, O., Bell, E. F., Dickinson, M., Donley, J. L., Faber, S. M., Ferguson, H. C., Giavalisco, M., Grogin, N. A., Kocevski, D. D., Koekemoer, A. M., Koo, D. C., Lai, K., Newman, J. A., and Somerville, R. S. (2012). THE NATURE OF EXTREMELY RED $H - [4.5] > 4$ GALAXIES REVEALED WITH SEDS AND CANDELS. *The Astrophysical Journal Letters*, 750(1):L20. Publisher: The American Astronomical Society.
- Caputi, K. I., Ilbert, O., Laigle, C., McCracken, H. J., Le Fèvre, O., Fynbo, J., Milvang-Jensen, B., Capak, P., Salvato, M., and Taniguchi, Y. (2015). Spitzer Bright, UltraV-

- ISTA Faint Sources in COSMOS: The Contribution to the Overall Population of Massive Galaxies at $z = 3-7$. *The Astrophysical Journal*, 810:73. Publisher: IOP ADS Bibcode: 2015ApJ...810...73C.
- Carnall, A. C., Leja, J., Johnson, B. D., McLure, R. J., Dunlop, J. S., and Conroy, C. (2019). How to measure galaxy star-formation histories I: Parametric models. *The Astrophysical Journal*, 873(1):44. arXiv: 1811.03635.
- Carnall, A. C., McLeod, D. J., McLure, R. J., Dunlop, J. S., Begley, R., Cullen, F., Donnan, C. T., Hamadouche, M. L., Jewell, S. M., Jones, E. W., Pollock, C. L., and Wild, V. (2022). A first look at JWST CEERS: massive quiescent galaxies from $3 < z < 5$. arXiv:2208.00986 [astro-ph].
- Carnall, A. C., McLure, R. J., Dunlop, J. S., McLeod, D. J., Wild, V., Cullen, F., Magee, D., Begley, R., Cimatti, A., Donnan, C. T., Hamadouche, M. L., Jewell, S. M., and Walker, S. (2023). A massive quiescent galaxy at redshift 4.658. arXiv:2301.11413 [astro-ph].
- Carnall, A. C., Walker, S., McLure, R. J., Dunlop, J. S., McLeod, D. J., Cullen, F., Wild, V., Amorin, R., Bolzonella, M., Castellano, M., Cimatti, A., Cucciati, O., Fontana, A., Gargiulo, A., Garilli, B., Jarvis, M. J., Pentericci, L., Pozzetti, L., Zamorani, G., Calabro, A., Hathi, N. P., and Koekemoer, A. M. (2020). Timing the earliest quenching events with a robust sample of massive quiescent galaxies at $2 < z < 5$. *Monthly Notices of the Royal Astronomical Society*, 496(1):695–707. arXiv: 2001.11975.
- Casey, C. M., Kartaltepe, J. S., Drakos, N. E., Franco, M., Ilbert, O., Rose, C., Cox, I. G., Nightingale, J. W., Robertson, B. E., Silverman, J. D., Koekemoer, A. M., Massey, R., McCracken, H. J., Rhodes, J., Akins, H. B., Amvrosiadis, A., Arango-Toro, R. C., Bagley, M. B., Capak, P. L., Champagne, J. B., Chartab, N., Ortiz, O. A. C., Cooke, K. C., Cooper, O. R., Darvish, B., Ding, X., Faisst, A. L., Finkelstein, S. L., Fujimoto, S., Gentile, F., Gillman, S., Gould, K. M. L., Gozaliasl, G., Harish, S., Hayward, C. C., He, Q., Hemmati, S., Hirschmann, M., Jin, S., Khostovan, A. A., Kokorev, V., Lambrides, E., Laigle, C., Leung, G. C. K., Liu, D., Liaudat, T., Long, A. S., Magdis, G., Mahler, G., Mainieri, V., Manning, S. M., Maraston, C., Martin, C. L., McCleary, J. E., McKinney, J., McPartland, C. J. R., Mobasher, B., Pattnaik, R., Renzini, A., Rich, R. M., Sanders, D. B., Sattari, Z., Scognamiglio, D., Scoville, N., Sheth, K., Shuntov, M., Sparre, M., Suzuki, T. L., Talia, M., Toft, S., Trakhtenbrot, B., Urry, C. M., Valentino, F., Vanderhoof, B. N., Vardoulaki, E., Weaver, J. R., Whitaker, K. E., Wilkins, S. M., Yang, L., and Zavala, J. A. (2022). COSMOS-Web: An Overview of the JWST Cosmic Origins Survey. arXiv:2211.07865 [astro-ph].
- Casey, C. M., Narayanan, D., and Cooray, A. (2014). Dusty star-forming galaxies at high redshift. *Physics Reports*, 541:45–161. ADS Bibcode: 2014PhR...541...45C.

Casey, C. M., Zavala, J. A., Manning, S. M., Aravena, M., Béthermin, M., Caputi, K. I., Champagne, J. B., Clements, D. L., Drew, P., Finkelstein, S. L., Fujimoto, S., Hayward, C. C., Koekemoer, A., Kokorev, V., Del P. Lagos, C., Long, A. S., Magdis, G. E., Man, A. W. S., Mitsuhashi, I., Popping, G., Spilker, J., Staguhn, J., Talia, M., Toft, S., Treister, E., Weaver, J. R., and Yun, M. (2021). Mapping Obscuration to Reionization with ALMA (MORA): 2 mm Efficiently Selects the Highest-redshift Obscured Galaxies. *The Astrophysical Journal*, 923(2):215.

Cecchi, R., Bolzonella, M., Cimatti, A., and Girelli, G. (2019). Quiescent galaxies at $z \sim 2.5$: observations vs. models. *The Astrophysical Journal*, 880(1):L14. arXiv:1906.11842.

Chabrier, G. (2003). Galactic Stellar and Substellar Initial Mass Function. *Publications of the Astronomical Society of the Pacific*, 115:763–795. ADS Bibcode: 2003PASP..115..763C.

Chapman, S. C., Blain, A. W., Smail, I., and Ivison, R. J. (2005). A Redshift Survey of the Submillimeter Galaxy Population. *The Astrophysical Journal*, 622:772–796. Publisher: IOP ADS Bibcode: 2005ApJ...622..772C.

Chauhan, G., Lagos, C. d. P., Obreschkow, D., Power, C., Oman, K., and Elahi, P. J. (2019). The H I velocity function: a test of cosmology or baryon physics? *Monthly Notices of the Royal Astronomical Society*, 488:5898–5915. ADS Bibcode: 2019MNRAS.488.5898C.

Chen, Y.-M., Shi, Y., Wild, V., Tremonti, C., Rowlands, K., Bizyaev, D., Yan, R., Lin, L., and Riffel, R. (2019). Post-Starburst Galaxies in SDSS-IV MaNGA. *Monthly Notices of the Royal Astronomical Society*, 489(4):5709–5722. arXiv:1909.01658 [astro-ph].

Cheng, C., Huang, J.-S., Smail, I., Yan, H., Cohen, S. H., Jansen, R. A., Windhorst, R. A., Ma, Z., Koekemoer, A., Willmer, C. N. A., Willner, S. P., Diego, J. M., Frye, B., Conselice, C. J., Ferreira, L., Petric, A., Yun, M., Gim, H. B., Polletta, M. d. C., Duncan, K. J., Honor, R., Holwerda, B. W., Röttgering, H. J. A., Hathi, N. P., Kamieneski, P. S., Adams, N. J., Coe, D., Broadhurst, T., Summers, J., Tompkins, S., Driver, S. P., Grogin, N. A., Marshall, M. A., Pirzkal, N., Robotham, A., and Ryan Jr, R. E. (2022). JWST’s PEARLS: A JWST/NIRCam view of ALMA sources. arXiv:2210.08163 [astro-ph].

Cimatti, A., Cassata, P., Pozzetti, L., Kurk, J., Mignoli, M., Renzini, A., Daddi, E., Bolzonella, M., Brusa, M., Rodighiero, G., Dickinson, M., Franceschini, A., Zamorani, G., Berta, S., Rosati, P., and Halliday, C. (2008). GMASS ultradeep spectroscopy of galaxies at $z \sim 2$ - II. Superdense passive galaxies: how did they form and evolve? *Astronomy & Astrophysics*, 482(1):21–42. Number: 1 Publisher: EDP Sciences.

Coe, D., Salmon, B., Bradač, M., Bradley, L. D., Sharon, K., Zitrin, A., Acebron, A., Cerny, C., Cibirka, N., Strait, V., Paterno-Mahler, R., Mahler, G., Avila, R. J., Ogaz, S., Huang, K.-H., Pelliccia, D., Stark, D. P., Mainali, R., Oesch, P. A., Trenti, M., Carrasco, D., Dawson, W. A., Rodney, S. A., Strolger, L.-G., Riess, A. G., Jones, C., Frye, B. L., Czakon, N. G., Umetsu, K., Vulcani, B., Graur, O., Jha, S. W., Graham, M. L., Molino, A., Nonino, M., Hjorth, J., Selsing, J., Christensen, L., Kikuchihara, S., Ouchi, M., Oguri, M., Welch, B., Lemaux, B. C., Andrade-Santos, F., Hoag, A. T., Johnson, T. L., Peterson, A., Past, M., Fox, C., Agulli, I., Livermore, R., Ryan, R. E., Lam, D., Sendra-Server, I., Toft, S., Lovisari, L., and Su, Y. (2019). RELICS: Reionization Lensing Cluster Survey. *The Astrophysical Journal*, 884:85. Publisher: IOP ADS Bibcode: 2019ApJ...884...85C.

Collaboration, A., Robitaille, T. P., Tollerud, E. J., Greenfield, P., Droettboom, M., Bray, E., Aldcroft, T., Davis, M., Ginsburg, A., Price-Whelan, A. M., Kerzendorf, W. E., Conley, A., Crighton, N., Barbary, K., Muna, D., Ferguson, H., Grollier, F., Parikh, M. M., Nair, P. H., Unther, H. M., Deil, C., Woillez, J., Conseil, S., Kramer, R., Turner, J. E. H., Singer, L., Fox, R., Weaver, B. A., Zabalza, V., Edwards, Z. I., Azalee Bostroem, K., Burke, D. J., Casey, A. R., Crawford, S. M., Dencheva, N., Ely, J., Jenness, T., Labrie, K., Lim, P. L., Pierfederici, F., Pontzen, A., Ptak, A., Refsdal, B., Servillat, M., and Streicher, O. (2013). Astropy: A community Python package for astronomy. *Astronomy and Astrophysics*, 558:A33.

Conroy, C. and Gunn, J. E. (2010). The Propagation of Uncertainties in Stellar Population Synthesis Modeling. III. Model Calibration, Comparison, and Evaluation. *The Astrophysical Journal*, 712:833–857. ADS Bibcode: 2010ApJ...712..833C.

Conroy, C., Gunn, J. E., and White, M. (2009). THE PROPAGATION OF UNCERTAINTIES IN STELLAR POPULATION SYNTHESIS MODELING. I. THE RELEVANCE OF UNCERTAIN ASPECTS OF STELLAR EVOLUTION AND THE INITIAL MASS FUNCTION TO THE DERIVED PHYSICAL PROPERTIES OF GALAXIES. *The Astrophysical Journal*, 699(1):486–506.

Cunha, E. d., Walter, F., Smail, I. R., Swinbank, A. M., Simpson, J. M., Decarli, R., Hodge, J. A., Weiss, A., Werf, P. P. v. d., Bertoldi, F., Chapman, S. C., Cox, P., Danielson, A. L. R., Dannerbauer, H., Greve, T. R., Ivison, R. J., Karim, A., and Thomson, A. (2015). AN ALMA SURVEY OF SUB-MILLIMETER GALAXIES IN THE EXTENDED CHANDRA DEEP FIELD SOUTH: PHYSICAL PROPERTIES DERIVED FROM ULTRAVIOLET-TO-RADIO MODELING. *The Astrophysical Journal*, 806(1):110. Publisher: The American Astronomical Society.

Cutler, S. E., Whitaker, K. E., Weaver, J. R., Wang, B., Pan, R., Bezanson, R., Furtak, L. J., Labbe, I., Leja, J., Price, S. H., Cheng, Y., Clausen, M., Cullen, F., Dayal, P., de Graaff, A., Dickinson, M., Dunlop, J. S., Feldmann, R., Franx, M., Giavalisco, M., Glazebrook, K., Greene, J. E., Grogin, N. A., Illingworth, G., Koekemoer, A. M., Kokorev, V., Marchesini, D., Maseda, M. V., Miller, T. B., Nanayakkara, T., Nelson, E. J., Setton, D. J., Shipley, H., and Suess, K. A. (2023). Two Distinct Classes of Quiescent Galaxies at Cosmic Noon Revealed by JWST PRIMER and UNCOVER. Publication Title: arXiv e-prints ADS Bibcode: 2023arXiv231215012C.

Daddi, E., Cimatti, A., Renzini, A., Fontana, A., Mignoli, M., Pozzetti, L., Tozzi, P., and Zamorani, G. (2004a). A New Photometric Technique for the Joint Selection of Star-forming and Passive Galaxies at $1.4 < z < 2.5$. *The Astrophysical Journal*, 617:746–764. ADS Bibcode: 2004ApJ...617..746D.

Daddi, E., Cimatti, A., Renzini, A., Vernet, J., Conselice, C., Pozzetti, L., Mignoli, M., Tozzi, P., Broadhurst, T., di Serego Alighieri, S., Fontana, A., Nonino, M., Rosati, P., and Zamorani, G. (2004b). Near-Infrared Bright Galaxies at $z \sim 2$. Entering the Spheroid Formation Epoch? *The Astrophysical Journal*, 600:L127–L130. ADS Bibcode: 2004ApJ...600L.127D.

Daddi, E., Delvecchio, I., Dimauro, P., Magnelli, B., Gomez-Guijarro, C., Coogan, R., Elbaz, D., Kalita, B. S., Le Bail, A., Rich, R. M., and Tan, Q. (2022). The bending of the star-forming main sequence traces the cold- to hot-accretion transition mass over $0 < z < 4$. *Astronomy and Astrophysics*, 661:L7. ADS Bibcode: 2022A&A...661L...7D.

Dalton, G. B., Caldwell, M., Ward, A. K., Whalley, M. S., Woodhouse, G., Edeson, R. L., Clark, P., Beard, S. M., Gallie, A. M., Todd, S. P., Strachan, J. M. D., Bezawada, N. N., Sutherland, W. J., and Emerson, J. P. (2006). The VISTA infrared camera. 6269:6269oX. Conference Name: Society of Photo-Optical Instrumentation Engineers (SPIE) Conference Series ADS Bibcode: 2006SPIE.6269E..oXD.

Dantas, M. L. L., Coelho, P. R. T., and Sánchez-Blázquez, P. (2020). UV upturn versus UV weak galaxies: differences and similarities of their stellar populations unveiled by a de-biased sample. *arXiv:2009.03915 [astro-ph]*. arXiv: 2009.03915.

Davidzon, I., Ilbert, O., Laigle, C., Coupon, J., McCracken, H. J., Delvecchio, I., Masters, D., Capak, P. L., Hsieh, B. C., Tresse, L., Fevre, O. L., Bethermin, M., Chang, Y.-Y., Faisst, A. L., Floc'h, E. L., Steinhardt, C., Toft, S., Aussel, H., Dubois, C., Hasinger, G., Salvato, M., Sanders, D. B., Scoville, N., and Silverman, J. D. (2017). The COSMOS2015 galaxy stellar mass function: 13 billion years of stellar mass assembly in 10 snapshots. *Astronomy & Astrophysics*, 605:A70. arXiv:1701.02734 [astro-ph].

- Davies, R. L., Belli, S., Park, M., Mendel, J. T., Johnson, B. D., Conroy, C., Benton, C., Bugiani, L., Emami, R., Leja, J., Li, Y., Maheson, G., Mathews, E. P., Naidu, R. P., Nelson, E. J., Tacchella, S., Terrazas, B. A., and Weinberger, R. (2024). JWST Reveals Widespread AGN-Driven Neutral Gas Outflows in Massive $z \sim 2$ Galaxies. *Monthly Notices of the Royal Astronomical Society*, 528(3):4976–4992. arXiv:2310.17939 [astro-ph].
- de Graaff, A., Rix, H.-W., Carniani, S., Suess, K. A., Charlot, S., Curtis-Lake, E., Arribas, S., Baker, W. M., Boyett, K., Bunker, A. J., Cameron, A. J., Chevallard, J., Curti, M., Eisenstein, D. J., Franx, M., Hainline, K., Hausen, R., Ji, Z., Johnson, B. D., Jones, G. C., Maiolino, R., Maseda, M. V., Nelson, E., Parlanti, E., Rawle, T., Robertson, B., Tacchella, S., Übler, H., Williams, C. C., Willmer, C. N. A., and Willott, C. (2023). Ionised gas kinematics and dynamical masses of $z \sim 6$ galaxies from JADES/NIRSpec high-resolution spectroscopy. arXiv:2308.09742 [astro-ph].
- de Graaff, A., Setton, D. J., Brammer, G., Cutler, S., Suess, K. A., Labbe, I., Leja, J., Weibel, A., Maseda, M. V., Whitaker, K. E., Bezanson, R., Boogaard, L. A., Cleri, N. J., De Lucia, G., Franx, M., Greene, J. E., Hirschmann, M., Matthee, J., McConachie, I., Naidu, R. P., Oesch, P. A., Price, S. H., Rix, H.-W., Valentino, F., Wang, B., and Williams, C. C. (2024). Efficient formation of a massive quiescent galaxy at redshift 4.9. arXiv:2404.05683 [astro-ph].
- Desprez, G., Martis, N. S., Asada, Y., Sawicki, M., Willott, C. J., Muzzin, A., Abraham, R. G., Bradač, M., Brammer, G., Estrada-Carpenter, V., Iyer, K. G., Matharu, J., Mowla, L., Noirot, G., Sarrouh, G. T. E., Strait, V., Gledhill, R., and Rihtaršič, G. (2023). Λ CDM not dead yet: massive high- z Balmer break galaxies are less common than previously reported. Publication Title: arXiv e-prints ADS Bibcode: 2023arXiv231003063D.
- D’Eugenio, C., Daddi, E., Gobat, R., Strazzullo, V., Lustig, P., Delvecchio, I., Jin, S., Cimatti, A., and Onodera, M. (2020a). HST grism spectroscopy of $z \sim 3$ massive quiescent galaxies: Approaching the metamorphosis. arXiv:2012.02767 [astro-ph]. arXiv: 2012.02767.
- D’Eugenio, C., Daddi, E., Gobat, R., Strazzullo, V., Lustig, P., Delvecchio, I., Jin, S., Puglisi, A., Calabró, A., Mancini, C., Dickinson, M., Cimatti, A., and Onodera, M. (2020b). The Typical Massive Quiescent Galaxy at $z \sim 3$ is a Post-starburst. *The Astrophysical Journal Letters*, 892:L2.
- Di Matteo, T., Springel, V., and Hernquist, L. (2005). Energy input from quasars regulates the growth and activity of black holes and their host galaxies. *Nature*, 433:604–607. ADS Bibcode: 2005Natur.433..604D.

- Dome, T., Tacchella, S., Fialkov, A., Ceverino, D., Dekel, A., Ginzburg, O., Lapiner, S., and Looser, T. J. (2024). Mini-quenching of $z = 4-8$ galaxies by bursty star formation. *Monthly Notices of the Royal Astronomical Society*, 527:2139–2151. Publisher: OUP ADS Bibcode: 2024MNRAS.527.2139D.
- Domínguez, A., Siana, B., Henry, A. L., Scarlata, C., Bedregal, A. G., Malkan, M., Atek, H., Ross, N. R., Colbert, J. W., Teplitz, H. I., Rafelski, M., McCarthy, P., Bunker, A., Hathi, N. P., Dressler, A., Martin, C. L., and Masters, D. (2013). DUST EXTINCTION FROM BALMER DECREMENTS OF STAR-FORMING GALAXIES AT $0.75 < z < 1.5$ WITH *HUBBLE SPACE TELESCOPE* /WIDE-FIELD-CAMERA 3 SPECTROSCOPY FROM THE WFC3 INFRARED SPECTROSCOPIC PARALLEL SURVEY. *The Astrophysical Journal*, 763(2):145.
- Donnan, C. T., McLeod, D. J., Dunlop, J. S., McLure, R. J., Carnall, A. C., Begley, R., Cullen, F., Hamadouche, M. L., Bowler, R. A. A., Magee, D., McCracken, H. J., Milvang-Jensen, B., Moneti, A., and Targett, T. (2023). The evolution of the galaxy UV luminosity function at redshifts $z < 8 - 15$ from deep JWST and ground-based near-infrared imaging. *Monthly Notices of the Royal Astronomical Society*, 518:6011–6040. Publisher: OUP ADS Bibcode: 2023MNRAS.518.6011D.
- Draine, B. T., Aniano, G., Krause, O., Groves, B., Sandstrom, K., Braun, R., Leroy, A., Klaas, U., Linz, H., Rix, H.-W., Schinnerer, E., Schmiedeke, A., and Walter, F. (2014). Andromeda's Dust. *The Astrophysical Journal*, 780:172. ADS Bibcode: 2014ApJ...780..172D.
- Draine, B. T. and Li, A. (2007). Infrared Emission from Interstellar Dust. IV. The Silicate-Graphite-PAH Model in the Post-Spitzer Era. *The Astrophysical Journal*, 657(2):810. Publisher: IOP Publishing.
- Dressler, A. and Gunn, J. E. (1983). Spectroscopy of galaxies in distant clusters. II. The population of the 3C 295 cluster. *The Astrophysical Journal*, 270:7–19. ADS Bibcode: 1983ApJ...270....7D.
- Driver, S. P., Popescu, C. C., Tuffs, R. J., Graham, A. W., Liske, J., and Baldry, I. (2008). The Energy Output of the Universe from 0.1 to 1000 μm . *The Astrophysical Journal*, 678:L101. ADS Bibcode: 2008ApJ...678L.101D.
- Díaz-Santos, T., Armus, L., Charmandaris, V., Lu, N., Stierwalt, S., Stacey, G., Malhotra, S., Werf, P. P. v. d., Howell, J. H., Privon, G. C., Mazzarella, J. M., Goldsmith, P. F., Murphy, E. J., Barcos-Muñoz, L., Linden, S. T., Inami, H., Larson, K. L., Evans, A. S., Appleton, P., Iwasawa, K., Lord, S., Sanders, D. B., and Surace, J. A. (2017). A Herschel/PACS

- Far-infrared Line Emission Survey of Local Luminous Infrared Galaxies. *The Astrophysical Journal*, 846(1):32. Publisher: The American Astronomical Society.
- D'Eugenio, C., Daddi, E., Liu, D., and Gobat, R. (2023). The [CII] 158 μm emission line as a gas mass tracer in high redshift quiescent galaxies. *Astronomy & Astrophysics*, 678:L9. Publisher: EDP Sciences.
- Eddington, A. S. (1926). *The Internal Constitution of the Stars*. Publication Title: The Internal Constitution of the Stars ADS Bibcode: 1926ics..book.....E.
- Eggen, O. J., Lynden-Bell, D., and Sandage, A. R. (1962). Evidence from the motions of old stars that the Galaxy collapsed. *The Astrophysical Journal*, 136:748. ADS Bibcode: 1962ApJ...136..748E.
- Emerson, J., McPherson, A., and Sutherland, W. (2006). Visible and Infrared Survey Telescope for Astronomy: Progress Report. *The Messenger*, 126:41–42. ADS Bibcode: 2006Msngr.126...41E.
- Esdaile, J., Glazebrook, K., Labbe, I., Taylor, E., Schreiber, C., Nanayakkara, T., Kacprzak, G. G., Oesch, P. A., Tran, K.-V. H., Papovich, C., Spitler, L., and Straatman, C. M. S. (2020). Confirmation of stellar masses and potential light IMF in massive quiescent galaxies at $3 < z < 4$ using velocity dispersions measurements with MOSFIRE. *arXiv:2010.09738 [astro-ph]*. arXiv: 2010.09738.
- Faisst, A. L. and Morishita, T. (2024). Dead or Alive? How Bursty Star Formation and Patchy Dust Can Cause Temporary Quiescence in High Redshift Galaxies. Publication Title: arXiv e-prints ADS Bibcode: 2024arXiv240213316F.
- Feldmann, R., Hopkins, P. F., Quataert, E., Faucher-Giguere, C.-A., and Keres, D. (2016). The formation of massive, quiescent galaxies at cosmic noon. *Monthly Notices of the Royal Astronomical Society: Letters*, 458(1):L14–L18. arXiv:1601.04704 [astro-ph].
- Ferguson, H. C., Dickinson, M., and Williams, R. (2000). The Hubble Deep Fields. *Annual Review of Astronomy and Astrophysics*, 38(1):667–715. _eprint: <https://doi.org/10.1146/annurev.astro.38.1.667>.
- Fernández-Soto, A., Lanzetta, K. M., and Yahil, A. (1999). A New Catalog of Photometric Redshifts in the Hubble Deep Field*. *The Astrophysical Journal*, 513(1):34.
- Finkelstein, S. L., Bagley, M. B., Ferguson, H. C., Wilkins, S. M., Kartaltepe, J. S., Papovich, C., Yung, L. Y. A., Arrabal Haro, P., Behroozi, P., Dickinson, M., Kocevski, D. D., Koekoer, A. M., Larson, R. L., Le Bail, A., Morales, A. M., Pérez-González, P. G., Burgarella,

D., Davé, R., Hirschmann, M., Somerville, R. S., Wuyts, S., Bromm, V., Casey, C. M., Fontana, A., Fujimoto, S., Gardner, J. P., Giallisco, M., Grazian, A., Grogin, N. A., Hathi, N. P., Hutchison, T. A., Jha, S. W., Jogee, S., Kewley, L. J., Kirkpatrick, A., Long, A. S., Lotz, J. M., Pentericci, L., Pierel, J. D. R., Pirzkal, N., Ravindranath, S., Ryan, R. E., Trump, J. R., Yang, G., Bhatawdekar, R., Bisigello, L., Buat, V., Calabrò, A., Castellano, M., Cleri, N. J., Cooper, M. C., Croton, D., Daddi, E., Dekel, A., Elbaz, D., Franco, M., Gawiser, E., Holwerda, B. W., Huertas-Company, M., Jaskot, A. E., Leung, G. C. K., Lucas, R. A., Mobasher, B., Pandya, V., Tacchella, S., Weiner, B. J., and Zavala, J. A. (2023). CEERS Key Paper. I. An Early Look into the First 500 Myr of Galaxy Formation with JWST. *The Astrophysical Journal*, 946:L13. ADS Bibcode: 2023ApJ...946L..13F.

Fontana, A., Santini, P., Grazian, A., Pentericci, L., Fiore, F., Castellano, M., Giallongo, E., Menci, N., Salimbeni, S., Cristiani, S., Nonino, M., and Vanzella, E. (2009). The Fraction of Quiescent Massive Galaxies in the Early Universe. *arXiv:0901.2898 [astro-ph]*. arXiv: 0901.2898.

Foreman-Mackey, D., Hogg, D. W., Lang, D., and Goodman, J. (2013). emcee: The MCMC Hammer. *Publications of the Astronomical Society of the Pacific*, 125(925):306–312. arXiv:1202.3665 [astro-ph, physics:physics, stat].

Forrest, B., Annunziatella, M., Wilson, G., Marchesini, D., Muzzin, A., Cooper, M. C., Marsan, Z. C., McConachie, I., Chan, J. C. C., Gomez, P., Kado-Fong, E., La Barbera, F., Labbé, I., Lange-Vagle, D., Nantais, J., Nonino, M., Peña, T., Saracco, P., Stefanon, M., and van der Burg, R. F. J. (2020a). An Extremely Massive Quiescent Galaxy at $z=3.493$: Evidence of Insufficiently Rapid Quenching Mechanisms in Theoretical Models. *The Astrophysical Journal*, 890(1):L1. arXiv: 1910.10158.

Forrest, B., Marsan, Z. C., Annunziatella, M., Wilson, G., Muzzin, A., Marchesini, D., Cooper, M. C., Chan, J. C. C., McConachie, I., Gomez, P., Kado-Fong, E., La Barbera, F., Lange-Vagle, D., Nantais, J., Nonino, M., Saracco, P., Stefanon, M., and van der Burg, R. F. J. (2020b). The Massive Ancient Galaxies At $z>3$ NEar-infrared (MAGAZ₃NE) Survey: Confirmation of Extremely Rapid Star-Formation and Quenching Timescales for Massive Galaxies in the Early Universe. *arXiv:2009.07281 [astro-ph]*. arXiv: 2009.07281.

Forrest, B., Wilson, G., Muzzin, A., Marchesini, D., Cooper, M. C., Marsan, Z. C., Annunziatella, M., McConachie, I., Zaidi, K., Gomez, P., Stawinski, S. M. U., Chang, W., de Lucia, G., La Barbera, F., Lubin, L., Nantais, J., Peña, T., Saracco, P., Surace, J., and Stefanon, M. (2022). MAGAZ₃NE: High Stellar Velocity Dispersions for Ultra-Massive Quiescent Galaxies at $z\gtrsim 3$. arXiv:2208.04329 [astro-ph].

- Franco, M., Elbaz, D., Béthermin, M., Magnelli, B., Schreiber, C., Ciesla, L., Dickinson, M., Nagar, N., Silverman, J., Daddi, E., Alexander, D. M., Wang, T., Pannella, M., Floc'h, E. L., Pope, A., Giavalisco, M., Maury, A. J., Bournaud, F., Chary, R., Demarco, R., Ferguson, H., Finkelstein, S. L., Inami, H., Iono, D., Juneau, S., Lagache, G., Leiton, R., Lin, L., Magdis, G., Messias, H., Motohara, K., Mullaney, J., Okumura, K., Papovich, C., Pforr, J., Rujopakarn, W., Sargent, M., Shu, X., and Zhou, L. (2018). GOODS-ALMA: 1.1 mm galaxy survey - I. Source catalog and optically dark galaxies. *Astronomy & Astrophysics*, 620:A152. Publisher: EDP Sciences.
- Franx, M., Labbé, I., Rudnick, G., Dokkum, P. G. v., Daddi, E., Schreiber, N. M. F., Moorwood, A., Rix, H.-W., Röttgering, H., Wel, A. v. d., Werf, P. v. d., and Starckenburg, L. v. (2003). A Significant Population of Red, Near-Infrared-selected High-Redshift Galaxies*. *The Astrophysical Journal*, 587(2):L79. Publisher: IOP Publishing.
- French, K. D. (2021). Evolution Through the Post-Starburst Phase: Using Post-Starburst Galaxies as Laboratories for Understanding the Processes that Drive Galaxy Evolution. *arXiv:2106.05982 [astro-ph]*. arXiv: 2106.05982 version: 1.
- Fujimoto, S., Kohno, K., Ouchi, M., Oguri, M., Kokorev, V., Brammer, G., Sun, F., Gonzalez-Lopez, J., Bauer, F. E., Caminha, G. B., Hatsukade, B., Richard, J., Smail, I., Tsujita, A., Ueda, Y., Uematsu, R., Zitrin, A., Coe, D., Kneib, J.-P., Postman, M., Umetsu, K., Lagos, C. d. P., Popping, G., Ao, Y., Bradley, L., Caputi, K., Dessauges-Zavadsky, M., Egami, E., Espada, D., Ivison, R. J., Jauzac, M., Knudsen, K. K., Koekemoer, A. M., Magdis, G. E., Mahler, G., Arancibia, A. M. M., Rawle, T., Shimasaku, K., Toft, S., Uemehata, H., Valentino, F., Wang, T., and Wang, W.-H. (2023). ALMA Lensing Cluster Survey: Deep 1.2 mm Number Counts and Infrared Luminosity Functions at $z \sim 1-8$. *arXiv:2303.01658 [astro-ph]*.
- Fumagalli, M., Labbe, I., Patel, S. G., Franx, M., van Dokkum, P., Brammer, G., da Cunha, E., Schreiber, N. M. F., Kriek, M., Quadri, R., Rix, H.-W., Wake, D., Whitaker, K. E., Lundgren, B., Marchesini, D., Maseda, M., Momcheva, I., Nelson, E., Pacifici, C., and Skelton, R. E. (2014). How dead are dead galaxies? Mid-Infrared fluxes of quiescent galaxies at redshift $0.3 < z < 2.5$: implications for star formation rates and dust heating. *The Astrophysical Journal*, 796(1):35. arXiv: 1308.4132.
- Gaia Collaboration, Vallenari, A., Brown, A. G. A., Prusti, T., de Bruijne, J. H. J., Arenou, F., Babusiaux, C., Biermann, M., Creevey, O. L., Ducourant, C., Evans, D. W., Eyer, L., Guerra, R., Hutton, A., Jordi, C., Klioner, S. A., Lammers, U. L., Lindgren, L., Luri, X., Mignard, F., Panem, C., Pourbaix, D., Randich, S., Sartoretti, P., Soubiran, C., Tanga, P., Walton, N. A., Bailer-Jones, C. A. L., Bastian, U., Drimmel, R., Jansen, F., Katz, D.,

Lattanzi, M. G., van Leeuwen, F., Bakker, J., Cacciari, C., Castañeda, J., De Angeli, F., Fabricius, C., Fouesneau, M., Frémat, Y., Galluccio, L., Guerrier, A., Heiter, U., Masana, E., Messineo, R., Mowlavi, N., Nicolas, C., Nienartowicz, K., Pailler, F., Panuzzo, P., Rickett, F., Roux, W., Seabroke, G. M., Sordo, R., Thévenin, F., Gracia-Abril, G., Portell, J., Teyssier, D., Altmann, M., Andrae, R., Audard, M., Bellas-Velidis, I., Benson, K., Berthier, J., Blomme, R., Burgess, P. W., Busonero, D., Busso, G., Cánovas, H., Carry, B., Cellino, A., Cheek, N., Clementini, G., Damerdj, Y., Davidson, M., de Teodoro, P., Nuñez Campos, M., Delchambre, L., Dell’Oro, A., Esquej, P., Fernández-Hernández, J., Fraile, E., Garabato, D., García-Lario, P., Gosset, E., Haigron, R., Halbwachs, J. L., Hambly, N. C., Harrison, D. L., Hernández, J., Hestroffer, D., Hodgkin, S. T., Holl, B., Janßen, K., Jevardat de Fombelle, G., Jordan, S., Krone-Martins, A., Lanzafame, A. C., Löffler, W., Marchal, O., Marrese, P. M., Moitinho, A., Muinonen, K., Osborne, P., Pancino, E., Pauwels, T., Recio-Blanco, A., Reyly, C., Riello, M., Rimoldini, L., Roegiers, T., Rybizki, J., Sarro, L. M., Siopis, C., Smith, M., Sozzetti, A., Utrilla, E., van Leeuwen, M., Abbas, U., Abraham, P., Abreu Aramburu, A., Aerts, C., Aguado, J. J., Ajaj, M., Aldea-Montero, F., Altavilla, G., Álvarez, M. A., Alves, J., Anders, F., Anderson, R. I., Anglada Varela, E., Antoja, T., Baines, D., Baker, S. G., Balaguer-Núñez, L., Balbinot, E., Balog, Z., Barache, C., Barbato, D., Barros, M., Barstow, M. A., Bartolomé, S., Bassilana, J. L., Bauchet, N., Becciani, U., Bellazzini, M., Berihuete, A., Bernet, M., Bertone, S., Bianchi, L., Binnenfeld, A., Blanco-Cuaresma, S., Blazere, A., Boch, T., Bombrun, A., Bossini, D., Bouquillon, S., Bragaglia, A., Bramante, L., Breedt, E., Bressan, A., Brouillet, N., Brugaletta, E., Bucciarelli, B., Burlacu, A., Butkevich, A. G., Buzzi, R., Caffau, E., Cancelliere, R., Cantat-Gaudin, T., Carballo, R., Carlucci, T., Carnerero, M. I., Carrasco, J. M., Casamiquela, L., Castellani, M., Castro-Ginard, A., Chaoul, L., Charlot, P., Chemin, L., Chiaramida, V., Chiavassa, A., Chornay, N., Comoretto, G., Contursi, G., Cooper, W. J., Cornez, T., Cowell, S., Crifo, F., Cropper, M., Crosta, M., Crowley, C., Dafonte, C., Dapergolas, A., David, M., David, P., de Laverny, P., De Luise, F., De March, R., De Ridder, J., de Souza, R., de Torres, A., del Peloso, E. F., del Pozo, E., Delbo, M., Delgado, A., Delisle, J. B., Demouchy, C., Dharmawardena, T. E., Di Matteo, P., Diakite, S., Diener, C., Distefano, E., Dolding, C., Edvardsson, B., Enke, H., Fabre, C., Fabrizio, M., Faigler, S., Fedorets, G., Fernique, P., Fienga, A., Figueras, F., Fournier, Y., Fouron, C., Fragkoudi, F., Gai, M., Garcia-Gutierrez, A., Garcia-Reinaldos, M., García-Torres, M., Garofalo, A., Gavel, A., Gavras, P., Gerlach, E., Geyer, R., Giacobbe, P., Gilmore, G., Girona, S., Giuffrida, G., Gommel, R., Gomez, A., González-Núñez, J., González-Santamaría, I., González-Vidal, J. J., Granvik, M., Guillout, P., Guiraud, J., Gutiérrez-Sánchez, R., Guy, L. P., Hatzidimitriou, D., Hauser, M., Hayward, M., Helmer, A., Helmi, A., Sarmiento, M. H., Hidalgo, S. L., Hilger, T., Hładczuk, N., Hobbs, D., Holland, G., Huckle, H. E., Jardine, K., Jasniewicz, G., Jean-Antoine Piccolo, A., Jiménez-Arranz, ♦., Jorissen, A., Juaristi Campillo, J., Julbe, F., Karbevská, L.,

Kervella, P., Khanna, S., Kontizas, M., Kordopatis, G., Korn, A. J., Kóspál, ♦, Kostrzewa-Rutkowska, Z., Kruszyńska, K., Kun, M., Laizeau, P., Lambert, S., Lanza, A. F., Lasne, Y., Le Campion, J. F., Lebreton, Y., Lebzelter, T., Leccia, S., Leclerc, N., Lecoœur-Taïbi, I., Liao, S., Licata, E. L., Lindstrøm, H. E. P., Lister, T. A., Livanou, E., Lobel, A., Lorca, A., Loup, C., Madrero Pardo, P., Magdaleno Romeo, A., Managau, S., Mann, R. G., Manteiga, M., Marchant, J. M., Marconi, M., Marcos, J., Marcos Santos, M. M. S., Marín Pina, D., Marinoni, S., Marocco, F., Marshall, D. J., Martin Polo, L., Martín-Fleitas, J. M., Marton, G., Mary, N., Masip, A., Massari, D., Mastrobuono-Battisti, A., Mazeh, T., McMillan, P. J., Messina, S., Michalik, D., Millar, N. R., Mints, A., Molina, D., Molinaro, R., Molnár, L., Monari, G., Monguió, M., Montegriffo, P., Montero, A., Mor, R., Mora, A., Morbidelli, R., Morel, T., Morris, D., Muraveva, T., Murphy, C. P., Musella, I., Nagy, Z., Noval, L., Ocaña, F., Ogden, A., Ordenovic, C., Osinde, J. O., Pagani, C., Pagano, I., Palaversa, L., Palicio, P. A., Pallas-Quintela, L., Panahi, A., Payne-Wardenaar, S., Peñalosa Esteller, X., Penttilä, A., Pichon, B., Piersimoni, A. M., Pineau, F. X., Plachy, E., Plum, G., Poggio, E., Prša, A., Pulone, L., Racero, E., Ragaini, S., Rainer, M., Raiteri, C. M., Rambaux, N., Ramos, P., Ramos-Lerate, M., Re Fiorentin, P., Regibo, S., Richards, P. J., Rios Diaz, C., Ripepi, V., Riva, A., Rix, H. W., Rixon, G., Robichon, N., Robin, A. C., Robin, C., Roelens, M., Rogues, H. R. O., Rohrbasser, L., Romero-Gómez, M., Rowell, N., Royer, F., Ruz Mieres, D., Rybicki, K. A., Sadowski, G., Sáez Núñez, A., Sagristà Sellés, A., Sahlmann, J., Salguero, E., Samaras, N., Sanchez Gimenez, V., Sanna, N., Santoveña, R., Sarasso, M., Schultheis, M., Sciacca, E., Segol, M., Segovia, J. C., Ségransan, D., Semeux, D., Shahaf, S., Siddiqui, H. I., Siebert, A., Siltala, L., Silvelo, A., Slezak, E., Slezak, I., Smart, R. L., Snaith, O. N., Solano, E., Solitro, F., Souami, D., Souchay, J., Spagna, A., Spina, L., Spoto, F., Steele, I. A., Steidelmüller, H., Stephenson, C. A., Süveges, M., Surdej, J., Szabados, L., Szegedi-Elek, E., Taris, F., Taylor, M. B., Teixeira, R., Tolomei, L., Tonello, N., Torra, F., Torra, J., Torralba Elipe, G., Trabucchi, M., Tsounis, A. T., Turon, C., Ulla, A., Unger, N., Vaillant, M. V., van Dillen, E., van Reeven, W., Vanel, O., Vecchiato, A., Viala, Y., Vicente, D., Voutsinas, S., Weiler, M., Wevers, T., Wyrzykowski, ♦, Yoldas, A., Yvard, P., Zhao, H., Zorec, J., Zucker, S., and Zwitter, T. (2023). Gaia Data Release 3. Summary of the content and survey properties. *Astronomy and Astrophysics*, 674:A1. ADS Bibcode: 2023A&A...674A...1G.

Galametz, A., Grazian, A., Fontana, A., Ferguson, H. C., Ashby, M. L. N., Barro, G., Castellano, M., Dahlen, T., Donley, J. L., Faber, S. M., Grogin, N., Guo, Y., Huang, K.-H., Kocevski, D. D., Koekemoer, A. M., Lee, K.-S., McGrath, E. J., Peth, M., Willner, S. P., Almaini, O., Cooper, M., Cooray, A., Conselice, C. J., Dickinson, M., Dunlop, J. S., Fazio, G. G., Foucaud, S., Gardner, J. P., Giavalisco, M., Hathi, N. P., Hartley, W. G., Koo, D. C., Lai, K., de Mello, D. F., McLure, R. J., Lucas, R. A., Paris, D., Pentericci, L., Santini, P.,

- Simpson, C., Sommariva, V., Targett, T., Weiner, B. J., Wuyts, S., and CANDELS Team (2013). CANDELS Multiwavelength Catalogs: Source Identification and Photometry in the CANDELS UKIDSS Ultra-deep Survey Field. *The Astrophysical Journal Supplement Series*, 206:10. Publisher: IOP ADS Bibcode: 2013ApJS..206...10G.
- Gelli, V., Salvadori, S., Ferrara, A., and Pallottini, A. (2024). Can Supernovae Quench Star Formation in High- z Galaxies? *The Astrophysical Journal*, 964:76. Publisher: IOP ADS Bibcode: 2024ApJ...964...76G.
- Gelli, V., Salvadori, S., Ferrara, A., Pallottini, A., and Carniani, S. (2023). Quiescent low-mass galaxies observed by JWST in the Epoch of Reionization. arXiv:2303.13574 [astro-ph].
- Giménez-Arteaga, C., Fujimoto, S., Valentino, F., Brammer, G. B., Mason, C. A., Rizzo, F., Rusakov, V., Colina, L., Prieto-Lyon, G., Oesch, P. A., Espada, D., Heintz, K. E., Knudsen, K. K., Dessauges-Zavadsky, M., Laporte, N., Lee, M., Magdis, G. E., Ono, Y., Ao, Y., Ouchi, M., Kohno, K., and Koekemoer, A. M. (2024). Outshining in the Spatially Resolved Analysis of a Strongly-Lensed Galaxy at $z=6.072$ with JWST NIRCam. arXiv:2402.17875 [astro-ph].
- Girelli, G., Bolzonella, M., and Cimatti, A. (2019). Massive and old quiescent galaxies at high redshift. *Astronomy & Astrophysics*, 632:A80.
- Glazebrook, K., Nanayakkara, T., Esdaile, J., Espejo, J. M., Jacobs, C., Kacprzak, G. G., Labbe, I., Marchesini, D., Marsan, C., Oesch, P., Papovich, C., Remus, R.-S., Schreiber, C., Straatman, C., Tran, K.-V., and Urbina, C. L. (2021). How Many Quiescent Galaxies are There at z . *JWST Proposal. Cycle 1*, page 2565. ADS Bibcode: 2021jwst.prop.2565G.
- Glazebrook, K., Nanayakkara, T., Schreiber, C., Lagos, C., Kawinwanichakij, L., Jacobs, C., Chittenden, H., Brammer, G., Kacprzak, G. G., Labbe, I., Marchesini, D., Marsan, Z. C., Oesch, P. A., Papovich, C., Remus, R.-S., Tran, K.-V. H., Esdaile, J., and Chandro-Gomez, A. (2024). A massive galaxy that formed its stars at $z \approx 11$. *Nature*, 628:277–281. ADS Bibcode: 2024Natur.628..277G.
- Glazebrook, K., Schreiber, C., Labbé, I., Nanayakkara, T., Kacprzak, G. G., Oesch, P. A., Papovich, C., Spitler, L. R., Straatman, C. M. S., Tran, K.-V. H., and Yuan, T. (2017). A massive, quiescent galaxy at redshift of $z=3.717$. *Nature*, 544(7648):71–74. arXiv: 1702.01751.
- Goto, T. (2005). 266 E+A galaxies selected from the Sloan Digital Sky Survey Data Release 2: the origin of E+A galaxies. *Monthly Notices of the Royal Astronomical Society*, 357(3):937–944.

- Gottumukkala, R., Barrufet, L., Oesch, P. A., Weibel, A., Allen, N., Pampliega, B. A., Nelson, E. J., Williams, C. C., Brammer, G., Fudamoto, Y., González, V., Heintz, K. E., Illingworth, G., Magee, D., Naidu, R. P., Shuntov, M., Stefanon, M., Toft, S., Valentino, F., and Xiao, M. (2023). Unveiling the hidden universe with JWST: The contribution of dust-obscured galaxies to the stellar mass function at $\mathbf{z \sim 3-8}$. arXiv:2310.03787 [astro-ph].
- Gould, K. M. L., Brammer, G., Valentino, F., Whitaker, K. E., Weaver, J. R., Lagos, C. d. P., Rizzo, F., Franco, M., Hsieh, B.-C., Ilbert, O., Jin, S., Magdis, G., McCracken, H. J., Mobasher, B., Shuntov, M., Steinhardt, C. L., Strait, V., and Toft, S. (2023). COSMOS2020: Exploring the Dawn of Quenching for Massive Galaxies at $3 < z < 5$ with a New Color-selection Method. *The Astronomical Journal*, 165(6):248. Publisher: The American Astronomical Society.
- Greggio, L. and Renzini, A. (1990). Clues on the Hot Star Content and the Ultraviolet Output of Elliptical Galaxies. *The Astrophysical Journal*, 364:35. ADS Bibcode: 1990ApJ...364...35G.
- Guarnieri, P., Maraston, C., Thomas, D., Pforr, J., Gonzalez-Perez, V., Etherington, J., Carlsen, J., Morice-Atkinson, X., Conselice, C. J., Gschwend, J., Carrasco Kind, M., Abbott, T., Allam, S., Brooks, D., Burke, D., Carnero Rosell, A., Carretero, J., Cunha, C., D’Andrea, C., da Costa, L., De Vincente, J., DePoy, D., Thomas Diehl, H., Doel, P., Frieman, J., Garcia-Bellido, J., Gruen, D., Gutierrez, G., Hanley, D., Hollowood, D., Honscheid, K., James, D., Jeltema, T., Kuehn, K., Lima, M., Maia, M. A. G., Marshall, J., Martini, P., Melchior, P., Menanteau, F., Miquel, R., Plazas Malagon, A., Richardson, S., Romer, K., Sanchez, E., Scarpine, V., Schindler, R., Sevilla, I., Smith, M., Soares-Santos, M., Sobreira, F., Suchyta, E., Tarle, G., Walker, A., and Wester, W. (2019). Candidate massive galaxies at $z \sim 4$ in the Dark Energy Survey. *Monthly Notices of the Royal Astronomical Society*, 483(3):3060–3081.
- Gómez-Guijarro, C., Toft, S., Karim, A., Magnelli, B., Magdis, G. E., Jiménez-Andrade, E. F., Capak, P. L., Fraternali, F., Fujimoto, S., Riechers, D. A., Schinnerer, E., Smolčić, V., Aravena, M., Bertoldi, F., Cortzen, I., Hasinger, G., Hu, E. M., Jones, G. C., Koekemoer, A. M., Lee, N., McCracken, H. J., Michałowski, M. J., Navarrete, F., Pović, M., Puglisi, A., Romano-Díaz, E., Sheth, K., Silverman, J. D., Staguhn, J., Steinhardt, C. L., Stockmann, M., Tanaka, M., Valentino, F., van Kampen, E., and Zirm, A. (2018). Starburst to Quiescent from HST/ALMA: Stars and Dust Unveil Minor Mergers in Submillimeter Galaxies at $z \sim 4.5$. *The Astrophysical Journal*, 856:121. Publisher: IOP ADS Bibcode: 2018ApJ...856..121G.

- Hamilton, D. (1985). The spectral evolution of galaxies. I. an observational approach. *The Astrophysical Journal*, 297:371–389. ADS Bibcode: 1985ApJ...297..371H.
- Harris, C. R., Millman, K. J., van der Walt, S. J., Gommers, R., Virtanen, P., Cournapeau, D., Wieser, E., Taylor, J., Berg, S., Smith, N. J., Kern, R., Picus, M., Hoyer, S., van Kerkwijk, M. H., Brett, M., Haldane, A., del Río, J. F., Wiebe, M., Peterson, P., Gérard-Marchant, P., Sheppard, K., Reddy, T., Weckesser, W., Abbasi, H., Gohlke, C., and Oliphant, T. E. (2020). Array programming with NumPy. *Nature*, 585(7825):357–362. Number: 7825 Publisher: Nature Publishing Group.
- Heintz, K. E., Brammer, G. B., Watson, D., Oesch, P. A., Keating, L. C., Hayes, M. J., Abdurro'uf, Arellano-Córdova, K. Z., Carnall, A. C., Christiansen, C. R., Cullen, F., Davé, R., Dayal, P., Ferrara, A., Finlator, K., Fynbo, J. P. U., Flury, S. R., Gelli, V., Gillman, S., Gottumukkala, R., Gould, K., Greve, T. R., Hardin, S. E., Y. Y Hsiao, T., Hutter, A., Jakobsson, P., Killi, M., Khosravaninezhad, N., Laursen, P., Lee, M. M., Magdis, G. E., Matthee, J., Naidu, R. P., Narayanan, D., Pollock, C., Prescott, M., Rusakov, V., Shuntov, M., Sneppen, A., Smit, R., Tanvir, N. R., Terp, C., Toft, S., Valentino, F., Vijayan, A. P., Weaver, J. R., Wise, J. H., and Witstok, J. (2024). The JWST-PRIMAL Legacy Survey. A JWST/NIRSpec reference sample for the physical properties and Lyman- α absorption and emission of ~ 500 galaxies at $z=5.5-13.4$. Publication Title: arXiv e-prints ADS Bibcode: 2024arXiv240402211H.
- Hinshaw, G., Larson, D., Komatsu, E., Spergel, D. N., Bennett, C. L., Dunkley, J., Nolta, M. R., Halpern, M., Hill, R. S., Odegard, N., Page, L., Smith, K. M., Weiland, J. L., Gold, B., Jarosik, N., Kogut, A., Limon, M., Meyer, S. S., Tucker, G. S., Wollack, E., and Wright, E. L. (2013). Nine-year Wilkinson Microwave Anisotropy Probe (WMAP) Observations: Cosmological Parameter Results. *The Astrophysical Journal Supplement Series*, 208:19. ADS Bibcode: 2013ApJS..208...19H.
- Horne, K. (1986). AN OPTIMAL EXTRACTION ALGORITHM FOR CCD SPECTROSCOPY. *Publications of the Astronomical Society of the Pacific*, 98(604):609. Publisher: IOP Publishing.
- Howarth, I. D. and Schmutz, W. (1992). Near-infrared spectroscopy of galactic Wolf-Rayet stars. *Astronomy and Astrophysics*, 261:503–522. ADS Bibcode: 1992A&A...261..503H.
- Hunter, J. D. (2007). Matplotlib: A 2D Graphics Environment. *Computing in Science & Engineering*, 9(3):90–95. Conference Name: Computing in Science & Engineering.
- Hwang, Y.-H., Wang, W.-H., Chang, Y.-Y., Lim, C.-F., Chen, C.-C., Gao, Z.-K., Dunlop, J. S., Gao, Y., Ho, L. C., Hwang, H. S., Koprowski, M., Michałowski, M. J., Peng,

- Y.-j., Shim, H., Simpson, J. M., and Toba, Y. (2021). Revisiting the Color-Color Selection: Submillimeter and AGN Properties of NUV-r-J Selected Quiescent Galaxies. *arXiv:2103.14336 [astro-ph]*. arXiv: 2103.14336.
- Ichikawa, A. and Matsuoka, Y. (2017). Recently Quenched Galaxies at $z = 0.2 - 4.8$ in the COSMOS UltraVISTA Field. *The Astrophysical Journal*, 843(1):L7. arXiv: 1706.03438.
- Ilbert, O., McCracken, H. J., Fevre, O. L., Capak, P., Dunlop, J., Karim, A., Renzini, M. A., Caputi, K., Boissier, S., Arnouts, S., Aussel, H., Comparat, J., Guo, Q., Hudelot, P., Kartaltepe, J., Kneib, J. P., Krogager, J. K., Floc'h, E. L., Lilly, S., Mellier, Y., Milvang-Jensen, B., Moutard, T., Onodera, M., Richard, J., Salvato, M., Sanders, D. B., Scoville, N., Silverman, J., Taniguchi, Y., Tasca, L., Thomas, R., Toft, S., Tresse, L., Vergani, D., Wolk, M., and Zirm, A. (2013). Mass assembly in quiescent and star-forming galaxies since $z=4$ from UltraVISTA. *Astronomy & Astrophysics*, 556:A55. arXiv: 1301.3157.
- Ishibashi, W. and Fabian, A. C. (2012). Active galactic nucleus feedback and triggering of star formation in galaxies. *Monthly Notices of the Royal Astronomical Society*, 427(4):2998–3005.
- Ito, K., Tanaka, M., Miyaji, T., Ilbert, O., Kauffmann, O. B., Koekemoer, A. M., Marchesi, S., Shuntov, M., Toft, S., Valentino, F., and Weaver, J. R. (2022). COSMOS2020: Ubiquitous AGN Activity of Massive Quiescent Galaxies at $0 < z < 5$ Revealed by X-ray and Radio Stacking. *arXiv:2203.04322 [astro-ph]*. arXiv: 2203.04322.
- Ito, K., Valentino, F., Brammer, G., Faisst, A. L., Gillman, S., Gómez-Guijarro, C., Gould, K. M. L., Heintz, K. E., Ilbert, O., Jespersen, C. K., Kokorev, V., Kubo, M., Magdis, G. E., McPartland, C. J. R., Onodera, M., Rizzo, F., Tanaka, M., Toft, S., Vijayan, A. P., Weaver, J. R., Whitaker, K. E., and Wright, L. (2024). Size–Stellar Mass Relation and Morphology of Quiescent Galaxies at $z \geq 3$ in Public JWST Fields. *The Astrophysical Journal*, 964(2):192. Publisher: The American Astronomical Society.
- Iverson, R. J., Lewis, A. J. R., Weiss, A., Arumugam, V., Simpson, J. M., Holland, W. S., Maddox, S., Dunne, L., Valiante, E., Werf, P. v. d., Omont, A., Dannerbauer, H., Smail, I., Bertoldi, F., Bremer, M., Busmann, R. S., Cai, Z.-Y., Clements, D. L., Cooray, A., Zotti, G. D., Eales, S. A., Fuller, C., Gonzalez-Nuevo, J., Ibar, E., Negrello, M., Oteo, I., Pérez-Fournon, I., Riechers, D., Stevens, J. A., Swinbank, A. M., and Wardlow, J. (2016). THE SPACE DENSITY OF LUMINOUS DUSTY STAR-FORMING GALAXIES AT $z > 4$: SCUBA-2 AND LABOCA IMAGING OF ULTRARED GALAXIES FROM HERSCHEL-ATLAS. *The Astrophysical Journal*, 832(1):78. Publisher: The American Astronomical Society.

- Iyer, K. and Gawiser, E. (2017). Reconstruction of Galaxy Star Formation Histories through SED Fitting: The Dense Basis Approach. *The Astrophysical Journal*, 838(2):127. Publisher: American Astronomical Society.
- Iyer, K. G., Gawiser, E., Faber, S. M., Ferguson, H. C., Kartaltepe, J., Koekemoer, A. M., Pacifici, C., and Somerville, R. S. (2019). Nonparametric Star Formation History Reconstruction with Gaussian Processes. I. Counting Major Episodes of Star Formation. *The Astrophysical Journal*, 879(2):116. Publisher: American Astronomical Society.
- Ji, Z. and Giavalisco, M. (2022). Reconstructing the Assembly of Massive Galaxies. II. Galaxies Develop Massive and Dense Stellar Cores as They Evolve and Head Toward Quiescence at Cosmic Noon. arXiv:2208.04325 [astro-ph].
- Jin, S., Daddi, E., Liu, D., Smolčić, V., Schinnerer, E., Calabrò, A., Gu, Q., Delhaize, J., Delvecchio, I., Gao, Y., Salvato, M., Puglisi, A., Dickinson, M., Bertoldi, F., Sargent, M., Novak, M., Magdis, G., Aretxaga, I., Wilson, G. W., and Capak, P. (2018). “Superdeblended” Dust Emission in Galaxies. II. Far-IR to (Sub)millimeter Photometry and High-redshift Galaxy Candidates in the Full COSMOS Field. *The Astrophysical Journal*, 864(1):56. Publisher: The American Astronomical Society.
- Johnson, B. D., Leja, J., Conroy, C., and Speagle, J. S. (2020). Stellar Population Inference with Prospector. arXiv:2012.01426 [astro-ph]. arXiv: 2012.01426.
- Johnson, H. L. (1955). A photometric system. *Annales d’Astrophysique*, 18:292. ADS Bibcode: 1955AnAp...18..292J.
- Kaasinen, M., Kewley, L., Bian, F., Groves, B., Kashino, D., Silverman, J., and Kartaltepe, J. (2018). The ionization parameter of star-forming galaxies evolves with the specific star formation rate. *Monthly Notices of the Royal Astronomical Society*, 477:5568–5589. ADS Bibcode: 2018MNRAS.477.5568K.
- Kashino, D., Silverman, J. D., Rodighiero, G., Renzini, A., Arimoto, N., Daddi, E., Lilly, S. J., Sanders, D. B., Kartaltepe, J., Zahid, H. J., Nagao, T., Sugiyama, N., Capak, P., Carollo, C. M., Chu, J., Hasinger, G., Ilbert, O., Kajisawa, M., Kewley, L. J., Koekemoer, A. M., Kovač, K., Le Fèvre, O., Masters, D., McCracken, H. J., Onodera, M., Scoville, N., Strazullo, V., Symeonidis, M., and Taniguchi, Y. (2013). THE FMOS-COSMOS SURVEY OF STAR-FORMING GALAXIES AT $z \sim 1.6$. I. H α -BASED STAR FORMATION RATES AND DUST EXTINCTION. *The Astrophysical Journal*, 777(1):L8.
- Kauffmann, G., Charlot, S., and White, S. D. M. (1996). Detection of strong evolution in the population of early-type galaxies. *Monthly Notices of the Royal Astronomical Society*, 283:L117–L122. ADS Bibcode: 1996MNRAS.283L.117K.

- Kauffmann, G., Heckman, T. M., Simon White, D. M., Charlot, S., Tremonti, C., Brinchmann, J., Bruzual, G., Peng, E. W., Seibert, M., Bernardi, M., Blanton, M., Brinkmann, J., Castander, F., Csábai, I., Fukugita, M., Ivezić, Z., Munn, J. A., Nichol, R. C., Padmanabhan, N., Thakar, A. R., Weinberg, D. H., and York, D. (2003). Stellar masses and star formation histories for 10^5 galaxies from the Sloan Digital Sky Survey. *Monthly Notices of the Royal Astronomical Society*, 341(1):33–53.
- Kauffmann, G., White, S. D. M., and Guiderdoni, B. (1993). The formation and evolution of galaxies within merging dark matter haloes. *Monthly Notices of the Royal Astronomical Society*, 264:201–218. ADS Bibcode: 1993MNRAS.264..201K.
- Kennicutt, J. (1998). Star Formation in Galaxies Along the Hubble Sequence. *Annual Review of Astronomy and Astrophysics*, 36(1):189–231. arXiv:astro-ph/9807187.
- Kewley, L. J. and Dopita, M. A. (2002). Using Strong Lines to Estimate Abundances in Extragalactic H ii Regions and Starburst Galaxies. *The Astrophysical Journal Supplement Series*, 142(1):35–52.
- Kewley, L. J., Dopita, M. A., Leitherer, C., Davé, R., Yuan, T., Allen, M., Groves, B., and Sutherland, R. (2013). Theoretical Evolution of Optical Strong Lines across Cosmic Time. *The Astrophysical Journal*, 774:100. ADS Bibcode: 2013ApJ...774..100K.
- Kewley, L. J., Nicholls, D. C., and Sutherland, R. S. (2019). Understanding Galaxy Evolution Through Emission Lines. *Annual Review of Astronomy and Astrophysics*, 57(1):511–570. _eprint: <https://doi.org/10.1146/annurev-astro-081817-051832>.
- Khoperskov, S., Haywood, M., Di Matteo, P., Lehnert, M. D., and Combes, F. (2018). Bar quenching in gas-rich galaxies. *Astronomy and Astrophysics*, 609:A60. ADS Bibcode: 2018A&A...609A..60K.
- Kirkpatrick, A., Pope, A., Sajina, A., Roebuck, E., Yan, L., Armus, L., Díaz-Santos, T., and Stierwalt, S. (2015). The Role of Star Formation and an AGN in Dust Heating of $z = 0.3$ – 2.8 Galaxies. I. Evolution with Redshift and Luminosity. *The Astrophysical Journal*, 814:9. ADS Bibcode: 2015ApJ...814....9K.
- Koekemoer, A. M., Aussel, H., Calzetti, D., Capak, P., Giavalisco, M., Kneib, J. P., Leauthaud, A., Le Fèvre, O., McCracken, H. J., Massey, R., Mobasher, B., Rhodes, J., Scoville, N., and Shopbell, P. L. (2007). The COSMOS Survey: Hubble Space Telescope Advanced Camera for Surveys Observations and Data Processing. *The Astrophysical Journal Supplement Series*, 172:196–202. ADS Bibcode: 2007ApJS..172..196K.

Kohno, K., Fujimoto, S., Tsujita, A., Kokorev, V., Brammer, G., Magdis, G. E., Valentino, F., Laporte, N., Sun, F., Egami, E., Bauer, F. E., Guerrero, A., Nagar, N., Caputi, K. I., Caminha, G. B., Jolly, J. B., Knudsen, K. K., Uematsu, R., Ueda, Y., Oguri, M., Zitrin, A., Ouchi, M., Ono, Y., Gonzalez-Lopez, J., Richard, J., Smail, I., Coe, D., Postman, M., Bradley, L., Koekemoer, A. M., Munoz Arancibia, A. M., Dessauges-Zavadsky, M., Espada, D., Umehata, H., Hatsukade, B., Egusa, F., Shimasaku, K., Matsui-Morokuma, K., Wang, W. H., Wang, T., Ao, Y., Baker, A. J., Lee, M. M., Lagos, C. d. P., Hughes, D. H., and ALCS collaboration (2023). Unbiased surveys of dust-enshrouded galaxies using ALMA. Publication Title: arXiv e-prints ADS Bibcode: 2023arXiv230515126K.

Kokorev, V., Brammer, G., Fujimoto, S., Kohno, K., Magdis, G. E., Valentino, F., Toft, S., Oesch, P., Davidzon, I., Bauer, F. E., Coe, D., Egami, E., Oguri, M., Ouchi, M., Postman, M., Richard, J., Jolly, J.-B., Knudsen, K. K., Sun, F., Weaver, J. R., Ao, Y., Baker, A. J., Bradley, L., Caputi, K. I., Dessauges-Zavadsky, M., Espada, D., Hatsukade, B., Koekemoer, A. M., Muñoz Arancibia, A. M., Shimasaku, K., Umehata, H., Wang, T., and Wang, W.-H. (2022). ALMA Lensing Cluster Survey: $\text{\$HST}$ and $\text{\$Spitzer}$ Photometry of 33 Lensed Fields Built with CHARGE. Technical report. Publication Title: arXiv e-prints ADS Bibcode: 2022arXiv220707125K Type: article.

Kokorev, V., Jin, S., Magdis, G. E., Caputi, K. I., Valentino, F., Dayal, P., Trebitsch, M., Brammer, G., Fujimoto, S., Bauer, F., Iani, E., Kohno, K., Sese, D. B., and Gómez-Guijarro, C. (2023). $\text{\$JWST}$ Insight Into a Lensed $\text{\$HST}$ -dark Galaxy and its Quiescent Companion at $z=2.58$. arXiv:2301.04158 [astro-ph].

Kokorev, V., Magdis, G., Davidzon, I., Brammer, G., Valentino, F., Daddi, E., Ciesla, L., Liu, D., Jin, S., Cortzen, I., Delvecchio, I., Giménez-Arteaga, C., Gómez-Guijarro, C., Sargent, M., Toft, S., and Weaver, J. R. (2021). The Evolving Interstellar Medium of Star-Forming Galaxies, as traced by $\text{\$Stardust}$. *The Astrophysical Journal*, 921(1):40. arXiv: 2109.06209.

Kriek, M., Beverage, A. G., Price, S. H., Suess, K. A., Barro, G., Bezanson, R. S., Conroy, C., Cutler, S. E., Franx, M., Lin, J., Lorenz, B., Ma, Y., Momcheva, I. G., Mowla, L. A., Pasha, I., van Dokkum, P., and Whitaker, K. E. (2023). The Heavy Metal Survey: Star Formation Constraints and Dynamical Masses of 21 Massive Quiescent Galaxies at $z\sim 1.4-2.2$. Publication Title: arXiv e-prints ADS Bibcode: 2023arXiv231116232K.

Kriek, M. and Conroy, C. (2013). The Dust Attenuation Law in Distant Galaxies: Evidence for Variation with Spectral Type. *The Astrophysical Journal*, 775(1):L16. arXiv:1308.1099 [astro-ph].

- Kriek, M., Conroy, C., van Dokkum, P. G., Shapley, A. E., Choi, J., Reddy, N. A., Siana, B., van de Voort, F., Coil, A. L., and Mobasher, B. (2016). A massive, quiescent, population II galaxy at a redshift of 2.1. *Nature*, 540(7632):248–251. Number: 7632 Publisher: Nature Publishing Group.
- Kriek, M., Dokkum, P. G. v., Labbé, I., Franx, M., Illingworth, G. D., Marchesini, D., and Quadri, R. F. (2009). AN ULTRA-DEEP NEAR-INFRARED SPECTRUM OF A COMPACT QUIESCENT GALAXY AT $z = 2.2$. *The Astrophysical Journal*, 700(1):221. Publisher: The American Astronomical Society.
- Kriek, M., van Dokkum, P. G., Franx, M., Förster Schreiber, N. M., Gawiser, E., Illingworth, G. D., Labbé, I., Marchesini, D., Quadri, R., Rix, H.-W., Rudnick, G., Toft, S., van der Werf, P., and Wuyts, S. (2006). Direct Measurements of the Stellar Continua and Balmer/4000 Å Breaks of Red $z > 2$ Galaxies: Redshifts and Improved Constraints on Stellar Populations I. *The Astrophysical Journal*, 645:44–54. ADS Bibcode: 2006ApJ...645...44K.
- Kriek, M., van Dokkum, P. G., Franx, M., Illingworth, G. D., Coppi, P., Förster Schreiber, N. M., Gawiser, E., Labbé, I., Lira, P., Marchesini, D., Quadri, R., Rudnick, G., Taylor, E. N., Urry, C. M., and van der Werf, P. P. (2007). The Origin of Line Emission in Massive $z \sim 2.3$ Galaxies: Evidence for Cosmic Downsizing of AGN Host Galaxies. *The Astrophysical Journal*, 669:776–790. ADS Bibcode: 2007ApJ...669..776K.
- Kron, R. G. (1980). Photometry of a complete sample of faint galaxies. *The Astrophysical Journal Supplement Series*, 43:305–325. Publisher: IOP ADS Bibcode: 1980ApJS...43..305K.
- Kubo, M., Uchimoto, Y. K., Yamada, T., Kajisawa, M., Ichikawa, T., Matsuda, Y., Akiyama, M., Hayashino, T., Konishi, M., Nishimura, T., Omata, K., Suzuki, R., Tanaka, I., Yoshikawa, T., Alexander, D. M., Fazio, G. G., Huang, J.-S., and Lehmer, B. D. (2013). THE FORMATION OF THE MASSIVE GALAXIES IN THE SSA22 $z = 3.1$ PROTOCLUSTER. *The Astrophysical Journal*, 778(2):170. Publisher: The American Astronomical Society.
- Kubo, M., Umehata, H., Matsuda, Y., Kajisawa, M., Steidel, C. C., Yamada, T., Tanaka, I., Hatsukade, B., Tamura, Y., Nakanishi, K., Kohno, K., Lee, C.-F., and Matsuda, K. (2021). A massive quiescent galaxy confirmed in a protocluster at $z=3.09$. *arXiv:2106.10798 [astro-ph]*. arXiv: 2106.10798 version: 1.
- Labbé, I., Huang, J., Franx, M., Rudnick, G., Barmby, P., Daddi, E., van Dokkum, P. G., Fazio, G. G., Förster Schreiber, N. M., Moorwood, A. F. M., Rix, H.-W., Röttgering, H.,

- Trujillo, I., and van der Werf, P. (2005). IRAC Mid-Infrared Imaging of the Hubble Deep Field-South: Star Formation Histories and Stellar Masses of Red Galaxies at $z > 2$. *The Astrophysical Journal*, 624:L81–L84. ADS Bibcode: 2005ApJ...624L..81L.
- Labbé, I., van Dokkum, P., Nelson, E., Bezanson, R., Suess, K. A., Leja, J., Brammer, G., Whitaker, K., Mathews, E., Stefanon, M., and Wang, B. (2023). A population of red candidate massive galaxies ~ 600 Myr after the Big Bang. *Nature*, 616(7956):266–269. Publisher: Nature Publishing Group.
- Lagos, C. d. P., da Cunha, E., Robotham, A. S. G., Obreschkow, D., Valentino, F., Fujimoto, S., Magdis, G. E., and Tobar, R. (2020). Physical properties and evolution of (sub-)millimetre-selected galaxies in the galaxy formation simulation SHARK. *Monthly Notices of the Royal Astronomical Society*, 499:1948–1971. ADS Bibcode: 2020MNRAS.499.1948L.
- Lagos, C. d. P., Robotham, A. S. G., Trayford, J. W., Tobar, R., Bravo, M., Bellstedt, S., Davies, L. J. M., Driver, S. P., Elahi, P. J., Obreschkow, D., and Power, C. (2019). From the far-ultraviolet to the far-infrared - galaxy emission at $0 \leq z \leq 10$ in the SHARK semi-analytic model. *Monthly Notices of the Royal Astronomical Society*, 489:4196–4216. ADS Bibcode: 2019MNRAS.489.4196L.
- Lagos, C. d. P., Tobar, R. J., Robotham, A. S. G., Obreschkow, D., Mitchell, P. D., Power, C., and Elahi, P. J. (2018). Shark: introducing an open source, free, and flexible semi-analytic model of galaxy formation. *Monthly Notices of the Royal Astronomical Society*, 481(3):3573–3603.
- Laigle, C., McCracken, H. J., Ilbert, O., Hsieh, B. C., Davidzon, I., Capak, P., Hasinger, G., Silverman, J. D., Pichon, C., Coupon, J., Aussel, H., Borgne, D. L., Caputi, K., Cassata, P., Chang, Y.-Y., Civano, F., Dunlop, J., Fynbo, J., kartaltepe, J. S., Koekemoer, A., Fevre, O. L., Floc'h, E. L., Leauthaud, A., Lilly, S., Lin, L., Marchesi, S., Milvang-Jensen, B., Salvato, M., Sanders, D. B., Scoville, N., Smolcic, V., Stockmann, M., Taniguchi, Y., Tasca, L., Toft, S., Vaccari, M., and Zabl, J. (2016). The COSMOS2015 Catalog: Exploring the $1 < z < 6$ Universe with half a million galaxies. *The Astrophysical Journal Supplement Series*, 224(2):24. arXiv:1604.02350 [astro-ph].
- Lang, D., Hogg, D. W., and Mykytyn, D. (2016). The Tractor: Probabilistic astronomical source detection and measurement. *Astrophysics Source Code Library*, page ascl:1604.008. ADS Bibcode: 2016ascl.soft04008L.
- Lawrence, A., Warren, S. J., Almaini, O., Edge, A. C., Hambly, N. C., Jameson, R. F., Lucas, P., Casali, M., Adamson, A., Dye, S., Emerson, J. P., Foucaud, S., Hewett, P.,

- Hirst, P., Hodgkin, S. T., Irwin, M. J., Lodieu, N., McMahon, R. G., Simpson, C., Smail, I., Mortlock, D., and Folger, M. (2007). The UKIRT Infrared Deep Sky Survey (UKIDSS). *Monthly Notices of the Royal Astronomical Society*, 379:1599–1617. ADS Bibcode: 2007MNRAS.379.1599L.
- Leauthaud, A., Massey, R., Kneib, J.-P., Rhodes, J., Johnston, D. E., Capak, P., Heymans, C., Ellis, R. S., Koekemoer, A. M., Le Fèvre, O., Mellier, Y., Réfrégier, A., Robin, A. C., Scoville, N., Tasca, L., Taylor, J. E., and Van Waerbeke, L. (2007). Weak Gravitational Lensing with COSMOS: Galaxy Selection and Shape Measurements. *The Astrophysical Journal Supplement Series*, 172:219–238. ADS Bibcode: 2007ApJS..172..219L.
- Leighly, K. M., Dietrich, M., and Barber, S. (2011). THE DISCOVERY OF THE FIRST He I λ 10830 BROAD ABSORPTION LINE QUASAR. *The Astrophysical Journal*, 728(2):94.
- Leja, J., Carnall, A. C., Johnson, B. D., Conroy, C., and Speagle, J. S. (2019a). How to Measure Galaxy Star Formation Histories II: Nonparametric Models. *The Astrophysical Journal*, 876(1):3. arXiv: 1811.03637.
- Leja, J., Johnson, B. D., Conroy, C., van Dokkum, P., Speagle, J. S., Brammer, G., Momcheva, I., Skelton, R., Whitaker, K. E., Franx, M., and Nelson, E. J. (2019b). An Older, More Quiescent Universe from Panchromatic SED Fitting of the 3D-HST Survey. *The Astrophysical Journal*, 877:140. ADS Bibcode: 2019ApJ...877..140L.
- Leja, J., Johnson, B. D., Conroy, C., van Dokkum, P. G., and Byler, N. (2017). Deriving Physical Properties from Broadband Photometry with Prospector: Description of the Model and a Demonstration of its Accuracy Using 129 Galaxies in the Local Universe. *The Astrophysical Journal*, 837(2):170. arXiv: 1609.09073.
- Leja, J., Tacchella, S., and Conroy, C. (2019c). Beyond UVJ: More Efficient Selection of Quiescent Galaxies with Ultraviolet/Mid-infrared Fluxes. *The Astrophysical Journal Letters*, 880:L9.
- Lilly, S., Le Fèvre, O., Hammer, F., Crampton, D., Schade, D. J., Hudon, J. D., and Tresse, L. (1996). The Evolution of Field Galaxies. 171:209. Conference Name: New Light on Galaxy Evolution ADS Bibcode: 1996IAUS..171..209L.
- Lindgren, L., Klioner, S. A., Hernández, J., Bombrun, A., Ramos-Lerate, M., Steidelmüller, H., Bastian, U., Biermann, M., de Torres, A., Gerlach, E., Geyer, R., Hilger,

T., Hobbs, D., Lammers, U., McMillan, P. J., Stephenson, C. A., Castañeda, J., Davidson, M., Fabricius, C., Gracia-Abril, G., Portell, J., Rowell, N., Teyssier, D., Torra, F., Bartolomé, S., Clotet, M., Garralda, N., González-Vidal, J. J., Torra, J., Abbas, U., Altmann, M., Anglada Varela, E., Balaguer-Núñez, L., Balog, Z., Barache, C., Becciani, U., Bernet, M., Bertone, S., Bianchi, L., Bouquillon, S., Brown, A. G. A., Bucciarelli, B., Busonero, D., Butkevich, A. G., Buzzzi, R., Cancelliere, R., Carlucci, T., Charlot, P., Cioni, M. R. L., Crosta, M., Crowley, C., del Peloso, E. F., del Pozo, E., Drimmel, R., Esquej, P., Fienga, A., Fraile, E., Gai, M., Garcia-Reinaldos, M., Guerra, R., Hambly, N. C., Hauser, M., Janßen, K., Jordan, S., Kostrzewa-Rutkowska, Z., Lattanzi, M. G., Liao, S., Licata, E., Lister, T. A., Löffler, W., Marchant, J. M., Masip, A., Mignard, F., Mints, A., Molina, D., Mora, A., Morbidelli, R., Murphy, C. P., Pagani, C., Panuzzo, P., Peñalosa Esteller, X., Poggio, E., Re Fiorentin, P., Riva, A., Sagristà Sellés, A., Sanchez Gimenez, V., Sarasso, M., Sciacca, E., Siddiqui, H. I., Smart, R. L., Souami, D., Spagna, A., Steele, I. A., Taris, F., Utrilla, E., van Reeven, W., and Vecchiato, A. (2021). Gaia Early Data Release 3. The astrometric solution. *Astronomy and Astrophysics*, 649:A2. ADS Bibcode: 2021A&A...649A...2L.

Long, A. S., Casey, C. M., Lagos, C. d. P., Lambrides, E. L., Zavala, J. A., Champagne, J., Cooper, O. R., and Cooray, A. R. (2022). Missing Giants: Predictions on Dust-Obscured Galaxy Stellar Mass Assembly Throughout Cosmic Time. arXiv:2211.02072 [astro-ph].

Looser, T. J., D'Eugenio, F., Maiolino, R., Tacchella, S., Curti, M., Arribas, S., Baker, W. M., Baum, S., Bonaventura, N., Boyett, K., Bunker, A. J., Carniani, S., Charlot, S., Chevillard, J., Curtis-Lake, E., Danhaive, A. L., Eisenstein, D. J., de Graaff, A., Hainline, K., Ji, Z., Johnson, B. D., Kumari, N., Nelson, E., Parlanti, E., Rix, H.-W., Robertson, B., Del Pino, B. R., Sandles, L., Scholtz, J., Smit, R., Stark, D. P., Übler, H., Williams, C. C., Willott, C., and Witstok, J. (2023). JADES: Differing assembly histories of galaxies – Observational evidence for bursty SFHs and (mini-)quenching in the first billion years of the Universe. arXiv:2306.02470 [astro-ph].

Lovell, C. C., Roper, W., Vijayan, A. P., Seeyave, L., Irodotou, D., Wilkins, S. M., Conselice, C. J., Fortuni, F., Kuusisto, J. K., Merlin, E., Santini, P., and Thomas, P. (2022). FLARES VIII. The Emergence of Passive Galaxies in the Early Universe ($z > 5$). arXiv:2211.07540 [astro-ph].

Lovell, C. C., Roper, W., Vijayan, A. P., Seeyave, L., Irodotou, D., Wilkins, S. M., Conselice, C. J., Fortuni, F., Kuusisto, J. K., Merlin, E., Santini, P., and Thomas, P. (2023). First light and reionisation epoch simulations (FLARES) - VIII. The emergence of passive galaxies at $z \geq 5$. *Monthly Notices of the Royal Astronomical Society*, 525:5520–5539. Publisher: OUP ADS Bibcode: 2023MNRAS.525.5520L.

- Lower, S., Narayanan, D., Leja, J., Johnson, B. D., Conroy, C., and Davé, R. (2020). How Well Can We Measure the Stellar Mass of a Galaxy: The Impact of the Assumed Star Formation History Model in SED Fitting. *arXiv:2006.03599 [astro-ph]*. arXiv: 2006.03599.
- Lustig, P., Strazzullo, V., D'Eugenio, C., Daddi, E., Pannella, M., Renzini, A., Cimatti, A., Gobat, R., Jin, S., Mohr, J. J., and Onodera, M. (2020). Compact, bulge dominated structures of spectroscopically confirmed quiescent galaxies at $z \sim 3$. *arXiv:2012.02766 [astro-ph]*. arXiv: 2012.02766.
- Lustig, P., Strazzullo, V., Remus, R.-S., D'Eugenio, C., Daddi, E., Burkert, A., De Lucia, G., Delvecchio, I., Dolag, K., Fontanot, F., Gobat, R., Mohr, J. J., Onodera, M., Pannella, M., Pillepich, A., and Renzini, A. (2022). Massive quiescent galaxies at $z \sim 3$: a comparison of selection, stellar population and structural properties with simulation predictions. *arXiv:2201.09068 [astro-ph]*. arXiv: 2201.09068.
- Lyman Spitzer, J. (1990). Report to project rand: Astronomical advantages of an extra-terrestrial observatory. *Astronomy Quarterly*, 7(3):131–142.
- Ma, Z., Fang, G., Kong, X., and Fan, L. (2015). Physical properties of distant red galaxies in the COSMOS/UltraVISTA field. *Publications of the Astronomical Society of Japan*, 67(91).
- Madau, P. and Dickinson, M. (2014). Cosmic Star Formation History. *Annual Review of Astronomy and Astrophysics*, 52(1):415–486. arXiv: 1403.0007.
- Magdis, G. E., Gobat, R., Valentino, F., Daddi, E., Zanella, A., Kokorev, V., Toft, S., Jin, S., and Whitaker, K. (2021). The Interstellar Medium of Quiescent Galaxies and its Evolution With Time. *arXiv:2101.04700 [astro-ph]*. arXiv: 2101.04700.
- Man, A. and Belli, S. (2018). Star formation quenching in massive galaxies. *Nature Astronomy*, 2(9):695–697. Number: 9 Publisher: Nature Publishing Group.
- Manning, S. M., Casey, C. M., Zavala, J. A., Magdis, G. E., Drew, P. M., Champagne, J. B., Aravena, M., Béthermin, M., Clements, D. L., Finkelstein, S. L., Fujimoto, S., Hayward, C. C., Hodge, J. A., Ilbert, O., Kartaltepe, J. S., Knudsen, K. K., Koekemoer, A. M., Man, A. W. S., Sanders, D. B., Sheth, K., Spilker, J. S., Staguhn, J., Talia, M., Treister, E., and Yun, M. S. (2022). Characterization of Two 2 mm detected Optically Obscured Dusty Star-forming Galaxies. *The Astrophysical Journal*, 925(1):23. Publisher: The American Astronomical Society.
- Mao, Z., Kodama, T., Pérez-Martínez, J. M., Suzuki, T. L., Yamamoto, N., and Adachi, K. (2022). Revealing impacts of stellar mass and environment on galaxy quenching. *Astronomy & Astrophysics*, 666:A141. Publisher: EDP Sciences.

Marchesini, D., Brammer, G., Morishita, T., Bergamini, P., Wang, X., Bradac, M., Roberts-Borsani, G., Strait, V., Treu, T., Fontana, A., Jones, T., Santini, P., Vulcani, B., Acebron, A., Calabrò, A., Castellano, M., Glazebrook, K., Grillo, C., Mercurio, A., Nanayakkara, T., Rosati, P., Tubthong, C., and Vanzella, E. (2023). Early Results from GLASS-JWST. IX. First Spectroscopic Confirmation of Low-mass Quiescent Galaxies at $z > 2$ with NIRISS. *The Astrophysical Journal Letters*, 942(2):L25. Publisher: The American Astronomical Society.

Marchesini, D., Whitaker, K. E., Brammer, G., van Dokkum, P. G., Labbé, I., Muzzin, A., Quadri, R. F., Kriek, M., Lee, K.-S., Rudnick, G., Franx, M., Illingworth, G. D., and Wake, D. (2010). The Most Massive Galaxies at $3.0 \leq z < 4.0$ in the Newfirm Medium-band Survey: Properties and Improved Constraints on the Stellar Mass Function. *The Astrophysical Journal*, 725:1277–1295. ADS Bibcode: 2010ApJ...725.1277M.

Marsan, Z. C., Marchesini, D., Brammer, G. B., Geier, S., Kado-Fong, E., Labbé, I., Muzzin, A., and Stefanon, M. (2017). A Spectroscopic Follow-up Program of Very Massive Galaxies at $3 \leq z \leq 4$: Confirmation of Spectroscopic Redshifts, and a High Fraction of Powerful AGNs. *The Astrophysical Journal*, 842(1):21. Publisher: American Astronomical Society.

Marsan, Z. C., Marchesini, D., Brammer, G. B., Stefanon, M., Muzzin, A., Fernandez-Soto, A., Geier, S., Hainline, K. N., Intema, H., Karim, A., Labbe, I., Toft, S., and van Dokkum, P. G. (2015). Spectroscopic Confirmation of an Ultra Massive and Compact Galaxy at $z=3.35$: A Detailed Look at an Early Progenitor of Local Most Massive Ellipticals. *The Astrophysical Journal*, 801(2):133. arXiv: 1406.0002.

Marsan, Z. C., Muzzin, A., Marchesini, D., Stefanon, M., Martis, N., Annunziatella, M., Chan, J. C. C., Cooper, M. C., Forrest, B., Gomez, P., McConachie, I., and Wilson, G. (2020). The Number Densities and Stellar Populations of Massive Galaxies at $3 < z < 6$: A Diverse, Rapidly Forming Population in the Early Universe. *arXiv:2010.04725 [astro-ph]*. arXiv: 2010.04725.

Martig, M., Bournaud, F., Teyssier, R., and Dekel, A. (2009). Morphological Quenching of Star Formation: Making Early-Type Galaxies Red. *The Astrophysical Journal*, 707:250–267. Publisher: IOP ADS Bibcode: 2009ApJ...707..250M.

Martin, D. C., Fanson, J., Schiminovich, D., Morrissey, P., Friedman, P. G., Barlow, T. A., Conrow, T., Grange, R., Jelinsky, P. N., Milliard, B., Siegmund, O. H. W., Bianchi, L., Byun, Y.-I., Donas, J., Forster, K., Heckman, T. M., Lee, Y.-W., Madore, B. F., Malina, R. F., Neff, S. G., Rich, R. M., Small, T., Surber, F., Szalay, A. S., Welsh, B., and Wyder,

- T. K. (2005). The Galaxy Evolution Explorer: A Space Ultraviolet Survey Mission. *The Astrophysical Journal*, 619:L1–L6. ADS Bibcode: 2005ApJ...619L...1M.
- Martis, N. S., Sarrouh, G. T. E., Willott, C. J., Abraham, R., Asada, Y., Bradač, M., Brammer, G., Harshan, A., Muzzin, A., Noirot, G., Sawicki, M., and Rihtaršič, G. (2024). Modelling and Subtracting Diffuse Cluster Light in JWST Images: A Relation between the Spatial Distribution of Globular Clusters, Dwarf Galaxies, and Intracluster Light in the Lensing Cluster SMACS 0723. Publication Title: arXiv e-prints ADS Bibcode: 2024arXiv240101945M.
- Matharu, J., Muzzin, A., Sarrouh, G. T. E., Brammer, G., Abraham, R., Asada, Y., Bradač, M., Desprez, G., Martis, N., Mowla, L., Noirot, G., Sawicki, M., Strait, V., Willott, C. J., Gould, K. M. L., Grindlay, T., and Harshan, A. T. (2023). A First Look at Spatially Resolved Balmer Decrements at $1.0 < z < 2.4$ from JWST NIRISS Slitless Spectroscopy. *The Astrophysical Journal*, 949:L11. Publisher: IOP ADS Bibcode: 2023ApJ...949L...11M.
- Maíz Apellániz, J. (2006). A Recalibration of Optical Photometry: Tycho-2, Strömgen, and Johnson Systems. *The Astronomical Journal*, 131:1184–1199. ADS Bibcode: 2006AJ....131.1184M.
- McCarthy, P. J. (2004). Eros and Faint Red Galaxies. *Annual Review of Astronomy and Astrophysics*, 42:477–515. ADS Bibcode: 2004ARA&A..42..477M.
- McConachie, I., Wilson, G., Forrest, B., Marsan, Z. C., Muzzin, A., Cooper, M. C., Annunziatella, M., Marchesini, D., Chan, J. C. C., Gomez, P., Abdullah, M. H., Saracco, P., and Nantais, J. (2021). Spectroscopic Confirmation of a Protocluster at $z=3.37$ with a High Fraction of Quiescent Galaxies. *arXiv:2109.07696 [astro-ph]*. arXiv: 2109.07696 version: 1.
- McCracken, H. J., Milvang-Jensen, B., Dunlop, J., Franx, M., Fynbo, J. P. U., Le Fèvre, O., Holt, J., Caputi, K. I., Goranova, Y., Buitrago, F., Emerson, J. P., Freudling, W., Hudelot, P., López-Sanjuan, C., Magnard, F., Mellier, Y., Møller, P., Nilsson, K. K., Sutherland, W., Tasca, L., and Zabl, J. (2012). UltraVISTA: a new ultra-deep near-infrared survey in COSMOS. *Astronomy and Astrophysics*, 544:A156. ADS Bibcode: 2012A&A...544A.156M.
- McKinney, J., Manning, S. M., Cooper, O. R., Long, A. S., Akins, H., Casey, C. M., Faisst, A. L., Franco, M., Hayward, C. C., Lambrides, E., Magdis, G., Whitaker, K. E., Yun, M., Champagne, J. B., Drakos, N. E., Gentile, F., Gillman, S., Gozaliasl, G., Ilbert, O., Jin, S., Koekemoer, A. M., Kokorev, V., Liu, D., Rich, R. M., Robertson, B. E., Valentino, F., Weaver, J. R., Zavala, J. A., Allen, N., Kartaltepe, J. S., McCracken, H. J., Paquereau, L., Rhodes, J., Shuntov, M., and Toft, S. (2023). A Near-infrared-faint, Far-infrared-luminous

Dusty Galaxy at $z \sim 5$ in COSMOS-Web. *The Astrophysical Journal*, 956:72. Publisher: IOP ADS Bibcode: 2023ApJ...956...72M.

Merlin, E., Fontana, A., Castellano, M., Santini, P., Torelli, M., Boutsia, K., Wang, T., Grazian, A., Pentericci, L., Schreiber, C., Ciesla, L., McLure, R., Derriere, S., Dunlop, J. S., and Elbaz, D. (2018). Chasing passive galaxies in the early Universe: a critical analysis in CANDELS GOODS-South. *Monthly Notices of the Royal Astronomical Society*, 473(2):2098–2123. arXiv:1709.00429 [astro-ph].

Merlin, E., Fortuni, F., Torelli, M., Santini, P., Castellano, M., Fontana, A., Grazian, A., Pentericci, L., Pilo, S., and Schmidt, K. B. (2019). Red & Dead CANDELS: massive passive galaxies at the dawn of the Universe. *Monthly Notices of the Royal Astronomical Society*, 490(3):3309–3328. arXiv:1909.07996 [astro-ph].

Michałowski, M. J., Dunlop, J. S., Koprowski, M. P., Cirasuolo, M., Geach, J. E., Bowler, R. A. A., Mortlock, A., Caputi, K. I., Aretxaga, I., Arumugam, V., Chen, C.-C., McLure, R. J., Birkinshaw, M., Bourne, N., Farrah, D., Ibar, E., van der Werf, P., and Zemcov, M. (2017). The SCUBA-2 Cosmology Legacy Survey: the nature of bright submm galaxies from 2 deg² of 850- μ m imaging. *Monthly Notices of the Royal Astronomical Society*, 469:492–515. Publisher: OUP ADS Bibcode: 2017MNRAS.469..492M.

Mihos, J. C. and Hernquist, L. (1996). Gasdynamics and Starbursts in Major Mergers. *The Astrophysical Journal*, 464:641. Publisher: IOP ADS Bibcode: 1996ApJ...464..641M.

Miller, T. B. and van Dokkum, P. (2021). Bayesian Fitting of Multi-Gaussian Expansion Models to Galaxy Images. *The Astrophysical Journal*, 923:124. ADS Bibcode: 2021ApJ...923..124M.

Miyazaki, S., Komiyama, Y., Kawanomoto, S., Doi, Y., Furusawa, H., Hamana, T., Hayashi, Y., Ikeda, H., Kamata, Y., Karoji, H., Koike, M., Kurakami, T., Miyama, S., Morokuma, T., Nakata, F., Namikawa, K., Nakaya, H., Nariai, K., Obuchi, Y., Oishi, Y., Okada, N., Okura, Y., Tait, P., Takata, T., Tanaka, Y., Tanaka, M., Terai, T., Tomono, D., Uraguchi, F., Usuda, T., Utsumi, Y., Yamada, Y., Yamanoi, H., Aihara, H., Fujimori, H., Mineo, S., Miyatake, H., Oguri, M., Uchida, T., Tanaka, M. M., Yasuda, N., Takada, M., Murayama, H., Nishizawa, A. J., Sugiyama, N., Chiba, M., Futamase, T., Wang, S.-Y., Chen, H.-Y., Ho, P. T. P., Liaw, E. J. Y., Chiu, C.-F., Ho, C.-L., Lai, T.-C., Lee, Y.-C., Jeng, D.-Z., Iwamura, S., Armstrong, R., Bickerton, S., Bosch, J., Gunn, J. E., Lupton, R. H., Loomis, C., Price, P., Smith, S., Strauss, M. A., Turner, E. L., Suzuki, H., Miyazaki, Y., Muramatsu, M., Yamamoto, K., Endo, M., Ezaki, Y., Ito, N., Kawaguchi, N., Sofuku, S., Taniike, T., Akutsu, K., Dojo, N., Kasumi, K., Matsuda, T., Imoto, K., Miwa, Y., Suzuki, M., Takeshi, K., and Yokota, H.

(2018). Hyper Suprime-Cam: System design and verification of image quality. *Publications of the Astronomical Society of Japan*, 70:S1. ADS Bibcode: 2018PASJ...70S...1M.

Mobasher, B., Dickinson, M., Ferguson, H. C., Giavalisco, M., Wiklind, T., Stark, D., Ellis, R. S., Fall, S. M., Grogin, N. A., Moustakas, L. A., Panagia, N., Sosey, M., Stiavelli, M., Bergeron, E., Casertano, S., Ingraham, P., Koekemoer, A., Labbé, I., Livio, M., Rodgers, B., Scarlata, C., Vernet, J., Renzini, A., Rosati, P., Kuntschner, H., Kümmel, M., Walsh, J. R., Chary, R., Eisenhardt, P., Pirzkal, N., and Stern, D. (2005). Evidence for a Massive Poststarburst Galaxy at $z \sim 6.5$. *The Astrophysical Journal*, 635:832–844. ADS Bibcode: 2005ApJ...635..832M.

Moneti, A., Euclid, C., McCracken, H. J., Shuntov, M., Kauffmann, O. B., Capak, P., Davidzon, I., Ilbert, O., Scarlata, C., Toft, S., Weaver, J., Chary, R., Cuby, J., Faisst, A. L., Masters, D. C., McPartland, C., Mobasher, B., Sanders, D. B., Scaramella, R., Stern, D., Szapudi, I., Teplitz, H., Zalesky, L., Amara, A., Auricchio, N., Bodendorf, C., Bonino, D., Branchini, E., Brau-Nogue, S., Brescia, M., Brinchmann, J., Capobianco, V., Carbone, C., Carretero, J., Castander, F. J., Castellano, M., Cavuoti, S., Cimatti, A., Cledassou, R., Congedo, G., Conselice, C. J., Conversi, L., Copin, Y., Corcione, L., Costille, A., Cropper, M., Da Silva, A., Degaudenzi, H., Douspis, M., Dubath, F., Duncan, C. a. J., Dupac, X., Dusini, S., Farrens, S., Ferriol, S., Fosalba, P., Frailis, M., Franceschi, E., Fumana, M., Garilli, B., Gillis, B., Giocoli, C., Granett, B. R., Grazian, A., Grupp, F., Haugan, S. V. H., Hoekstra, H., Holmes, W., Hormuth, F., Hudelot, P., Jahnke, K., Kermiche, S., Kiessling, A., Kilbinger, M., Kitching, T., Kohley, R., Kümmel, M., Kunz, M., Kurki-Suonio, H., Liori, S., Lilje, P. B., Lloro, I., Maiorano, E., Mansutti, O., Marggraf, O., Markovic, K., Marulli, F., Massey, R., Maurogordato, S., Meneghetti, M., Merlin, E., Meylan, G., Moresco, M., Moscardini, L., Munari, E., Niemi, S. M., Padilla, C., Paltani, S., Pasian, F., Pedersen, K., Pires, S., Poncet, M., Popa, L., Pozzetti, L., Raison, F., Rebolo, R., Rhodes, J., Rix, H., Roncarelli, M., Rossetti, E., Saglia, R., Schneider, P., Secroun, A., Seidel, G., Serrano, S., Sirignano, C., Sirri, G., Stanco, L., Tallada-Crespí, P., Taylor, A. N., Tereno, I., Toledo-Moreo, R., Torradeflot, F., Wang, Y., Welikala, N., Weller, J., Zamorani, G., Zoubian, J., Andreon, S., Bardelli, S., Camera, S., Graciá-Carpio, J., Medinaceli, E., Mei, S., Polenta, G., Romelli, E., Sureau, F., Tenti, M., Vassallo, T., Zacchei, A., Zucca, E., Baccigalupi, C., Balaguera-Antolínez, A., Bernardeau, F., Biviano, A., Bolzonella, M., Bozzo, E., Burigana, C., Cabanac, R., Cappi, A., Carvalho, C. S., Casas, S., Castignani, G., Colodro-Conde, C., Coupon, J., Courtois, H. M., Di Ferdinando, D., Farina, M., Finelli, F., Flose-Reimberg, P., Fotopoulou, S., Galeotta, S., Ganga, K., Garcia-Bellido, J., Gaztanaga, E., Gozaliasl, G., Hook, I., Joachimi, B., Kansal, V., Keihänen, E., Kirkpatrick, C. C., Lindholm, V., Mainetti, G., Maino, D., Maoli, R., Martinelli, M., Martinet, N., Maturi, M., Metcalf, R. B., Morgante, G., Morisset, N., Nucita, A., Patrizzii, L., Potter, D., Renzi, A., Riccio,

- G., Sánchez, A. G., Sapone, D., Schirmer, M., Schultheis, M., Scottez, V., Sefusatti, E., Teyssier, R., Tubio, O., Tutusaus, I., Valiviita, J., Viel, M., and Hildebrandt, H. (2022). Euclid preparation. XVII. Cosmic Dawn Survey: Spitzer Space Telescope observations of the Euclid deep fields and calibration fields. *Astronomy & Astrophysics, Volume 658, id.A126*, <NUMPAGES>15</NUMPAGES> pp., 658:A126.
- Moneti, A., McCracken, H. J., Hudelot, P., Rouberol, S., Herent, O., and Mellier, Y. (2019). The fourth UltraVISTA data release. page 15.
- Morisset, C., Delgado-Inglada, G., Sánchez, S. F., Galbany, L., García-Benito, R., Husemann, B., Marino, R. A., Mast, D., Roth, M. M., and CALIFA collaboration (2016). Photoionization models of the CALIFA H II regions: I. Hybrid models. *Astronomy & Astrophysics*, 594:A37.
- Moster, B. P., Somerville, R. S., Newman, J. A., and Rix, H.-W. (2011). A Cosmic Variance Cookbook. *The Astrophysical Journal*, 731:113. ADS Bibcode: 2011ApJ...731..113M.
- Moustakas, L. A., Davis, M., Graham, J. R., Silk, J., Peterson, B. A., and Yoshii, Y. (1997). Colors and K-Band Counts of Extremely Faint Field Galaxies* **. *The Astrophysical Journal*, 475(2):445. Publisher: IOP Publishing.
- Mowla, L., Iyer, K. G., Desprez, G., Estrada-Carpenter, V., Martis, N. S., Noirot, G., Sarrouh, G. T., Strait, V., Asada, Y., Abraham, R. G., Brammer, G., Sawicki, M., Willott, C. J., Bradac, M., Doyon, R., Muzzin, A., Pacifici, C., Ravindranath, S., and Zabl, J. (2022). The Sparkler: Evolved High-redshift Globular Cluster Candidates Captured by JWST. *The Astrophysical Journal*, 937:L35. Publisher: IOP ADS Bibcode: 2022ApJ...937L..35M.
- Mowla, L. A., van Dokkum, P., Brammer, G. B., Momcheva, I., van der Wel, A., Whitaker, K., Nelson, E., Bezanson, R., Muzzin, A., Franx, M., MacKenty, J., Leja, J., Kriek, M., and Marchesini, D. (2019). COSMOS-DASH: The Evolution of the Galaxy Size-Mass Relation since $z \sim 3$ from New Wide-field WFC3 Imaging Combined with CANDELS/3D-HST. *The Astrophysical Journal*, 880:57. ADS Bibcode: 2019ApJ...880...57M.
- Mullaney, J. R., Alexander, D. M., Goulding, A. D., and Hickox, R. C. (2011). Defining the intrinsic AGN infrared spectral energy distribution and measuring its contribution to the infrared output of composite galaxies. *Monthly Notices of the Royal Astronomical Society*, 414:1082–1110. ADS Bibcode: 2011MNRAS.414.1082M.
- Muzzin, A., Marchesini, D., Stefanon, M., Franx, M., McCracken, H. J., Milvang-Jensen, B., Dunlop, J. S., Fynbo, J. P. U., Brammer, G., Labbé, I., and van Dokkum, P. G. (2013). The Evolution of the Stellar Mass Functions of Star-forming and Quiescent Galaxies to z

= 4 from the COSMOS/UltraVISTA Survey. *The Astrophysical Journal*, 777:18. ADS Bibcode: 2013ApJ...777...18M.

Muzzin, A., van Dokkum, P., Franx, M., Marchesini, D., Kriek, M., and Labbé, I. (2009). How Massive are Massive Compact Galaxies? *The Astrophysical Journal*, 706:L188–L191. ADS Bibcode: 2009ApJ...706L.188M.

Mármol-Queraltó, E., McLure, R. J., Cullen, F., Dunlop, J. S., Fontana, A., and McLeod, D. J. (2016). The evolution of the equivalent width of the H α emission line and specific star formation rate in star-forming galaxies at $1 < z < 5$. *Monthly Notices of the Royal Astronomical Society*, 460:3587–3597. ADS Bibcode: 2016MNRAS.460.3587M.

Naidu, R. P., Oesch, P. A., Setton, D. J., Matthee, J., Conroy, C., Johnson, B. D., Weaver, J. R., Bouwens, R. J., Brammer, G. B., Dayal, P., Illingworth, G. D., Barrufet, L., Belli, S., Bezanson, R., Bose, S., Heintz, K. E., Leja, J., Leonova, E., Marques-Chaves, R., Stefanon, M., Toft, S., van der Wel, A., van Dokkum, P., Weibel, A., and Whitaker, K. E. (2022). Schrodinger’s Galaxy Candidate: Puzzlingly Luminous at $z \approx 17$, or Dusty/Quenched at $z \approx 5$? Publication Title: arXiv e-prints ADS Bibcode: 2022arXiv220802794N.

Nanayakkara, T., Esdaile, J., Glazebrook, K., Salcedo, J. M. E., Durre, M., and Jacobs, C. (2021). Massive High-Redshift Quiescent Galaxies With JWST. *arXiv:2103.01459 [astro-ph]*. arXiv: 2103.01459.

Nanayakkara, T., Glazebrook, K., Jacobs, C., Kawinwanichakij, L., Schreiber, C., Brammer, G., Esdaile, J., Kacprzak, G. G., Labbe, I., Lagos, C., Marchesini, D., Marsan, Z. C., Oesch, P. A., Papovich, C., Remus, R.-S., and Tran, K.-V. H. (2024). A population of faint, old, and massive quiescent galaxies at $3 < z < 4$ revealed by JWST NIRSpec Spectroscopy. *Scientific Reports*, 14(1):3724. Publisher: Nature Publishing Group.

Nanayakkara, T., Glazebrook, K., Jacobs, C., Schreiber, C., Brammer, G., Esdaile, J., Kacprzak, G. G., Labbe, I., Lagos, C., Marchesini, D., Marsan, Z. C., Nateghi, H., Oesch, P. A., Papovich, C., Remus, R.-S., and Tran, K.-V. H. (2022). A population of faint, old, and massive quiescent galaxies at $3 < z < 4$ revealed by JWST NIRSpec Spectroscopy. *arXiv:2212.11638 [astro-ph]*.

Nelson, E. J., Suess, K. A., Bezanson, R., Price, S. H., Van Dokkum, P., Leja, J., Wang, B., Whitaker, K. E., Labbé, I., Barrufet, L., Brammer, G., Eisenstein, D. J., Gibson, J., Hartley, A. I., Johnson, B. D., Heintz, K. E., Mathews, E., Miller, T. B., Oesch, P. A., Sandles, L., Setton, D. J., Speagle, J. S., Tacchella, S., Tadaki, K.-i., Übler, H., and Weaver, J. R. (2023).

JWST Reveals a Population of Ultrared, Flattened Galaxies at $2 < z < 6$ Previously Missed by HST. *The Astrophysical Journal Letters*, 948(2):L18.

Nelson, E. J., Suess, K. A., Bezanson, R., Price, S. H., van Dokkum, P., Leja, J., Wang, B., Whitaker, K. E., Labbé, I., Barrufet, L., Brammer, G., Eisenstein, D. J., Heintz, K. E., Johnson, B. D., Mathews, E., Miller, T. B., Oesch, P. A., Sandles, L., Setton, D. J., Speagle, J. S., Tacchella, S., Tadaki, K.-i., and Weaver, H. ♦. J. (2022). JWST reveals a population of ultra-red, flattened disk galaxies at z . Technical report. Publication Title: arXiv e-prints ADS Bibcode: 2022arXiv220801630N Type: article.

Noiro, G., Sawicki, M., Abraham, R., Bradač, M., Iyer, K., Moutard, T., Pacifici, C., Ravindranath, S., and Willott, C. J. (2022). Across the Green Valley with HST grisms: colour evolution, crossing time-scales and the growth of the red sequence at $z=1.0-1.8$. *arXiv:2203.06185 [astro-ph]*. arXiv: 2203.06185.

Nomoto, K., Tominaga, N., Umeda, H., Kobayashi, C., and Maeda, K. (2006). Nucleosynthesis yields of core-collapse supernovae and hypernovae, and galactic chemical evolution. *Nuclear Physics A*, 777:424–458. ADS Bibcode: 2006NuPhA.777..424N.

Oke, J. B. and Gunn, J. E. (1983). Secondary standard stars for absolute spectrophotometry. *The Astrophysical Journal*, 266:713–717. ADS Bibcode: 1983ApJ...266..713O.

Ostriker, J. P., Choi, E., Ciotti, L., Novak, G. S., and Proga, D. (2010). Momentum Driving: Which Physical Processes Dominate Active Galactic Nucleus Feedback? *The Astrophysical Journal*, 722:642–652. Publisher: IOP ADS Bibcode: 2010ApJ...722..642O.

Pacifici, C., Kassin, S. A., Weiner, B. J., Holden, B., Gardner, J. P., Faber, S. M., Ferguson, H. C., Koo, D. C., Primack, J. R., Bell, E. F., Dekel, A., Gawiser, E., Giavalisco, M., Rafelski, M., Simons, R. C., Barro, G., Croton, D. J., Dave, R., Fontana, A., Grogin, N. A., Koekoer, A. M., Lee, S.-K., Salmon, B., Somerville, R., and Behroozi, P. (2016). The evolution of star formation histories of quiescent galaxies. *The Astrophysical Journal*, 832(1):79. arXiv: 1609.03572.

Padovani, P., Alexander, D. M., Assef, R. J., De Marco, B., Giommi, P., Hickox, R. C., Richards, G. T., Smolčić, V., Hatziminaoglou, E., Mainieri, V., and Salvato, M. (2017). Active galactic nuclei: what's in a name? *The Astronomy and Astrophysics Review*, 25(1):2.

Papovich, C. (2006). Spitzer observations of red galaxies: Implication for high-redshift star formation. *New Astronomy Reviews*, 50:134–139. ADS Bibcode: 2006NewAR..50..134P.

- Papovich, C., Bassett, R., Lotz, J. M., Wel, A. v. d., Tran, K.-V., Finkelstein, S. L., Bell, E. F., Conselice, C. J., Dekel, A., Dunlop, J. S., Guo, Y., Faber, S. M., Farrah, D., Ferguson, H. C., Finkelstein, K. D., Häussler, B., Kocevski, D. D., Koekemoer, A. M., Koo, D. C., McGrath, E. J., McLure, R. J., McIntosh, D. H., Momcheva, I., Newman, J. A., Rudnick, G., Weiner, B., Willmer, C. N. A., and Wuyts, S. (2012). CANDELS OBSERVATIONS OF THE STRUCTURAL PROPERTIES OF CLUSTER GALAXIES AT $z = 1.62$. *The Astrophysical Journal*, 750(2):93. Publisher: The American Astronomical Society.
- Papovich, C., Labbé, I., Quadri, R., Tilvi, V., Behroozi, P., Bell, E. F., Glazebrook, K., Spitler, L., Straatman, C. M. S., Tran, K.-V., Cowley, M., Davé, R., Dekel, A., Dickinson, M., Ferguson, H. C., Finkelstein, S. L., Gawiser, E., Inami, H., Faber, S. M., Kacprzak, G. G., Kawinwanichakij, L., Kocevski, D., Koekemoer, A., Koo, D. C., Kurczynski, P., Lotz, J. M., Lu, Y., Lucas, R. A., McIntosh, D., Mehrtens, N., Mobasher, B., Monson, A., Morrison, G., Nanayakkara, T., Persson, S. E., Salmon, B., Simons, R., Tomczak, A., Dokkum, P. v., Weiner, B., and Willner, S. P. (2015). ZFOURGE/CANDELS: ON THE EVOLUTION OF M^* GALAXY PROGENITORS FROM $z = 3$ TO 0.5^* . *The Astrophysical Journal*, 803(1):26. Publisher: The American Astronomical Society.
- Park, M., Belli, S., Conroy, C., Tacchella, S., Leja, J., Cutler, S. E., Johnson, B. D., Nelson, E. J., and Emami, R. (2022). Rapid Quenching of Galaxies at Cosmic Noon. arXiv:2210.03747 [astro-ph].
- Pedregosa, F., Varoquaux, G., Gramfort, A., Michel, V., Thirion, B., Grisel, O., Blondel, M., Prettenhofer, P., Weiss, R., Dubourg, V., Vanderplas, J., Passos, A., Cournapeau, D., Brucher, M., Perrot, M., and Duchesnay, \diamond . (2011). Scikit-learn: Machine Learning in Python. *Journal of Machine Learning Research*, 12(85):2825–2830.
- Pellegrini, S. and Renzini, A. (1991). WINDS, OUTFLOWS, AND INFLOWS IN X-RAY ELLIPTICAL GALAXIES. I. Luca Ciotti Dipartimento di Astronomia, Università di Bologna, CP 596, I-40100, Bologna, Italy Annibale D’Ercole Osservatorio Astronomico di Bologna, CP 596, I-40100, Bologna, Italy AND. *ApJ* . . , 376.
- Phillipps, S., Ali, S. S., Bremer, M. N., De Propriis, R., Sansom, A. E., Cluver, M. E., Alpaslan, M., Brough, S., Brown, M. J. I., Davies, L. J. M., Driver, S. P., Grootes, M. W., Holwerda, B. W., Hopkins, A. M., James, P. A., Pimblet, K., Robotham, A. S. G., Taylor, E. N., and Wang, L. (2020). Galaxy And Mass Assembly (GAMA): Defining passive galaxy samples and searching for the UV upturn. *Monthly Notices of the Royal Astronomical Society*, 492(2):2128–2139.
- Pickles, A. J. (1998). A Stellar Spectral Flux Library: 1150–25000 Å. *Publications of the Astronomical Society of the Pacific*, 110(749):863. Publisher: IOP Publishing.

Planck Collaboration, Ade, P. A. R., Aghanim, N., Arnaud, M., Ashdown, M., Aumont, J., Baccigalupi, C., Banday, A. J., Barreiro, R. B., Barrena, R., Bartlett, J. G., Bartolo, N., Battaner, E., Battye, R., Benabed, K., Benoît, A., Benoit-Lévy, A., Bernard, J. P., Bersanelli, M., Bielewicz, P., Bikmaev, I., Böhringer, H., Bonaldi, A., Bonavera, L., Bond, J. R., Borrill, J., Bouchet, F. R., Bucher, M., Burenin, R., Burigana, C., Butler, R. C., Calabrese, E., Cardoso, J. F., Carvalho, P., Catalano, A., Challinor, A., Chamballu, A., Chary, R. R., Chiang, H. C., Chon, G., Christensen, P. R., Clements, D. L., Colombi, S., Colombo, L. P. L., Combet, C., Comis, B., Couchot, F., Coulais, A., Crill, B. P., Curto, A., Cuttaia, F., Dahle, H., Danese, L., Davies, R. D., Davis, R. J., de Bernardis, P., de Rosa, A., de Zotti, G., Delabrouille, J., Désert, F. X., Dickinson, C., Diego, J. M., Dolag, K., Dole, H., Donzelli, S., Doré, O., Douspis, M., Ducout, A., Dupac, X., Efstathiou, G., Eisenhardt, P. R. M., Elsner, F., Enßlin, T. A., Eriksen, H. K., Falgarone, E., Fergusson, J., Feroz, F., Ferragamo, A., Finelli, F., Forni, O., Frailis, M., Fraisse, A. A., Franceschi, E., Frejsel, A., Galeotta, S., Galli, S., Ganga, K., Génova-Santos, R. T., Giard, M., Giraud-Héraud, Y., Gjerløw, E., González-Nuevo, J., Górski, K. M., Grainge, K. J. B., Gratton, S., Gregorio, A., Gruppuso, A., Gudmundsson, J. E., Hansen, F. K., Hanson, D., Harrison, D. L., Hempel, A., Henrot-Versillé, S., Hernández-Monteagudo, C., Herranz, D., Hildebrandt, S. R., Hivon, E., Hobson, M., Holmes, W. A., Hornstrup, A., Hovest, W., Huffenberger, K. M., Hurier, G., Jaffe, A. H., Jaffe, T. R., Jin, T., Jones, W. C., Juvela, M., Keihänen, E., Keskitalo, R., Khamitov, I., Kisner, T. S., Kneissl, R., Knoche, J., Kunz, M., Kurki-Suonio, H., Lagache, G., Lamarre, J. M., Lasenby, A., Lattanzi, M., Lawrence, C. R., Leonardi, R., Lesgourgues, J., Levrier, F., Liguori, M., Lilje, P. B., Linden-Vørnle, M., López-Caniiego, M., Lubin, P. M., Macías-Pérez, J. F., Maggio, G., Maino, D., Mak, D. S. Y., Mandolesi, N., Mangilli, A., Martin, P. G., Martínez-González, E., Masi, S., Matarrese, S., Mazzotta, P., McGehee, P., Mei, S., Melchiorri, A., Melin, J. B., Mendes, L., Mennella, A., Migliaccio, M., Mitra, S., Miville-Deschênes, M. A., Moneti, A., Montier, L., Morgante, G., Mortlock, D., Moss, A., Munshi, D., Murphy, J. A., Naselsky, P., Nastasi, A., Nati, F., Natoli, P., Netterfield, C. B., Nørgaard-Nielsen, H. U., Noviello, F., Novikov, D., Novikov, I., Olamaie, M., Oxborrow, C. A., Paci, F., Pagano, L., Pajot, F., Paoletti, D., Pasian, F., Patanchon, G., Pearson, T. J., Perdereau, O., Perotto, L., Perrott, Y. C., Perrotta, F., Pettorino, V., Piacentini, F., Piat, M., Pierpaoli, E., Pietrobon, D., Plaszczynski, S., Pointecouteau, E., Polenta, G., Pratt, G. W., Prézeau, G., Prunet, S., Puget, J. L., Rachen, J. P., Reach, W. T., Rebolo, R., Reinecke, M., Remazeilles, M., Renault, C., Renzi, A., Ristorcelli, I., Rocha, G., Rosset, C., Rossetti, M., Roudier, G., Rozo, E., Rubiño-Martín, J. A., Rumsey, C., Rusholme, B., Rykoff, E. S., Sandri, M., Santos, D., Saunders, R. D. E., Savelainen, M., Savini, G., Schammel, M. P., Scott, D., Seiffert, M. D., Shellard, E. P. S., Shimwell, T. W., Spencer, L. D., Stanford, S. A., Stern, D., Stolyarov, V., Stompor, R., Streblyanska, A., Sudiwala, R., Sunyaev, R., Sutton, D., Suur-Uski, A. S., Sygnet, J. F., Tauber, J. A., Terenzi, L., Tof-

- folatti, L., Tomasi, M., Tramonte, D., Tristram, M., Tucci, M., Tuovinen, J., Umana, G., Valenziano, L., Valiviita, J., Van Tent, B., Vielva, P., Villa, F., Wade, L. A., Wandelt, B. D., Wehus, I. K., White, S. D. M., Wright, E. L., Yvon, D., Zacchei, A., and Zonca, A. (2016). Planck 2015 results. XXVII. The second Planck catalogue of Sunyaev-Zeldovich sources. *Astronomy and Astrophysics*, 594:A27. ADS Bibcode: 2016A&A...594A..27P.
- Price, S. H., Kriek, M., Barro, G., Shapley, A. E., Reddy, N. A., Freeman, W. R., Coil, A. L., Shivaei, I., Azadi, M., Groot, L. d., Siana, B., Mobasher, B., Sanders, R. L., Leung, G. C. K., Fetherolf, T., Zick, T. O., Übler, H., and Schreiber, N. M. F. (2020). The MOSDEF Survey: Kinematic and Structural Evolution of Star-forming Galaxies at $1.4 \leq z \leq 3.8$. *The Astrophysical Journal*, 894(2):91. Publisher: The American Astronomical Society.
- Pérez-González, P. G., Barro, G., Annunziatella, M., Costantin, L., García-Argumánuez, ♦., McGrath, E. J., Mérida, R. M., Zavala, J. A., Haro, P. A., Bagley, M. B., Backhaus, B. E., Behroozi, P., Bell, E. F., Buat, V., Calabrò, A., Casey, C. M., Cleri, N. J., Coogan, R. T., Cooper, M. C., Cooray, A. R., Dekel, A., Dickinson, M., Elbaz, D., Ferguson, H. C., Finkelstein, S. L., Fontana, A., Franco, M., Gardner, J. P., Giavalisco, M., Gómez-Guijarro, C., Grazian, A., Grogin, N. A., Guo, Y., Jogee, S., Kartaltepe, J. S., Kewley, L. J., Kirkpatrick, A., Kocevski, D. D., Koekemoer, A. M., Long, A. S., Lotz, J. M., Lucas, R. A., Papovich, C., Pirzkal, N., Ravindranath, S., Somerville, R. S., Tacchella, S., Trump, J. R., Wang, W., Wilkins, S. M., Wuyts, S., Yang, G., and Yung, L. Y. A. (2022). CEERS Key Paper V: A triality on the nature of HST-dark galaxies. arXiv:2211.00045 [astro-ph].
- Reddy, N. A., Erb, D. K., Steidel, C. C., Shapley, A. E., Adelberger, K. L., and Pettini, M. (2005). A Census of Optical and Near-Infrared Selected Star-forming and Passively Evolving Galaxies at Redshift $z \sim 2$. *The Astrophysical Journal*, 633:748–767. ADS Bibcode: 2005ApJ...633..748R.
- Reddy, N. A., Topping, M. W., Sanders, R. L., Shapley, A. E., and Brammer, G. (2023a). A JWST/NIRSpec Exploration of the Connection between Ionization Parameter, Electron Density, and Star-formation-rate Surface Density in $z = 2.7–6.3$ Galaxies. *The Astrophysical Journal*, 952(2):167.
- Reddy, N. A., Topping, M. W., Sanders, R. L., Shapley, A. E., and Brammer, G. (2023b). Paschen-line Constraints on Dust Attenuation and Star Formation at $z \sim 1–3$ with JWST/NIRSpec. arXiv:2301.07249 [astro-ph].
- Rees, M. J. and Ostriker, J. P. (1977). Cooling, dynamics and fragmentation of massive gas clouds: clues to the masses and radii of galaxies and clusters. *Monthly Notices of the Royal Astronomical Society*, 179:541–559. Publisher: OUP ADS Bibcode: 1977MNRAS.179..541R.

Rigby, J., Perrin, M., McElwain, M., Kimble, R., Friedman, S., Lallo, M., Doyon, R., Feinberg, L., Ferruit, P., Glasse, A., Rieke, M., Rieke, G., Wright, G., Willott, C., Colon, K., Milam, S., Neff, S., Stark, C., Valenti, J., Abell, J., Abney, F., Abul-Huda, Y., Acton, D. S., Adams, E., Adler, D., Aguilar, J., Ahmed, N., Albert, L., Alberts, S., Aldridge, D., Allen, M., Altenburg, M., de Oliveira, C. A., Anderson, G., Anderson, H., Anderson, S., Argyriou, I., Armstrong, A., Arribas, S., Artigau, E., Arvai, A., Atkinson, C., Bacon, G., Bair, T., Banks, K., Barrientes, J., Barringer, B., Bartosik, P., Bast, W., Baudoz, P., Beatty, T., Bechtold, K., Beck, T., Bergeron, E., Bergkoetter, M., Bhatawdekar, R., Birkmann, S., Blazek, R., Blome, C., Boccaletti, A., Boeker, T., Boia, J., Bonaventura, N., Bond, N., Bosley, K., Boucarut, R., Bourque, M., Bouwman, J., Bower, G., Bowers, C., Boyer, M., Brady, G., Braun, H., Breda, D., Bresnahan, P., Bright, S., Britt, C., Bromenschenkel, A., Brooks, B., Brooks, K., Brown, B., Brown, M., Brown, P., Bunker, A., Burger, M., Bushouse, H., Cale, S., Cameron, A., Cameron, P., Canipe, A., Caplinger, J., Caputo, F., Carey, L., Carniani, S., Carrasquilla, M., Carruthers, M., Case, M., Chance, D., Chapman, G., Charlot, S., Charlow, B., Chayer, P., Chen, B., Cherinka, B., Chichester, S., Chilton, Z., Chonis, T., Clark, C., Clark, K., Coe, D., Coleman, B., Comber, B., Comeau, T., Connolly, D., Cooper, R., Cooper, J., Coppock, E., Correnti, M., Cossou, C., Coulais, A., Coyle, L., Cracraft, M., Curti, M., Cuturic, S., Davis, K., Davis, M., Dean, B., DeLisa, A., deMeester, W., Dencheva, N., Dencheva, N., DePasquale, J., Deschenes, J., Detre, H., Diaz, R., Dicken, D., DiFelice, A., Dillman, M., Dixon, W., Doggett, J., Donaldson, T., Douglas, R., DuPrie, K., Dupuis, J., Durning, J., Easmin, N., Eck, W., Edeani, C., Egami, E., Ehrenwinkler, R., Eisenhamer, J., Eisenhower, M., Elie, M., Elliott, J., Elliott, K., Ellis, T., Engesser, M., Espinoza, N., Etienne, O., Etxaluze, M., Falini, P., Feeney, M., Ferry, M., Filippazzo, J., Fincham, B., Fix, M., Flagey, N., Florian, M., Flynn, J., Fontanella, E., Ford, T., Forshay, P., Fox, O., Franz, D., Fu, H., Fullerton, A., Galkin, S., Galyer, A., Marin, M. G., Gardner, L., Gardner, J., Garland, D., Gasman, D., Gaspar, A., Gaudreau, D., Gauthier, P., Geers, V., Geithner, P., Gennaro, M., Giardino, G., Girard, J., Giuliano, M., Glassmire, K., Glauser, A., Glazer, S., Godfrey, J., Golimowski, D., Gollnitz, D., Gong, F., Gonzaga, S., Gordon, M., Gordon, K., Goudfrooij, P., Greene, T., Greenhouse, M., Grimaldi, S., Groebner, A., Grundy, T., Guillard, P., Gutman, I., Ha, K. Q., Haderlein, P., Hagedorn, A., Hainline, K., Haley, C., Hami, M., Hamilton, F., Hammel, H., Hansen, C., Harkins, T., Harr, M., Hart, Q., Hart, J., Hartig, G., Hashimoto, R., Haskins, S., Hathaway, W., Havey, K., Hayden, B., Hecht, K., Heller-Boyer, C., Henry, A., Hermann, K., Hernandez, S., Hesman, B., Hicks, B., Hilbert, B., Hines, D., Hoffman, M., Holfeltz, S., Holler, B. J., Hoppa, J., Hott, K., Howard, J., Hunter, D., Hunter, A., Hurst, B., Husemann, B., Hustak, L., Ignat, L. I., Irish, S., Jackson, W., Jahromi, A., Jakobsen, P., James, L., James, B., Januszewski, W., Jenkins, A., Jirdeh, H., Johnson, P., Johnson, T., Jones, O., Jones, D., Jones, R., Jones, V., Jordan, I., Jordan, M., Jurczyk, S., Jurling, A., Kaleida, C.,

Kalmanson, P., Kammerer, J., Kang, H., Kao, S.-H., Karakla, D., Kavanagh, P., Kelly, D., Kendrew, S., Kennedy, H., Kenny, D., Keski-kuha, R., Keyes, C., Kidwell, R., Kinzel, W., Kirk, J., Kirkpatrick, M., Kirshenblat, D., Klaassen, P., Knapp, B., Knight, J. S., Knollenberg, P., Koehler, R., Koekemoer, A., Kovacs, A., Kulp, T., Kumari, N., Kyprianou, M., La Massa, S., Labador, A., Ortega, A. L., Lagage, P.-O., Lajoie, C.-P., Lallo, M., Lam, M., Lamb, T., Lambros, S., Lampenfield, R., Langston, J., Larson, K., Law, D., Lawrence, J., Lee, D., Leisenring, J., Lepo, K., Leveille, M., Levenson, N., Levine, M., Levy, Z., Lewis, H., Lewis, D., Libralato, M., Lightsey, P., Link, M., Liu, L., Lo, A., Lockwood, A., Logue, R., Long, D., Long, C., Loomis, C., Lopez-Caniego, M., Alvarez, J. L., Love-Pruitt, J., Lucy, A., Luetzendorf, N., Maghami, P., Maiolino, R., Major, M., Malla, S., Malumuth, E., Manjavacas, E., Mannfolk, C., Marrione, A., Marston, A., Martel, A., Maschmann, M., Masci, G., Masciarelli, M., Maszkiewicz, M., Mather, J., McKenzie, K., McLean, B., McMaster, M., Melbourne, K., Meléndez, M., Menzel, M., Merz, K., Meyett, M., Meza, L., Miskey, C., Misselt, K., Moller, C., Morrison, J., Morse, E., Moseley, H., Mosier, G., Mountain, M., Mueckay, J., Mueller, M., Mullally, S., Murphy, J., Murray, K., Murray, C., Muzerolle, J., Mycroft, M., Myers, R., Myrick, K., Nanavati, S., Nance, E., Nayak, O., Naylor, B., Nelan, E., Nickson, B., Nielson, A., Nieto-Santisteban, M., Nikolov, N., Noriega-Crespo, A., O'Shaughnessy, B., O'Sullivan, B., Ochs, W., Ogle, P., Oleszczuk, B., Olmsted, J., Osborne, S., Ottens, R., Owens, B., Pacifici, C., Pagan, A., Page, J., Parrish, K., Patapis, P., Pauly, T., Pavlovsky, C., Pedder, A., Peek, M., Pena-Guerrero, M., Pennanen, K., Perez, Y., Perna, M., Perriello, B., Phillips, K., Pietraszkiewicz, M., Pinaud, J.-P., Pirzkal, N., Pitman, J., Piwowar, A., Platais, V., Player, D., Plesha, R., Pollizi, J., Polster, E., Pontoppidan, K., Porterfield, B., Proffitt, C., Pueyo, L., Pulliam, C., Quirt, B., Neira, I. Q., Alarcon, R. R., Ramsay, L., Rapp, G., Rapp, R., Rauscher, B., Ravindranath, S., Rawle, T., Regan, M., Reichard, T. A., Reis, C., Ressler, M. E., Rest, A., Reynolds, P., Rhue, T., Richon, K., Rickman, E., Ridgaway, M., Ritchie, C., Rix, H.-W., Robberto, M., Robinson, O., Robinson, M., Robinson, G., Rock, F., Rodriguez, D., Del Pino, B. R., Roellig, T., Rohrbach, S., Roman, A., Romelfanger, F., Rose, P., Roteliuk, A., Roth, M., Rothwell, B., Rowlands, N., Roy, A., Royer, P., Royle, P., Rui, C., Rumler, P., Runnels, J., Russ, M., Rustamkulov, Z., Ryden, G., Ryer, H., Sabata, M., Sabatke, D., Sabbi, E., Samuelson, B., Sappington, B., Sargent, B., Sauer, A., Scheithauer, S., Schlawin, E., Schlitz, J., Schmitz, T., Schneider, A., Schreiber, J., Schulze, V., Schwab, R., Scott, J., Sembach, K., Shaughnessy, B., Shaw, R., Shawger, N., Shay, C., Sheehan, E., Shen, S., Sherman, A., Shiao, B., Shih, H.-Y., Shivaei, I., Sienkiewicz, M., Sing, D., Sirianni, M., Sivaramakrishnan, A., Skipper, J., Sloan, G., Slocum, C., Slowinski, S., Smith, E., Smith, E., Smith, D., Smith, C., Snyder, G., Soh, W., Sohn, T., Soto, C., Spencer, R., Stallcup, S., Stansberry, J., Starr, E., Starr, C., Stewart, A., Stiavelli, M., Straughn, A., Strickland, D., Stys, J., Summers, F., Sun, F., Sunnquist, B., Swade, D., Swam, M., Swaters, R., Swoish, R., Taylor, J., Taylor,

R., Plate, M. T., Tea, M., Teague, K., Telfer, R., Temim, T., Thatte, D., Thompson, L., Thompson, C., Thomson, S., Tikkanen, T., Tippet, W., Todd, C., Toolan, S., Tran, H., Trejo, E., Truong, J., Tsukamoto, C., Tustain, S., Tyra, H., Ubeda, L., Underwood, K., Uzzo, M., Van Campen, J., Vandal, T., Vandenbussche, B., Vila, B., Volk, K., Wahlgren, G., Waldman, M., Walker, C., Wander, M., Warfield, C., Warner, G., Wasiaik, M., Watkins, M., Weilert, M., Weiser, N., Weiss, B., Weissman, S., Welty, A., West, G., Wheate, L., Wheatley, E., Wheeler, T., White, R., Whiteaker, K., Whitehouse, P., Whiteleather, J., Whitman, W., Williams, C., Willmer, C., Willoughby, S., Wilson, A., Wirth, G., Wislowski, E., Wolf, E., Wolfe, D., Wolff, S., Workman, B., Wright, R., Wu, R., Wu, C., Wymer, K., Yates, K., Yates, J., Yeager, C., Yerger, E., Yoon, J., Young, A., Yu, S., Zak, D., Zeidler, P., Zhou, J., Zielinski, T., Zincke, C., and Zonak, S. (2022). Characterization of JWST science performance from commissioning. arXiv:2207.05632 [astro-ph].

Robotham, A. S. G., Bellstedt, S., Lagos, C. d. P., Thorne, J. E., Davies, L. J., Driver, S. P., and Bravo, M. (2020). ProSpect: generating spectral energy distributions with complex star formation and metallicity histories. *Monthly Notices of the Royal Astronomical Society*, 495:905–931. ADS Bibcode: 2020MNRAS.495..905R.

Rodighiero, G., Bisigello, L., Iani, E., Marasco, A., Grazian, A., Sinigaglia, F., Cassata, P., and Gruppioni, C. (2023). JWST unveils heavily obscured (active and passive) sources up to $z \approx 13$. *Monthly Notices of the Royal Astronomical Society*, 518:L19–L24. ADS Bibcode: 2023MNRAS.518L..19R.

Rodighiero, G., Cimatti, A., Franceschini, A., Brusa, M., Fritz, J., and Bolzonella, M. (2007). Unveiling the oldest and most massive galaxies at very high redshift. *Astronomy and Astrophysics*, 470:21–37. ADS Bibcode: 2007A&A...470...21R.

Salpeter, E. E. (1955). The Luminosity Function and Stellar Evolution. *The Astrophysical Journal*, 121:161. Publisher: IOP ADS Bibcode: 1955ApJ...121..161S.

Sanders, R. L., Jones, T., Shapley, A. E., Reddy, N. A., Kriek, M., Coil, A. L., Siana, B., Mobasher, B., Shivaee, I., Price, S. H., Freeman, W. R., Azadi, M., Leung, G. C. K., Fetherolf, T., Zick, T. O., de Groot, L., Barro, G., and Fornasini, F. M. (2019). The MOS-DEF Survey: [SIII] as a New Probe of Evolving ISM Conditions. arXiv:1910.13594 [astro-ph].

Sandles, L., D’Eugenio, F., Helton, J. M., Maiolino, R., Hainline, K., Baker, W. M., Williams, C. C., Alberts, S., Bunker, A. J., Carniani, S., Charlot, S., Chevallard, J., Curti, M., Curtis-Lake, E., Eisenstein, D. J., Ji, Z., Johnson, B. D., Looser, T. J., Rawle, T., Robertson, B., Del Pino, B. R., Tacchella, S., Übler, H., Willmer, C. N. A., and Willott, C. (2023).

JADES: deep spectroscopy of a low-mass galaxy at redshift 2.3 quenched by environment. [arXiv:2307.08633 \[astro-ph\]](#).

Santini, P., Castellano, M., Fontana, A., Fortuni, F., Menci, N., Merlin, E., Pagul, A., Testa, V., Calabrò, A., Paris, D., and Pentericci, L. (2022a). The Stellar Mass Function in CANDELS and Frontier Fields: The Buildup of Low-mass Passive Galaxies since $z \approx 3$. *The Astrophysical Journal*, 940:135. ADS Bibcode: 2022ApJ...940..135S.

Santini, P., Castellano, M., Merlin, E., Fontana, A., Fortuni, F., Kodra, D., Magnelli, B., Menci, N., Calabrò, A., Lovell, C. C., Pentericci, L., Testa, V., and Wilkins, S. M. (2020). The emergence of passive galaxies in the early Universe. [arXiv:2011.10584 \[astro-ph\]](#). [arXiv:2011.10584](#).

Santini, P., Fontana, A., Castellano, M., Leethochawalit, N., Trenti, M., Treu, T., Belfiori, D., Birrer, S., Bonchi, A., Merlin, E., Mason, C., Morishita, T., Nonino, M., Paris, D., Polenta, G., Rosati, P., Yang, L., Bradac, M., Calabrò, A., Dressler, A., Glazebrook, K., Marchesini, D., Mascia, S., Nanayakkara, T., Pentericci, L., Roberts-Borsani, G., Scarlata, C., Vulcani, B., and Wang, X. (2022b). Early results from GLASS-JWST. XI: Stellar masses and mass-to-light ratio of $z > 7$ galaxies. [arXiv:2207.11379 \[astro-ph\]](#).

Saracco, P., Marchesini, D., La Barbera, F., Gargiulo, A., Annunziatella, M., Forrest, B., Vagle, D. J. L., Marsan, Z. C., Muzzin, A., Stefanon, M., and Wilson, G. (2020). The Rapid Build-up of Massive Early-type Galaxies. Supersolar Metallicity, High Velocity Dispersion and Young Age for an ETG at $z=3.35$. [arXiv:2011.04657 \[astro-ph\]](#). [arXiv:2011.04657](#).

Sarrouh, G. T., Muzzin, A., Iyer, K. G., Mowla, L., Abraham, R. G., Asada, Y., Bradac, M., Brammer, G. B., Desprez, G., Martis, N. S., Matharu, J., Noirot, G., Sawicki, M., Strait, V., Willott, C., and Zabl, J. (2024). Exposing Line Emission: A First Look At The Systematic Differences of Measuring Stellar Masses With JWST NIRCам Medium Versus Wide Band Photometry. Publication Title: [arXiv e-prints ADS Bibcode: 2024arXiv240108781S](#).

Sawicki, M., Arnouts, S., Huang, J., Coupon, J., Golob, A., Gwyn, S., Foucaud, S., Moutard, T., Iwata, I., Liu, C., Chen, L., Desprez, G., Harikane, Y., Ono, Y., Strauss, M. A., Tanaka, M., Thibert, N., Balogh, M., Bundy, K., Chapman, S., Gunn, J. E., Hsieh, B.-C., Ilbert, O., Jing, Y., LeFèvre, O., Li, C., Matsuda, Y., Miyazaki, S., Nagao, T., Nishizawa, A. J., Ouchi, M., Shimasaku, K., Silverman, J., de la Torre, S., Tresse, L., Wang, W.-H., Willott, C. J., Yamada, T., Yang, X., and Yee, H. K. C. (2019). The CFHT large area U-band deep survey (CLAUDS). *Monthly Notices of the Royal Astronomical Society*, 489:5202–5217. ADS Bibcode: 2019MNRAS.489.5202S.

- Schawinski, K., Urry, C. M., Simmons, B. D., Fortson, L., Kaviraj, S., Keel, W. C., Lintott, C. J., Masters, K. L., Nichol, R. C., Sarzi, M., Skibba, R., Treister, E., Willett, K. W., Wong, O. I., and Yi, S. K. (2014). The green valley is a red herring: Galaxy Zoo reveals two evolutionary pathways towards quenching of star formation in early- and late-type galaxies. *Monthly Notices of the Royal Astronomical Society*, 440:889–907. ADS Bibcode: 2014MNRAS.440..889S.
- Schlaflly, E. F. and Finkbeiner, D. P. (2011). MEASURING REDDENING WITH SLOAN DIGITAL SKY SURVEY GALAXY SPECTRA AND RECALIBRATING SFD. *The Astrophysical Journal*, 737(2):103. Publisher: The American Astronomical Society.
- Schreiber, C., Glazebrook, K., Nanayakkara, T., Kacprzak, G. G., Labbe, I., Oesch, P., Yuan, T., Tran, K.-V., Papovich, C., Spitler, L., and Straatman, C. (2018). Near infrared spectroscopy and star-formation histories of $3 < z < 4$ quiescent galaxies. *Astronomy & Astrophysics*, 618:A85. arXiv: 1807.02523.
- Schreiber, C., Glazebrook, K., Papovich, C., Diaz-Santos, T., Verma, A., Elbaz, D., Kacprzak, G. G., Nanayakkara, T., Oesch, P., Pannella, M., Spitler, L., Straatman, C., Tran, K.-V., and Wang, T. (2020). A low [CII]/[NII] ratio in the center of a massive galaxy at $z=3.7$: witnessing the transition to quiescence at high-redshift? *arXiv:2011.13700 [astro-ph]*. arXiv: 2011.13700.
- Schreiber, C., Pannella, M., Elbaz, D., Béthermin, M., Inami, H., Dickinson, M., Magnelli, B., Wang, T., Aussel, H., Daddi, E., Juneau, S., Shu, X., Sargent, M. T., Buat, V., Faber, S. M., Ferguson, H. C., Giavalisco, M., Koekemoer, A. M., Magdis, G., Morrison, G. E., Papovich, C., Santini, P., and Scott, D. (2015). The Herschel view of the dominant mode of galaxy growth from $z = 4$ to the present day. *Astronomy & Astrophysics*, 575:A74. Publisher: EDP Sciences.
- Scoville, N., Aussel, H., Brusa, M., Capak, P., Carollo, C. M., Elvis, M., Giavalisco, M., Guzzo, L., Hasinger, G., Impey, C., Kneib, J. P., LeFevre, O., Lilly, S. J., Mobasher, B., Renzini, A., Rich, R. M., Sanders, D. B., Schinnerer, E., Schminovich, D., Shopbell, P., Taniguchi, Y., and Tyson, N. D. (2007). The Cosmic Evolution Survey (COSMOS): Overview. *The Astrophysical Journal Supplement Series*, 172:1–8. ADS Bibcode: 2007ApJS..172....1S.
- Setton, D. J., Khullar, G., Miller, T. B., Bezanson, R., Greene, J. E., Suess, K. A., Whitaker, K. E., Antwi-Danso, J., Atek, H., Brammer, G., Cutler, S. E., Dayal, P., Feldmann, R., Furtak, L. J., Fujimoto, S., Glazebrook, K., Goulding, A. D., Kokorev, V., Labbe, I., Leja, J., Ma, Y., Marchesini, D., Nanayakkara, T., Pan, R., Price, S. H., Siegel, J. C., Shipley,

H., Weaver, J. R., van Dokkum, P., Wang, B., and Williams, C. C. (2024). UNCOVER NIRSpec/PRISM Spectroscopy Unveils Evidence of Early Core Formation in a Massive, Centrally Dusty Quiescent Galaxy at $z_{\text{spec}}=3.97$. Publication Title: arXiv e-prints ADS Bibcode: 2024arXiv240205664S.

Shahidi, A., Mobasher, B., Nayyeri, H., Hemmati, S., Wiklind, T., Chartab, N., Dickinson, M., Finkelstein, S. L., Pacifici, C., Papovich, C., Ferguson, H. C., Fontana, A., Giavalisco, M., Koekemoer, A., Newman, J., Sattari, Z., and Somerville, R. (2020). Selection of massive evolved galaxies at $3 \leq z \leq 4.5$ in the CANDELS fields. *The Astrophysical Journal*, 897(1):44. arXiv: 2005.12507.

Shapley, A. E., Reddy, N. A., Sanders, R. L., Topping, M. W., and Brammer, G. B. (2023). JWST/NIRSpec Measurements of the Relationships Between Nebular Emission-line Ratios and Stellar Mass at $z \sim 3-6$. Technical report. Publication Title: arXiv e-prints ADS Bibcode: 2023arXiv230300410S Type: article.

Sherman, S., Jogee, S., Florez, J., Stevans, M. L., Kawinwanichakij, L., Wold, I., Finkelstein, S. L., Papovich, C., Ciardullo, R., Gronwall, C., Cora, S. A., Hough, T., and Vega-Martínez, C. A. (2020). Investigating The Growing Population of Massive Quiescent Galaxies at Cosmic Noon. *arXiv:2010.04741 [astro-ph]*. arXiv: 2010.04741.

Shi, K., Toshikawa, J., Lee, K.-S., Wang, T., Cai, Z., and Fang, T. (2021). Accelerated galaxy growth and environmental quenching in a protocluster at $z=3.24$. *arXiv:2102.06499 [astro-ph]*. arXiv: 2102.06499.

Shuntov, M., McCracken, H. J., Gavazzi, R., Laigle, C., Weaver, J. R., Davidzon, I., Ilbert, O., Kauffmann, O. B., Faisst, A., Dubois, Y., Koekemoer, A. M., Moneti, A., Milvang-Jensen, B., Mobasher, B., Sanders, D. B., and Toft, S. (2022). COSMOS2020: Cosmic evolution of the stellar-to-halo mass relation for central and satellite galaxies up to $z \sim 5$. *Astronomy and Astrophysics*, 664:A61. ADS Bibcode: 2022A&A...664A..61S.

Skelton, R. E., Whitaker, K. E., Momcheva, I. G., Brammer, G. B., van Dokkum, P. G., Labbé, I., Franx, M., van der Wel, A., Bezanson, R., Da Cunha, E., Fumagalli, M., Förster Schreiber, N., Kriek, M., Leja, J., Lundgren, B. F., Magee, D., Marchesini, D., Maseda, M. V., Nelson, E. J., Oesch, P., Pacifici, C., Patel, S. G., Price, S., Rix, H.-W., Tal, T., Wake, D. A., and Wuyts, S. (2014). 3D-HST WFC3-selected Photometric Catalogs in the Five CANDELS/3D-HST Fields: Photometry, Photometric Redshifts, and Stellar Masses. *The Astrophysical Journal Supplement Series*, 214:24. ADS Bibcode: 2014ApJS..214...24S.

- Skrutskie, M. F., Cutri, R. M., Stiening, R., Weinberg, M. D., Schneider, S., Carpenter, J. M., Beichman, C., Capps, R., Chester, T., Elias, J., Huchra, J., Liebert, J., Lonsdale, C., Monet, D. G., Price, S., Seitzer, P., Jarrett, T., Kirkpatrick, J. D., Gizis, J. E., Howard, E., Evans, T., Fowler, J., Fullmer, L., Hurt, R., Light, R., Kopan, E. L., Marsh, K. A., McCallon, H. L., Tam, R., Van Dyk, S., and Wheelock, S. (2006). The Two Micron All Sky Survey (2MASS). *The Astronomical Journal*, 131:1163–1183. ADS Bibcode: 2006AJ....131.1163S.
- Slob, M., Kriek, M., Beverage, A. G., Suess, K. A., Barro, G., Bezanson, R., Cheng, C. M., Conroy, C., de Graaff, A., Förster Schreiber, N. M., Franx, M., Lorenz, B., Mancera Piña, P. E., Marchesini, D., Muzzin, A., Newman, A. B., Price, S. H., Shapley, A. E., Stefanon, M., van Dokkum, P., and Weisz, D. R. (2024). The JWST-SUSPENSE Ultradeep Spectroscopic Program: Survey Overview and Star-Formation Histories of Quiescent Galaxies at $1 < z < 3$. Publication Title: arXiv e-prints ADS Bibcode: 2024arXiv240412432S.
- Smail, I., Ivison, R. J., and Blain, A. W. (1997). A Deep Submillimeter Survey of Lensing Clusters: A New Window on Galaxy Formation and Evolution. *The Astrophysical Journal*, 490(1):L5. Publisher: IOP Publishing.
- Speagle, J. S., Steinhardt, C. L., Capak, P. L., and Silverman, J. D. (2014). A Highly Consistent Framework for the Evolution of the Star-Forming "Main Sequence" from $z \sim 0-6$. *The Astrophysical Journal Supplement Series*, 214(2):15. arXiv: 1405.2041.
- Spilker, J. S., Aravena, M., Béthermin, M., Chapman, S. C., Chen, C.-C., Cunningham, D. J. M., De Breuck, C., Dong, C., Gonzalez, A. H., Hayward, C. C., Hezaveh, Y. D., Litke, K. C., Ma, J., Malkan, M., Marrone, D. P., Miller, T. B., Morningstar, W. R., Narayanan, D., Phadke, K. A., Sreevani, J., Stark, A. A., Vieira, J. D., and Weiß, A. (2018). Fast molecular outflow from a dusty star-forming galaxy in the early Universe. *Science*, 361(6406):1016–1019. Publisher: American Association for the Advancement of Science.
- Spitler, L. R., Straatman, C. M. S., Labbe, I., Glazebrook, K., Tran, K.-V. H., Kacprzak, G. G., Quadri, R. F., Papovich, C., Persson, S. E., van Dokkum, P., Allen, R., Kawinwanichakij, L., Kelson, D. D., McCarthy, P. J., Mehrtens, N., Monson, A. J., Nanayakkara, T., Rees, G., Tilvi, V., and Tomczak, A. R. (2014). Exploring the $z=3-4$ massive galaxy population with ZFOURGE: the prevalence of dusty and quiescent galaxies. *The Astrophysical Journal*, 787(2):L36. arXiv: 1405.1048.
- Stahler, S. W. and Palla, F. (2004). *The Formation of Stars*. Publication Title: The Formation of Stars ADS Bibcode: 2004fost.book.....S.

- Stawinski, S. M. U., Cooper, M. C., Forrest, B., Muzzin, A., Marchesini, D., Wilson, G., Gomez, P., McConachie, I., Marsan, Z. C., Annuziatella, M., and Chang, W. (2024). Spectroscopic Confirmation of an Ultra-Massive Galaxy in a Protocluster at $z \sim 4.9$. arXiv:2404.16036 [astro-ph].
- Steinhardt, C. L., Capak, P., Masters, D., and Speagle, J. S. (2016). The Impossibly Early Galaxy Problem. *The Astrophysical Journal*, 824:21. ADS Bibcode: 2016ApJ...824...21S.
- Steinhardt, C. L., Jespersen, C. K., and Linzer, N. B. (2021). Finding High-Redshift Galaxies with JWST. *The Astrophysical Journal*, 923(1):8. arXiv:2111.14865 [astro-ph].
- Stevans, M. L., Finkelstein, S. L., Kawinwanichakij, L., Wold, I., Papovich, C., Somerville, R. S., Yung, L. Y. A., Sherman, S., Ciardullo, R., Dave, R., Florez, J., Gronwall, C., and Jogee, S. (2021). The NEWFIRM HETDEX Survey: Photometric Catalog and a Conservative Sample of Massive Quiescent Galaxies at $z=3-5$ over 17.5 deg^2 in the SHELA Field. arXiv:2103.14690 [astro-ph]. arXiv: 2103.14690.
- Stockmann, M., Toft, S., Gallazzi, A., Zibetti, S., Conselice, C. J., Margalef-Bentabol, B., Zabl, J., Jørgensen, I., Magdis, G. E., Gómez-Guijarro, C., Valentino, F. M., Brammer, G. B., Ceverino, D., Cortzen, I., Davidzon, I., Demarco, R., Faisst, A., Hirschmann, M., Krogager, J.-K., Lagos, C. D., Man, A. W. S., Mundy, C. J., Peng, Y., Selsing, J., Steinhardt, C. L., and Whitaker, K. E. (2019). X-shooter Spectroscopy and HST Imaging of 15 Ultra Massive Quiescent Galaxies at $z \gtrsim 2$. *The Astrophysical Journal*, 888(1):4. arXiv: 1912.01619.
- Straatman, C. M. S., Labbé, I., Spitler, L. R., Allen, R., Altieri, B., Brammer, G. B., Dickinson, M., van Dokkum, P., Inami, H., Glazebrook, K., Kacprzak, G. G., Kawinwanichakij, L., Kelson, D. D., McCarthy, P. J., Mehrrens, N., Monson, A., Murphy, D., Papovich, C., Persson, S. E., Quadri, R., Rees, G., Tomczak, A., Tran, K.-V. H., and Tilvi, V. (2014). A substantial population of massive quiescent galaxies at $z \sim 4$ from ZFOURGE. *The Astrophysical Journal*, 783(1):L14. arXiv: 1312.4952.
- Straatman, C. M. S., Labbé, I., Spitler, L. R., Glazebrook, K., Tomczak, A., Allen, R., Brammer, G. B., Cowley, M., Dokkum, P. v., Kacprzak, G. G., Kawinwanichakij, L., Mehrrens, N., Nanayakkara, T., Papovich, C., Persson, S. E., Quadri, R. F., Rees, G., Tilvi, V., Tran, K.-V. H., and Whitaker, K. E. (2015). THE SIZES OF MASSIVE QUIESCENT AND STAR-FORMING GALAXIES AT $z \sim 4$ WITH ZFOURGE AND CANDELS*. *The Astrophysical Journal Letters*, 808(1):L29. Publisher: The American Astronomical Society.
- Straatman, C. M. S., Spitler, L. R., Quadri, R. F., Labbé, I., Glazebrook, K., Persson, S. E., Papovich, C., Tran, K.-V. H., Brammer, G. B., Cowley, M., Tomczak, A., Nanayakkara,

T., Alcorn, L., Allen, R., Broussard, A., Dokkum, P. v., Forrest, B., Houdt, J. v., Kacprzak, G. G., Kawinwanichakij, L., Kelson, D. D., Lee, J., McCarthy, P. J., Mehrrens, N., Monson, A., Murphy, D., Rees, G., Tilvi, V., and Whitaker, K. E. (2016). THE FOURSTAR GALAXY EVOLUTION SURVEY (ZFOURGE): ULTRAVIOLET TO FAR-INFRARED CATALOGS, MEDIUM-BANDWIDTH PHOTOMETRIC RED-SHIFTS WITH IMPROVED ACCURACY, S_{DLA} MASSES, AND CONFIRMATION OF QUIESCENT GALAXIES TO $z \sim 3.5^*$. *The Astrophysical Journal*, 830(1):51. Publisher: The American Astronomical Society.

Strait, V., Brammer, G., Muzzin, A., Desprez, G., Asada, Y., Abraham, R., Bradač, M., Iyer, K. G., Martis, N., Mowla, L., Noirot, G., Sarrouh, G. T. E., Sawicki, M., Willott, C., Gould, K., Grindlay, T., Matharu, J., and Rihtaršič, G. (2023). An Extremely Compact, Low-mass Galaxy on its Way to Quiescence at $z = 5.2$. *The Astrophysical Journal Letters*, 949(2):L23. Publisher: The American Astronomical Society.

Suess, K. A., Bezanson, R., Nelson, E. J., Setton, D. J., Price, S. H., Dokkum, P. v., Brammer, G., Labbé, I., Leja, J., Miller, T. B., Robertson, B., Wel, A. v. d., Weaver, J. R., and Whitaker, K. E. (2022a). Rest-frame Near-infrared Sizes of Galaxies at Cosmic Noon: Objects in JWST's Mirror Are Smaller than They Appeared. *The Astrophysical Journal Letters*, 937(2):L33. Publisher: The American Astronomical Society.

Suess, K. A., Leja, J., Johnson, B. D., Bezanson, R., Greene, J. E., Kriek, M., Lower, S., Narayanan, D., Setton, D. J., and Spilker, J. S. (2022b). Recovering the star formation histories of recently-quenched galaxies: the impact of model and prior choices. arXiv:2207.02883 [astro-ph].

Sun, F., Egami, E., Fujimoto, S., Rawle, T., Bauer, F. E., Kohno, K., Smail, I., Pérez-González, P. G., Ao, Y., Chapman, S. C., Combes, F., Dessauges-Zavadsky, M., Espada, D., González-López, J., Koekemoer, A. M., Kokorev, V., Lee, M. M., Morokuma-Matsui, K., Muñoz Arancibia, A. M., Oguri, M., Pelló, R., Ueda, Y., Uematsu, R., Valentino, F., Van der Werf, P., Walth, G. L., Zemcov, M., and Zitrin, A. (2022). ALMA Lensing Cluster Survey: ALMA-Herschel Joint Study of Lensed Dusty Star-forming Galaxies across $z \square 0.5 - 6$. *The Astrophysical Journal*, 932(2):77.

Sun, F., Egami, E., Pérez-González, P. G., Smail, I., Caputi, K. I., Bauer, F. E., Rawle, T. D., Fujimoto, S., Kohno, K., Dudzevičiūtė, U., Atek, H., Bianconi, M., Chapman, S. C., Combes, F., Jauzac, M., Jolly, J.-B., Koekemoer, A. M., Magdis, G. E., Rodighiero, G., Rujopakarn, W., Schaerer, D., Steinhardt, C. L., Van der Werf, P., Walth, G. L., and Weaver, J. R. (2021). Extensive Lensing Survey of Optical and Near-infrared Dark Objects

(El Sonido): HST H-faint Galaxies behind 101 Lensing Clusters. *The Astrophysical Journal*, 922:114. Publisher: IOP ADS Bibcode: 2021ApJ...922..114S.

Sun, F., Helton, J. M., Egami, E., Hainline, K. N., Rieke, G. H., Willmer, C. N. A., Eisenstein, D. J., Johnson, B. D., Rieke, M. J., Robertson, B., Tacchella, S., Alberts, S., Baker, W. M., Bhatawdekar, R., Boyett, K., Bunker, A. J., Charlot, S., Chen, Z., Chevallard, J., Curtis-Lake, E., Danhaive, A. L., DeCoursey, C., Ji, Z., Lyu, J., Maiolino, R., Rujopakarn, W., Sandles, L., Shivaiei, I., Übler, H., Willott, C., and Witstok, J. (2024). JADES: Resolving the Stellar Component and Filamentary Overdense Environment of Hubble Space Telescope (HST)-dark Submillimeter Galaxy HDF850.1 at $z = 5.18$. *The Astrophysical Journal*, 961:69. Publisher: IOP ADS Bibcode: 2024ApJ...961...69S.

Suzuki, T. L., Glazebrook, K., Schreiber, C., Kodama, T., Kacprzak, G. G., Leiton, R., Nanayakkara, T., Oesch, P. A., Papovich, C., Spitler, L., Straatman, C. M. S., Tran, K.-V., and Wang, T. (2022). Low star-formation activity and low gas content of quiescent galaxies at $z = 3.5-4.0$ constrained with ALMA. arXiv:2206.14238 [astro-ph].

Tabatabaei, F. S., Minguez, P., Prieto, M. A., and Fernández-Ontiveros, J. A. (2018). Discovery of massive star formation quenching by non-thermal effects in the centre of NGC 1097. *Nature Astronomy*, 2:83–89. ADS Bibcode: 2018NatAs...2...83T.

Talia, M., Cimatti, A., Giulietti, M., Zamorani, G., Bethermin, M., Faisst, A., Fèvre, O. L., and Smolčić, V. (2021). Illuminating the Dark Side of Cosmic Star Formation Two Billion Years after the Big Bang. *The Astrophysical Journal*, 909(1):23. Publisher: The American Astronomical Society.

Toft, S., Smolčić, V., Magnelli, B., Karim, A., Zirm, A., Michalowski, M., Capak, P., Sheth, K., Schawinski, K., Krogager, J. K., Wuyts, S., Sanders, D., Man, A. W. S., Lutz, D., Staguhn, J., Berta, S., Mccracken, H., Krpan, J., and Riechers, D. (2014). Submillimeter Galaxies as Progenitors of Compact Quiescent Galaxies. *The Astrophysical Journal*, 782:68. Publisher: IOP ADS Bibcode: 2014ApJ...782...68T.

Toft, S., van Dokkum, P., Franx, M., Labbe, I., Förster Schreiber, N. M., Wuyts, S., Webb, T., Rudnick, G., Zirm, A., Kriek, M., van der Werf, P., Blakeslee, J. P., Illingworth, G., Rix, H. W., Papovich, C., and Moorwood, A. (2007). Hubble Space Telescope and Spitzer Imaging of Red and Blue Galaxies at $z \sim 2.5$: A Correlation between Size and Star Formation Activity from Compact Quiescent Galaxies to Extended Star-forming Galaxies. *The Astrophysical Journal*, 671:285–302. ADS Bibcode: 2007ApJ...671..285T.

- Tokunaga, A. T. and Vacca, W. D. (2005). The Mauna Kea Observatories Near-Infrared Filter Set. III. Isophotal Wavelengths and Absolute Calibration. *Publications of the Astronomical Society of the Pacific*, 117:421–426. ADS Bibcode: 2005PASP..117..421T.
- Tomczak, A. R., Quadri, R. F., Tran, K.-V. H., Labbé, I., Straatman, C. M. S., Papovich, C., Glazebrook, K., Allen, R., Brammer, G. B., Kacprzak, G. G., Kawinwanichakij, L., Kelson, D. D., McCarthy, P. J., Mehrtens, N., Monson, A. J., Persson, S. E., Spitler, L. R., Tilvi, V., and Dokkum, P. v. (2014). GALAXY Σ LAR MASS FUNCTIONS FROM ZFOURGE/CANDELS: AN EXCESS OF LOW-MASS GALAXIES SINCE $z = 2$ AND THE RAPID BUILDUP OF QUIESCENT GALAXIES*. *The Astrophysical Journal*, 783(2):85. Publisher: The American Astronomical Society.
- Totani, T. and Yoshii, Y. (1998). Does the Number Density of Elliptical Galaxies Change at $z < 1$? *The Astrophysical Journal*, 501(2):L177. Publisher: IOP Publishing.
- Trayford, J. W., Lagos, C. d. P., Robotham, A. S. G., and Obreschkow, D. (2020). Fade to grey: systematic variation of galaxy attenuation curves with galaxy properties in the EAGLE simulations. *Monthly Notices of the Royal Astronomical Society*, 491:3937–3951. ADS Bibcode: 2020MNRAS.491.3937T.
- Valentino, F., Brammer, G., Fujimoto, S., Heintz, K. E., Weaver, J. R., Strait, V., Gould, K. M. L., Mason, C., Watson, D., Laursen, P., and Toft, S. (2022). The archival discovery of a strong Lyman- α and [CII] emitter at $z = 7.677$. *The Astrophysical Journal Letters*, 929(1):L9. arXiv:2203.03657 [astro-ph].
- Valentino, F., Brammer, G., Gould, K. M. L., Kokorev, V., Fujimoto, S., Jespersen, C. K., Vijayan, A. P., Weaver, J. R., Ito, K., Tanaka, M., Ilbert, O., Magdis, G. E., Whitaker, K. E., Faisst, A. L., Gallazzi, A., Gillman, S., Gimenez-Arteaga, C., Gomez-Guijarro, C., Kubo, M., Heintz, K. E., Hirschmann, M., Oesch, P., Onodera, M., Rizzo, F., Lee, M., Strait, V., and Toft, S. (2023). An Atlas of Color-selected Quiescent Galaxies at $z > 3$ in Public JWST Fields. arXiv:2302.10936 [astro-ph].
- Valentino, F., Tanaka, M., Davidzon, I., Toft, S., Gomez-Guijarro, C., Stockmann, M., Onodera, M., Brammer, G., Ceverino, D., Faisst, A. L., Gallazzi, A., Hayward, C. C., Ilbert, O., Kubo, M., Magdis, G. E., Selsing, J., Shimakawa, R., Sparre, M., Steinhardt, C., Yabe, K., and Zabl, J. (2020). Quiescent galaxies 1.5 billion years after the Big Bang and their progenitors. *The Astrophysical Journal*, 889(2):93. arXiv: 1909.10540.
- van Dokkum, P. G., Franx, M., Fabricant, D., Kelson, D. D., and Illingworth, G. D. (1999). A High Merger Fraction in the Rich Cluster MS 1054-03 at $Z = 0.83$: Direct Evidence

for Hierarchical Formation of Massive Galaxies. *The Astrophysical Journal*, 520:L95–L98. Publisher: IOP ADS Bibcode: 1999ApJ...520L..95V.

van Dokkum, P. G., Kriek, M., and Franx, M. (2009a). A high stellar velocity dispersion for a compact massive galaxy at redshift $z = 2.186$. *Nature*, 460(7256):717–719. Number: 7256 Publisher: Nature Publishing Group.

van Dokkum, P. G., Labbé, I., Marchesini, D., Quadri, R., Brammer, G., Whitaker, K. E., Kriek, M., Franx, M., Rudnick, G., Illingworth, G., Lee, K.-S., and Muzzin, A. (2009b). The NEWFIRM Medium-Band Survey: Filter Definitions and First Results. *Publications of the Astronomical Society of the Pacific*, 121:2. ADS Bibcode: 2009PASP..121....2V.

Virtanen, P., Gommers, R., Oliphant, T. E., Haberland, M., Reddy, T., Cournapeau, D., Burovski, E., Peterson, P., Weckesser, W., Bright, J., van der Walt, S. J., Brett, M., Wilson, J., Millman, K. J., Mayorov, N., Nelson, A. R. J., Jones, E., Kern, R., Larson, E., Carey, C. J., Polat, ♦., Feng, Y., Moore, E. W., VanderPlas, J., Laxalde, D., Perktold, J., Cimrman, R., Henriksen, I., Quintero, E. A., Harris, C. R., Archibald, A. M., Ribeiro, A. H., Pedregosa, F., and van Mulbregt, P. (2020). SciPy 1.0: fundamental algorithms for scientific computing in Python. *Nature Methods*, 17(3):261–272. Number: 3 Publisher: Nature Publishing Group.

Wang, B., de Graaff, A., Davies, R. L., Greene, J. E., Leja, J., Goulding, A. D., Williams, C. C., Brammer, G. B., Suess, K. A., Weibel, A., Bezanson, R., Boogaard, L. A., Cleri, N. J., Hirschmann, M., Katz, H., Labbe, I., Maseda, M. V., Matthee, J., McConachie, I., Naidu, R. P., Oesch, P. A., Rix, H.-W., Setton, D. J., and Whitaker, K. E. (2024a). RUBIES: JWST/NIRSpec Confirmation of an Infrared-luminous, Broad-line Little Red Dot with an Ionized Outflow. arXiv:2403.02304 [astro-ph].

Wang, T., Elbaz, D., Schreiber, C., Pannella, M., Shu, X., Willner, S. P., Ashby, M. L. N., Huang, J.-S., Fontana, A., Dekel, A., Daddi, E., Ferguson, H. C., Dunlop, J., Ciesla, L., Koekemoer, A. M., Giavalisco, M., Boutsia, K., Finkelstein, S., Juneau, S., Barro, G., Koo, D. C., Michałowski, M. J., Orellana, G., Lu, Y., Castellano, M., Bourne, N., Buitrago, F., Santini, P., Faber, S. M., Hathi, N., Lucas, R. A., and Pérez-González, P. G. (2016). INFRARED COLOR SELECTION OF MASSIVE GALAXIES AT $z > 3$. *The Astrophysical Journal*, 816(2):84.

Wang, T., Schreiber, C., Elbaz, C., Yoshimura, Y., Kohno, K., Shu, X., Yamaguchi, Y., Pannella, M., Franco, M., Huang, J., Lim, C. F., and Wang, W. H. (2019). A dominant population of optically invisible massive galaxies in the early Universe. *Nature*, 572(7768):211–214. arXiv:1908.02372 [astro-ph].

Wang, T., Sun, H., Zhou, L., Xu, K., Cheng, C., Li, Z., Chen, Y., Mo, H. J., Dekel, A., Zheng, X., Cai, Z., Yang, T., Dai, Y. S., Elbaz, D., and Huang, J. S. (2024b). The true number density of massive galaxies in the early Universe revealed by JWST/MIRI. Publication Title: arXiv e-prints ADS Bibcode: 2024arXiv240302399W.

Wang, W., Wylezalek, D., De Breuck, C., Vernet, J., Rupke, D. S. N., Zakamska, N. L., Vayner, A., Lehnert, M. D., Nesvadba, N. P. H., and Stern, D. (2024c). JWST discovers an AGN ionization cone but only weak radiative-driven feedback in a powerful ≈ 3.5 radio-loud AGN. arXiv:2401.02479 [astro-ph].

Weaver, J. R., Davidzon, I., Toft, S., Ilbert, O., McCracken, H. J., Gould, K. M. L., Jespersen, C. K., Steinhardt, C., Lagos, C. D. P., Capak, P. L., Casey, C. M., Chartab, N., Faisst, A. L., Hayward, C. C., Kartaltepe, J. S., Kauffmann, O. B., Koekemoer, A. M., Kokorev, V., Laigle, C., Liu, D., Long, A., Magdis, G. E., McPartland, C. J. R., Milvang-Jensen, B., Mobasher, B., Moneti, A., Peng, Y., Sanders, D. B., Shuntov, M., Sneppen, A., Valentino, F., Zalesky, L., and Zamorani, G. (2022). COSMOS2020: The Galaxy Stellar Mass Function: On the assembly and star formation cessation of galaxies at $0.2 \leq z \leq 7.5$. arXiv:2212.02512 [astro-ph].

Weaver, J. R., Kauffmann, O. B., Ilbert, O., McCracken, H. J., Moneti, A., Toft, S., Brammer, G., Shuntov, M., Davidzon, I., Hsieh, B. C., Laigle, C., Anastasiou, A., Jespersen, C. K., Vinther, J., Capak, P., Casey, C. M., McPartland, C. J. R., Milvang-Jensen, B., Mobasher, B., Sanders, D. B., Zalesky, L., Arnouts, S., Aussel, H., Dunlop, J. S., Faisst, A., Franx, M., Furtak, L. J., Fynbo, J. P. U., Gould, K. M. L., Greve, T. R., Gwyn, S., Kartaltepe, J. S., Kashino, D., Koekemoer, A. M., Kokorev, V., Fevre, O. L., Lilly, S., Masters, D., Magdis, G., Mehta, V., Peng, Y., Riechers, D. A., Salvato, M., Sawicki, M., Scarlata, C., Scoville, N., Shirley, R., Sneppen, A., Smolcic, V., Steinhardt, C., Stern, D., Tanaka, M., Taniguchi, Y., Teplitz, H. I., Vaccari, M., Wang, W.-H., and Zamorani, G. (2021). COSMOS2020: A panchromatic view of the Universe to $z \sim 10$ from two complementary catalogs. arXiv:2110.13923 [astro-ph]. arXiv: 2110.13923.

Weaver, J. R., Zalesky, L., Kokorev, V., McPartland, C. J. R., Chartab, N., Gould, K. M. L., Shuntov, M., Davidzon, I., Faisst, A., Stickley, N., Capak, P. L., Toft, S., Masters, D., Mobasher, B., Sanders, D. B., Kauffmann, O. B., McCracken, H. J., Ilbert, O., Brammer, G., and Moneti, A. (2023). The Farmer: A Reproducible Profile-fitting Photometry Package for Deep Galaxy Surveys. *The Astrophysical Journal Supplement Series*, 269(1):20. Publisher: The American Astronomical Society.

Wel, A. v. d., Franx, M., Dokkum, P. G. v., Skelton, R. E., Momcheva, I. G., Whitaker, K. E., Brammer, G. B., Bell, E. F., Rix, H.-W., Wuyts, S., Ferguson, H. C., Holden, B. P., Barro,

- G., Koekemoer, A. M., Chang, Y.-Y., McGrath, E. J., Häussler, B., Dekel, A., Behroozi, P., Fumagalli, M., Leja, J., Lundgren, B. F., Maseda, M. V., Nelson, E. J., Wake, D. A., Patel, S. G., Labbé, I., Faber, S. M., Grogin, N. A., and Kocevski, D. D. (2014). 3D-HST+CANDELS: THE EVOLUTION OF THE GALAXY SIZE–MASS DISTRIBUTION SINCE $z = 3$. *The Astrophysical Journal*, 788(1):28. Publisher: The American Astronomical Society.
- Werner, M. W., Roellig, T. L., Low, F. J., Rieke, G. H., Rieke, M., Hoffmann, W. F., Young, E., Houck, J. R., Brandl, B., Fazio, G. G., Hora, J. L., Gehrz, R. D., Helou, G., Soifer, B. T., Stauffer, J., Keene, J., Eisenhardt, P., Gallagher, D., Gautier, T. N., Irace, W., Lawrence, C. R., Simmons, L., Van Cleve, J. E., Jura, M., Wright, E. L., and Cruikshank, D. P. (2004). The Spitzer Space Telescope Mission. *The Astrophysical Journal Supplement Series*, 154:1–9. Publisher: IOP ADS Bibcode: 2004ApJS..154....1W.
- Whitaker, K. E., Franx, M., Leja, J., van Dokkum, P. G., Henry, A., Skelton, R. E., Fumagalli, M., Momcheva, I. G., Brammer, G. B., Labbe, I., Nelson, E. J., and Rigby, J. R. (2014). Constraining the Low-Mass Slope of the Star Formation Sequence at $0.5 < z < 2.5$. *The Astrophysical Journal*, 795(2):104. arXiv: 1407.1843.
- Whitaker, K. E., Kriek, M., van Dokkum, P. G., Bezanson, R., Brammer, G., Franx, M., and Labbé, I. (2012). A Large Population of Massive Compact Post-starburst Galaxies at $z > 1$: Implications for the Size Evolution and Quenching Mechanism of Quiescent Galaxies. *The Astrophysical Journal*, 745:179. ADS Bibcode: 2012ApJ...745..179W.
- Whitaker, K. E., Labbé, I., van Dokkum, P. G., Brammer, G., Kriek, M., Marchesini, D., Quadri, R. F., Franx, M., Muzzin, A., Williams, R. J., Bezanson, R., Illingworth, G. D., Lee, K.-S., Lundgren, B., Nelson, E. J., Rudnick, G., Tal, T., and Wake, D. A. (2011). The NEWFIRM Medium-band Survey: Photometric Catalogs, Redshifts, and the Bimodal Color Distribution of Galaxies out to $z \sim 3$. *The Astrophysical Journal*, 735:86. ADS Bibcode: 2011ApJ...735...86W.
- Whitaker, K. E., Narayanan, D., Williams, C. C., Li, Q., Spilker, J. S., Davé, R., Akhshik, M., Akins, H. B., Bezanson, R., Katz, N., Leja, J., Magdis, G. E., Mowla, L., Nelson, E. J., Pope, A., Privon, G. C., Toft, S., and Valentino, F. (2021). High Molecular-Gas to Dust Mass Ratios Predicted in Most Quiescent Galaxies. *arXiv:2111.05349 [astro-ph]*. arXiv: 2111.05349.
- Whitaker, K. E., van Dokkum, P. G., Brammer, G., Kriek, M., Franx, M., Labbé, I., Marchesini, D., Quadri, R. F., Bezanson, R., Illingworth, G. D., Lee, K.-S., Muzzin, A., Rudnick, G., and Wake, D. A. (2010). The Age Spread of Quiescent Galaxies with the NEWFIRM

Medium-band Survey: Identification of the Oldest Galaxies Out to $z \sim 2$. *The Astrophysical Journal*, 719:1715–1732. ADS Bibcode: 2010ApJ...719.1715W.

Whitaker, K. E., van Dokkum, P. G., Brammer, G., Momcheva, I. G., Skelton, R., Franx, M., Kriek, M., Labbé, I., Fumagalli, M., Lundgren, B. F., Nelson, E. J., Patel, S. G., and Rix, H.-W. (2013). QUIESCENT GALAXIES IN THE 3D-HST SURVEY: SPECTROSCOPIC CONFIRMATION OF A LARGE NUMBER OF GALAXIES WITH RELATIVELY OLD STELLAR POPULATIONS AT $z \sim 2$. *The Astrophysical Journal*, 770(2):L39.

Wiklind, T., Mobasher, B., Dickinson, M., Ferguson, H., Giavalisco, M., Grogin, N., and Panagia, N. (2007). Massive and Evolved Galaxies at $z \geq 5$. 235:368–372. Conference Name: Galaxy Evolution across the Hubble Time ADS Bibcode: 2007IAUS..235..368W.

Wild, V., Almaini, O., Cirasuolo, M., Dunlop, J., McLure, R., Bowler, R., Ferreira, J., Bradshaw, E., Chuter, R., and Hartley, W. (2014). A new method for classifying galaxy SEDs from multiwavelength photometry. *Monthly Notices of the Royal Astronomical Society*, 440(2):1880–1898.

Wild, V., Taj Aldeen, L., Carnall, A., Maltby, D., Almaini, O., Werle, A., Wilkinson, A., Rowlands, K., Bolzonella, M., Castellano, M., Gargiulo, A., McLure, R., Pentericci, L., and Pozzetti, L. (2020). The star formation histories of $z \sim 1$ post-starburst galaxies. *Monthly Notices of the Royal Astronomical Society*, 494:529–548.

Wild, V., Walcher, C. J., Johansson, P. H., Tresse, L., Charlot, S., Pollo, A., Le Fèvre, O., and De Ravel, L. (2009). Post-starburst galaxies: more than just an interesting curiosity. *Monthly Notices of the Royal Astronomical Society*, 395(1):144–159.

Wilkinson, A., Almaini, O., Wild, V., Maltby, D., Hartley, W. G., Simpson, C., and Rowlands, K. (2021). From starburst to quiescence: post-starburst galaxies and their large-scale clustering over cosmic time. *Monthly Notices of the Royal Astronomical Society*, 504(3):4533–4550. arXiv: 2104.07676.

Williams, C. C., Alberts, S., Ji, Z., Hainline, K. N., Lyu, J., Rieke, G., Endsley, R., Suess, K. A., Johnson, B. D., Florian, M., Shivaee, I., Rujopakarn, W., Baker, W. M., Bhatawdekar, R., Boyett, K., Bunker, A. J., Carniani, S., Charlot, S., Curtis-Lake, E., DeCoursey, C., de Graaff, A., Egami, E., Eisenstein, D. J., Gibson, J. L., Hausen, R., Helton, J. M., Maiolino, R., Maseda, M. V., Nelson, E. J., Perez-Gonzalez, P. G., Rieke, M. J., Robertson, B. E., Sun, F., Tacchella, S., Willmer, C. N. A., and Willott, C. J. (2023). The galaxies missed by Hubble and ALMA: the contribution of extremely red galaxies to the cosmic census at $z \sim 3$. Publication Title: arXiv e-prints ADS Bibcode: 2023arXiv231107483W.

Williams, C. C., Giavalisco, M., Bezanson, R., Cappelluti, N., Cassata, P., Liu, T., Lee, B., Tundo, E., and Vanzella, E. (2017). Morphology Dependence of Stellar Age in Quenched Galaxies at Redshift ~ 1.2 : Massive Compact Galaxies Are Older than More Extended Ones. *The Astrophysical Journal*, 838:94. Publisher: IOP ADS Bibcode: 2017ApJ...838...94W.

Williams, C. C., Giavalisco, M., Lee, B., Tundo, E., Mobasher, B., Nayyeri, H., Ferguson, H. C., Koekemoer, A., Trump, J. R., Cassata, P., Dekel, A., Guo, Y., Lee, K.-S., Pentericci, L., Bell, E. F., Castellano, M., Finkelstein, S. L., Fontana, A., Grazian, A., Grogin, N., Kocevski, D., Koo, D. C., Lucas, R. A., Ravindranath, S., Santini, P., Vanzella, E., and Weiner, B. J. (2015). The Interstellar Medium and Feedback in the Progenitors of the Compact Passive Galaxies at $z \sim 2$. *The Astrophysical Journal*, 800:21. Publisher: IOP ADS Bibcode: 2015ApJ...800...21W.


Williams, C. C., Labbe, I., Spilker, J., Stefanon, M., Leja, J., Whitaker, K., Bezanson, R., Narayanan, D., Oesch, P., and Weiner, B. (2019). Discovery of a Dark, Massive, ALMA-only Galaxy at $z \sim 5-6$ in a Tiny 3 mm Survey. *The Astrophysical Journal*, 884:154. Publisher: IOP ADS Bibcode: 2019ApJ...884..154W.

Williams, R. E., Blacker, B., Dickinson, M., Dixon, W. V. D., Ferguson, H. C., Fruchter, A. S., Giavalisco, M., Gilliland, R. L., Heyer, I., Katsanis, R., Levay, Z., Lucas, R. A., McElroy, D. B., Petro, L., Postman, M., Adorf, H.-M., and Hook, R. (1996). The Hubble Deep Field: Observations, Data Reduction, and Galaxy Photometry. *The Astronomical Journal*, 112:1335. Publisher: IOP ADS Bibcode: 1996AJ...112.1335W.

Williams, R. J., Quadri, R. F., Franx, M., van Dokkum, P., and Labbe, I. (2009). Detection of quiescent galaxies in a bicolor sequence from $z=0-2$. *The Astrophysical Journal*, 691(2):1879–1895. arXiv: 0806.0625.

Willott, C. J., Abraham, R. G., Albert, L., Bradac, M., Brammer, G., Chayer, P., Dixon, W. V. D., Doyon, R., Dupuis, J., Ferrarese, L., Goudfrooij, P., Hutchings, J., Martel, A., Pacifici, C., Ravindranath, S., and Sawicki, M. (2017). CANUCS: The CANadian NIRISS Unbiased Cluster Survey. *JWST Proposal. Cycle 1*, page 1208. ADS Bibcode: 2017jwst.prop.1208W.

Willott, C. J., Desprez, G., Asada, Y., Sarrouh, G. T. E., Abraham, R., Bradač, M., Brammer, G., Estrada-Carpenter, V., Iyer, K. G., Martis, N. S., Matharu, J., Mowla, L., Muzzin, A., Noirot, G., Sawicki, M., Strait, V., Rihtaršič, G., and Withers, S. (2023). A Steep Decline in the Galaxy Space Density Beyond Redshift 9 in the CANUCS UV Luminosity Function. Publication Title: arXiv e-prints ADS Bibcode: 2023arXiv231112234W.

- Willott, C. J., Doyon, R., Albert, L., Brammer, G. B., Dixon, W. V., Muzic, K., Ravindranath, S., Scholz, A., Abraham, R., Artigau, , Bradač, M., Goudfrooij, P., Hutchings, J. B., Iyer, K. G., Jayawardhana, R., LaMassa, S., Martis, N., Meyer, M. R., Morishita, T., Mowla, L., Muzzin, A., Noirot, G., Pacifici, C., Rowlands, N., Sarrouh, G., Sawicki, M., Taylor, J. M., Volk, K., and Zabl, J. (2022). The Near-infrared Imager and Slitless Spectrograph for the James Webb Space Telescope. II. Wide Field Slitless Spectroscopy. *Publications of the Astronomical Society of the Pacific*, 134(1032):025002. Publisher: The Astronomical Society of the Pacific.
- Wisnioski, E., Schreiber, N. M. F., Wuyts, S., Wuyts, E., Bandara, K., Wilman, D., Genzel, R., Bender, R., Davies, R., Fossati, M., Lang, P., Mendel, J. T., Beifiori, A., Brammer, G., Chan, J., Fabricius, M., Fudamoto, Y., Kulkarni, S., Kurk, J., Lutz, D., Nelson, E. J., Momcheva, I., Rosario, D., Saglia, R., Seitz, S., Tacconi, L. J., and Dokkum, P. G. v. (2015). THE KMOS₃D SURVEY: DESIGN, FIRST RESULTS, AND THE EVOLUTION OF GALAXY KINEMATICS FROM $0.7 \leq z \leq 2.7^*$. *The Astrophysical Journal*, 799(2):209. Publisher: The American Astronomical Society.
- Withers, S., Muzzin, A., Ravindranath, S., Sarrouh, G. T. E., Abraham, R., Asada, Y., Bradač, M., Brammer, G., Desprez, G., Iyer, K., Martis, N., Mowla, L., Noirot, G., Sawicki, M., Strait, V., and Willott, C. J. (2023). Spectroscopy from Photometry: A Population of Extreme Emission Line Galaxies at $1.7 \leq z \leq 6.7$ Selected with JWST Medium Band Filters. *The Astrophysical Journal*, 958:L14. Publisher: IOP ADS Bibcode: 2023ApJ...958L..14W.
- Wu, P.-F., Wel, A. v. d., Bezanson, R., Gallazzi, A., Pacifici, C., Straatman, C. M. S., Barišić, I., Bell, E. F., Chauke, P., D'Eugenio, F., Franx, M., Muzzin, A., Sobral, D., and Houdt, J. v. (2020). The Colors and Sizes of Recently Quenched Galaxies: A Result of Compact Starburst before Quenching. *The Astrophysical Journal*, 888(2):77.
- Wu, P.-F., Wel, A. v. d., Bezanson, R., Gallazzi, A., Pacifici, C., Straatman, C. M. S., Barišić, I., Bell, E. F., Chauke, P., Houdt, J. v., Franx, M., Muzzin, A., Sobral, D., and Wild, V. (2018). Fast and Slow Paths to Quiescence: Ages and Sizes of 400 Quiescent Galaxies from the LEGA-C Survey. *The Astrophysical Journal*, 868(1):37.
- Wuyts, S., Labbé, I., Förster Schreiber, N. M., Franx, M., Rudnick, G., Brammer, G. B., and van Dokkum, P. G. (2008). FIREWORKS U_{38-to-24} μ m Photometry of the GOODS Chandra Deep Field-South: Multiwavelength Catalog and Total Infrared Properties of Distant Ks-selected Galaxies. *The Astrophysical Journal*, 682:985–1003. ADS Bibcode: 2008ApJ...682..985W.
- Xiao, M., Oesch, P., Elbaz, D., Bing, L., Nelson, E., Weibel, A., Naidu, R., Daddi, E., Bouwens, R., Matthee, J., Wuyts, S., Chisholm, J., Brammer, G., Dickinson, M., Magnelli,

B., Leroy, L., van Dokkum, P., Schaerer, D., Herard-Demanche, T., Barrufet, L., Endsley, R., Fudamoto, Y., Gómez-Guijarro, C., Gottumukkala, R., Illingworth, G., Labbe, I., Magee, D., Marchesini, D., Maseda, M., Qin, Y., Reddy, N., Shapley, A., Shivaiei, I., Shuntov, M., Stefanon, M., Whitaker, K., and Wytthe, J. S. (2023a). Massive Optically Dark Galaxies Unveiled by JWST Challenge Galaxy Formation Models. Publication Title: arXiv e-prints ADS Bibcode: 2023arXiv230902492X.

Xiao, M.-Y., Elbaz, D., Gómez-Guijarro, C., Leroy, L., Bing, L.-J., Daddi, E., Magnelli, B., Franco, M., Zhou, L., Dickinson, M., Wang, T., Rujopakarn, W., Magdis, G. E., Treister, E., Inami, H., Demarco, R., Sargent, M. T., Shu, X., Kartaltepe, J. S., Alexander, D. M., Béthermin, M., Bournaud, F., Ciesla, L., Ferguson, H. C., Finkelstein, S. L., Giavalisco, M., Gu, Q.-S., Iono, D., Juneau, S., Lagache, G., Leiton, R., Messias, H., Motohara, K., Mullaney, J., Nagar, N., Pannella, M., Papovich, C., Pope, A., Schreiber, C., and Silverman, J. (2023b). The hidden side of cosmic star formation at $z > 3$ - Bridging optically dark and Lyman-break galaxies with GOODS-ALMA. *Astronomy & Astrophysics*, 672:A18. Publisher: EDP Sciences.

Xie, L., De Lucia, G., Fontanot, F., Hirschmann, M., Bahé, Y. M., Balogh, M. L., Muzzin, A., Vulcani, B., Baxter, D. C., Forrest, B., Wilson, G., Rudnick, G. H., Cooper, M. C., and Rescigno, U. (2024). The first quenched galaxies, when and how? Publication Title: arXiv e-prints ADS Bibcode: 2024arXiv240201314X.

Yan, H., Dickinson, M., Eisenhardt, P. R. M., Ferguson, H. C., Grogin, N. A., Paolillo, M., Chary, R.-R., Casertano, S., Stern, D., Reach, W. T., Moustakas, L. A., and Fall, S. M. (2004). High-Redshift Extremely Red Objects in the Hubble Space Telescope Ultra Deep Field Revealed by the GOODS Infrared Array Camera Observations. *The Astrophysical Journal*, 616:63–70. ADS Bibcode: 2004ApJ...616...63Y.

Yi, S., Demarque, P., and Kim, Y.-C. (1997). On the Ultraviolet-bright Phase of Metal-rich Horizontal-Branch Stars. *The Astrophysical Journal*, 482(2):677. Publisher: IOP Publishing.

Zavala, J. A., Casey, C. M., Manning, S. M., Aravena, M., Béthermin, M., Caputi, K. I., Clements, D. L., Cunha, E. D., Drew, P., Finkelstein, S. L., Fujimoto, S., Hayward, C., Hodge, J., Kartaltepe, J. S., Knudsen, K., Koekemoer, A. M., Long, A. S., Magdis, G. E., Man, A. W. S., Popping, G., Sanders, D., Scoville, N., Sheth, K., Staguhn, J., Toft, S., Treister, E., Vieira, J. D., and Yun, M. S. (2021). The Evolution of the IR Luminosity Function and Dust-obscured Star Formation over the Past 13 Billion Years. *The Astrophysical Journal*, 909(2):165.

Zibetti, S., Rossi, E., and Gallazzi, A. R. (2024). On the maximum age resolution achievable through stellar population synthesis models. *Monthly Notices of the Royal Astronomical Society*, 528:2790–2804. Publisher: OUP ADS Bibcode: 2024MNRAS.528.2790Z.

Zolotov, A., Dekel, A., Mandelker, N., Tweed, D., Inoue, S., DeGraf, C., Ceverino, D., Primack, J. R., Barro, G., and Faber, S. M. (2015). Compaction and quenching of high- z galaxies in cosmological simulations: blue and red nuggets. *Monthly Notices of the Royal Astronomical Society*, 450:2327–2353. Publisher: OUP ADS Bibcode: 2015MNRAS.450.2327Z.